Hochschule für Angewandte Wissenschaften Hamburg

Hamburg University of Applied Sciences

Diplomarbeit

Department Fahrzeugtechnik und Flugzeugbau

Integration of a Noise Analysis Module into a Multidisciplinary Aircraft Design Process

Philip Krammer

27. August 2008

Hochschule für Angewandte Wissenschaften Hamburg
Department Fahrzeugtechnik + Flugzeugbau
Berliner Tor 9
20099 Hamburg

in Zusammenarbeit mit:

Technische Universität Carolo-Wilhelmina zu Braunschweig*
Institut für Flugzeugbau und Leichtbau
Hermann-Blenk-Straße 35
38108 Braunschweig

Deutsches Zentrum für Luft- und Raumfahrt[§]
Institut für Aerodynamik und Strömungstechnik, Konfigurativer Entwurf
Lilienthalplatz 7
38108 Braunschweig

Verfasser: Philip Krammer
Abgabedatum: 27.08.2008

1. Prüfer: Prof. Dr.-Ing. Dieter Scholz, MSME
2. Prüfer: Dipl.-Ing. Christan Werner-Westphal

Industrielle Betreuer: Dipl.-Ing. Christan Werner-Westphal*
                         M.S., Dipl.-Ing. Lothar Bertsch[§]

Kurzreferat

Eine Reduzierung des Fluglärms kann sowohl durch Änderung primärer Lärmquellen am Flugzeug selbst, als auch durch Anpassung relevanter Flugzeugentwurfs- und Flugleistungs-parameter erreicht werden. Eine getrennte Betrachtung beider Ansätze muss nicht unmittelbar zu dem gewünschten Ergebnis führen. Eine methodische Herangehensweise ist daher unumgänglich und nur mittels multidisziplinärer Optimierung realisierbar. Fluglärm kann mit Hilfe von PANAM (Parametric Aircraft Noise Analysis Module) analysiert werden. PrADO (Preliminary Aircraft Design Optimization) bietet eine Entwicklungsumgebung um neuartige Flugzeugkonfigurationen zu untersuchen. Ziel der vorliegenden Arbeit ist die Anbindung von PANAM an PrADO, um den Fluglärm am Boden, als eine direkte Antwort auf eine angepasste Flugzeugkonfiguration und deren Auswirkung auf Flugleistungen, bewerten zu können. Dazu müssen Parameter der Flugzeuggeometrie, des Triebwerkes und diskretisierter Flugtrajektorien übergeben werden. Mittels der Eulerschen Turbinengleichung ist es möglich, aus einem thermodynamischen Kreisprozess auf die Fanblattspitzengeschwindigkeit zu schließen. Der maximale Steigwinkel wird aus der Überschussleistung gewonnen. Danach wird ein An- bzw. Abflug am Computer simuliert, um die Auswirkungen des Lärms am Boden zu analysieren. Der so gewonnene EPNL (Effective Perceived Noise Level) ermöglicht einen Vergleich mit ICAO-zertifizierten Werten aus Überflugsmessungen. Des Weiteren zeigt ein -um 40 % in Leistung gesteigertes- Mittelstreckenflugzeug Lärmminderungspotential während des Starts. Hierbei konnte die 80 EPNdB Isokonturfläche, im Vergleich mit dem Referenzflugzeug, um mehr als 20 % reduziert werden. Eine weitere Anwendung der Schnittstelle an einem größeren Frachtflugzeug (ungefähr 330 Tonnen maximales Abfluggewicht) liefert brauchbare Lärmergebnisse, obwohl semi-empirische, parametrische Lärmquellmodelle auf Überflugsmessungen eines Airbus A319 basieren. Eine einzigartige Visualisierung charakteristischer Lärmabstrahlungen, macht verständlich, wie implementierte Lärmquellmodelle auf Änderungen in der Flugzeugkonfiguration und im Flugzustand reagieren.

Abstract

Aircraft noise reduction can be achieved not only by noise reduction at source but also by modification of parameters in aircraft design and performance. Treating both merely independent from each other does not necessarily lead to the favoured results. As a matter of fact, a balanced approach is necessary to combine both methodologies with each other for multidisciplinary optimization. Aircraft noise analysis can be conducted with the Parametric Aircraft Noise Analysis Module (PANAM). PrADO (Preliminary Aircraft Design Optimization) provides a framework to investigate state-of-the art aircraft configurations already in an early stage of conceptual design. The objective of the thesis is the interconnection of both programs that allows for a direct response in noise impact on ground due to changes in aircraft configuration and performance. Parameters of aircraft geometry, the propulsion system and discretised trajectories are extracted out of PrADOs modules and databases. Application of the Euler turbine equation was necessary to gather fan blade tip speed from thermodynamic engine cycle analysis results. Maximum climb angle is observed by making use of the excess power. The aircraft is then "flown" to evaluate noise impact on ground. Results show not only that obtained Effective Perceived Noise Levels (EPNL) provide comparability with ICAOs noise certification reference values but also that a short- to medium range aircraft with a 40 % increase in static thrust exhibits a potential in a noise reduction during take-off. The ground area enclosed by the 80 EPNdB noise contour of constant EPNL is decreased by more than 20 % with respect to the conventional baseline aircraft. Another application of the derived interface on a larger freighter aircraft with a maximum take-off weight of about 330 tons indicates valuable results although semi-empiric, parametric noise source models are based on noise measurements of an Airbus A319. A unique visualisation of characteristic noise radiation has been conducted successfully. Changes in directivities and dimensions contribute to a generic understanding how implemented noise source models respond to changes in aircraft configuration and condition.

DEPARTMENT OF AUTOMOTIVE AND AERONAUTICAL ENGINEERING

Integration of a Noise Analysis Module into a Multidisciplinary Aircraft Design Process

Diplomarbeit at Hamburg University of Applied Sciences

Background

Community noise caused by aircraft during the initial and terminal phases of flight is a matter of increasing importance for the civil aviation industry. With airports increasingly operating near or at their capacity limit, one of the most promising means to enable further air traffic growth is to develop aircraft with minimum community noise impact, allowing them to avoid night time flying restrictions.

From an aircraft designer's standpoint, reducing aircraft noise to the levels needed to achieve this goal is a very challenging task. It is to be expected that such drastic noise reductions will not be achieved by merely working on mitigating noise sources on the aircraft in isolated form. Instead, the interactions of noise sources as well as shielding effects have to be considered and used to one's advantage. Aircraft noise becomes a configuration issue and thus has to be considered in the preliminary design stage [1].

At the DLR Institute of Aerodynamics and Flow Technology (AS), the Parametric Aircraft Noise Analysis Module (PANAM) has been developed which allows the prediction of noise impact on the ground along arbitrary flight trajectories [2]. The module takes into account major airframe and engine noise components, as well as diverse effects on sound propagation.

At the Institute of Aircraft Design and Lightweight Structures (IFL), Technische Universität Braunschweig, the multidisciplinary integrated preliminary aircraft design process PrADO has been in development for some time [3]. The process features a modular structure which allows the easy addition of disciplines and analysis methods to the design process.

At HAW Hamburg the Green Freighter (GF) research project investigates environmentally friendly freighters. Aircraft configurations investigated in the GF project can be used for investigations in this thesis.

Objective

The objective of this thesis is the interconnection between PANAM and PrADO. This includes two modes of operation: On the one hand, PANAM shall be able to retrieve necessary configuration data for noise analysis from the PrADO databases (geometry, engine data, flight trajectories for take-off and final approach, etc.). On the other hand, PrADO shall be able to retrieve noise analysis results in a format allowing easy visualization, but also in a format suitable for use as an optimization target function. The completed process is to be applied to several aircraft designs, allowing a thorough discussion of process capabilities and of depicted parameter sensitivities. A written report shall document the theoretical background, the work performed and the results obtained, including an assessment of these results.

The following tasks have to be performed:
- Familiarization with the design tool PrADO as well as the noise analysis tool PANAM. Literature research concerning the topic of noise analysis.
- Definition of interfaces which allow PANAM to use configuration data derived out of PrADO, such as aircraft geometric data and engine characteristics
- Definition of interfaces which allow PANAM to use PrADO's flight simulation modules for the calculation of symmetrical flight trajectories during take-off and landing
- Formulation of a target function suitable for the consideration of aircraft noise as an optimization parameter in the preliminary aircraft design process
- Definition of interfaces which allow PrADO to use PANAM noise analysis results for evaluation of the formulated target function
- Implementation of the defined interfaces in the form of FORTRAN programs
- Application of the developed processes on different aircraft designs. Verification if expected parameter sensitivities are depicted. If possible, comparison of calculated noise data with literature data for the examined aircraft
- Documentation of the conducted work and discussion of the obtained results

Literatur

[1]   SMITH, M. J. T.: Aircraft Noise. Cambridge University Press, Cambridge, New York, Port Chester, Melbourne, Sydney, 1989

[2]   BERTSCH L.; DOBRZYNSKI, W.; GUÉRIN, S.: Tool Development for Low-Noise Aircraft Design, AIAA/CEAS Paper 2008-2995, 14th AIAA/CEAS Aeroacoustics Conference, 5-7 May 2008, Vancouver, Canada

[3]   HEINZE, W.: Ein Beitrag zur quantitativen Analyse der technischen und wirtschaftlichen Auslegungsgrenzen verschiedener Flugzeugkonzepte für den Transport großer Nutzlasten, ZLR-Forschungsbericht 94-01, Braunschweig, 1994

The results have to be documented in a report. The report has to be written in a form up to internationally excepted scientific standards. The application of the German DIN standards is one excepted method to achieve the required scientific format.

**Deutsches Zentrum
für Luft- und Raumfahrt** e.V.
in der Helmholtz-Gemeinschaft

Institut für Aerodynamik und Strömungstechnik
Abteilung Konfigurativer Entwurf
Prof. Dr.-Ing. Karl-Heinz Horstmann
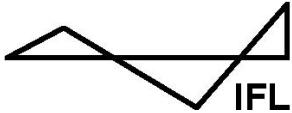
Institut für **F**lugzeugbau und **L**eichtbau
Technische Universität Braunschweig
Universitätsprof. Dr.-Ing. Peter Horst

This thesis is conducted in cooperation with the Institute of Aerodynamics and Flow Technology (AS) of the German Aerospace Center (DLR) and with the Institute of Aircraft Design and Lightweight Structures (IFL), Technische Universität Braunschweig.

Statutory Declaration

"I declare in lieu of an oath that I have written this diploma thesis myself and that I have not used any sources or resources other than stated for its preparation. I further declare that I have clearly indicated all direct and indirect quotations. This diploma thesis has not been submitted elsewhere for examination purposes."

August 27, 2008   Philip Krammer

Table of Contents

11

List of Figures

List of Tables

Nomenclature

Symbols

A	attenuation, A-weighted
C	EPNL tone correction
c	speed of sound, absolute velocity
d	duration / flyover time
D	EPNL duration correction / aerodynamic drag
DI_M	directivity index of radiated sound
f	frequency
h	enthalpy
H	height
i	one-third octave band number
K	Geometrical spreading
k	time increment (k-th) / wavenumber
L	Aerodynamic lift
M	Mach number
m	mass
n	perceived noisiness, rotational speed
N	total perceived noisiness
O	origin
P	power; spatial defined through x, y, and z-coordinates
p	pressure
P_W	sound power
Q	volume flux
R	radius; radiation vector (between S and O)
S	entropy
T	time period absolute value / engine thrust
t	time
u	local mean stream speed (flow velocity), circumferential velocity
v	flight velocity vector, relative velocity, specific volume
V	volume (absolute)

x	Cartesian coordinate
y	Cartesian coordinate (y_0 for sound pressure amplitude in Pa)
z	Cartesian coordinate

Greek Letters

α	angle of attack
β	sideslip angle
γ	climb angle
Δ	difference (delta)
δ	ratio for corrected pressure
ζ	exit flow angle (fan blade)
η	efficiency
θ	directivity/polar angle, ratio for corrected temperature
Θ	inclination angle; zenith
λ	wavelength
ρ	density
σ	ground resistivity to air
τ	engine throttle setting
Φ	bank angle
φ	radiation angle
Ψ	azimuth angle
ψ	directivity/polar angle referenced to lateral axis
ω	angular speed, rad/s

Subscripts

$()_a$	air-path axis system
$()_c$	corrected quantities
$()_D$	design point
$()_F$	flight position of the aircraft
$()_N$	net quantities
$()_O$	observer
$()_{ref}$	reference value
$()_{rms}$	root-mean-square
$()_{RT}$	rotor tip
$()_S$	source
$()_t$	total quantities, tangential
$()_0$	earth-fixed axis system
$()'$	displaced axis system
$(\_)$	vector (within text)

Abbreviations

ACARE	Advisory Council for Aeronautics Research in Europe
ANOPP	Aircraft Noise Prediction Program
ASCII	American Standard Code for Information Interchange
ATA	Air Transport Association
CFM56	CFM International turbofan engine
CPU	Central Processing Unit
DLR	Deutsches Zentrum für Luft- und Raumfahrt e.V.
DMS	Data Management System
DOC	Direct Operating Costs

EPNL	Effective Perceived Noise Level
ESPL	Equivalent Sound Pressure Level
FAR	Federal Aviation Regulation
FL	Flight Level (100 ft)
GE90	General Electric GE90 turbofan engine
GUI	Graphical User Interface
ICAO	International Civil Aviation Organization
IFL	Inst. of Aircraft Design and Lightweight Structures
ISA	International Standard Atmosphere
LDLP	Low Drag-Low Power
LNA	Low Noise Aircraft
MDA	Multidisciplinary Design Analysis
MDO	Multidisciplinary Design Optimization
MSL	Mean Sea Level
MTOW	Maximum Take-Off Weight
NACRE	New Aircraft Concepts REsearch
NADP	Noise Abatement Departure Procedure
OASPL	Overall Sound Pressure Level
OWE	Operating Weight Empty
PANAM	Parametric Aircraft Noise Analysis Module
PNL	Perceived Noise Level
PNLT	Tone Corrected Perceived Noise Level
PNLTM	Maximum Tone Corrected Perceived Noise Level
PrADO	Preliminary Aircraft Design and Optimization (program)
PWL	Sound Power Level
QSTOL	Quiet Short Take-Off and Landing
SPL	Sound Pressure Level
TET	Turbine Exhaust Temperature
VITAL	EnVIronmenTALly Friendly Aero Engines
ZTL	Turbofan, from German Zweistrom-Turbo-Luftstrahl-Triebwerk

1 Introduction

One day, humans will have to combat noise as relentlessly as the Cholera and the Pest.
(free translation; Robert Koch, 1910)

1.1 Background

Over the past years, the reduction of perceived aircraft noise has become a central factor in aircraft design and aircraft operations. By focusing on noise reduction at source (quieter aircraft), land-use planning, noise abatement procedures and aircraft operating restrictions, the "noise problem" can be identified and analysed. Bearing all aspects in mind gives rise to the so-called balanced approach to aircraft noise management that has been endorsed by the ICAO Assembly in 2001 (**ICAO 2008**). Today, aircraft noise has become a major problem in Europe. To adapt to expected traffic growth[1] in air transport at no environmental cost, stakeholders as well as policy makers await an economically and quieter global airline fleet. This can already be seen in a decreasing average age of large aircraft due to a significant advantage in fuel-efficient operation compared to short-range aircraft (**DLR Annual Report 2007,** p. 66). The expected low noise level of new aircraft is emphasized by looking at numerous airports that have already reached their noise capacity level despite simultaneous runway extensions and terminal infrastructure (**ACARE Report 2001**, p. 83). With this in mind, as of January 1st 2006 a more stringent chapter 4 was introduced by the Committee on Aviation Environmental Protection (CAEP/5) and became applicable to new as well as to older aircraft at re-certification. It can also be seen that many airports need to apply noise alleviation or prevention measurers (**ICAO 2008**). Remarkably often, airports have already introduced a noise surcharge through an individual set of measures according to their specific needs (**DLR Annual Report 2007**, pp. 161-2). To drive research towards those new challenges outlined by the Advisory Council for Aeronautics Research in Europe (ACARE), besides other environmental goals, to reduce perceived noise by half the 2002 averaged levels that have been associated with a 10 EPNdB reduction for fixed-wing aircraft per operation. The aim is to achieve this target concept by the year 2020 using complementary technologies

---

[1] An average traffic growth out of different global forecast studies (Airbus, Boeing, ICAO) would be an increase of about 126 % in passenger kilometres within the time frame 2008 - 2025 (**DLR Annual Report 2007**, p. 128).

and noise abatement procedures (**ACARE Report 2001**, pp. 83-4). The challenge in achieving this goal was documented in the report entitled "Trends in Global Noise and Emissions from Commercial Aviation". The paper was expected but not presented at an FAA conference in Barcelona last year (**Spiegel Online 2008**). Results of the report show that the population affected by noise will significantly increase over the next 15 years , especially in Western Europe (increase of 125% in the population above 65 dB day-night average sound level from now up to the year 2025), although new technologies and methods will emerge (**Fleming 2008**). This emphasizes the need for outstanding technologies and research to be conducted in the related field of minimizing aircraft noise in combination with other constraints such as fuel burn and green house gases.

The German Aerospace Center (DLR) explored and analysed numerous possibilities for aircraft noise reduction within the interdisciplinary project Quiet Air Traffic (in German: Leiser Flugverkehr) and QSTOL (Quiet Short Take-Off and Landing). ACARE goals have been approached and short- to mid-term solutions have been provided. Further studies dealt with noise prediction models that had recently been put together into one framework. The so derived noise prediction module was designed, particularly with regard to being implemented into a multidisciplinary design analysis process for aircraft preliminary sizing, to address noise reduction at source while taking the aircraft behaviour during take-off and landing into account. This approach is unique and allows judging perceived noise on a generic level and at an early stage of new aircraft projects.

1.2 Objective

The Parametric Noise Analysis Module (PANAM) facilitates a framework for aircraft noise prediction. The program commands aircraft geometric parameters, engine characteristics and flight trajectories. The second framework, the Preliminary Aircraft Design Optimization program (PrADO) that allows for parameter-, sensitivity-, and feasibility studies provides an access to derive required input data for PANAM. The objective of this thesis is the interface of the both program frameworks. Available design codes as implemented in PrADO are used to obtain the necessary information. As a result, execution of PANAM will deliver noise

analysis upon results that can be traced back to PrADO allowing noise to become a design constraint or an objective function in a multidisciplinary aircraft design process. More precisely, aircraft geometric parameters are readily available information obtainable out of PrADOs databases. Engine characteristics shall be provided in the form of an engine map dependent on Mach number, flight altitude and thrust setting. Engine thermodynamic cycle analysis as in PrADO can be used to derive the necessary temperatures, mass flows and pressures of a turbofan engine at any given engine- and flight condition. Flight trajectory modules have already been designed for PrADO, after addressing consecutive modules, flight mechanical parameters have to be transferred into the correct format for PANAM. The interface shall moreover be responsible for the execution sequence. Any wrong input might preferably lead to an error message. Interfaces shall be implemented in the form of FORTRAN-programs and PANAM requires all data in an ASCII-file format. Formulation of a target function suitable for the consideration of noise as an optimization parameter is necessary before initiating a multidisciplinary design process. Assets and drawbacks of the chosen form of the traced back noise parameter ought to be discussed. With the so derived interface, the overall process shall be applied upon different aircraft designs. Obtained results are to be discussed and verified if expected parameter sensitivities are depicted. If possible, calculated noise data is to be compared with data as found in literature.

1.3   Definition of Terms

Aircraft Noise

Aircraft noise encompasses overall noise out of engine and airframe noise sources as depicted in figure A.1. Engine associated noise has a strong influence (predominantly during take-off) and can be broadly subdivided into fan and jet noise. Those engine parts most contributing to engine noise are the fan (including the stator), exhaust, compressor, combustor and turbine.

Fan Noise

Fan noise is primarily caused by fan blades with transonic rotational tip speed and a high fan pressure ratio. The former is referred to as shock associated noise and becomes significant at fan rotational tip speeds above Mach number of 0.72. Shock strength is influenced by fan

blade leading edge design. The latter is associated with broadband noise due to turbulences in the secondary mass flow stream after passing the fan blade and further down the stators. Discrete tones develop with the shock at the fan blades and are referred to as buzz-saw noise (**Smith 1989**, pp. 134-6), which can be reduced by using acoustically absorbent material in the inner nacelle. Turbulence and therefore noise is also due to vibrations. As a result of that fan blades are manufactured   geometrically as identical as possible including consideration of elastic deformations with the engine at high rotational speed. This can also be achieved by midspan snubbers on the fan blades that are used as a damping element if the fan blade aspect ratio gets too high.

Jet Noise

According to the theory of Sir James Lighthill (1924-1998) jet associated noise increases with stream velocity. With the introduction of the turbofan engine in the 1950s jet noise was significantly lowered. A turbofan engine produces a slower, cooler exhaust stream with a considerably larger cross section. The noise "remaining" out of the turbofan exhaust stream is due to combinations of temperature and velocity differences as well as formation and decomposition of vortices (**DLR News May 2008**, p. 18).

Airframe Noise

Flaps, slats and landing gear are the primary contributors to airframe noise. All three have similar amplitudes with the peak at different frequencies. Flap noise originates primarily from the flap side edge where a strong vortex is formed. This is due to a sharp change in lift between wing and flap. Slat noise is caused by resonances due to slat trailing edge vortex shedding and the gap between slat and wing. Landing gear noise is broadly associated as broadband noise due to bluff body separation and shedding from various components of various sizes. Additionally, noise radiating from the clean aircraft is a strong function of lift coefficient. This is due to different turbulent boundary layer characteristics along the wing upper surface (**Lockard 2004**, p. 5-12).

Multidisciplinary Aircraft Design Process

Aircraft design is essentially affected by strong interactions between related disciplines and the economical framework during aircraft operations that have to be well balanced in respect of the airplane as an overall system. The interactions are additionally most likely to be opposed. The objective is to find the best aircraft configuration out of many possible ones that

cope with the transport task i.e. compliance with the required design mission, compliance with maximum permissible runway lengths, etc. The chosen configuration shall provide technical and economical benefits to the customer in order to be on a competitive basis (**Heinze 2004**, front page). The basic set of design parameters contains thrust to weight ratio, wing loading, aspect ratio, sweep, and thickness (**Raymer 1999**, p. 612). As a logical consequence, the question arises how an optimization of this basic set of design parameters could be achieved. A six-dimensional carpet plot does not exist. Multidisciplinary Design Analysis (MDA) and optimization (MDO) are nowadays, with the help of high-capacity data processors, commonly applied upon preliminary aircraft design. Systems that are complex and feature strong interactions between disciplines can be handled with MDA/MDO. This allows for simultaneous manipulation of variables and a highly optimized system design with respect to all main disciplines (**Werner-Westphal 2008**, p. 581). Concerning a multidisciplinary aircraft design processes the following questions may be of interest (**Heinze 2004**, front page):

- Is the suggested aircraft configuration with respect to the design mission and the chosen technology standard feasible? (Feasibility studies)
- What influence is exerted on the overall system aircraft by design parameters, alteration of the design mission and the impact of new technologies? (Parameter- and sensitivity studies)
- How can a designed aircraft technically and economically be improved by changing the aircraft configuration e.g.: wing area, wing aspect ratio, number of engines and arrangement? (Configuration optimization)
- To what degree is the preferred aircraft configuration more (or less) economical in comparison with other related concepts? (Configuration finding)

Supplementary, MDO becomes additionally important considering unconventional aircraft configurations[2]. The greater the number of additional new constraints, the more complex the observed system. A remedy can be found by applying statistic and empirical data that is however not broadly available for unconventional aircraft configurations. Therefore, higher fidelity methods that take more physical laws into account are necessary in combination with

---

[2] Unconventional aircraft configurations differ at least in one basic feature out of the design features of a conventional aircraft configuration (characterized by a fuselage and a wing as well as a horizontal tailplane and vertical tailplanes located at the tail of the aircraft (**Scholz 1999**, p. 4.7)

multidisciplinary design tools (**Werner-Westphal 2008**, p. 581). Interactions between related disciplines are enforced by e.g. the so called snowball effect[3] and the square-cube law that puts the term "multidisciplinary" into the correct spotlight.

1.4   Outline of the Thesis

The chapter on theory with appendix B comprehends a thorough explanation of acoustic theory as well as the programs used. All relevant aspects to be considered for a noise prediction in aircraft preliminary design are explained and derived from generally excepted formula. Beyond other mentioned frequency weightings the generally accepted scale for evaluating aircraft noise, the effective perceived noise level, is explained in more detail. The description of acoustic source models besides sound propagation effects leads consequently into the next sub-chapter: development and explanation of PANAM. With an introduction to PrADOs principal set-up and philosophy a basis should have been provided to the reader to reconstruct the method applied for interconnection of both programs.

Chapter 4 presents the method applied in transferring parameters of aircraft geometry, the propulsion system and discretised trajectories out of PrADOs modules and databases. The respective appendix C contains a list of all parameters that have to be passed. Appendix F contains further information of the interface on a supporting level.

Chapter 5 together with appendix D contains considerations how noise could be implemented in a multidisciplinary design optimization process. Additionally, a detailed description of those aircraft parameters that are influencing the noise impact on ground directly and primarily has been provided. With this in mind, the reader should be able to comprehend influences that are decisive for obtained and discussed results.

Chapter 6 presents the results of the applied interface upon two aircraft configurations. A parameter study has been conducted that focuses on the engine thrust and resulting aircraft

---

[3] The heavier the aircraft, the more lift and thrust is needed. With more thrust required, the bigger the engine the more aircraft weight and so on…

take-off behaviour. The chapter comprises a pre-discussion of outputs of the derived interface. Especially those outputs of the engine map are examined. The complementary to chapter 6 is appendix E that can be subdivided into figures for the short- to medium range aircraft, the Green Freighter and source model directivities (see list of figures).

The chapter on discussion focuses primarily on the analysis of obtained noise results and leads into chapter 7: summary and concluding remarks.

2   Literature Review

The overall European collaborative network dedicated to the reduction of aircraft noise, X-Noise, coordinates research projects that are contributing to the aeroacoustical knowledge base and addresses aircraft noise challenges set by the ACARE 2020 Vision (**X-Noise 2008**). Over the past ten years, many of those research projects have been accomplished with a few still going on: The technology platform SILENCE(R) links turbomachinery-, exhaust- and airframe noise reduction technologies and was the largest research project conducted. Over six years a total of 25 source noise reduction technologies have been studied and evaluated such as the ultra-high bypass ratio engine concept, negatively scarfed inlets, zero-splice inlet liners, low-noise fairings on landing gears, etc. (**Snecma 2007**). Besides those projects dealing with basic tool development and understanding, two thematic areas in X-Noise are left: advanced configuration and noise abatement procedures that are to be associated with the topic in this thesis. NACRE (New Aircraft Concepts REsearch) deals with aircraft architecture and VITAL (EnVIronmenTALly Friendly Aero Engines) with engine architecture making up the advanced configuration platform. Both are in their final phase and considered as large validation and multidisciplinary projects. SOURDINE (Study of Optimisation procedURes for Decreasing the Impact of NoisE) dealt with the evaluation of noise abatement procedures (**SOURDINE 2008**). The NACRE consortium, headed by Airbus, strives for solutions at a generic aircraft component level (wing, fuselage, and engine) where noise related aspects are taken into account. Resulting aircraft designs are therefore not primarily driven by low noise aspects. Different aircraft concepts or even slightly changed aircraft configurations exhibit different behaviour during take-off and landing. Such an interconnection of aircraft architectures and noise abatement procedures projects might exist in X-Noise but is at least not shown on the road-map (**X-Noise 2008**). To demonstrate and validate technology breakthroughs so far obtained the Clean Sky JTI was launched (Joint Technology Initiative) as one of the future European research projects (**Clean Sky 2008**).

The Silent Aircraft Initiative project carried out in partnership between the University of Cambridge and the Massachusetts Institute of Technology, focused on the conceptual design of an ultra low noise, fuel efficient aircraft (figure A.2). The derived concept is said to be as quiet as 63 dBA (OASPL) at airport perimeter besides additionally being very fuel efficient (**Silent Aircraft Initiative 2008**). For accomplishing this derived aircraft concept, many

technical challenges have been introduced such as vectored thrust, distributed propulsion systems, pressure vessel for the unconventional airframe, etc. (novel centrebody shape with leading edge carving initially based on the Blended-Wing-Body concept). With this in mind, sound prediction becomes very challenging not only because relating noise source models do not exist but also considering engine noise shielding effects. Someone might therefore put the above mentioned noise exposure value into question. However, the derived concept will be significantly less noisy than today's aircraft but with still many technical challenges to overcome.

Novel aircraft concepts to reduce noise developed by Cranfield University are linked to the Silent Aircraft Initiative. The derived configuration is a conventional fuselage combined with a low aspect ratio delta wing (broad delta) and a V-tail. Noise prediction is done by semi-empirical low fidelity models based on conventional aircraft but for the new derived configuration it is not quite clear, out of the given information as in the paper, how noise prediction is done. Noise reduction potentials are mentioned such as undercarriage fairings (minus 8-10 dBA), 6 degree steep approaches (minus 8-12 dBA), displaced thresholds (minus 5 dBA), etc. As a conclusion in **Mistry 2007** (p. 597): "It can thus be seen that the BD (Broad Delta, authors note) has the potential for meeting the extremely challenging 60 dBA target." Assuming that a first rough noise prediction is done by subtracting constant noise values from derived noise levels may lead to the question if interferences between the noise sources are still to be of negligible amplitude (e.g. engines placed near to each other over the wing).

At DLR Institute for Aerodynamics and Flow Technology a promising Low Noise Aircraft (LNA) has been developed (**DLR Report 2008)** that has been analyzed in PrADO at the Institute of Aircraft Design and Lightweight Structures (IFL) (**Werner-Westphal 2008**). The wide-body aircraft configuration includes above wing mounted engines as well as forward swept outer wings with an increased reference area for a better fan noise shielding (figure A.3). As a consequence, the whole wing is moved backwards to reduce cabin noise. The resulting configuration is a canard with penalties in aircraft structural weights and direct operating costs, but with less noise emission compared to conventional aircraft configurations due to fan noise shielding. Estimated noise reduction in terms of sound pressure levels is not possible to predict due to the lack of acoustic shielding effects and influences.

For evaluating engine noise shielding in the design phase of new aircraft concepts a ray-tracing tool called SHADOW is currently under development at DLR (**DLR Report 2008**). Solving ordinary differential equations allows for a very fast prediction of geometrical shielding effects. Of crucial importance are for such cases diffraction effects that are also considered within the program. A first application of the program upon the LNA configuration can be seen in figure A.4.

By searching for aircraft conceptual design in relation with aircraft noise, response surface equations are often encountered (**Olson 2006**; **Geoffrey 2004**). First-principles analysis combined with response surface methods (composition of statistical techniques for empirically relating an output variable to input variables) are considered as powerful tools for evaluating new technologies upon which empirical methods cannot be applied. As a result, trend lines for the entire design space are plotted for several different constraint scenarios. Those parametric sensitivity plots are said to assist the designer in understanding the tradeoffs involved. The advantage is seen in fairly fast analysis and plotting sensitivities over the entire design space rather than for a selected number of optimized points. By contrast, difficulties have been encountered in the level of detail out of first-principles analysis and many sensitivity plots are depicted for only one design constraint influenced by a number of specific parameters. For the latter, influences shown are therefore not on a generic level.

Also often encountered in literature is the Aircraft Noise Prediction Program ANOPP that is a semi-empirical code using publicly available noise prediction schemes (**Leifsson 2005**, p. 30). It is continuously updated by NASA Langley Research Center and often used at research institutes in the United States.

A similar approach as used in this thesis has been found in **Leifsson 2006**. Noise is added as a design constraint into a multidisciplinary design optimization framework. The aircraft is first optimized without considering noise. The obtained reference configuration is analysed at approach to obtain a reference noise level that is subsequently added as a noise constraint. Noise prediction is accomplished with ANOPP. One of the results showed, by increasing the wing reference area with a weight penalty of about 3.8 % and thereby reducing the approach speed from 150 to 130 knots, total airframe noise can be reduced by 3 EPNdBs. As a further result, out of a trailing edge flap elimination by increasing wing reference area and angle of attack, total airframe noise can be reduced by only 1 EPNdB.

Another approach for decreasing noise impact on ground is by optimizing flight trajectories. Here, the objective function is based on noise models and terminal area population density data and constraints are based on flight envelopes (**Xue 2006**). In contrast, different standard approaches are also possible to compare with respect to perceived noise on the ground as in **LAnAb 2007** (project 1630).

Many ongoing research activities and different approaches have been found to reduce aircraft noise. Unconventional aircraft configurations exhibit a high potential of noise reduction upon which empirical or semi-empirical noise analysis modules cannot be applied elementarily. Here, noise prediction with related noise impact on ground gets more complex when dealing with noise shielding effects that are difficult to estimate not only because of the arising acoustical diffractions and refractions. Multidisciplinary design optimization in connection with noise analysis that takes alterable mechanical flight parameters (due to a change in the aircraft configuration) as well as responding semi-empirical noise models into account, has not been found in this manner in available literature.

3   Theory

... for administrative and control purposes, all the real and imaginary effects that people perceive (from aircraft noise, authors note) have to be rolled into a simple indicator; otherwise it would be far too complicated to quantify and judge the impact of changes to the general pattern of aviation, and the results might be misleading. For this reason, rating aircraft noise has become something of an art.” (Smith, Aircraft Noise p. 3)

Many rating scales can be found in literature. These include the generally accepted A-weighting as well as the commonly used effective perceived noise levels developed for the purpose of aircraft noise measurements. The comparability of other rating scales, such as aircraft noise exposure modelling, got lost by using somehow independently defined annoyance descriptors. Additionally, recently developed, state of the art rating scales can be found in literature, e.g. the criteria of a human wake-up probability (**LAnAb 2007**, project 1635, p. 101), sound exposure modelling based on an averaged sound pressure of all observers or ground microphones (**Ishii 2005**, p. 5), or even the more complex Zwicker Tone Illusion[4] (**Franosch 2003**, abstract) that is transferred to the unbiased annoyance or UBA-rating (**Kollmeier ca. 2006**, p. 71). Still, a lot of research is needed in human reaction to aircraft noise since there is no fully reliable scale (**Smith 1989**, p. 19).

Noise prediction results are presented in this thesis either as A-weighted sound pressure levels or as effective perceived noise level to be consistent, obtain comparability and use commonly accepted scales. The following chapter includes the formulation of the mentioned scales and theoretical foundations of general acoustics and aeroacoustics. Subsequently, the principal philosophy of the two main programs used for interconnection is explained.

3.1   Noise Analysis

Noise consists ordinarily of many frequency components. A pure tone, for comparison, is a sinusoidal pressure fluctuation at one single frequency. Therefore, sound waves in air are

---

[4] “The Zwicker tone is an auditory aftereffect. For instance, after switching off a broadband noise with a spectral gap, one perceives it as a lingering pure tone with the pitch in the gap. … it cannot be explained by known properties of the auditory periphery alone.” (**Franosch 2003**, abstract)

characterized by adiabatic[5] expansions and contractions. A forward travelling pure tone sound wave may be described with the following equation (**Wilson 1989**, pp. 11-3):

$$p(\vec{x},t) = y_0 \cos\left[\frac{\omega}{c}(\vec{x} - ct)\right] \tag{3.1}$$

where $p(t)$ = instantaneous sound pressure (Pa)

y_0 = sound pressure amplitude (Pa)

ω = angular frequency (rad/s) = $2\pi f$

c = speed of sound = λf = 340 m/s

λ = wavelength (m)

An oscillating particle causes a difference between instantaneous absolute sound pressure and the prevailing ambient pressure. The variation of the squared sound pressure over a given time t, or any number of periods T considering pure tones, can be calculated by integration in the form of:

$$p_{rms}^{\ 2} = \frac{1}{T}\int_0^T p(t)^2\, dt \tag{3.2}$$

where $p_{rms}^{\ 2}$ = mean-square sound pressure

p_{rms} = root-mean-square sound pressure (Pa)

The mean-square sound pressure of a pure tone can be determined solving equation 3.1 in equation 3.2 (derivation has been reproduced but not stated):

$$p_{rms}^{\ 2} = \frac{y_0^{\ 2}}{T}\int_0^T \cos^2\left(\frac{\omega x}{c} - \omega t\right) dt = \frac{y_0^{\ 2}}{2} \tag{3.3}$$

3.1.1   Sound Pressure Level

Since the human ear recognizes pressure fluctuations in a specific way it seems logical to evaluate sound similarly. In principal the ear does not react in the same way pressure varies.

---

[5] The heat exchange between compression and expansion is negligible.

Moreover, the ear does respond to an energy input more or less logarithmically. This input is proportional to the mean-square or square of sound pressure. The threshold of hearing is at about 20 μPa. A rock concert in front of the loud speaker causes a sound pressure in the ear of about 20 Pa which is close to the level where pain is experienced. This remarkable wide range of sound pressure information the human ear can detect is transferred to the human brain which is not able to react in a linear way. As a consequence measuring by comparing with a logarithmic scale becomes more convenient (**Bies 2003**, p. 36). The sound pressure level, L_p or SPL in dB is defined in **DIN 45630 1971** as follows:

$$\text{SPL} = 10 \lg \frac{p_{rms}^2}{p_{ref}^2} = 20 \lg \frac{p_{rms}}{p_{ref}} \tag{3.4}$$

where p_{ref} is the reference sound pressure (expressed by the same unit as p) and set at the threshold of hearing that equals as a matter of fact to 0 dB of sound pressure level:

$$p_{ref} = 2 \cdot 10^{-5} \frac{\text{N}}{\text{m}^2} = 20 \mu\text{Pa} \tag{3.5}$$

For the avoidance of a too compressed scale a factor of 10 is introduced (**Bies 2003**, p. 37), changing the unit "bel" to "decibel". The logarithmic unit decibel is used to describe the above mentioned ratio with its reference. According to **DIN 45630 1971** the sound power level PWL[6] in dB is defined with the reference power $P_{W,ref} = 10^{-12}\text{W} = 1$ pW as in equation 3.4a.

$$\text{PWL} = 10 \lg \frac{P_W}{P_{W,ref}} \tag{3.4a}$$

Due to the logarithmic scale a doubling of the root-mean-square sound pressure level leads to a change of only 6 dB (using equation 3.6 in equation 3.7),

---

[6] Sound power is in available literature alternatively identified by the letter "W" (L_W). This is probably done in order not to confuse the level of sound pressure L_p (SPL) with sound power level L_P (PWL), although this is suggested by **DIN 45630 1979**. To be consistent, in this thesis SPL and PWL are used only instead of identifying a sound level by the letter "L". As a consequence P can be used for the sound power (according do DIN) without confusing the reader. Still, pressure p and power P are likely to be mistaken. Therefore, as a definition in this thesis, the sound power receives the subscript "W".

$$p_{rms,NEW} = 2p_{rms} \tag{3.6}$$

$$\text{SPL} = 10\lg\left(\frac{2p_{rms}}{p_{ref}}\right)^2 = 10\lg\left[\left(\frac{p_{rms}}{p_{ref}}\right)^2 \cdot 4\right]$$

$$= 10\lg\left(\frac{p_{rms}}{p_{ref}}\right)^2 + 10\lg 4$$

$$= 10\lg\left(\frac{p_{rms}}{p_{ref}}\right)^2 + 6.021\,\text{dB} \tag{3.7}$$

whereas a doubling of the mean-square sound pressure results in an approximate 3 dB increase ($\Delta\text{SPL} = 10{\cdot}\lg 2$). The respective sound pressure of a given sound pressure level can be obtained using equation 3.4:

$$\lg\frac{p_{rms}}{p_{ref}} = \frac{\text{SPL}}{20}$$

$$p_{rms} = p_{ref} \cdot 10^{\text{SPL}/20} \tag{3.8}$$

$$p_{rms} = 20 \cdot 10^{-6}\,\text{Pa} \cdot 10^{90\,\text{dB}/20} = 0.633\,\text{Pa} \tag{3.9}$$

Assuming a sound pressure level of a very loud sound, say about 90 dB, the magnitude of the respective root-mean-square sound pressure is only 0.632 Pa (equation 3.9). In the special case of a pure tone it is possible to estimate the sound pressure amplitude y_0 with the help of equation 3.3:

$$y_0 = \sqrt{2} \cdot p_{rms} = \sqrt{2} \cdot 0.633\,\text{Pa} = 0.894\,\text{Pa} \tag{3.10}$$

The standard atmospheric absolute pressure at mean sea level is set at 101,325 Pa. With this in mind, the corresponding sound pressure to a pure tone of about 90 dB sound pressure level is less than 1/100,000th of atmospheric pressure. This sensibility is responsible for the just noticeable difference that equals 1 dB, with a sound power increase of about 26 % (**Wolfe 2006**), depending on frequency and absolute SPL, whereas an average individual perceives an increase in 10 dB of SPL as a doubling in loudness (compare **Wilson 1989**, p. 13).

3.1.2 Broadband Noise

Considering two pure tones of the same amplitude and frequency that are in phase, the root-mean-square sound pressure doubles as a consequence on a combination of both. With a phase angle of about π the resulting pressure would theoretically be zero. Essentially, aircraft noise is produced by many uncorrelated sources, comprising various amplitudes and frequencies. For the description of such random sounds, the sound pressure is resolved into its frequency components referred to as sound spectra. The model used by **Bies 2003** (pp. 39-41) to discuss sound spectra is based on an oscillatory piston in an open tube. When the piston goes for the compression stroke only the element of air at the top face of the piston is forced to move. The pressure in the element of air increases. The second element of air which is next to the translated one but not in direct contact with the piston surface does not move at the very first moment. This is because air exhibits inertia. In the following moment the pressurized element of air is expanding causing the second element to move. A pressure pulse with the velocity of the speed of sound emerges. The same explanation model can be found in the area of gas dynamics in relation with the development of shock waves. During the inverse movement of the piston an equivalent negative pressure pulse is formed since the volume on the top of the piston is expanding. The reciprocating motion of the piston creates a pressure distribution equally to a sine wave with a frequency proportional to the revolutions per minute of the engine. Therefore, a pressure disturbance caused by harmonic motion is characterized by a single frequency. However, if the movement of the piston is irregular the pressure distribution of the sound wave must be described with a frequency spectrum consisting of a combination of several sinusoids with various frequencies. A special case is the cyclic motion of the piston. The spectrum can then be described with discrete frequencies. Typically recorded sounds in general may show single-frequency components but are more likely to consist of very disordered and random waveforms such as broadband noise. Erratic pressure disturbances may be decomposed into basic functions by Fourier analyses. Here, it has to be said, that tonal components found within the frequency analysis should be examined differently since they are not considered as broadband noise. A description of the waveform in terms of separating and collecting all waves of all frequencies becomes possible with the help of a frequency spectrum. The spectrum is divided into frequency bands which cover a dedicated frequency range for easier explanation.

In order to compare measured sound spectra more easily a table of preferred frequencies has been standardized. The standard **EN ISO 266 1997** of the International Organization for Standardization defines the preferred frequencies for acoustical measurements. The frequency sequence refers to a reference frequency f_{ref} = 1000 Hz. The preferred frequencies are based on the system of preferred numbers within the R10 series after international standard ISO 3. In general, geometrical series are favoured due to constant percentage increments before rounding. The exact frequency can be computed by using following coherence:

$$f = 10^{n/10} f_{ref} \tag{3.11}$$

where n is a positive or negative integer. The frequency sequence is determined by the power of ten and can therefore be easily adapted or extended to infrasonic and ultrasonic frequency bands. An octave is defined as the interval between two sounds with a basic frequency ratio of $1:2$ (**Wilson 1989**, p. 545). More detailed information of sound can be obtained by using standardized one-third octave band centre frequencies that are set at each value of the R 10 series. With $n = 3$ in equation 3.11 a factor of about 2 results between frequency f and reference frequency f_{ref}. Hence, every third one-third octave band centre frequency is an octave.

Table 3.1   Preferred centre frequencies

Band number[a]	Octave band centre frequency	One-third octave band centre frequency	Calculated frequency[b]	Band limits[c]	
				Lower	Upper
30	1,000	1,000	1,000.0	880	1,130
31		1,250	1,258.9	1,130	1,414
32		1,600	1,584.9	1,414	1,760
33	2,000	2,000	1,995.3	1,760	2,250
34		2,500	2,511.9	2,250	2,825
35		3,150	3,162.3	2,825	3,535
36	4,000	4,000	3,981.1	3,535	4,400
37		5,000	5,011.9	4,400	5,650
38		6,300	6,309.6	5,650	7,070
39	8,000	8,000	7,943.3	7,070	8,800

Notes:

[a]   band number is related to f_c: BN = 10lg f_c (**Bies 2003**, p. 42)

[b]   equation 3.11, in round figures of 5 significant decimals (**EN ISO 266 1997**)

[c]   calculated with 1/3 octave band width as stated above

Every frequency band holds an upper and a lower band limit where the band with Δf of each band can be calculated as $\Delta f = 0.2316 f_C$ for 1/3 octave bands and $\Delta f = 0.7071 f_C$ for octave

bands, with f_C as the respective centre frequency. A detailed description can be found in **Bies 2003** (pp. 42-3). An extract of preferred frequencies is depicted in table 3.1. The table can be expanded indefinitely in either direction by multiplication or division of powers of ten.

A sound is usually described in a 1/3 octave band frequency spectra where each of those frequency bands most likely represents a different sound pressure level. For combining these incoherent sounds, a linear energy basis has to be applied i.e. the summation of perceived sound in the form of mean-square sound pressures or root mean-square sound pressures. Therefore, SPL that are represented on a logarithmic basis have to be transferred to pressure values before summation. The obtained result converted back to SPL is often referred to in literature as Overall Sound Pressure Level (OASPL). With equation 3.4, OASPL yields the following formula[7]:

$$\text{SPL} = 10 \lg \frac{p_{rms}^2}{p_{ref}^2} \Rightarrow p_{rms}^2 = p_{ref}^2 \cdot 10^{SPL/10}$$

$$\left\langle p_{1rms}^2 \right\rangle + \left\langle p_{2rms}^2 \right\rangle + \ldots = \sum_{i=1}^{N} \left\langle p_{(i)rms}^2 \right\rangle = p_{ref}^2 \sum_{i=1}^{N} 10^{SPL(i)/10}$$

$$\text{OASPL} = 10 \lg \frac{\sum_{i=1}^{N} \left\langle p_{(i)rms}^2 \right\rangle}{p_{ref}^2} = 10 \lg \left(\sum_{i=1}^{N} 10^{\text{SPL}(i)/10} \right) \tag{3.11a}$$

The same formulation can be obtained by using root mean-square sound pressures. The reference pressure p_{ref} is set to be constant for all frequency bands and can therefore be excluded from the summation symbol. An equivalent sound level is obtained by averaging OASPL over a time interval (one hour, one day, etc.) and similarly converting back to decibels by using the same principle as described above. For broadband noise, the calculation of the OASPL is necessary before computing an Equivalent Sound Pressure Level (ESPL). For e.g. pure tones, ESPL may be derived directly out of mean-square sound pressures. ESPL (or L_{eq} respectively as used in some literature) is to be calculated as follows (**Wilson 1989**, p. 25):

$$\text{ESPL} = 10 \lg \left(\frac{1}{T} \int_{0}^{T} 10^{OASPL/10} \, dt \right) \tag{3.11b}$$

---

[7] The time average of the product of two or more time-varying quantities, which have been averaged over the time beforehand, are indicated by angle brackets (**Bies 2003**, p.30).

3.1.3 Frequency Weighting

Human hearing is most sensitive in the frequency range of 500 Hz to 5 kHz. The apparent loudness of a sound i.e. the subjective response of the ear that varies with frequency and sound pressure is therefore not to be considered in a proportional context. The divergence of perceived and actual sound is decreasing with increasing sound pressure level (**Bies 2003**, p. 100; **Wilson 1989**, p. 24). In other words, a soft sound at a specified low sound pressure level (say, near 20 dB) cannot be heard by the human ear at frequencies below 130 Hz. For comparison a sound at 100 dB sound pressure level can be sensed between 20 Hz and 20 kHz that is the full audible range of a human. The audible range as described in this context is depicted in figure B.1. Taking this behaviour of the human ear into account, electronic weighting networks, commonly implemented as electronic filters, have been established. Simply by adjusting the sound level in each frequency band to a value of the first audible (low) sound level i.e. the soft sound margin in figure B.1., the A-weighted circuit can be determined. A-weighting is therefore a measure of loudness. B and C networks have been designed for sound levels above 55 dB and should therefore be used when dealing with louder sounds due to a more appropriate weighing. However, A-weighting is most common because it (a) correlates reasonably well with hearing thresholds, (b) is used by many commercial sound-level meters and (c) is the basis for B- and C-weighting, which do not offer a clear advantage (**Lamancusa 2000**; **Smith 1989** pp. 285-6). Figure 3.1 shows the A-weighting and C-weighting network corrections in dB in comparison. The corrected sound pressure levels are specified with the unit dBA or dBC respectively. D-weighting has been solely developed to approximate perceived aircraft flyover noise. Data for the D-weighted circuit has been found in **Lamancusa 2000** and plotted in figure 3.1. The D-weighting circuit additionally penalizes the perceived noise between 1 kHz and 10 kHz of frequency range. The reason for that is a better description of aircraft noise based on annoyance rather than loudness. D-weighting has been used in airport-monitoring systems as a basis for the approximation of the Perceived Noise Level (PNL) whereas C-weighting has been used to describe sonic boom overpressures (**Smith 1989**, p. 286). The relative contribution of each one-third octave band to overall loudness varies additionally with overall loudness (**Lamancusa 2000**). The so far explained weighting circuits have been set up with a specified condition and cover therefore only a specific range. However, considering A-weighting with sound pressure levels below 55 dB may not necessarily lead to huge discrepancies. With the introduction of equal

noisiness contours, perceived noise level can be calculated, taking human annoyance to aircraft noise at different frequencies and sound pressure levels into account. PNL is the basis for the complex unit Effective Perceived Noise Level (EPNL). The calculation of EPNL data from measured noise data is specified in **ICAO Annex 16 1989** and **FAR Part 36** respectively. In principal, EPNL can be computed in five steps out of the three basic physical properties of sound pressure (level, frequency distribution and time variation): (1) The sound pressure levels of each of the 24 one-third octave bands are first converted to perceived noisiness $n(i,k)$ by means of a noy[8] table. The noy values are combined and converted to instantaneous PNL(k). A tone correction factor C(k) is calculated (2) and then added (3) to the PNL(k) which results in the Tone Corrected Perceived Noise Level PNLT(k). The maximum value PNLTM of PNLT(k) is determined. With the calculation (4) of a duration correction factor D, EPNL is determined by the algebraic sum of PNLTM and D (5). Noise analysis must be conducted in the range of one-third octave nominal midband frequencies from 50 Hz through 10 kHz inclusive (**FAR Part 36**, A36.3.7.3) i.e. a total of 24 one-third octave bands. This range has been marked as an "audible" range for aircraft noise analysis in figure 3.1. The index i represents therefore the one-third octave band number whereas k is set for the increment of time.
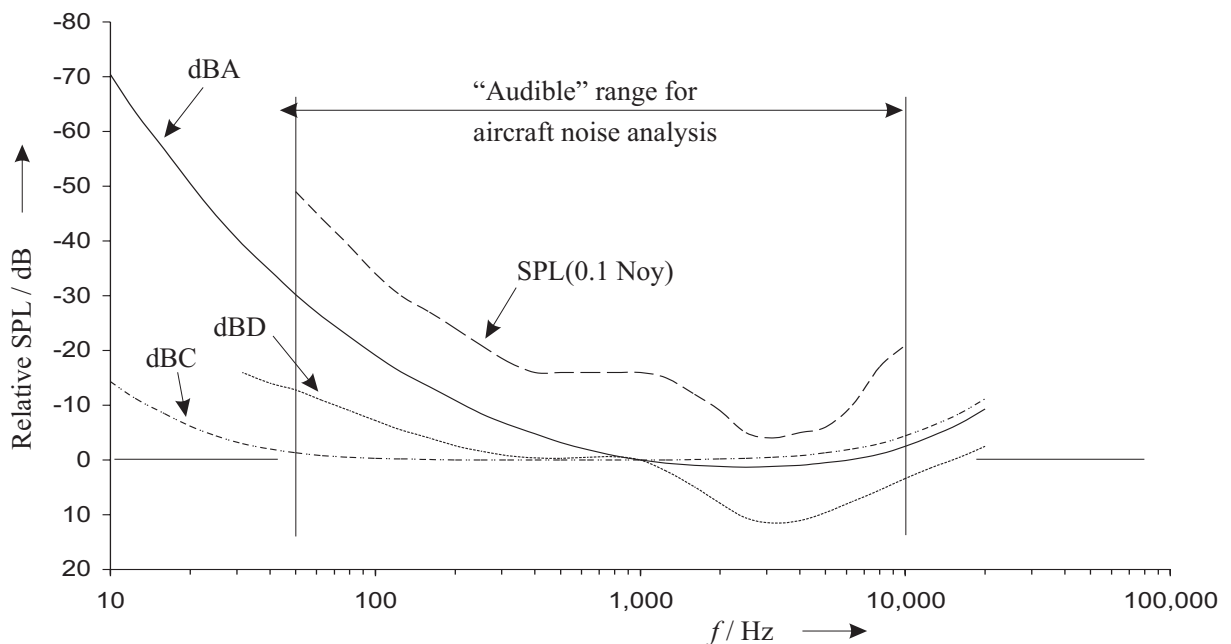
Figure 3.1 Plot of A-, C-, D-weighting relative response curves and relative sound pressure level of constant perceived noisiness 0.1 (audible annoyance curve) within relevant one third-octave band centre frequencies. Data provided in table B.1.

---

[8] unit used for the calculation of PNdB

The first step in calculation of EPNL may be surveyed. The conversion of each one-third octave band sound pressure value SPL(i,k) to perceived noisiness n(i,k) can be achieved by either a reference table (noys as a function of SPL) or by using the provided mathematical formulation. The mathematical formulation contains different slopes, intercepts and coordinates of discontinuities depending on the frequency band i. To visualize a correlation of the so far explained weighting circuits without going into too much detail with the complex mathematical formulation, the SPL of 0.1 noys has been plotted in figure 3.1. This perceived noisiness value may represent the beginning or the threshold of annoyance. Figure 3.1 indicates that the "annoyance" defined by the mentioned authorities' starts at a somewhat higher SPL than the predefined SPL of the audible range. Secondly, the characteristics of the derived curvature are very similar to that of the D-weighted. As a consequence PNL may have used the former D-weighted network as a basis.

The understanding of the interconnection of the perceived noisiness n(i,k) as well as the resultant PNL(k) and the frequency is advantageous. The total perceived noisiness is derived out of the following formulation (**ICAO Annex 16 1989**; **FAR Part 36**):

$$N(k) = 0.85n(k) + 0.15\sum_{i=1}^{24} n(i,k) \tag{3.12}$$

Where n(k) is the greatest value of the 24 values of n(i,k). Putting this equation into words, all perceived noisiness except the largest one are accumulated and then multiplied by a factor of 0.15. Thus, the magnitude of each of those noys is decreased by 85 % whereas the largest perceived noise value remains unchanged. The PNL(k) is then computed by

$$\text{PNL}(k) = 40.0 + 10\log_2 N(k) \tag{3.13}$$

With this logarithmic relationship to the base two a total perceived noisiness of $N(k) = 10$ Noys corresponds to a PNL = 74 PNdB. In contrast, for $N(k) = 1000$, the PNL reaches a value of about 140 PNdB. The frequency reference for the perceived noisiness is the same as for the above described weighting networks namely 1 kHz. For a better understanding of the noy-weighting, a constant SPL(i,k) has been moved through the one-third octave frequency bands and converted to perceived noisiness n(k) and total perceived noisiness N(k) as a second step. Typical SPL(i,k) have been chosen with respect to the upper and lower SPL

margin of a normal aircraft noise contour plot. Figure 3.2 depicts the correlation of the perceived noisiness over the frequency range. The 60 dB signal remains almost without a noise penalty. In contrast, the 90 dB signal gets keenly punished within the range from 1 kHz to 10 kHz where the human ear is more sensitive. The slope between 100 Hz and 1 kHz is also remarkably different. However, the maxima of both curvatures are approximately at the same frequency. For the 90 dB signal the maximum is at about 67.2 Noys in contrast to 8.5 Noys for the 60 dB signal. By applying equation 3.12, the total perceived noisiness $N(k)_{60\,dB}$ becomes 23.4 Noys and $N(k)_{90\,dB} = 191.5$ Noys as shown in table B.2. The maximum value counts for both around 35 % of the total perceived noisiness. As a consequence the loudest signal for the calculation of a PNL is punished by approximately 35 %. With equation 3.13, $PNL(k)_{60\,dB}$ amounts 85.5 PNdB and $PNL(k)_{90\,dB}$ finally rises up to 115.8 PNdB. In conclusion, the Perceived Noisiness Level scale makes it possible to raise the defined level of perceived noise with respect to perceived annoyance in the most sensible frequency range. The human hearing system is more perceptible to discrete tones and tends to disregard broadband sound in the subsequent frequency range. The annoyance of these discrete tones may often even be higher than the plain PNL scale would indicate (**Smith 1989**, p. 10).
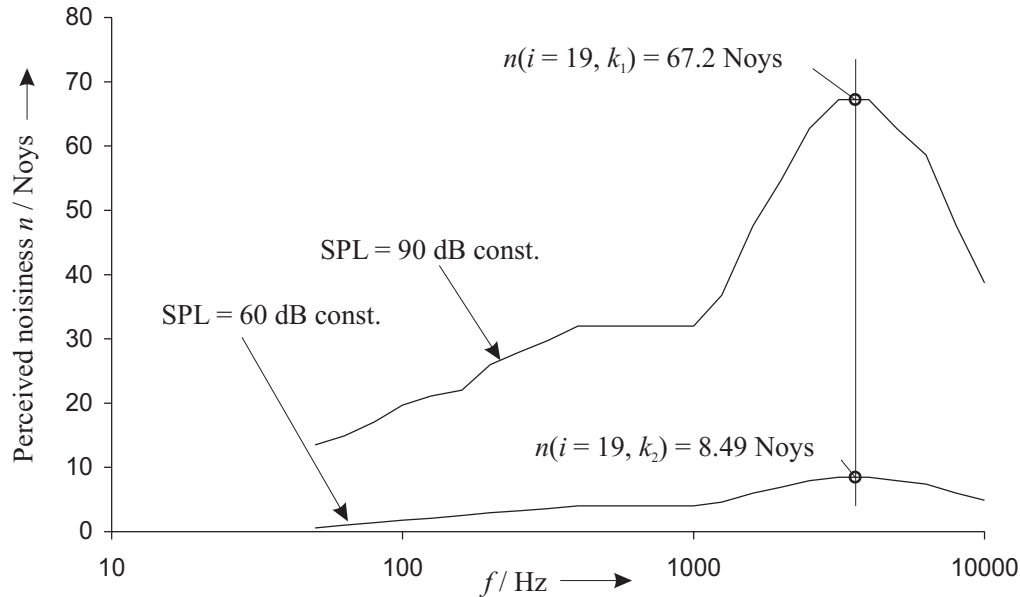
Figure 3.2　Perceived noisiness n as a function of frequency f with constant Sound Pressure Levels. Data as in table B.2.

The second step in EPNL calculation requires the calculation of the tone correction factor $C(k)$. The scale used to allow for tone-sensing characteristics, defined by spectral irregularities such as maximum discrete frequency components or tones (**ICAO Annex 16**

1989), is the Tone Corrected Perceived Noise Level, PNLT(k) in units of TPNdB. Discrete tones are a measure for the penalty $C(k)$ depending on both frequency and degree of intrusion (**Smith 1989**, p.10). The latter is examined by somehow taking the PNL(k) difference ΔPNL(k) between two frequency bands into account. A description of the comprehensive calculation can be found in the relevant wordings of law. The equation for step three for EPNL calculation is as follows:

$$\mathrm{PNLT}(k) = \mathrm{PNL}(k) + C(k) \tag{3.14}$$

As a final step, a "duration" correction D of the increasing and decreasing nature of aircraft noise during an aircraft flyover is added. The duration varies with both aircraft type and mode of operation (**Smith 1989**, p. 12). D is calculated by integration. The summation of incoherent sounds i.e. sounds of random phases, is done by a linear energy basis and their representation on a logarithmic basis (**Bies 2003**, p.47). Usually, mean-square sound pressure rather than root-mean-square sound pressure are summarized since it gives the same result after converting back to the logarithmic basis. This explains the division by 10 in the exponent in equation 3.15 for calculating D (**ICAO Annex 16 1989**):

$$\mathrm{D} = 10 \cdot \lg\left[\left(\frac{1}{T}\right)\int_{t(1)}^{t(2)} \text{antilog} \frac{\mathrm{PNLT}}{10}\right] dt - \mathrm{PNLTM} \tag{3.15}$$

$$\mathrm{D} = 10 \cdot \lg\left[\left(\frac{1}{T}\right)\sum_{k=0}^{d/\Delta t} \Delta t \, \text{antilog} \frac{\mathrm{PNLT}(k)}{10}\right] - \mathrm{PNLTM} \tag{3.16}$$

where T is a normalizing time constant and PNLTM is the maximum value of PNLT. PNLT is derived from SPL data. Therefore, equation 3.15 is rewritten with a summation sign instead of an integral where Δt is the time increment for which PNLT(k) is calculated and d is the time interval. d is found by identifying PNLTM and decreasing the level by 10 TPNdB. Figure 3.3 depicts two different aircraft flyovers for comparison. $\overline{pnlt}$ is the mean value of PNLTs(k) during flyover time d.

In the relevant wordings of law the final step in calculating EPNL is defined as in equation 3.17. Equation 3.16 in equation 3.17 reduces EPNL to the mean value of PNLT(k):

$$\overline{pnlt} = \text{PNLTM} + D \tag{3.17}$$

$$\overline{pnlt} = \text{PNLTM} + 10 \cdot \lg\left[\left(\frac{1}{T}\right)\sum_{k=0}^{d/\Delta t} \Delta t \, \text{antilog} \frac{\text{PNLT}(k)}{10}\right] - \text{PNLTM}$$

$$\overline{pnlt} = 10 \cdot \lg\left[\left(\frac{1}{T}\right)\sum_{k=0}^{d/\Delta t} \Delta t \, \text{antilog} \frac{\text{PNLT}(k)}{10}\right] \tag{3.18}$$

$$\text{EPNL} = 10 \cdot \lg\left[\left(\frac{1}{10 \text{ s}}\right)\sum_{k=0}^{d/\Delta t} \Delta t \, \text{antilog} \frac{\text{PNLT}(k)}{10}\right] \tag{3.18a}$$

Equation 3.18 contains a disadvantage. The information whether the occurrence was short and loud or even longer and e.g. louder to a lesser extent is lost. Figure 3.3 shows two flyover histories with the same maxima but different flyover times d_1 and d_2. Both occurrences would give approximately the same EPNL. Therefore, the aeronautical authorities set the time reference T to a focused value of $T = 10$ s as in equation 3.18a (compare **Bertsch 2007**, p. 22). In conclusion, EPNL is the integrated energy between PNLTM and the 10 dB threshold and normalised by a time constant of 10 s.

Figure 3.3   Perceived noise level corrected for tones as a function of aeroplane flyover time. Left curve and variable definitions from **ICAO Annex 16 1989**; right curve imaginary.

Sound pressure level samples must be measured for aircraft certification in time intervals of 500 ms ±5 milliseconds (**FAR Part 36**, **ICAO Annex 16 1989**). With this in mind and a normalized time reference equation 3.18 can be reduced to:

$$\text{EPNL} = 10 \cdot \lg \left[\sum_{k=0}^{2d} \Delta t \, \text{antilog} \, \frac{\text{PNLT}(k)}{10} \right] - 13 \text{ EPNdB} \qquad (3.19)$$

with   T = 10 s

Δt = 0.5 s   per definition.

Equation 3.19 is often found in literature without stating the predefined values of T and Δt (compare **Bertsch 2007**, p. 22). The time interval may be mandatory and constant for aircraft noise measuring, but for noise prediction, Δt diversifies and is far from a constant value. This is due to the flight points that result from a discretised flight trajectory. The moving frame of reference, the aircraft, radiates sound with the speed of sound. The observer on the ground, in the resting frame of reference, receives radiated sound more or less delayed (e.g. Doppler Effect). Additionally, flight points are changing position in space and distance to each other.

The left PNLT curve in figure 3.3 reflects a typical PNLT(k) over flyover time distribution. The two maximum points where the curve changes from increasing to decreasing are due to the engine directivity characteristics. Fan noise radiates forwards e.g. in an angle of 45° and jet noise rearwards with e.g. the same angle. Both are major contributors to overall aircraft noise. The observer on the ground is hit by fan noise first, experiences then a softer zone between the two radiances and finally gets hit by the jet noise beam. Noise source directivities will be discussed below.

3.1.4   Acoustic Source Models and Analogy

Essentially, sources of sound generation are generally complex models. As a consequence, simplified acoustic source models have been defined for the description of the noise-generation mechanism and noise analysis respectively. A monopole is a single spherical sound source, radiating sound waves that are only dependent on the radial distance R from the source. The wave equation is derived with the help of spherical coordinates (**Norton 1989**, p. 125). The time averaged mean-square acoustic pressure is defined as (**Bies 2003**, p. 177):

$$\left\langle p_{rms}^2 \right\rangle = \left(\frac{Qk\rho c}{4\pi R} \right)^2 \qquad (3.20)$$

where $k = \omega / c$ wavenumber (angular frequency divided by the speed of sound)

Q = volume flux as a function of the particle velocity of fluid produced a the surface of the pulsating spherical source

ρ = density

c = speed of sound

A point dipole is a special dipole and consists of two monopoles of equal strength in an indefinitely small distance to each other and oscillating 180° out of phase with each other. Indefinitely small is per definition very much less than the radiated wavelength. The model is much more complex when dealing with ordinary dipoles i.e. two sources in a distance larger than specified to each other (**Norton 1989**, pp. 130-4; **Bies 2003**, pp. 179-82). The time averaged mean-square acoustic pressure of a point dipole can be determined by:

$$\left\langle p_{rms}{}^2 \right\rangle = \left(\frac{hQk^2\rho c \cos\theta}{2\pi R} \right)^2 \tag{3.21}$$

where Q = volume flux of each point source

θ = directivity or polar angle reference to longitudinal axis

$2h$ = distance of dipole sources to each other

A further extension of the discussed models comprises two dipoles in an indefinitely small distance to each other and oscillating 180° out of phase with each other – the quadrupole. The consequence is no net flux of fluid and no net unbalanced force. The quadrupole does, however, apply a net shear force on the fluid, which could be reduced to a local stress on the fluid in the extreme. The importance lies on the fluids local stress time rate of change. Quadrupoles are relatively poor in radiating sound because fluids support shear forces poorly. However quadrupoles are used to describe jet noise that is produced by a mixing region of the jet and the quiescent atmosphere (**Bies 2003**, pp. 185-8). A longitudinal quadrupole has in contrast to the lateral quadrupole both dipole axes aligned. The radiated sound power of the lateral quadrupole P_W can be obtained from equation 3.22 and the time averaged mean-square acoustic pressure $p_{rms}{}^2$ from equation 3.23:

$$P_W = \rho c \frac{\left(2k^3 hLQ\right)^2}{15\pi} \tag{3.22}$$

$$\left\langle p_{\text{rms}}{}^2 \right\rangle = \left(\frac{\rho\, c\, hlQ\, k^3 \sin 2\theta \sin \psi}{2\pi R} \right)^2 \tag{3.23}$$

where l = rectangular source dimension

ψ = directivity or polar angle reference to lateral axis

Sound can be classified, depending on the generation of sound waves, into structure-borne sound (vibration of solid bodies) or into aerodynamic sound that results from pressure-fluctuations induced by turbulence and unsteady flows. For the latter the region between source and receiver contains sources of sound energy. These sources are permanently influenced and changed by the flow and are therefore to be included in the analysis of the homogeneous wave equation. The wave equation is then considered as inhomogeneous (**Norton 1989**, pp. 106-7) which makes the identification of the sound sources more difficult. Fan noise, jet noise, noise from aerofoils etc. is to be solved adequately with the inhomogeneous acoustic wave equation. Research relating to this topic was driven by the jet aircraft industry and Lighthill provided the first general theory of aerodynamic sound in the early 1950s. He located all non-linear terms in the fluid dynamic equations of motions on the right hand side of the inhomogeneous wave equation. With this in mind, the sources of sound are then the difference between the exact laws of fluid motion and the linearised acoustical approximations. Therefore, the non-linearitis are virtually generating the sound (**Norton 1989**, p. 155). Dowling, Ffowcs, Williams and Goldstein provide necessary fundamental equations to derive effects of the presence of solid bodies in the flow out of Lighthill's inhomogeneous wave equation. As a consequence, the three terms in the resulting equations represent a free turbulence component, a component due to fluctuating body forces and fluctuating motions of the solid body resulting from the unsteady flow. Each term is then evaluated independently by scaling with parameters associated to the turbulence components. This is possible with the restriction to low Mach numbers i.e. wave length λ of the exhaust flow of a jet nozzle much greater than the nozzle diameter. The derived equations suggest that the radiated sound power scales with the flow velocity is comparable to the flow velocity specified for monopoles, dipoles and quadrupoles referred to as Lighthill's acoustic analogy (**Norton 1989**, pp. 158-60). This coherence can be shown by relating the mean flow velocity to the radiated sound power as in **Bies 2003** (pp. 187-8) by using equation 3.22. The following assumptions (equations 3.24) are made: (a) source flux Q is proportional to the local mean stream speed u times the stream cross-sectional area S, (b) S is proportional to the square of either

characteristic source dimension l or h where l equals h and (c) k is proportional to u divided by h times c. Introducing the Mach number $M = u/c$ and substituting these expressions and in equation 3.22 yields:

$$k \propto u/(hc) \quad , \quad Q \propto uh^2 \quad , \quad h \approx l \tag{3.24}$$

$$P_W = \rho c \frac{\left(2k^3 hLQ\right)^2}{15\pi}$$

$$P_W = \frac{\rho c}{15\pi} \left(2 \frac{u^3}{h^3 c^3} h\, h u h^2\right)^2$$

$$P_W = \frac{\rho c}{15\pi} \left(\frac{2u^4 h}{c^3}\right)^2 = \frac{4}{15\pi} \cdot \frac{\rho u^8 h^2}{c^5}$$

$$P_{W,Quadrupole(lat)} \propto \frac{\rho u^8 S}{c^5} \propto \rho u^3 M^5 S \tag{3.25}$$

The solution of the first term of the inhomogeneous wave equations suggests that the radiated sound power scales with the eight power of the flow velocity similar to the u^8 relationship derived in equation 3.25. This is Lighthill's prediction for jet noise. The assumptions in equation 3.24 can be applied on monopoles and dipoles respectively. Further scaling and solving of the inhomogeneous wave equation results in a u^6 and u^4 relationship similar to that of dipoles and monopoles (compare **Norton 1989**, p. 159-60). Therefore:

$$P_{W,Dipole} \propto \rho u^3 M^3 S \tag{3.26}$$

$$P_{W,Monopole} \propto \rho u^3 M S \tag{3.27}$$

where - a quadrupole represents fluctuating motions of the solid body resulting from the unsteady flow,

- a dipole represents the component due to fluctuating body forces and
- a monopole represents a free turbulence component.

The derived interpretations further show that for a given Mach number the quadrupole is least efficient in converting stream power to noise followed by the dipole as a consequence from the Mach numbers power in the formulas. In contrast, the efficiency of quadrupole noise

generation increases much more rapidly so that the initial almost negligible source of noise might become a very important one.

3.1.5 Convective Amplification

Due to a relative speed between emitting source and observer, provoked by a motion of either part, the frequency observed is different in comparison to the permanently constant emitting source frequency. This effect is referred to as Doppler Effect and becomes considerably important in noise analysis since the source of noise i.e. the aircraft is moving. φ_x is the angle between the vector R (from source to observer) and the flight velocity vector v. With $\varphi_y = 0$ (figure 3.5), the decisive relative velocity component becomes $v_{rel} = v \cdot \cos(\varphi_x)$. This observed velocity is always lower than the prevailing flight speed due to the aircraft's altitude except for two cases: if observer and source are at the same altitude the observed velocity is the flight speed; in contrast, with the aircraft exactly above the observer, the relative velocity is null. The relationship of the observed frequency is therefore as follows:

$$\frac{f_{Observer}}{f_{Source}} = \frac{1}{1 - M \cos \varphi_x} \tag{3.28}$$

With the source moving towards the observer the ratio becomes greater than one and vice versa after the source or aircraft passing by (φ_x greater 90°; $\cos(\varphi_x)$ becomes negative). As described above, the frequency is decisive for the weighting of perceived sound pressure levels. Figure 3.4 shows that a frequency jump of a one-third octave band starts at a Mach number of $M = 0.25$ and at a Mach number of $M = 0.5$ for an octave band[9] respectively. These margins are moved to higher values with an increase in radiation angle φ_x as shown as in example of $\varphi_x = 45°$ in figure 3.4. The margins are then approximately $M = 0.35$ for the one third octave band and $M = 0.7$ for the octave. With the source at an indefinite distance from the observer, φ_x becomes zero or 180° that is the maximum slope since source and observer are levelled at the same height. With these boundaries in mind a potential range can be defined. The slope of the curve is decreasing with the source coming closer to the observer.

---

[9] With $f_{Observer}/f_{Source} = 2$ the observer frequency is twice the source frequency i.e. one octave.

Due to the characteristics of the power function defined in equation 3.28 the influence of the Doppler Effect after the source passing by the observer is low. Therefore, frequency shifting is more likely to occur and more dominant with the source coming towards the observer.
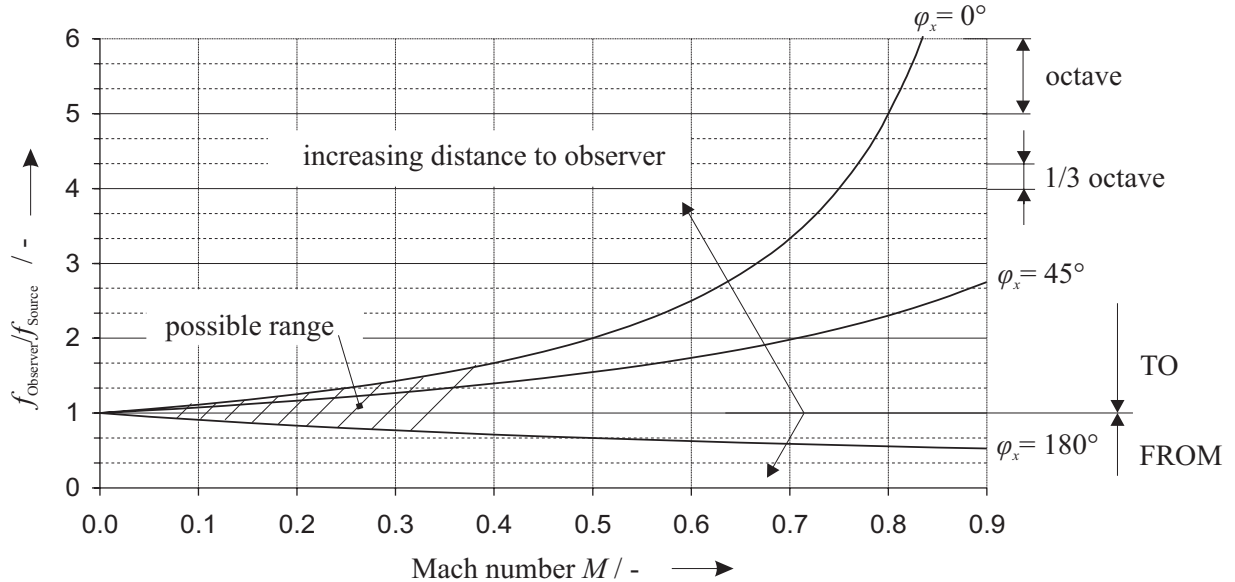
Figure 3.4 Doppler shifts against Mach number (towards or from the observer). Valid only for Mach numbers below 1.0.

This frequency shift has an additional influence on the time averaged mean-square acoustic sound pressures of the discussed monopoles, dipoles and quadrupoles. The wavenumber $k = \omega / c = 2\pi f / c$ is directly proportional to the frequency divided by the speed of sound. As a consequence, with an increasing frequency, k in equations 3.20, 3.21 and 3.23 is increasing, thus the sound pressure of the derived multipoles is increasing too. This effect is referred to as convective amplification of acoustic sources. The same dependency is valid for a decreasing k i.e. the source moving from the observer. **Maughan 1987** secured a loudspeaker onto a bicycle wheel, which was turned by an electric motor. A ground fixed microphone recorded the change in frequency as well as the oscillating amplified microphone output when the source on the wheel was moving at 1.25 m/s. The difference in sound pressure level for a monopole followed by dipoles and quadrupoles can be derived by substituting equation 3.20 with equation 3.28 (compare **Bertsch 2007**):

$$\Delta SPL_{conv} = SPL_{Observer} - SPL_{Source}$$

$$= 10 \lg \left(\frac{p_O}{p_{ref}} \right)^2 - 10 \lg \left(\frac{p_S}{p_{ref}} \right)^2$$

$$= 20\lg\left(\frac{p_O \,/\, p_{ref}}{p_S \,/\, p_{ref}}\right) = 20\lg\left(\frac{\langle p_O \rangle}{\langle p_S \rangle}\right)$$

$$= 20\lg\left(\frac{k_O}{k_S}\right) = 20\lg\left(\frac{f_{Observer}}{f_{Source}}\right)$$

$$= 20\lg\left(\frac{1}{1 - M\cos\theta}\right) = -20\lg(1 - M\cos\theta)$$

$$\Delta SPL_{conv} = -n \cdot 20\lg(1 - M\cos\theta) \tag{3.29}$$

where $n = 1$ for monopoles (from k^2 in equation 3.20)

$n = 2$ for dipoles (from k^4 in equation 3.21)

$n = 3$ for quadrupoles (from k^6 in equation 3.23)

The difference of observed and source sound pressure is therefore changing logarithmically with flight Mach number (influenced by φ_x). The factor n shows that quadrupoles are affected the most by a Doppler shifting followed by dipoles and monopoles. However, after **Dowling 2006** (abstract) the motion of a monopole must not be treated as a convected monopole due to additional coupled multipoles. With an additional amplification in the direction perpendicular to the flight path the obtained amplification is not the monopole convective amplification $(1 - M)^{-2}$. The minimum effect is found to be $(1 - M)^{-3}$ depending on the virtual mass tensor of the body. Considering dipoles the effect of convection is surprising and complicated and it cannot be described completely by Doppler factors. As a conclusion, the influence of moving source might be greater than calculated with the derived equations above.

3.1.6   Sound Propagation Effects

Sound propagation can be described as the transmission of acoustic energy through a medium (in most cases air) via sound waves (**Truax 1999**). SPL received at an observation point is affected by the Sound Power Level (PWL) and various attenuation factors. By separating the dominant factors a generalized expression for a single component source can be written as in **Bies 2003** (pp. 219-44):

$$\text{SPL}_{Observer} = \text{PWL} + DI_M - K - A_E$$

$$\text{SPL}_{Observer} = \text{PWL} + DI_M - K - A_a - A_{bhp} - A_f - A_g - A_m \tag{3.30}$$

with the following term definitions:

DI_M directivity index due to the fact the sound sources are radiating sound differently in amplitude in any direction. Those sources are referred to as directional source. Omni directional directivities can be changed by e.g. placing a monopole near a reflecting surface. Dipole and quadrupoles on the other hand are directional sound sources and exhibit already a characteristic directivity. DI_M is the logarithmic value of sound intensity in direction of the polar angles θ and ψ, divided by the sound intensity of a sphere (**Bies 2003**, p. 205).

K geometrical spreading i.e. spreading of the sound energy due to expansion of the wave fronts. K is independent of frequency and can be associated either with spherical or cylindrical spreading. E.g. the SPL of a monopole is reduced by 6 dB for each doubling distance from the source (**Truax 1999**). Equation 3.31 (**CONCAWE 1981**) for a monopole can be used to verify (similarities to be found in equation 3.20 and 3.7):

$$K = 10\lg\!\left(4\pi\, d^2\right) \tag{3.31}$$

$$\Delta K = \frac{K}{K_{ref}} = 10\lg\!\left(\frac{4\pi}{4\pi}\frac{d^2}{d_{ref}^{\,2}}\right)$$
$$= 10\lg 2 = 6.021\,\text{dB} \tag{3.32}$$

A_E the excess attenuation factor can be further subdivided into:

A_a attenuation due to air absorption dependent upon temperature and relative humidity. Well known and often cited as the Method for the Calculation of the Absorption of Sound by the Atmosphere (**ANSI 1995**) which provides the means for calculating atmospheric attenuation of sound from any source for a wide range of meteorological conditions.

A_{bhp} attenuation due to regular barriers, houses and process equipment

A_f attenuation due to forests

A_g attenuation due to ground reflection. Complex models exist. In most cases A_g is more likely a gain. As a basic correction, the increase in noise level for an acoustically hard surface (e.g. water, concrete) is simply 3 dB for all frequency bands and distances with a

hemispherical radiation from the source. Soft ground has no effect thus no difference in noise levels (**CONCAWE 1981**). However, with the observer near the reflecting surface (**Bies 2003**, pp. 206-7) i.e. distance under one-tenth of a wavelength, pressure doubling occurs that equals a 6 dB increase in sound pressure level according to equation 3.7. For greater distances and broadband noise, the path difference between direct and reflected waves is usually sufficiently large for a combination with random phase. This would be an increase in 3 dB of SPL. In the case of tonal noise, sound pressures can be calculated by taking reflecting laws and phase shifting into account.

A_m attenuation due to meteorological effects such as wind and atmospheric temperature gradients (could be both, a gain or a loss), which has an important effect in the received SPLs (**CONCAWE 1981**). Refractions can lead to e.g. a significant decrease in SPL with the wind blowing from the observer to the source. Aircraft noise measuring for certification is therefore restricted to special atmospheric conditions. As an example the ambient air temperature must be within 35 °C and -10 °C. The averaged wind velocity on the ground must not exceed 12 knots with a maximum crosswind velocity of about 7 knots (**FAR Part 36**). As a consequence of great impacts on received SPLs, alternative noise abatement procedures have been investigated taking the airport's predominant wind direction into account (**LAnAb 2007**, project 1636).

ISO 9613-2 1999 defines a procedure for calculating the attenuation of sound during propagation outdoors within accuracy class two. Geometrical spreading, air absorption, ground effect, reflexion on surfaces and the shielding of obstacles can be taken into account. **ISO 9613-1 1993** specifies an analytical method of calculating the attenuation of atmospheric absorption for a variety of meteorological conditions. Computer programs used for the prediction of aircraft noise are usually based on ISA conditions with no influences of wind. Temperature gradients may also be neglected if appropriate. Additionally, the ground surface is assumed to be planar with no obstacles in between. Ground reflection may be important due to the difference in SPL of the simulated observer i.e. the received noise, either on the ground or above. These assumptions in equation 3.30 yields:

$$\text{SPL}_{O,prediction} = \text{PWL} + DI_M - K - A_a - A_g \qquad (3.33)$$

3.2   PANAM

The Parametric Aircraft Noise Analysis Module (PANAM) has been developed by the German Aerospace Center DLR and is still undergoing further research and development. The software was developed with regard to multidisciplinary optimization requirements and the prospective to include noise analysis already in a preliminary design process. One of those requirements is low CPU demand. For this reason, high fidelity methods such as computational aeroacoustics or computational fluid dynamics are no more appropriate. As a consequence, empirical analysis becomes more attractive but with uncertainties in prediction accuracy by leaving the range of measured conditions. A remedy can be found by using semi-empirical models that (1) are most importantly based on physical effects, (2) have the advantage of fast and easy computation and (3) allow for a parametric variation (**Bertsch 2008**, introduction). Still, a disadvantage always arises by applying the module to foreign or different conditions that are not covered by the original measurement range. The results may be good but should always be accepted with reserve.

The current version of PANAM allows for noise evaluation of conventional aircraft configurations along arbitrary three dimensional flight trajectories. A componental approach has been chosen to provide a possibility to further include newly derived noise source models[10]. With this modular setup, overall noise, i.e. sound pressure levels and sound radiation, is calculated out of single, parametric, semi-empirical noise source models. PANAM requires about 50 input parameters for airframe noise and about 30 for engine noise. The following input data in the form of ASCII input files are requested for noise analysis:

- aircraft geometric parameters such as wing and landing gear dimensions
- a discretised flight trajectory composed of quasi-stationary aircraft positions that specifies both the aircraft configuration (e.g. gear and flaps extended) and the operating condition (e.g. climb with specified climb speed and thrust setting)
- engine characteristics in the form of an engine map
- observer (microphone) locations (can be placed in any order: plane arrays, structured or unstructured that can be used to visualize noise footprints. If observers are located above

---

[10] Of growing importance are for example noise source models for unconventional high lift concepts such as upper surface blowing and externally blown flaps.

ground, ground resistivity to air σ used as a parameter for the sound reflecting quality of the surface upon microphone height is decisive[11]).

3.2.1 Noise Prediction in PANAM

Noise emission is calculated for each quasi-stationary aircraft position. Two major loops are implemented into the code: the outer loop is defined as loop over all observers, whereupon for each observer all significant flight positions (depending on PANAMs fast mode) have to be considered (inner loop). A schema of the program's philosophy is depicted in figure 3.5.

Rotating coordinate system: ⟶ Noise emission to noise impact:

Figure 3.5 Coordinate system rotation, reference sphere, noise emission and impact on ground

Before entering the observer loop, the attitude of the body-fixed coordinate system relative to the earth-fixed coordinate system has to be known for each quasi-stationary aircraft position. This is because sound source model directivities are related to the body axis system. Each flight position along the flight trajectory is defined through earth-fixed x_0-, y_0-, and z_0-coordinates. The reference of the observer array is also the earth-fixed axis system with the z_0-

---

[11] **Bies 2003** (p. 209) suggests $\sigma = 1.5 \cdot 10^5$ - $3 \cdot 10^5$ Pa s·m^{-2} for grass or rough pasture on the airport, $\sigma = 3 \cdot 10^7$ Pa s·m^{-2} for asphalt and $\sigma = 2 \cdot 10^4$ - $8 \cdot 10^4$ Pa s·m^{-2} for forests with pines or hemlocks. As a matter of fact, more sound energy is absorbed on porous surfaces.

axis pointing upwards. For a given time t the aircraft is at a flight position $P_F(x_0'(t), y_0'(t), z_0'(t))$ where the apostrophe designates a displaced observer earth-fixed coordinate system. With this information it is possible to locate the flight position relative to the observer's earth-fixed origin. As a result, the observer P_O at position $P_O(x_0, y_0, z_0)$ is connected to the flight position P_F through the vector R (figure 3.5). Computation of the tangent line to the flight trajectory at the observer P_O is done through an interpolation of P_O and the flight trajectory points before and after it, by a polynomial. The derived tangent is the flight velocity vector v and the x_a-axis of the air-path axis system (x_a, y_a, z_a). According to **DIN 9300 1990**, a further rotation by the angle of attack α and the angle of sideslip β determines the body axis system (x_f, y_f, z_f)[12]. Figure 3.5 illustrates a coordinate transformation by rotating about the y-axis with all other angles at zero. With the aircraft at flight position P_F, sound emission on a reference sphere, relative to the respective body axis system, is computed. The reference sphere surface is loaded with various sound pressure levels for the whole frequency spectrum depending on source model directivities. Sound pressure levels change with aircraft configuration and aircraft operation condition. As a result, for each flight point along the flight trajectory, different sound emissions on the reference sphere are obtained since e.g. thrust setting, flap/slat setting may change. To obtain related SPLs for the whole one-third octave band frequency spectrum to an observer, the position on the reference sphere has to be known. The radiation vector R between P_F and the observer on the ground can be described either by ordinary coordinates or by two angles (right illustration in figure 3.5). The two angles, φ_x and φ_y, represent radiation angles[13]. As a next step, noise source models are fed with relevant data to predict sound emission on the reference sphere. With the predefined radiation angles relative to the body axis system it is possible to find the sound emission (SPL_S) on the reference sphere associated with the observer's position at a give time t. This is the noise that radiates from the source directly towards the respective observer. Sound emission contains for each one-third octave band related sound pressure levels. Therefore, a number of SPLs, dependent on the frequency f, are essential for each position on the spherical surface. The magnitude of the radiation vector $|R|$ is the distance from the source to the observer. Noise emission on the reference sphere is transferred to noise impact on the ground,

---

[12] The body axis system can also be derived out of the earth-fixed system with rotations by air-path angles and further rotations by α and β or even directly by Euler angles.

[13] φ_x is defined and implemented in PANAM as the angle between the vector R and the x_f-axis respectively. With φ_{y2} as the angle between R and the z_f-axis, the orientation of R would be exactly defined. However, the second angle φ_y, as per definition used in the noise prediction program, is defined as shown in figure 3.5 (left illustration). This results from the definition as used for flyover noise measurements in **Pott-Pollenske 2006**. Other possibilities of angle definitions do exist.

$SPL_O(x_0, y_0, z_0, t, f)$, upon sound propagation effects have to be considered. The current version takes the following effects into account:

- geometrical spreading K as in the preceding chapter
- attenuation due to ground reflection A_g as described in **Le Duc 2008**
- attenuation due to air absorption A_a according to the Method for the Calculation of the Absorption of Sound by the Atmosphere (**ANSI 1995**)
- directivity of each source model (D_{IM}) as implemented in PANAMs code.

As in equation 3.33, all relevant effects that should be considered for computerized sound propagation are implemented in PANAM. Additionally, convective amplification is taken into account since derived deviations are distinctive. The method used in the noise prediction algorithm is deduced in the preceding chapter (equation 3.29). Since convective amplification is due to frequency Doppler shift it may also be considered under the general term of sound propagation effects. However, in available literature, sound propagation effects are defined as used in this thesis.
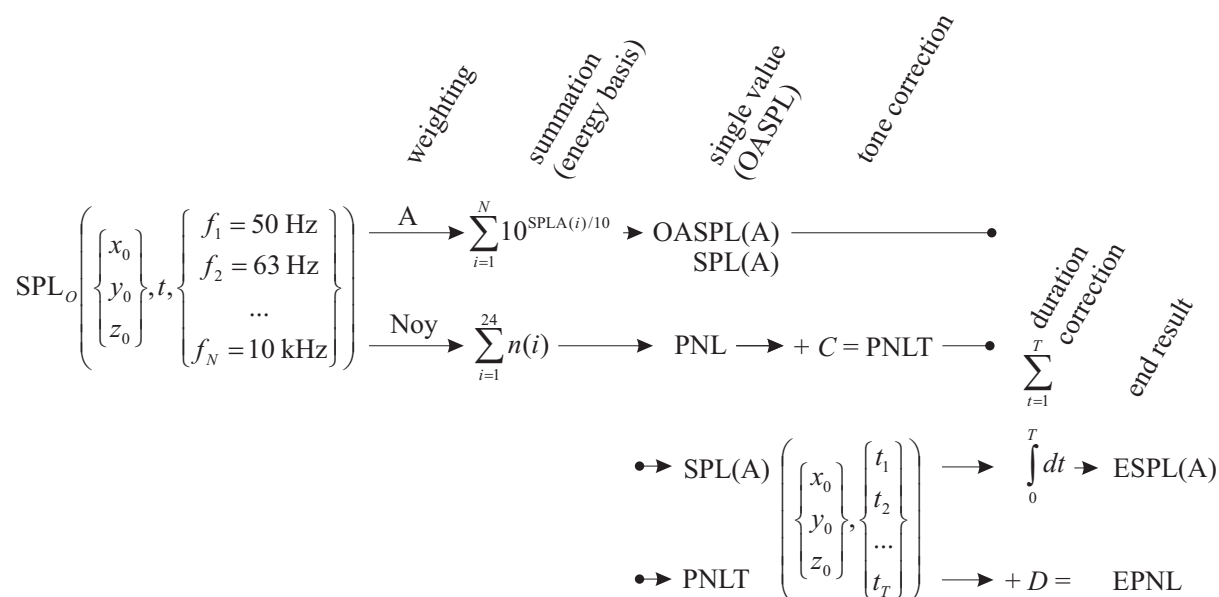
Figure 3.6   Weighting functions applied to spectra at observer (x_0, y_0 ,z_0) and at a given time t (compare figure 3.5). For the duration T (t_1 … t_T), ESPL(A) and EPNL can be computed out of a number of SPLs(A) and PNLTs.

With the so far derived sound emission of the observer it is now possible to apply different weighting functions upon the spectrum. This cannot be done beforehand because sound propagation effects influence the whole frequency spectrum. With a single value out of the

spectrum the frequency information gets lost, which would mean that e.g. Doppler shifting cannot be considered anymore. Figure 3.6 shows, with a given spectrum at an observer x_{0i}, y_{0i}, z_{0i} at a specific time t sound pressure levels are available for each considered one-third octave band centre frequency f_1 to f_N. Weighting applied upon this spectrum is either the A-weighting or the perceived noisiness weighting for EPNL calculation. The resulting spectrum is summarized on an energy basis that gives a single value usually referred to as OASPL. A-weighted spectra result in OASPL(A). In literature the "OA" of the OASPL(A) is often omitted that gives SPL(A). For EPNL calculation the tone correction C and the duration correction D is added to the PNL. Both computations are implemented in PANAM as defined by aeronautical authorities. To obtain a duration correction more than one SPL(A) or PNLT value has to be known. For an observer at x_{0i}, y_{0i}, z_{0i}, correlated sound levels at different times, t_1 to t_T, are used for obtaining a duration correction. Sound levels between a transmission time step[14], $\Delta t = t_{i+1} - t_i$, are assumed to be constant. For ESPL(A) calculation the duration correction is obtained by averaging over a time interval that is set to the whole flight time in the programs code. As a result, noise analyses as an output of PANAM are possible in scales and units of:

- SPL in dB
- SPL(A) in dBA/dB(A)
- ESPL(A) in dBA/dB(A)
- EPNL in EPNdB

PANAM comprises a fast mode computation. Maximum noise levels at a given observer are assumed to occur at that time, where the distance between observer and aircraft is at a minimum. Noise levels are computed forwards and backwards out of this position until obtained sound levels fall under a predefined threshold (**Bertsch 2008**, p. 4). Under normal circumstances, sound levels might not rise again after falling below the threshold. However, considering e.g. high flight speeds at a greater distance from the observer where convective amplification is dominant or noise sources with strong longitudinal- and weaker normal directives, sound levels may become more significant. Therefore, the threshold should be set to rather low noise levels.

---

[14] "The transmission time step starts when the observer receives the signal from one aircraft position. This time step lasts until the emitted sound from the consecutive aircraft position has reached the observer location." (**Bertsch 2008**, p. 4)

Overall aircraft noise is generally predicted by adding different noise source models. Each model is specified for one specific aeroacoustic source that further results from one specific aircraft element or aircraft feature. Noise originating from other sources that are so far not implemented in PANAM are therefore not considered in the analysis. Those new aircraft noise reduction technologies, which are currently under investigation, can however readily be implemented into PANAM due to its modular set up. Relevant and major noise source models for a general prediction of conventional aircraft noise are currently available and used. Within PANAM, airframe noise is predicted with sources models described in **Pott-Pollenske 2006**, jet noise with models by **Stone 1982** and fan noise is predicted according to the method of **Heidmann 1979**.

A validation of PANAM with aircraft flyover test results showed that noise levels for approach trajectories are predicted well. For take-off trajectories obtained noise levels are too high, but still satisfactory, especially when the aircraft is approaching the observer. This may either be (1) due to the lack of noise source models that reflect the effect of acoustic lining on fan noise or (2) already applied technologies on aircraft engines are not covered by used source models (**Bertsch 2008**, p. 4). All noise source models are concentrated in one point i.e. the quasi-stationary flight point along the discretised flight trajectory. This assumption is valid due to a significantly large distance between source and observer compared with the distance between the sources. As a result, interactions between noise sources are neglected, which is also due to the lack of appropriate prediction models. Summing up the facts that are to be considered when dealing with PANAM:

- Noise source models are concentrated in one point
- Interactions between noise components are neglected.
- Shielding effects such as engine noise shielding through airframe components are not yet surveyed.
- Noise prediction is a result of current, implemented noise source models.
- Acoustic lining on fan noise is not yet included.
- The general model used for computing convective amplification is put into question by Dowling 2006 (abstract).

- Parametric semi-empirical noise source models are based on flyover measurements of a conventional aircraft, powered by turbofan engines, of the size of the reference aircraft considered in this thesis.

3.3   PrADO

At the Institute of Aircraft Design and Lightweight Structures (IFL) a multidisciplinary integrated preliminary aircraft design and optimization tool has been under development for over 20 years. PrADO (Preliminary Aircraft Design and Optimization), consists of about more than 500 FORTRAN-77[15] programs that reflect various disciplines involved in aircraft design. The programs and routines are organized in 4 program levels and connected through a Data Management System (DMS) (**Heinze 2004**, chapter 2). A set of independent computer codes for a given, specific task within the design process are centralised and compendious in the design modules e.g. module 3: wing geometry conversion, module 22: total aircraft weight estimation. A list of all design modules with their actual status at the beginning of 2008 can be found in figure B.2.

The design modules only communicate with the DMS via the DMS program library to access configuration data. A data transfer between different design modules is not possible. This allows for quick activation or deactivation of an arbitrary design module. The addressed modules are selected with respect to the aircraft configuration that is to be investigated e.g. the geometry of a liquid hydrogen tank can be calculated by additionally activating module 10; module 8 can be skipped if winglets are not to be considered. Furthermore, this modular set up comprises the basis to further expand the tool easily. This is of great importance when for example new environmental considerations such as community noise and emission limits become driving parameters and call for additional analysis to be conducted. Relevant design data is written by the DMS in thematically sorted ASCII files, the databases. The database is initialized with data provided by the user including the transport mission, a basic parametric

---

[15] PrADO is originally designed in FORTRAN-77. However, since new compilers can handle variable names of arbitrary length, as is the standard in Fortran90, the restriction in FORTRAN-77 that variable names consist of maximum six characters, is no longer to be considered (as an example of one deviation to FORTRAN-77 definitions). New programs may also be written in Fortran90 or Fortran95 and adapted accordingly.

description of the configuration layout and all relevant constraints and design targets (compare **Werner-Westphal 2008**, p. 582). An overview of the provided databases is given in figure B.2.

3.3.1 Program Levels in PrADO

The four program levels and their associated elements are depicted in figure B.2. First level routines are responsible for initialising and arranging the databases out of preset user data. This data is collected in a specification file. Further programs process results in form of graphs, tables and three-D-view drawings for a basic interpretation. To make program operation easier a Graphical User Interface (GUI) has been adapted (**Heinze 2004**, chapter 2).

Within the second program level the selected mode of operation is addressed. The first out of three is design analysis. The sequence of executed design modules[16] is given by the arrangement of the design modules as in figure B.2, which is one arrangement out of many possible ones. The sequence is iteratively run until a convergence of all dependent design variables is achieved (**Werner-Westphal 2008**, p. 582). This process would be in accordance with the above explained feasibility study during aircraft design and provides one possible solution out of many. After passing module 27 the program may iteratively start over again (if it is the case that all following modules are specified as after iteration modules or do not exist). The reason for that are parameters set for verifying the convergence of the aircraft configuration. Usually selected dependent design variables that must show convergence are operating empty mass[17], fuel mass, maximum take-off mass[18], maximum take-off thrust and the number of engines. The two latter ones may not be treated as dependent design parameters unless explicitly specified by the user. For instance, in module 14 it may come out that provided maximum take-off mass is not sufficient and has to be increased. This would lead to a change in geometry, engine characteristics, aerodynamics etc. that are to be calculated once again in another loop sequence. As another example, the vertical tail plane is somehow geometrically defined out of preset data. Module 4 calculates its geometry that implicates a

---

[16] Other design sequences i.e. modular set ups of different aircraft design related disciplines can be found in literature (**Scholz 1999**, page 2.6).
[17] equivalent to Operating Weight Empty OEW
[18] equivalent to Maximum Take-Off Weight MTOW

specific vertical tail plane mass calculated in module 22. However, in module 27 it might be necessary to increase the volume of the vertical tail plane due to stability and control of the aircraft. This would change the vertical tail plane mass and as consequence the overall aircraft mass affecting all relevant disciplines such as aerodynamics and performance. As a rough assumption it might be said that after module 27, convergence of global aircraft masses has been achieved and the structural sizing of the aircraft configuration is accomplished. Regarding the operational mode of design analysis, modules 28 up to 30 have no direct influence on the design process and provide therefore, in this special case only, additional information for the user. However, with the two other modes of operation the modules are able to exert an influence.

The second mode of operation allows for variation of independent parameters within user specified limits. Each parameter in PrADO can be made independent by the user. A vast flexibility is a result of that. For each set of independent variables a design analysis i.e. the first mode of operation as explained above, is conducted. The obtained solutions out of the whole design space can be used for judging parametric influences and showing design trends referred to as parameter- and sensitivity studies.

In the second program level, the third and last mode of operation, optimization, requires a target function of independent design variables and design boundaries. Optimization algorithms are then used to find the parameter combination that minimises or maximises the target function. For each operation mode, complete design analysis are performed depending on design variable combinations. With this information out of every iteration step, the value of the target function can be evaluated (**Werner-Westphal 2008**, p. 582).

The third program level contains the intrinsic, interdisciplinary design process for the configuration to be analysed. As afore mentioned, the design modules feature relevant disciplines involved in aircraft design and share their data without exception via the DMS database. The design iteration aborts when the dependent design variables show convergence. Is this the case, program control is handed back to level two. With the selected operation mode of design analysis the program aborts with the output of the databases. In contrast, with the two other modes of operation a new aircraft configuration is described by specifying a new dataset of independent variables out of target function history and running a whole design analysis from the beginning (**Heinze 2004**, chapter 2).

The fourth program level concentrates the program libraries that contain the intrinsic physical calculation models used for determination of aerodynamic-, flight mechanic- and atmospheric characteristic data (**Heinze 2004**, chapter 2). Equally, further level four embedded subroutines contain e.g. a statistic processor, finite element methods, structural beam modelling, mathematical tools such as regression, thermodynamic laws, etc. that are more likely to be considered separately and referred to as problem oriented libraries. Those libraries that handle a whole design task are more comprehensive and are requested directly by the design modules. The database schema of the turbofan engine calculation model (ZTL11) is shown in figure B.2. The subroutine ZTL may be requested by module 6, 33 and 28 respectively for either computing an engine map or designing the engine. The subroutine ZTL therefore needs two modes of operation: design and off-design (refer to chapter 4.2.1). Those two in turn may need problem oriented libraries for calculating e.g. atmospheric data, temperatures, etc.

Fortran programs used for exchanging data between the design modules are arranged under the DMS program library from which only a few are depicted in figure B.2. The thematically sorted databases are located on the right hand side of the schema. The databases contain related variables in form of integer, real or character data types. A simple code assigns the appropriate type declaration and size of the variable e.g. vector with 10 elements, matrix etc. With such a unified code, DMS program libraries can be applied to every variable used in the program. As a result, a single variable name with a brief description and type declaration is correctly associated with only one defined variable value, additionally defined in unit and size.

PrADO's aircraft geometry model output is very detailed for the stage of preliminary design. The 3D-view of the aircraft depicts structural elements (e.g. skins, frames, spars, ribs), control surfaces, fuel tanks, cabin layout (e.g. seats, galleys, restrooms, separation walls), landing gear (extended or retracted), etc. besides geometry models for humans, cargo containers and ground vehicles for judging aircraft ground handling, ergonomic qualities etc.

PrADO also holds different implemented methods for several key disciplines (**Werner-Westphal 2008**, p. 582). The calculation method can be selected with regard to the desired analysis out of e.g. different handbook methods that are more or less detailed and therefore more or less CPU time demanding.

4   Method

"The propellers made a horrendous noise. The airplane rattled because it had piston engines. You couldn't even talk to your neighbour. It was not as romantic as I thought it would be. ... I thought flying should be elegant." (Hans von Ohain, Inventor of the jet engine)

The method used for the interconnection of PrADO and PANAM is described in this chapter. For noise prediction, aircraft geometry, engine characteristics and a flight trajectory are needed. All mentioned data computed are written as an output into separate files. The noise analysis program is then able to open each file on demand and read all necessary data for the computation of aircraft noise. Aircraft geometry is described through various parameters derived out of PrADO's databases. Calculation is needed for spoiler and flap geometry. Engine characteristics are computed depending on flight altitude, Mach number and thrust setting and written out in form of an engine map. Calculation is needed for the fan rotational speed N1 and other parameters such as fan total temperature rise through the fan. The flight trajectory is calculated by PrADOs flight mechanical subroutines. An additional subroutine was necessary to evaluate maximum climb angle. Data is formatted according to PANAMs input requirements. A supplement to PrADOs specification file was necessary (appendix F).

Input – Output PANAM (IOPANAM), is responsible for data processing. Figure 4.1 depicts a schema of the program flow and the implementation of the newly developed interface IOPANAM. Module 28, reserved for aircraft noise analysis, as well as 29 and 30 are defined as after iteration modules[19] since there is no direct related influence of direct operating costs or noise upon the structural sizing of the aircraft (figure B.2). Therefore, module 28 and, as a consequence, noise analysis is performed only once within the iteration loop of a design analysis. Within module 28 the user can decide to conduct noise analysis either with PANAM or with PrADOs former noise analysis version. The interface, IOPANAM, has two modes of operation: The first one is used in the case that PrADO is set to obtain noise analysis with the help of PANAM and the second one is for executing IOPANAM directly without PrADO. The latter, was programmed to allow for geometry-, engine map- or trajectory calculation independently. The interface uses all subroutines that are implemented in PrADO but does not necessarily go through an iterative process. The databases, however, must contain related data for computation. The output files can be used to obtain a thorough and detailed noise analysis

---

[19] modules that are requested after the iteration process. This is equivalent with the accomplishment of structural sizing of the aircraft configuration (see preceding chapter).

with the stand alone version of PANAM. In contrast to the second mode, the first mode calculates aircraft geometry as well as an engine map in any case. If there is neither a take-off- nor an approach trajectory selected, required data for performing the noise analysis is missing and IOPANAM aborts with an error message. After executing PANAM, noise analysis results are evaluated and written back into the database. If a design variable for noise is selected as dependent, convergence is verified after each iteration loop.
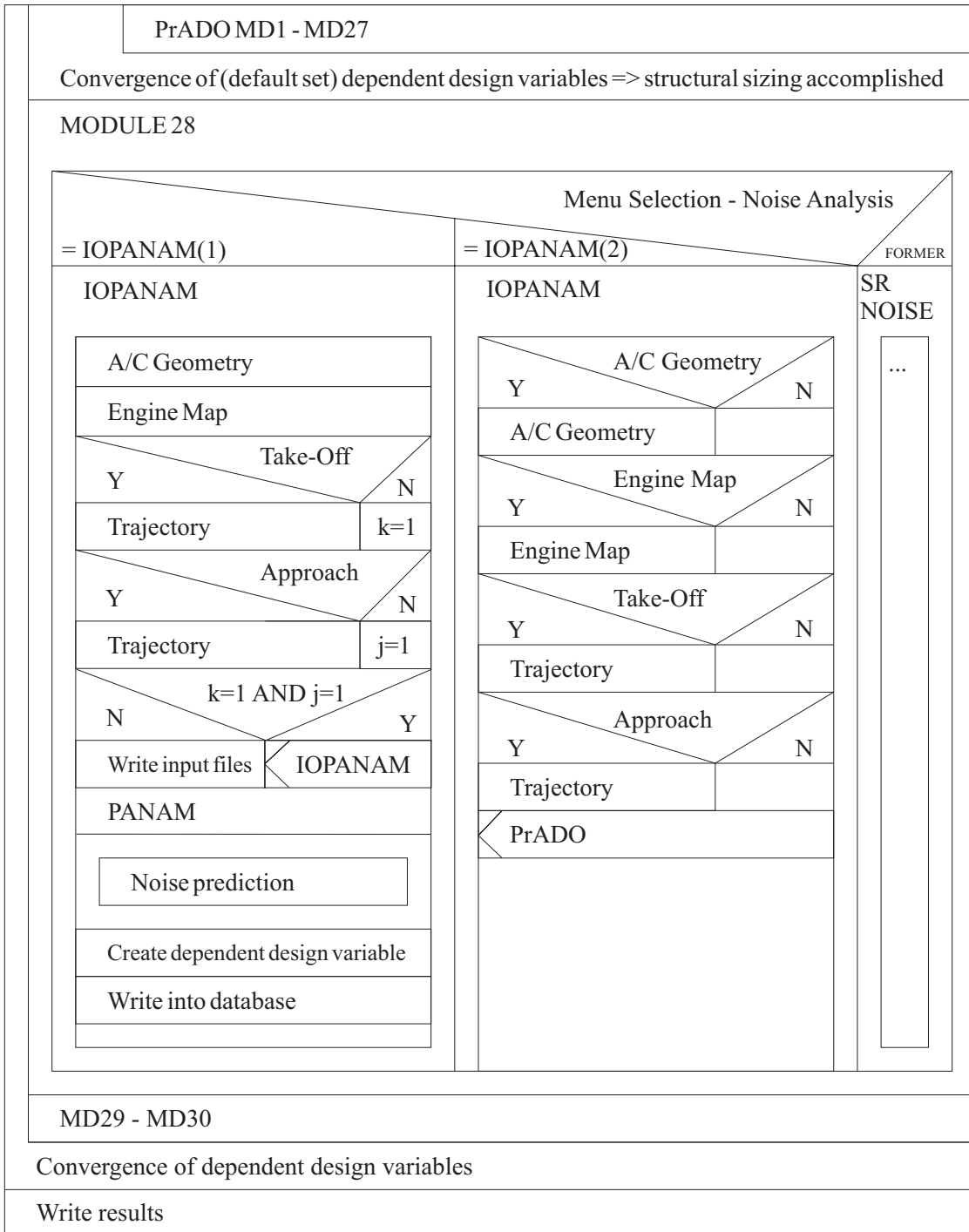
Figure 4.1   IOPANAM structogram (according to **DIN 66261 1985**). Y = yes, N = no.

4.1 Aircraft Geometry and Configuration

PANAMs parametric semi-empirical noise source models need geometric data to calculate noise emission. Data of wing geometry, horizontal tailplane, vertical tailplane and the landing gear is necessary. Furthermore, fuselage diameter and the number of engines are required as an input. Dedicated variable names can be found along with a short description in table C.1. Values of the reference aircraft are also provided. PrADO writes all data in classified databases as depicted in figure B.2. Table C.1 includes the database number in which the required parameter can be found. Furthermore, a few parameters from former data input files have been passed but not used on a later basis for noise prediction in PANAM (e.g. FNKBESF in table C.1). Other parameters used for checking e.g. the existence of flaps or the number of vertical tail planes became inessential since all checks are now handled by IOPANAM. Variable names of those parameters are crossed in table C.1 to indicate that they are not passed anymore in the current version. Additional vectors out of the database are needed for calculating parameters that are not included in the database in the requested format. For example, the slat length is not to be found in the database as an absolute value. Therefore, the plan view vector of the front wing box is used for computing the length. Vectors are read by applying a specific coding. These vectors of geometric information are essential for calculation only and are therefore also not passed as an input for PANAM.

Table 4.1   Aircraft configuration requirements (status in July 2008)

A/C component	Max. No. in PrADO	Max. No. for PANAM
airfoil wing	2	1
horizontal tailplane	4	1
vertical tailplane	4	1
gear strut	> 5	3
fuselage	2	1
identical engines	10	10

Before parameter values are read out of the database the basic aircraft configuration is surveyed. Numbers of major aircraft components must not exceed a specific value as shown in table 4.1, although greater quantities would be possible to consider in PrADO. Thus, only conventional aircraft configurations can be taken into account. A further restriction is defined by allowing only a single vertical tail plane and identical engines. The latter is not necessarily a restriction since common aircraft hold identical engines regardless of engine quantity. This limitation in aircraft configuration is due to PANAMs ability in computing only a specific

number of such aircraft components. Since PANAM would not be able to handle such issues, IOPANAM was programmed to give an error message if one of the maximum quantities, as stated in table 4.1, is exceeded by the user in PrADO.

The number of engines is taken into consideration as stated in equation 4.1. Engine noise source models compute noise emission of a single engine. Sound pressure levels are calculated for relevant one-third octave band frequencies. A doubling of sound pressure levels, as is the case with two engines, is therefore independently done for each octave band before determining the overall sound pressure. As stated in equation 3.7, this summation equals a doubling of the mean square sound pressure. Two engines result in a logarithmic increase of 3.01 dB, three engines in 4.77 dB and four engines in 6.02 dB respectively. With equation 4.1 in mind, only identical engines are to be considered.

$$\text{SPL}_{Engine}\left(f_{1/3}\right) = 10 \lg\left(\text{No}_{Engines} \cdot \text{antilog}\left(\frac{\text{SPL}_{SingleEngine}\left(f_{1/3}\right)}{10}\right)\right) \qquad (4.1)$$

4.1.2 Airframe Geometry

Aircraft wing parameters are among others: wing loading for take-off and landing, wing span, wing sweep, dihedral angle, length of flaps and slats, etc. For horizontal- and vertical tailplanes span, trailing edge sweep, dihedral angle and mean aerodynamic chord are required data. PrADO allows for different types of leading edge flaps: Krueger flap, leading edge flap and slats. As long as no flap (leading- or trailing edge) is extended, the airfoil wing is considered to be in a clean configuration. Parameter of flap position is provided by the trajectory file. With this input set for a clean configuration, PANAM calculates airframe noise for a cruise configuration with no influence of high lift devices. The noise source model for leading edge flaps is based on a slat. Although input parameters would be the same in quantity and definition for Krueger or leading edge flaps, only slats are considered in IOPANAM. In all other cases, the program writes an error message and aborts. This is because the so far implemented noise source model needs further research if applied on other

types than slats[20]. The geometric slat model is described by a spanwise length and an averaged depth as in figure 4.2. The η-coordinate in PrADO is defined perpendicularly to the aircraft's longitudinal axis for describing a percentage spanwise extension of various elements on the wing such as flaps, slats, wing tanks, ailerons, etc. Noise source models need spoiler length along the η-coordinate as an input and not the actual length of the spoiler. However, leading edge sweep φ_{LE} out of airfoil wing parameters, set as slat trailing edge sweep, is additionally considered in noise source modelling. Therefore, leading edge wing sweep is also important for the predication of slat noise. Slat length is computed out of a geometrical vector reserved for the front wing box. The sum of the percentage length of different segments is multiplied by the half wing span to obtain the spanwise length in units of meters. The projected area A_{proj} of each element (top view) is additionally added up to obtain an averaged slat depth. Thus, the sum of the projected area divided by the actual slat length (length in η-coordinate divided by the cosine of the leading edge wing sweep) gives the actual averaged slat chord c_S (equation 4.2). Finally, slat length is doubled to obtain the length on the right and left wing of the aircraft. This is necessary because the implemented noise source model accounts for only one piece of slat and assumes that therefore a slat, with a total length over the whole wing span, swept according to the leading edge and with an averaged slat chord.

$$\overline{c_S} = \frac{\left(\sum_{i=1}^{n} A_{proj}(i)\right)\cos(\varphi_{LE})}{\sum_{i=1}^{n} \eta(i+1) - \eta(i)} \tag{4.2}$$

with i-th slat element/coordinate.

The same principle is applied upon trailing edge flaps. Out of possible PrADO types i.e. split flap, plain flap, Fowler flap, single-, double-, or, triple slotted flap and single slotted flaps with upper surface blowing; only fowler flaps are to be considered. Flap geometry is taken from the aft wing box geometry vector. The same principle as in the preceding paragraph applies computing flap length and an averaged flap chord. A further simplification is made by averaging the trailing edge over a straight line, which is swept backwards according to an averaged trailing edge sweep (figure 4.2). A kink would normally subdivide the trailing edge

---

[20] e.g.: the noise source model, developed to predict noise originated from a slat, is based on an acoustic model that considers the gap between the slat and the aircraft wing. In the case of a Krueger flap, this gap would no longer exist and the aeroacoustic physics behind lose validity.

flaps into two pieces with separate tailing edge sweeps. The same principle is applied on spoilers whereas the spoiler length of upper- and lower wing spoilers is accumulated.
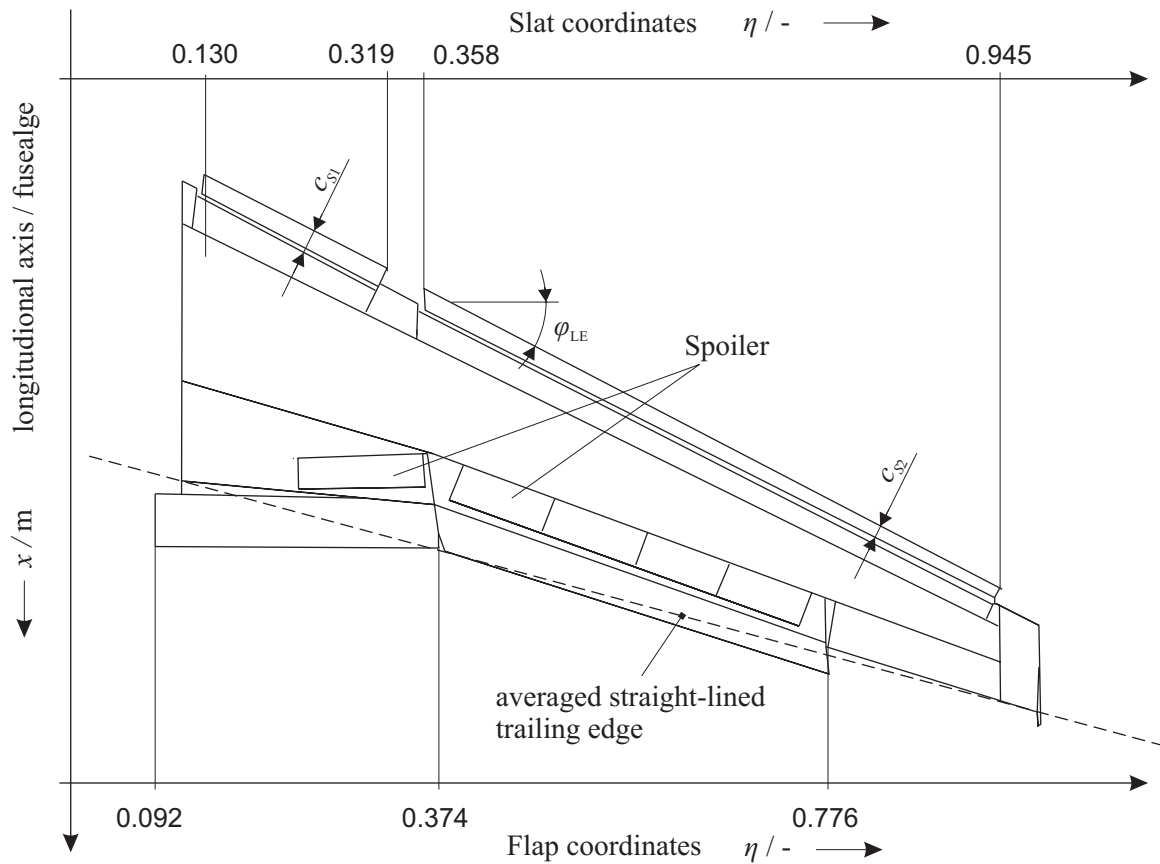
Figure 4.2   Calculation of averaged slat, spoiler and flap length

For the prediction of landing gear noise, gear leg length, tire diameter and the number of axles are required data out of PrADO. The noise source model in PANAM can be applied to multi-wheel main landing gears commonly referred to as bogie gears. The number of axles applied on one gear leg is a control parameter for the wheel arrangement. The implemented noise prediction model was validated on single- and double bogies (**Pott-Pollenske 2006**, p. 9). A further applicability for e.g. triple bogies might be possible. The landing gear arrangement must be tricycle due to the character of the implemented model in PANAM. Therefore, only three gear struts (with any number of axles and wheels) are available as a maximum as shown in table 4.1. The nose gear out of all gear struts is found by a parameter set for nose gear steering. The length of a gear strut is the sum of fully compressed gear strut length and maximum shock-absorber travel. Left- and right main gear are considered as identical. Therefore, data of the second main landing gear has not to be passed.

4.2   Engine Output

The turbofan engine is primarily used on commercial aircraft due to a higher efficiency, a more economical operation and low noise emission. The main advantage of the turbofan is an acceleration of a large amount of air with a lower velocity. Thus, the propulsive efficiency is higher (**Mattingly 1996**, p. 10) and jet noise lower (**Crichton 2007**, p. 176). A modern turbofan engine is characterized by a large diameter due to longer fan blades. The tangential velocity v_t (m/s) of the fan tip can be calculated as follows:

$$\omega = \frac{v_t}{r} = \frac{2 \cdot \pi \cdot \omega_{cyc}}{60\,\text{s}}$$

(4.3)

where ω is the angular speed ($\text{rad}\cdot\text{s}^{-1}$) and $\omega_{cyc}/60\text{s}$ the rotational speed n (rpm). Table C.2 summarises necessary parameters for a turbofan engine with about 100 kN static thrust that can be used for calculating the appropriate tangential velocity. The result is a tip mach number of about $M = 1.4$. Therefore excessive compressibility effects occur limiting the low pressure compressor design, more specifically, the fan diameter aerodynamically (**Mattingly 1996**, p. 10). The mass flow entering the engine at the front is, after passing the fan, subdivided into a core and bypassed mass flow. The nozzle at the end of both flows can be designed individually commonly referred to as turbofan with separate exhaust nozzles. The other way is by introducing a mixer unit to immingle both streams before passing the combined nozzle. This type of turbofan engine is referred to as mixed-flow turbofan engine characterized by a single engine nacelle. Cold air streams are less noise emitting than core flows heated by internal engine combustion (**Bräunling 2001**, p. 194). Mixing core- with fan flow results in a decrease of overall temperature and thus in a lower jet noise. However, a single nozzle does not necessarily mean a forced mixing of both streams. The IAE-V2500 for an example uses, at first sight, a single nozzle but can be compared with a separate exhaust nozzles turbofan engine (**Bräunling 2001**, pp. 231-2). The inner nozzle is inside the engine nacelle and the streams are not mixed together. In fact, the cold stream is more forced to envelop the hot stream where a slight mixing of both streams occurs. Engines provided with a mixer unit can be associated with models like the CFM56-5C installed on the Airbus A340-200/300 or the PW300. The idea of mixing the streams is usually considered to be less noise emitting. Therefore mixed flow ultra high bypass ratio turbofans are often seen as the best

engine type for an ultra low noise design (compare **Crichton 2007**, p. 4). However, recently developed technologies on turbofan engines with separate nozzles are to be found in literature (compare Woodward and Hughes 2004; **Huff 2007**). The implemented jet noise model is designed for jets exhausting from coaxial nozzles with conventional velocity profiles (**Stone 1982**, p. 341). As a matter of fact, engines equipped with a mixer unit i.e. engines with one single exhausting jet cannot be evaluated with the model. The model according to **Stone 1982** is based on two separate isolated streams that are primary and secondary jet. Therefore, only turbofan engines with separate exhaust nozzles are to be considered. A differentiation in engine nacelle length does not apply e.g. IAE-V2500 compared to a CFM56-5A5 (figure C.1). To ensure that the aircraft to be investigated in PrADO uses engines without a mixer unit the length of the mixer unit out of the database is read. If the length value is different from zero the program aborts and writes an error message.

Module 33 was already designed for computing an engine map. Data is written into a separate file and stored in the project directory. Engine parameters depending on flight altitude, Mach number and thrust setting are written into this file in tabular form. The calculation method computes engine performance data such as engine thrust, engine specific fuel consumption and emission values. However, jet- and fan noise source models need additional parameters such as exhaust velocity and fan rotational speed. Engine characteristics in a flight altitude of about 11 km are additionally not of interest for noise prediction. As a consequence, a new subroutine was set up to account for relevant parameters within a feasible range for noise prediction applications.

4.2.1 Selected Calculation Method

PrADO comprises different mathematical methods for engine performance estimation. Module 33 covers calculation of an engine map and calls directly the method selected. Table 4.2 gives an overview of the implemented methods. Not all methods account for respective engine components used in current turbofan engines.

Table 4.2   Implemented Engine Calculation Models in PrADO (1 = considered; 0 = not considered within the model)

Method	Year	Fan	Low pressure compressor	High pressure compressor	High pressure turbine	Low pressure turbine
VTW1	2001	x	x	x	x	x
TL2	1991	0	0	1	1	0
ZTL2	1999	1	0	1	1	0
ZTL10	1999	1	1	1	1	1
ZTL11	2008	1	1	1	1	1
ZTL12	2006	1	0	1	1	1

Subroutine ZTL11 requires input for Mach number, flight altitude and thrust setting. Output parameters are engine thrust, thrust specific fuel consumption and emission indices NOx, CO, HC and H2O. Emission values are not essential for engine noise prediction and therefore not passed. ZTL11 uses the maximum turbine entry temperature, depending on flight altitude and Mach number, for the estimation of other parameters via a regression analysis with four nodes. ZTL11 has two modes of operation: parametric cycle analysis referred to as design-point or on-design and engine performance analysis referred to as off-design. Parametric cycle analysis takes more than one engine into account and determines the performance at various flight conditions with different design choices and limits (e.g. compressor pressure ration, turbine entry temperature). Each considered engine in this model is operating at its design point. In contrast, engine performance analysis considers only one specified engine and determines the whole engine map in all flight conditions and throttle settings (**Mattingly 1996**, pp. 241-2). Latter is used for computing PANAMs engine map.

4.2.2   Necessary Engine Parameters

Necessary engine parameters are besides characteristic data, in form of an engine map, constant parameters that are set in advance. Those engine type specific parameters are to be redefined when dealing with another turbofan engine. As an example, the rotor stator spacing is a geometric parameter defined in figure C.2. Engine geometry is not accurately calculated by the implemented engine module. If there are no spacing values found in literature a sectional drawing of the concerned engine can be helpful. In the current version of PANAM rotor stator spacing was found to be 2.0. This value can be applied upon the reference engine with about 100 kN static thrust. In contrast to the example above, the constant parameter of

the total temperature rise through the fan was set in the program to constant value of 40.01K. However, total temperature rise is not constant over rotational speed. Later calculations showed the possibility of calculating the total temperature rise simply by thermodynamics formula. The parameter is now written into the engine map as a further characteristic value and as a consequence of that a better accuracy of engine noise prediction might be achieved.

For calculating the rotor speed out of the rotor speed in percent, also referred to as N1 engine speed, a reference speed value is required. For the engine currently used, the maximum permissible rotor speed of about 5100 rpm has been found in **FAA E28NE 1998** (p. 5) with the associated N1 speed of about 102%. Therefore, 5000 rpm of the low pressure shaft equals 100% N1 rotor speed as indicated in the cockpit. This reference is used for transferring data from rotor speed to N1 and backwards. The number of fan rotor blades and outlet guide vanes are also necessary data for starting PANAM. Therefore such data has to be made available through PrADOs database. Within database eight, already available data such as maximum shaft rotational speed N1 in rpm (n1_max in Table C.2 in cyc/s) and additionally maximum tangential fan velocity is found. These two parameters are directly related to each other through formula 4.3. The tangential fan velocity divided by the speed of sound is set to be the design tip relative Mach number. This assumption may not be accurate when dealing with another engine type. Table C.2 summarizes all parameters provided by PrADO in the current version. In the column of the former version in table C.2 it can be seen which parameters were set engine type specific to a constant value. Those are now requested as an input from the PrADO specification file (Appendix F). Data is transferred into the databases and made available for engine map calculation. Results are written into the engine map file. PANAM does not have a database. Therefore, those parameters formerly treated as constant within PANAM are now additionally transferred through the engine map file e.g. hub-to-tip ratio (hub radius divided by tip radius associated in our case with the dimensions of the fan rotor) for calculating the engine inlet area.

Temperatures, pressures etc. in an engine cycle are associated with engine components through sectional numbering. Undisturbed air in front of the engine is commonly referred as section zero, the inlet lip as section one and the compressor entry with section two. Compressor outlet i.e. combustor inlet is consequently numbered as section three (figure C.3).

Nozzle outlet is designated as section nine although different numbers have been found in literature[21].

4.2.2 Engine Map Range

The former engine map provides characteristic engine data up to flight level *FL* 320 and Mach number 0.8. During approach and departure such a remarkable wide range is not essential. With lower margins, data space can be used for more detailed results. An approach starting 50 km from the runway threshold, which is considered to be enough for a noise analysis on the ground, with a typical glide slope angle of about 3°, would start in 8600 ft or flight level *FL* 86. Considering airspace classifications in Germany, the maximum permissible flight speed, encompassing flight level *FL* 100, is approximately 130 m/s (**LAnAb 2007**, project 1635, p. 97). Air temperature according to the International Standard Atmosphere (ISA) in *FL* 100 is about 268.3 K with the speed of sound at 328.4 m/s. Maximum permissible Mach number in above mentioned airspaces is therefore $M = 0.39$. With this in mind, the range of the engine map is computed up to flight level *FL* 100 and Mach number 0.48.

4.2.3 Calculation of Fan Rotational Speed

Fan rotational speed N1 is a parameter for fan noise prediction with a strong influence. However, out of PrADOs thermodynamic derivations (as in ZTL11) no direct relation for N1 exists. Since engine calculation within PrADO is based on a gas turbine engine cycle analysis, only thermodynamic parameters are available. Thermodynamics of a fan can be treated the same way as of a compressor. As a result, a fan is equally characterized by its pressure ratio and efficiency (**Farokhi 2008**, p. 180) and additionally by mechanical or technical work *w* in thermodynamics. In general, power *P* equals force *F* multiplied by velocity *v*. Mechanical work *w* is force multiplied by travelled distance. Thus, by dividing the power by a mass flow rate gives the specific mechanical work based on one kilogram:

---

[21] **Mattingly 1996** (p. 10) uses section eight for the nozzle outlet whereas **Farokhi 2008** (p. 180) and **Bräunling 2001** (p. 194) use section nine.

$$w = \frac{P}{\dot{m}} = \frac{vF}{\dot{m}} \quad \left[\frac{N \cdot m \cdot s}{s \cdot kg} = \frac{N \cdot m}{kg} = \frac{J}{kg} \right] \tag{4.4}$$

When dealing with power out of an engine a difference must be made between the aircraft power P_F and the net power P_N. The ratio between those two can be described by the propulsive efficiency η_P. Net power i.e. power out of an engine cycle analysis is always greater than aircraft power that is force multiplied by velocity. Therefore the propulsive efficiency describes how much power out of the engine cycle can finally be used and transferred into flight speed.

$$\eta_P = P_F / P_N \tag{4.5}$$

In the present case net mechanical work is of significance and is gathered from the fan compression process on an *h-s* diagram as in figure 4.3:
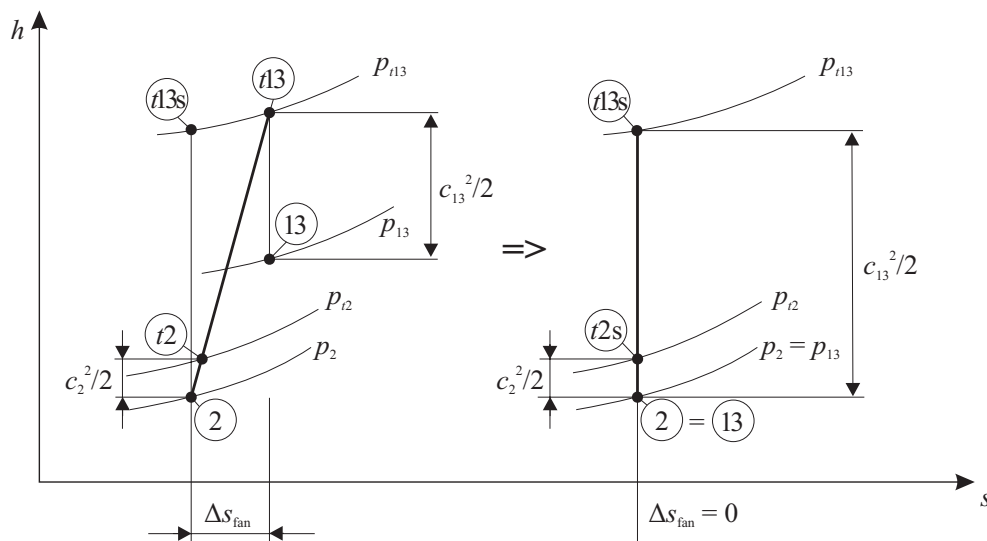
Figure 4.3 *h-s* diagram representing the flow process in an (adiabatic) fan, left illustration adapted from **Farokhi 2008** (p. 180)

Section two designates the fan entry and section 13 the fan outlet right behind the fan blade. In contrast fan nozzle is referred to as section 19 (figure C.3). Total quantities are designated through a further *t* in front of the section number and isentropic quantities through an *s* at the end. Therefore, the fluid entering the fan already exhibits a velocity c_2. Taking this velocity into account gives the total pressure p_{t2} that is then put to a higher value through the fan to p_{t3}. The difference between total pressure p_{t3} and ambient pressure p_3 is again described by the

kinetic energy of the fluid in section 13. The second law of thermodynamics calls for an increase in entropy for all irreversible processes (left illustration in figure 4.3). Now assuming a process with no friction (e.g. at the wall, in the fan bearing, etc.) the entropy change becomes zero and the process is isentropic with s = constant. A further assumption has been introduced to derive the process depicted in the right illustration in figure 4.3. The ambient pressure before and after the fan has been set to the same level $p_2 = p_{13}$. Therefore only the change in fluid flow velocity before and after the fan is taken into account. This step was necessary since no direct results are available out of PrADOs gas turbine engine cycle analysis. This becomes clearly visible by stating the formula used to derive the fan mechanical work. Out of the first law of thermodynamics total quantities can be written in the form:

$$q_{t2,t13} + \left(w_{friction}\right)_{t2,t13} + \int_{t2}^{t13} v \cdot dp = h_{t13} - h_{t2} = \int_{t2}^{t13} dh_t = c_p(T_{t13} - T_{t2}) \qquad (4.6)$$

Accounting for an adiabatic process, which is additionally considered isentropic equation 4.6 yields:

$$\int_{t2}^{t13} v \cdot dp = h_{t13} - h_{t2} = \int_{t2}^{t13} dh_t = c_p(T_{t13} - T_{t2}) \qquad (4.7)$$

with the total enthalpy:

$$h_{t13} = h_{13} + \frac{v_{13}^2}{2}; \quad h_{t2} = h_2 + \frac{v_2^2}{2} \qquad (4.8)$$

and by substituting the very left side of equation 4.7 for specific net mechanical work gives:

$$w_{N,fan} = h_{t13} - h_{t2} = h_{13} - h_2 + \frac{1}{2}\left(c_{13}^2 - c_2^2\right) \qquad (4.9)$$

Now the enthalpy h is the sum of internal energy and pressure multiplied by volume. Neither internal energy nor the ambient pressure of fan entry and outlet are known out of PrADOs thermodynamic cycle analysis. Therefore, setting the enthalpies before and after the fan to an equivalent level was a necessity. As a result, ambient pressure before and after the fan becomes equal as depicted in the right illustration in figure 4.3. Commonly, the velocity change through a compressor is neglected since the delta is diminutive and pressure difference

is taken into account. However, considering a fan, the increase in pressure might not be significant in contrast to the fluid velocity change. Therefore, equation 4.9 has become:

$$w_{N,fan} = \frac{1}{2}\left(c_{13}^2 - c_2^2\right)$$ (4.10)

As a result, the fan cycle output is the increase of kinetic energy imparted to the air. With this variable it is now possible to apply the fundamental equation of turbomachinery, the Euler turbine equation.

$$w_{N,fan} = u_{13}c_{13u} - u_2 c_{2u}$$ (4.11)

In words, the change of the fluid angular momentum between the exit and the inlet of a streamtube is equal to the applied torque exerted by the blade on the fluid (**Farokhi 2008**, p. 393). Absolute velocity c, relative velocity v and the rotor speed u are connected through the Galilean transformation (equation 4.12) and are applied on a cylindrical cut of a fan blade as in figure 4.4.
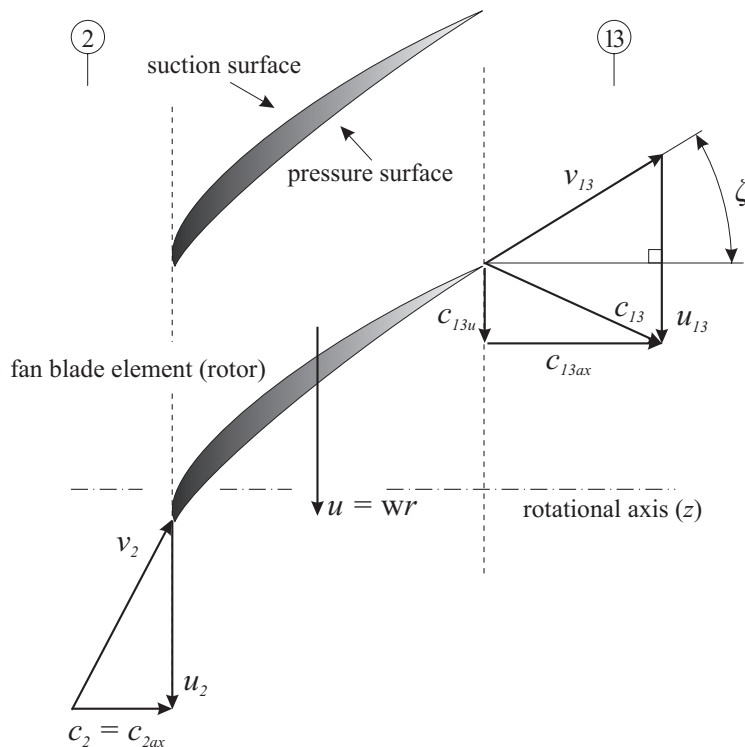
Figure 4.4   Cylindrical (r = constant) cut of a fan blade with velocity triangles (adapted from **Farokhi 2008** (p. 396) and **Bräunling 2001** (p. 298)

Absolute velocity c can be further broken down into a radial- c_u and an axial velocity c_{ax} component. c_u indicates a swirl and c_{ax} is a measure of flow rate. Commercial turbofan engines are usually not equipped with inlet guide vanes. Therefore, the flowfield entering is swirl-free and section two can be described by a pure axial velocity $c_2 = c_{2ax}$ parallel to the rotational z-axis. In an axial-flow turbomachinery, the fluid path is predominantly along the rotational axis. u_2 is therefore equal to u_{13} (**Farokhi 2008**, p. 394). With this in mind equation 4.11 yields:

$$\vec{c} = \vec{u} + \vec{v} \tag{4.12}$$

$$w_{N,fan} = u c_{13u} \tag{4.13}$$

At section 13 a swirl is already imparted into the air flow specifying c_{13u}. The exit flow angle ζ is assumed to be identical with the fan blade trailing edge angle. Exit flow angle ζ is therefore a function of the cylindrical cut radius of the fan r_{fan} (figure C.4), and prevailing flow conditions around the fan blade e.g. separated flow on the trailing edge. The ratio of circumferential- and axial velocity can be found by:

$$\tan \varsigma = \frac{u - c_{13u}}{c_{13ax}} \tag{4.14}$$

Additionally, the axial velocities c_{2ax} and c_{13ax} are roughly the same and treated accordingly: $c_{2ax} = c_{13ax}$. Out of the entering mass flow the axial velocity component c_{13ax} can be found by equation 4.14:

$$c_{13ax} = c_{2ax} \approx c_2 = \frac{\dot{m}}{\rho A_2} = \frac{4\left(\dot{m}_{fan} + \dot{m}_{core}\right)}{\rho \pi D_{Fan}^2} \tag{4.15}$$

c_{2ax} is not identical with the flight speed although section two may have identical quantities with section zero far ahead of the engine. Static thrust, as an example, is the thrust with the engine resting on the ground but with the fan at full rotational speed. c_{2ax} in front of the fan is certainly not zero in this case but the undisturbed air far ahead of the fan may still be at rest.

Finally, substituting c_{13ax} for equation 4.15 and c_{13u} for equation 4.13 in equation 4.14 makes it possible to determine the circumferential velocity u (equation 4.16). The quadratic equation is solved in a common mathematical way (negative velocities as solutions are ignored):

$$u = \tan \zeta\, c_{13ax} + \frac{w_{N,fan}}{u}$$

$$u^2 = u^1 \left[\tan \zeta\, c_{13ax}\right] + u^0 \left[w_{N,fan}\right]$$

$$u_{1,2} = \frac{\tan \zeta\, c_{13ax}}{2} \pm \sqrt{\left(\frac{\tan \zeta\, c_{13ax}}{2}\right)^2 + w_{N,fan}}$$

$$u = \frac{\tan \zeta\, c_{13ax}}{2} + \sqrt{\left(\frac{\tan \zeta\, c_{13ax}}{2}\right)^2 + \frac{1}{2}\left(c_{13} - c_{13ax}\right)} \tag{4.15}$$

Where c_{13ax} is the velocity of the entering fluid flow and c_{13} is the absolute velocity of the leaving fluid flow. After passing the fan stator, the fluid flow is ideally again almost swirl-free. The absolute velocity at section 19 is therefore aligned with the rotational axis and is additionally a parameter out of PrADOs cycle analysis. Assuming that the magnitude of the absolute velocity at section 19 is identical with that at section 13, c_{13} can finally be replaced by c_{19}. Now, by asking for fan rotational speed N1 equation 4.3 becomes of relevance upon one correlation of rpm and %N1 has to be known. According **FAA E28NE 1998**, 5000 rpm equal 100% N1 (table 6.1) for the reference engine as used in this thesis.

The derived circumferential velocity is only valid at one specific point along the fan radius. With an increasing distance to the fan rotational axis exit flow angle ζ decreases and vice versa. Fan blade geometry is often not known especially when dealing with recently developed three-dimensional optimized fans. However, the principle above does not change and fan blade trailing edge angles might be similar with other or new engines to be considered. With this in mind, the radial distance at which the currently found ζ is assumed to apply has become a relative value. Considering a new engine with no readily available data, only the absolute fan radius has to be approximated.

$$\zeta_{50\%} = \zeta\left(\frac{r_{fan}}{2}\right) = 8° \tag{4.16}$$

The fan total temperature rise equals fan mechanical work divided by the pressure coefficient:

$$w_{N,Fan} = c_p (T_{t13} - T_{t2})$$ (4.17)

4.2.4 Corrected Quantities

Speed triangles as depicted in figure 4.4 are changing permanently due to changes in pressure, density and mass flows. Additionally, acceleration of the engine is limited. At a certain point the relative incident flow to the rotor blade reaches a high angle of attack causing the compressor blade to stall (comparable to an aircraft wing stall). The pressure generation collapses, i.e. the compressor chokes and as a consequence the compressor is in an unstable condition (**Bräunling 2001**, pp. 499-519 and **Mattingly 1996**, pp. 672f). For analyzing this behaviour compressor maps are used. Typical compressor maps of two high-performance fan stages have been found in literature (figure C.5). These maps show that with only one constant fan rotational speed many conditions of mass flow versus fan pressure ratio are possible. Engines are optimized in one design point i.e. flight condition, where the exit flow angle ζ might be the extension of the sectional fan airfoil root chord as e.g. in figure 4.4. By leaving the design point as e.g. depicted in figure C.5, incident angle as well as exit flow angle change. Therefore, with the assumptions above and a constant exit flow angle ζ an inaccuracy in computing N1 emerges.

By using corrected quantities, as is the normal case for plotting a compressor map, rotational speed becomes directly proportional to the ratio of the axial to rotational velocity and mass flow rate becomes directly proportional to the Mach number of the entering flow (**Mattingly 1996**, p. 673). Referencing pressure and temperature to values corresponding to ISA sea level before calculating fan rotational speed might damp the inaccuracy. Therefore, the following ratios have been introduced:

$$\delta_2 = \frac{p_{t2}}{p_{ref}} = \frac{p_{t2}}{p_0} \cdot \frac{p_0}{p_{ref}} \qquad \theta_2 = \frac{T_{t2}}{T_{ref}} = \frac{T_{t2}}{T_0} \cdot \frac{T_0}{T_{ref}}$$ (4.18)

$$n_c = \frac{n}{\sqrt{\theta_i}} \qquad\qquad \dot{m}_c = \frac{\dot{m}\sqrt{\theta_2}}{\delta_2} \qquad\qquad (4.18a)$$

where p_{ref} = 1013.25 hPa and T_{ref} = 288.15 K with rotational speed n_c in rpm and mass flow $\dot{m}_c$ in kilograms per second. With an adiabatic flow process[22] (assumption to a very high degree of approximation) through the inlet cowl all total temperatures are of the same magnitude $T_{t0} = T_{t1} = T_{t2}$ as well as all total pressures $p_{t0} = p_{t1} = p_{t2}$. Total temperature and pressure are calculated within the troposphere as a polytropic atmosphere as follows:

$$\frac{T_{t2}}{T_0} = 1 + \frac{\kappa-1}{2}M_0^2 \qquad\qquad \frac{p_{t2}}{p_0} = \left(1 + \frac{\kappa-1}{2}M_0^2\right)^{\frac{\kappa}{\kappa-1}} \qquad\qquad (4.19)$$

$$T_0 = T_{ref}\left(1 - \frac{n-1}{n}\frac{H_0}{H_{ref}}\right) \qquad\qquad p_0 = p_{ref}\left(1 - \frac{n-1}{n}\frac{H_0}{H_{ref}}\right)^{\frac{n}{n-1}} \qquad\qquad (4.19a)$$

where H_{ref} = 8434 m and the polytropic index for air n = 1.235. Thus, with δ_2 and θ_2 the corrected mass flow can be computed upon the corrected rotational speed n_c will be obtained as result. n_c is then transferred back to rotational speed n as in equation 4.19.

---

[22] Wall frictions in the inlet cowl are in this case neglected. Therefore, the diffuser pressure ratio is one. Out of typical range the range of the diffuser pressure ratio a discrepancy of about 8 % can arise at lower Mach numbers and mass flows (**Bräunling 2001**, p. 431).

4.3   Flight Trajectories

One of the most promising noise abatement departure procedures for short-to medium range aircraft is the modified ATA-procedure. After rotating the aircraft climbs with a reduced constant[23] thrust or with maximum continuous thrust and at a constant speed (greater than take-off climb speed) up to a cut-back altitude (approximately 1500 ft). Sustaining the climb with reduced thrust, climb angle and climb rate (500 – 1000 ft/min), the aircraft is put into a clean configuration and accelerates before it goes into the final climb up to cruise altitude (**LAnAb 2007**, project 1635, p. 97).

The well-established Low Drag-Low Power (LDLP) procedure suggests the gear extension at a reduced altitude (2000 ft) compared to former standardized procedures. Due to a reduced drag of a retracted gear (LD) less power (LP) is necessary during the approach. The aircraft goes from level flight into an open descent with constant speed and the engines at idle. Before intercepting the glide path the aircraft will decrease airspeed and configure for the final approach at the intermediate altitude hold (**LAnAb 2007**, project 1631, p. 73). Both procedures are two-dimensional, have an influence on noise impact to ground and can be implemented into the PrADO framework. Both procedures applied on the reference aircraft as used in this thesis are shown in figures D.1 and D.2.

4.3.1 Parameters

PANAM requests the following flight trajectory parameters as an input: position coordinates relative to the observer's array point of origin, a time coordinate, True Air Speed (TAS), engine thrust, climb angle, Euler angles as well as positions of landing gear and high lift devices that are essential for defining symmetrical flight paths. Considering e.g. simultaneous and non-interfering traffic procedures, those parameters set at a constant value in the current version of IOPANAM are additionally requested since turns and descending spirals are flown. Flight modules in PrADO are not designed for such a special case. Therefore, y-coordinate,

---

[23] The procedure with reduced engine thrust is referred to as FLEX-procedure on Airbus-airplanes and derated-thrust procedure on Boeing-airplanes (**LAnAb 2007**, project 1635, p. 97).

bank angle etc. cannot be calculated and are therefore set to zero serving as a replacement character in the ASCII file. Further parameters additionally not passed are rotor speed (taken out of the engine map), aircraft acceleration (not necessary in the flight mechanics calculation), spoiler position (not necessary for departures and approaches) and wind parameters such as velocity and direction (not necessary for aircraft design). Table C.3 summarizes all prescribed parameters and the correlation to PrADOs variable names. All data was directly available except for the pitch-angle (climb angle plus angle of attack as in figure 4.5) and the z-coordinate (aircraft altitude minus aerodrome elevation that is usually mean sea level).

4.3.2 Segmented Calculation and Maximum Climb Angle

PrADO calculates trajectories by calling different flight segments, designed for one specific flight condition, in a logical sequence. For example, the take-off path is calculated as follows: take-off ground roll, rotating and lift-off manoeuvre, climb up to obstacle height, initial climb, intermediate climb and final climb. Those segments in the form of subroutines are requested in the same way to the point where the aircraft reaches the obstacle height. At this point the user can select a climb segment with one specific characteristic i.e. the climb segment can either be flown with a constant climb angle up to the maximum climb angle or with a constant true air speed. Any number of those climb segments can be arranged in any order providing a possibility to design case-specific take-off procedures. A more detailed description of the segments is to be found in appendix F. Unfortunately, flight segments in PrADO were designed to increase thrust over 100 % if the aircraft is not able to restrain the desired climb angle or climb speed. To avoid this effect, the climb angle is surveyed in advance to be lower than the maximum climb angle for the prevailing flight condition. By making use of the excess power maximum climb angle can be derived.

The earth-fixed axis system as defined in **DIN 9300 1990** has its origin in the aircraft's centre of gravity. The x-axis runs forward against the fluid flow, the y-axis through the starboard wing and as a result the z-axis is pointing downwards. To obtain the flight-path axis system a rotation by flight-path azimuth and climb angle is necessary. With no wind influence the

flight-path axis system becomes equally the air-path axis system. Therefore, rotations by the air-path azimuth angle χ_a (in this case identical to the flight path azimuth), the air-path inclination angle γ_a (in this case identical to the air-path climb angle) and the air-path bank angle μ_a are necessary to obtain the air-path axis system (x_a, y_a, z_a). A further rotation about the lateral air-path axis y_a by the angle of attack α determines the body axis system. The angle of sideslip β is set to zero. The body axis system can also be derived out of the earth-fixed system by applying the Euler angles[24] (figure C.6). In the present case of symmetrical flight trajectories ($\chi_a = \mu_a = \beta = 0$) the inclination angle Θ is the sum of air-path climb angle γ_a and angle of attack α. This summation is valid only in the case that all rotations are about the y-axis ($\Psi = \Phi = 0$).
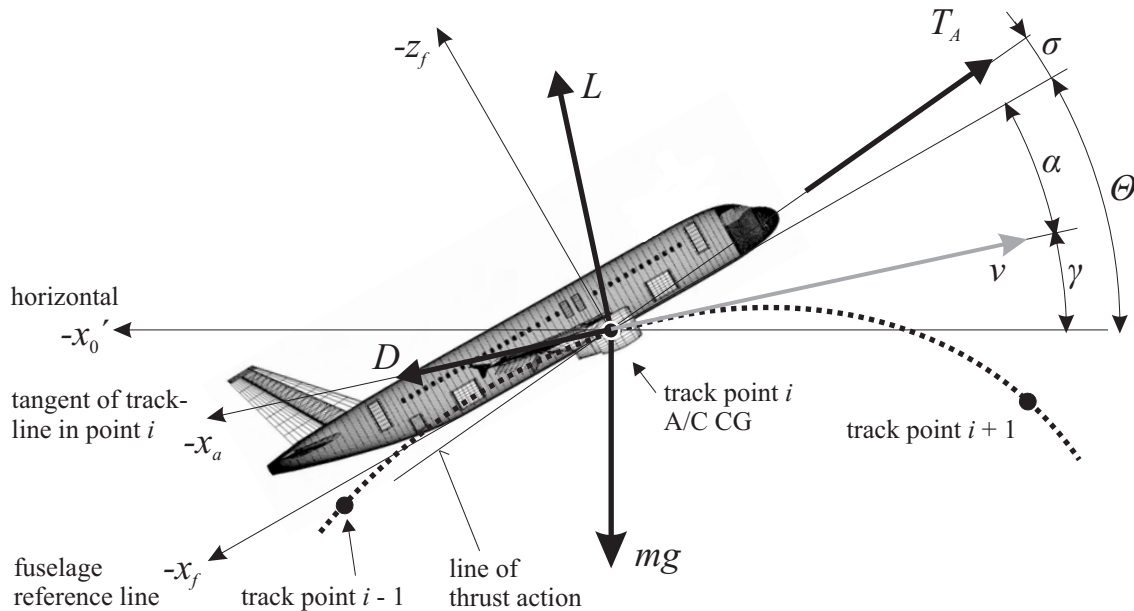
Figure 4.5   Forces and angle definitions during steady, symmetrical climbing flight

The flight trajectory is discretised into quasi-stationary flight positions. Any point along the trajectory assumes for a specified time increment a steady flight so that Newton's laws can be applied. Figure 4.5 illustrates forces acting on the aircraft during steady flight that are lift L, drag D, thrust available T_A and aircraft weight mg (aircraft mass multiplied by acceleration of gravity). Lift, drag and flight velocity vector v are perpendicular to each other. σ is the thrust vector inclination. A summation of all forces acting along the air-path axis x_a yields equation 4.20 along the normal air-path axis z_a yields equation 4.21.

---

[24] The three Euler angles are azimuth- Ψ, inclination- Θ, and bank angle Φ (**DIN 9300 1990**). The order of the three rotations to be completed is Ψ, Θ, Φ and must not be mistaken (a different attitude or position may result).

$$D = T_A \cos(\alpha + \sigma) - mg \sin \gamma \qquad (4.20)$$

$$L = mg \cos \gamma - T_A \sin(\alpha + \sigma) \qquad (4.21)$$

Equation 4.20 rearranged for the air-path climb angle γ and multiplied by flight velocity v determines the rate of climb v_C (equation 4.22). According to **Phillips 2004** (pp. 239-42) following assumption can be applied: climb angle γ is always small considering aircraft with low thrust-to-weight ratios. Therefore, the level flight drag $T_R.\cos(\alpha + \sigma)$ can be used in equation 4.22 instead of the actual drag D. Thus, the rate of climb can be approximated by equation 4.23 where the dot product of the velocity vector and thrust vector equals power.

$$v \sin \gamma = v_C = \frac{v T_A \cos(\alpha + \sigma) - vD}{mg} \qquad (4.22)$$

$$v_C = \frac{v T_A \cos(\alpha + \sigma) - v T_R \cos(\alpha + \sigma)}{mg} = \frac{P_A - P_R}{mg} \qquad (4.23)$$

$$\gamma = \arcsin\left[\frac{\cos(\alpha + \sigma)}{mg}(T_A - T_R) \right] \qquad (4.24)$$

The difference of the power available P_A and the power required P_R is the excess power and is a measure of climb performance. Climb angle γ can be calculated by equation 4.24 where the thrust available T_A is the actual thrust setting. Thrust required T_R is computed within a computational loop: thrust - lift coefficient – angle of attack – drag coefficient – drag force – and thrust again, until convergence occurs. This can be exemplified by rotating the airplane about the y-axis (figure 4.5) until equations 4.20 and 4.21 are satisfied. T_A must not be lower than T_R otherwise climb angle or climb speed are set too high or the aircraft descends (v_C negative). With T_A greater than T_R, the airplane is accelerating. With T_A equally T_R, a steady climbing flight with constant flight speed is performed. The desired airspeed is associated with only one specific rate of climb or sink rate respectively that is additionally dependent on the aircraft altitude. With all forces determined, load factors, accelerations, velocities and time increments can be computed. The aircraft is then reconsidered in the subsequent quasi-stationary flight position.

5   Explicit Design for Low Noise

"Ne pourroit-on pas conjecturer que le Bruit n'est point d'une autre nature que le Son? [...]
Pourquoi le Bruit ne seroit-il pas du Son?" Translation: Could we not imagine that noise ... is
sound. Why could noise not be sound? (Jean-Jacques Rousseau, Dictionnaire de Musique, 1767)

When trying to reduce aircraft noise the focus might be on various aspects driven by aeronautical authorities, airlines, airport or even a community exposed to aircraft noise. The design methodology for low-noise aircraft design can be implicit or explicit (**Leifsson 2005**, p. 18). An aircraft is implicitly designed with respect to a low-noise characteristic by selecting a configuration that has the potential for a significant noise reduction (e.g. Blended Wing Body with engines mounted on the upper surface). PANAM is in the current version not able to account for noise shielding, which would be the ultimate design feature. For this reason, the focus is on conventional aircraft configurations that are explicitly designed for low noise. This explicit design can be approached in two ways:

- reducing noise at source i.e. at the aircraft to minimize noise radiation and
- by optimizing noise abatement procedures to minimize noise impact on ground.

A balanced approach (**Airbus 2007**, **ICAO 2008**) can be found by considering both at the same level of significance. This becomes essential due to changes in flight mechanics when trying to reduce noise at source upon aircraft performance during take-off and landing changes. As an example, if high lift devices are reduced, the glideslope during approach as well as the climb performance in the first segment will be heavily influenced. This may result in a lower approach and departure altitude decreasing the distance to the observer on the ground and influencing the noise impact on ground. Therefore, the airplane with reduced high lift devices need not be necessarily quieter. This example demonstrates and emphasises multi-disciplinary optimization with respect to aircraft noise reduction.

5.1 Noise in a Multidisciplinary Optimization Process

Multidisciplinary Design Optimization (MDO) allows noise to be considered either as (**Leifsson 2005**, p. 19):

- an objective function that is to be minimized and/or
- a design constraint that needs to be met.

Before looking closer at both processes the question arises which noise level actually should be considered as a parameter to be applied on the objective function or design constraint. Here, creativity has no limits. Different forms of weighting scales and observer arrays can be used. Additionally, obtained noise levels can be averaged to obtain a broader level of predictions. Discrete values may be of interest by focusing on one of the three ICAO noise certification reference positions (figure D.14) to optimize an aircraft for certification purposes. So, many variations and combinations are possible. To obtain a better feeling of aviation related noise levels EPNL and SPL(A) have been plotted against each other (figure D.1 and D.2). Noise contours are cut below 48 dBA for A-weighted sound pressure levels. This level reflects approximately the ambient sound pressure level. As a rough guide, EPNLs are 10 dB higher compared to A-weighted sound pressure levels (as can be seen in two dimensional noise plots in appendix E). Therefore, EPNL is cut below 58 EPNdB. A doubling of the mean-square sound pressure level is equivalent to a 3 dB increase (equation 3.7). Each contour line in the plot represents therefore a doubling of the mean-square-, each second line a doubling of the root mean-square sound pressure level. Out of figures D.1 and D.2, the following characteristics have been found for EPNL:

- Effective perceived noise levels are higher compared to sound pressure levels. This increase still remains significant when an SPL(A) is considered equal to an 10 dB increased EPNL (same colours within the plot represent approximated equal sound pressure levels).
- The area of isocontours of effective perceived noise is larger.
- Discontinuities provoked by changes in the aircraft configuration (flap/slat setting, landing gear deployment) and changes in the aircraft condition (airspeed, engine thrust setting, etc) are smoothed by applying effective perceived noise weighting.

Out of EPNL and SPL(A) derivation as explained in the chapter on theory, one might say that A-weighting is a scale that only takes loudness into account whereas the EPNL is a result of both loudness and annoyance. The noys applied as a weighting upon sound pressure levels result from the former D-weighting scale and are in fact not comparable to the A-weighting. However, the perceived loudness might still have the strongest influence on perceived noise and therefore it might be considered that EPNL is a result out of the SPL(A). Therefore, it would be sufficient to bear SPL(A) levels in mind because they respond to changes in aircraft configurations and condition. In contrast, EPNL smoothes changes and discontinuities in obtained sound pressure levels. Differences in aircraft design might therefore be of negligible amplitude on an EPNL scale. As a result, the influence upon a multidisciplinary design process might be lowered. Additionally, this effect could be emphasised though, since expected noise levels differ only slightly from each other due to the summation of sound pressure levels on an energy basis. Here again, the response in EPNL might not be sensitive enough for an optimization process. However, this effect can be reduced by working with noise contours. A change of about 5 dB of noise radiating from the source causes a doubling (or halving) of ground area enclosed by a given noise contour of constant level. On the other hand this sensitivity might produce wrong results on contour areas when dealing with less accurate input noise data. This is the reason why noise footprints have not been readily used for aircraft noise certification (**Smith 1989**, p. 245). None the less, as a conclusion, EPNL is the recognized scale for rating aircraft noise and is therefore used in the first instance. And secondly, the area of a given noise contour in EPNdB is sensitive enough to be used within a multidisciplinary optimization. Inaccuracy in calculated data might lead to wrong results and has to be kept in mind. In a last step, the observer mesh can be chosen dependent on required accuracy and CPU time[25]. As depicted in figures D.1 and D.2, low EPNL contour lines are cut at the edge of the observer mesh. The computed area enclosed is therefore smaller and does not account for events beyond the observer mesh. By considering contour lines at a higher EPNL the analysed area becomes more concentrated about the *y*-axis. To catch all minor changes in a high-valued EPNL noise contour, a higher resolution about the *y*-axis should be used as shown in figure D.4.

Figure 5.1 depicts the process for considering noise as a parameter in a multidisciplinary design optimization framework. According to the design philosophy in PrADO (figure B.2),

---

[25] increases linearly with an increasing number of observers to be calculated.

the most important structural aircraft masses (max. take-off-, fuel- and operating empty mass) must show convergence before the design analysis is finished. By adding noise only as a design constraint the overall process ends after all design constraints are met. The ground area A_{ISO} enclosed by a given noise contour in EPNdB of a constant EPNL is computed after the design analysis. If the area enclosed is lower than a predefined area, the design constraint is met and the design loop is exited if all other possible design constraints are met as well. By running an optimization, an objective function is calculated where, in our case, the difference between the afore calculated isocontour $A_{ISO,old}$ and the newly calculated isocontour $A_{ISO,new}$ is to be minimized. Therefore, the optimization process ends, if the difference (probably along with others) is lower than a predefined value. If this is not the case, all independent design variables are varied and the whole process is started over again. Those variables are "independent" of the process because a variation occurs only outside the loop. Within the design analysis, all independent design variables are left constant. Upper and lower margins limit the value range of the independent design variables.
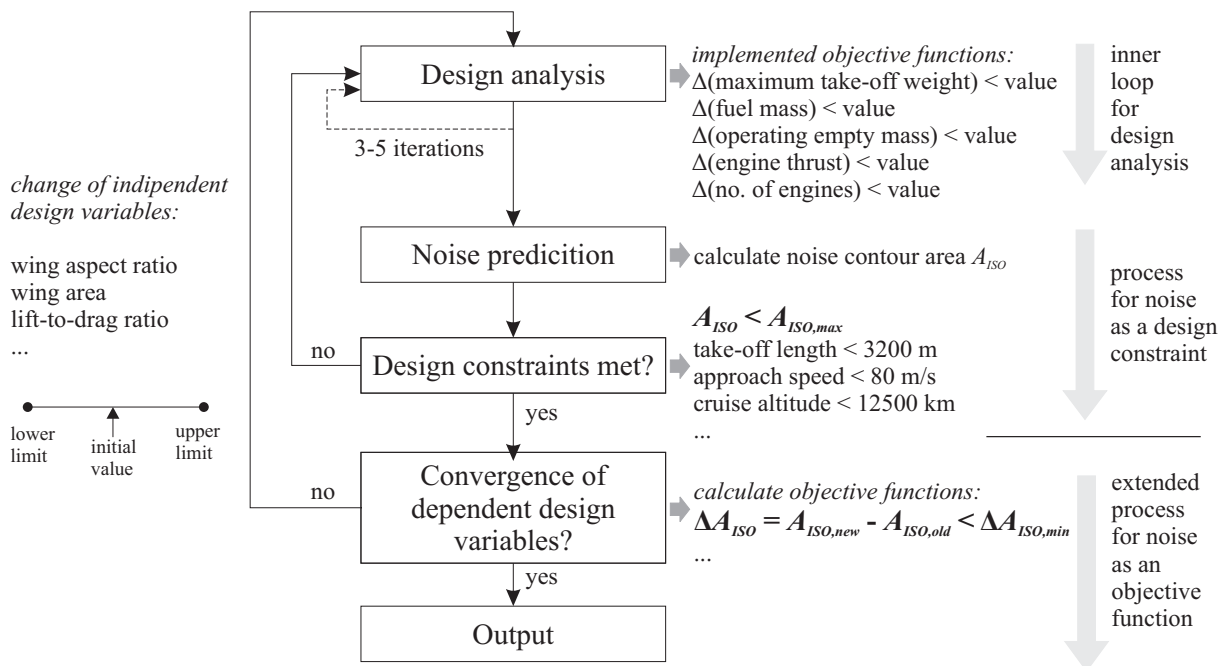
Figure 5.1   Procedures for optimizing aircraft for minimum noise

5.2 Sound Pressure on Reference Sphere

As discussed above, a balanced approach is to minimize noise on the source itself while additionally considering the noise impact on the ground. To evaluate the noise that radiates from the aircraft only, the idea came up to visualize sound pressure on a reference sphere.

The observer array is usually a plane consistent of any kind of microphones at or 1.2 m above ground level. But, the observer array can be arranged in any form (chapter on theory), thus, even spheres are possible. The program developed for computing a parametric spherical grid dependent on radius R, observer height and a discretisation factor n applies fundamental vector algebra. The starting grid with six nodes is predefined within the program code. The resulting shape equals an octahedron with each point at the distance R from the origin. As a next step, the grid is refined by splitting each spherical triangle to four further spherical triangles. This is done by halving each side length and connecting the new three derived points. As a result, a new inner triangle is within the outer triangle, splitting the geometry which can be considered as refining the grid. Figure 5.2 shows the idea behind this and the technique applied. Each spatial vector has the same initial point, the origin O, and an arbitrary endpoint P on the spherical surface. All vectors $\underline{a}$ are therefore position vectors (equation 5.1). Every two neighboured vectors are added (equation 5.2). The geometrical result $\underline{r}_{12}$ is the vector exactly between both and the parallelogram rule can be applied. The magnitude of $\underline{r}_{12}$ is not of interest. By normalizing the resulting vector and multiplying the unit vector by the constant radius R one gets the medial vector $\underline{a}_{12}$ with the correct magnitude and direction (equation 5.3). As a result a new grid point with the coordinates x_{12}, y_{12}, z_{12} has been found. These steps are repeated twice for each triangle. The newly obtained additional nodes are connected, representing the new triangle for refining the grid. The process is depicted in figures D.5-10. The derived triangles are not of equal size. The spherical surface of the new triangles in figure D.6 changes due to a slight difference in spherical excess[26]. This effect can be seen in figure D.10 (shows the upper hemisphere only) where a specific pattern in triangular shape can be identified on the spherical surface. The number of nodes increases with each refining step exponentially (figure D.11).

$$P_1 : \vec{a}_1 = \overline{OP_1} = \left(x_1, y_1, z_1 \right)$$

---

[26] The spherical excess is the difference between the sum of the angles of a spherical triangle and π.

$$P_2 : \vec{a}_2 = \overline{OP_2} = \left(x_2, y_2, z_2 \right) \tag{5.1}$$

$$\vec{a}_1 + \vec{a}_2 = \begin{Bmatrix} x_1 + x_2 \\ y_1 + y_2 \\ z_1 + z_2 \end{Bmatrix} = \vec{r}_{12} \tag{5.2}$$

$$\vec{a}_{12} = \frac{1}{\left| \vec{r}_{12} \right|} \vec{r}_{12} R \tag{5.3}$$

The spherical grid is used as an observer array for noise prediction. The trajectory must consist of at least three points (see chapter 3.2) that are within the sphere. The middle point is preferably set at the origin. With a radius of about 100 m all three discretised flight trajectory points are securely within the shape. Furthermore, due to small trajectory increments and circle dimensions the object is in a resting position. The derived sound impact on each observer is therefore a noise radiating snap-shot of an aircraft at a predefined aircraft condition and configuration.
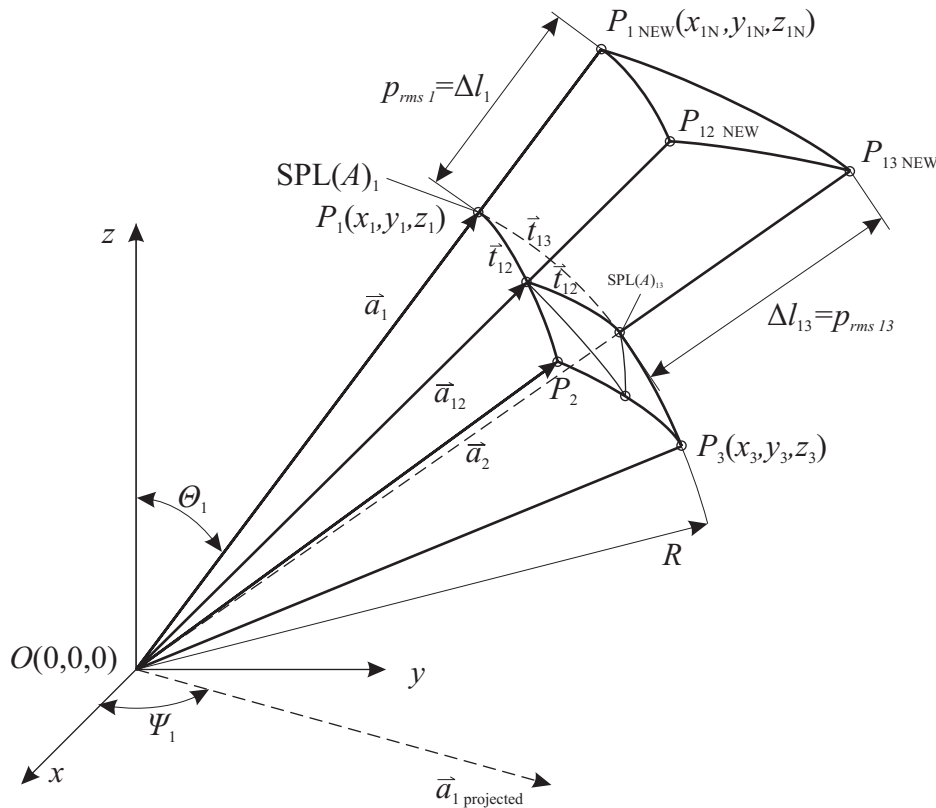
Figure 5.2   Spherical grid creation, refining and deforming

Each observer or microphone around the spherical surface contains a local sound pressure level. Levels can be computed either as OASPL(A), ESPL(A) or EPNL. For an OASPL(A)

level with no time correction it is possible to reverse computation and to obtain the root-mean-square sound pressure p_{rms} in Pascal of each observer (equation 3.8). However, OASPL(A) is derived from A-weighted sound pressure level by a summation on an energy basis. Therefore, the obtained value by applying equation 3.8 on the OASPL(A) is not equivalent to a single root-mean-square sound pressure value for a given frequency band. The derived root-mean-square sound pressure more likely represents the maximum A-weighted sound pressure level out of the whole frequency band. With this information it is possible to obtain a directivity characteristic simply by scaling the magnitude of each vector with the root-mean-square sound pressure. As a first step, coordinates of each position vector are converted out of the Cartesian coordinate system into the spherical coordinate system (equations 5.4-5 as in **Merziger 1999**, pp. 490, 533-4) that is described by zenith, azimuth and radial distance (Θ, ψ, R). The radius is extended by a scaled value of the root-mean-square sound pressure designated by the length Δl. The spherical coordinates with the new radius are converted back to Cartesian coordinates as in equation 5.6. Applications of a spherical deformation are presented in appendix E.1.

$$\Theta_1 = \arctan\left(\frac{\sqrt{x_1^2 + y_1^2}}{z_1}\right) \qquad 0 \leq \Theta_1 \leq \pi \tag{5.4}$$

$$\Psi_1 = \arctan\left(\frac{y_1}{x_1}\right) = \operatorname{atan2}\left(\frac{y_1}{x_1}\right) \qquad 0 \leq \Psi_1 \leq 2\pi \tag{5.5}$$

$$P_{11} = \left\{ \begin{array}{c} (R+\Delta l_1)\sin\Theta\cos\Psi \\ (R+\Delta l_1)\sin\Theta\sin\Psi \\ (R+\Delta l_1)\cos\Theta \end{array} \right\} = \left\{ \begin{array}{c} x_{1N} \\ y_{1N} \\ z_{1N} \end{array} \right\} \tag{5.6}$$

5.3 Parameters Dependent on Noise

All parameters that have to be passed for a noise analysis in PANAM can be considered as parameters exerting an influence on aircraft noise. A thorough list of all relevant parameters can be found in tables C.1-3. Those with a significant influence on the radiated sound of the

aircraft are to be discussed in the following chapter. However, in some cases, a generalization is not possible.

Fan Noise

PANAM computes fan noise and jet noise separately for the prediction of overall engine noise. The implemented fan noise model is described by **Heidmann 1979**. The model includes a modification on the basis of the Boeing Ames Method by **Dunn 1973** and has been designed in partial support of NASA's Aircraft Noise Prediction Program (ANOPP). The model used predicts sound pressure levels in dB referenced to 20 µPa. The tool allows the investigation of turbojet compressors, single-stage turbofans and two-stage turbofans with and without inlet guide vanes. However, the method is calibrated and examined on single stage fan test results. Compressors and fans are expected to operate near or below the design point. The inlet duct is assumed to be aerodynamically clean with no acoustic linings. The noise components broadband noise and discrete-tone noise are applied on the fan or compressor inlet duct as well as on the fan discharge duct. Furthermore, a combination tone noise component is used for the inlet duct (**Heidmann 1979**; **Dunn 1973**). Spectrum shape, level and free field directivity of each component is finally combined with a spectral summing. Free field sound pressure levels are presented along a circle and as a function of the polar angle (figure D.12). Comparisons with Airbus A319 data, equipped with CFM56-5A5 engines, indicate an over-prediction of resulting levels (**Bertsch 2008**, p. 4). Sound pressure levels are in **Heidmann 1979** normalized by:

$$\text{SPL}_{norm} = 20\lg\left(\frac{T_{t13} - T_{t2}}{0.555\,\text{K}}\right) + 10\lg\left(\frac{\dot{m}_{fan}}{0.453\,\text{kg/s}}\right) \tag{5.7}$$

Noise is then calculated as follows:

$$\text{SPL} = \text{SPL}_{norm} + 20\lg(M_{TRD}) + f(M_{TR}) + \Delta\text{dB}(\text{rotor - stator spacing}) + DI_M + \text{spectrum content} \tag{5.8}$$

where M_{TR} is the rotor-tip relative Mach number and M_{TRD} is the M_{TR} at the design point of the fan. Equation 5.8 shows that sound caused by the fan is proportional to M_{TRD} to the power of two. M_{TR} is used to adjust obtained SPLs upwards and downwards. Table 5.1 shows the correction factors if M_{TR} reaches a specific value and the possible range of resulting SPLs. It

can be seen that the discrete-tone noise for the fan has the strongest influence because it scales the noise by M_{TR} to the power of five. This increase of about 10 dB becomes significant when the rotor-tip relative Mach number reaches values above 0.72. The rotor stator spacing has a minor influence and differentiates between broadband and discrete-tone noise. Directivity corrections (D_{IM}) are virtually identical for discrete-tone- and broadband noise with a maximum correction of about 20 dB (figure D.12).

Table 5.1 Variation of noise radiating from the fan

noise components	constraint	correction	possible range [dB]	correction for rotor-stator spacing > 100 [dB]
fan inlet				
broadband	$M_{TR} > 0.90$	$-(M_{TR}/0.9)^2$	58 - 64	2.4
discrete-tone	$M_{TR} > 0.72$	$(M_{TR}/0.72)^5$	60 - 75	4.771
fan discharge				
broadband	$M_{TR} > 1.00$	$-(M_{TR})^2$	60 - 65	2.4
discrete-tone	$M_{TR} > 1.00$	$-(M_{TR})^2$	63 - 68	4.771

Jet Noise

Jet noise is predicted by **Stone 1982**. The model can be applied on coaxial jets having low to moderately high bypass ratios. Jet noise is a result of jet mixing noise and shock noise. For jet mixing noise, ratios of fully expanded primary- to secondary jet in temperature T_9/T_{19}, velocity v_{19}/v_9, and cross-sectional area A_{19}/A_9 ratio are taken into account. Influences of primary jet velocity and area ratio on jet noise are depicted in figure D.13. For a modern turbofan engine, such as the CFM56-5A4, the area ratio equals approximately $A_{19}/A_9 = 3$ that is responsible for low OASPLs. Therefore, the higher the cross-sectional area the lower are the predicted sound pressure levels. A strong influence is exerted on jet noise by the primary velocity of the jet, ranging from $v_9 = 217$ m/s up to $v_9 = 590$ m/s and resulting in an OASPL increase of about 30 dB (depicted in figure D.13). Shock noise is not likely to be dominant in future high-bypass engines (**Stone 1982**, p. 340). Therefore, by dealing with currently used and modern high-bypass engines shock noise is included only for the generality of the results.

Noise from Clean Airframe and High-Lift Devices

Sound pressure levels radiating from the clean aircraft are as much as 10 dB below sound pressure levels of the aircraft with deployed high lift devices and landing gear (**Pott-Pollenske 2006**, pp. 6-8). Clean airframe noise and noise that radiates from high-lift devices follow a v^5 power law. This means that the mean-square sound pressure is proportional to the fifth power of airspeed. The directivity for clean airframe noise is only in a lateral direction

taking the cosine of the wind dihedral angle into account. Generally speaking, slotted slats produce the most aerodynamic noise followed by noise radiating from the flap side edges and both show strong interactions. The acoustic model for slat noise consists of compact dipole sources with their axis perpendicular to the swept leading edge chord. The cosine of the wind leading edge sweep scales sound pressure levels by the power of three. Additionally, an influence of the slat spanwise extension over a selected radiation distance exists (ratio to the power of two). Noise source models have been derived out of flyover noise measurement results that have been conducted with an Airbus A319.

Landing Gear Noise

Noise radiating from the landing gear follows a v^6 power law (**Pott-Pollenske 2006**, pp. 9-10) and is presented in the from of a monopole and exhibits therefore no characteristic in directivity. Nose landing gears are more complex in their architecture and are therefore seen to produce a higher sound pressure level compared to a main landing gear (a 2 dB increase is expected). Also, the lift related circulation around the wing lowers the airspeed that actually hits the under-wing mounted main landing gear. Geometric design parameters of the gear (strut length, wheel diameter, etc.) are used to account for the source dimension.

It can be seen that the airspeed exerts the greatest impact on the overall airframe noise because it scales sound pressure levels of each noise component (clean airframe, high-lift devices-, and landing gear noise) to at least the power of five. Interactions of airframe noise sources cannot be calculated yet. Thus, a componential approach is used to account for each noise source individually and to summarize predicted sound pressure levels on an energy basis.

6 Results

Competition has always driven Aviation technology toward the most efficient aircraft. ... So, while we strive to do even more on fuel and the environment, we must also better explain how far we have come." (Olivier Villa, Senior Vice President Civil Aircraft Dassault Aviation, Aero May 2008)

6.1 Short- to Medium Range Aircraft Noise Analysis

The derived interface has been applied in the first instance to two short- to medium range aircraft configurations. Both feature the same geometrical dimensions. The reference aircraft is a 150 passenger, twin engine subsonic transport aircraft with a design range of about 4800 km at a cruise speed of about Mach 0.78 (figure E.1). The reference aircraft is powered by two turbofan engines with 98 kN static thrust. A design analysis in PrADO yields a converged maximum take-off mass of 69 tons, an operating empty mass of 37 tons and a fuel mass of about 14 tons for the design mission including domestic reserves. The high-powered aircraft configuration features in contrast to the reference aircraft an increase of 40 % in static thrust (figure E.2). This parameter has been selected in order to evaluate the influence of an increased maximum climb-angle on noise impact on ground during a departure in accordance with the modified ATA-procedure.

After a second design analysis in PrADO for the high-powered aircraft, the impact of a more powerful engine upon an aircraft configuration can be evaluated with respect to the baseline i.e. the reference aircraft. With engines that are heavier compared to those on the reference aircraft, overall aircraft weight increases. Thus, more lift is required to carry the weight. With a constant wing reference area, wing loading increases and as a consequence, structural dimensioning of the wing must be adapted to higher loads. This increase in wing weight further increases overall weights of the aircraft (figure 6.1). On the other hand, heavier engines on the wing act with their mass force against aerodynamic lift. This effect is, however, in our example, weaker compared to the mass surplus by the engines on overall aircraft masses.
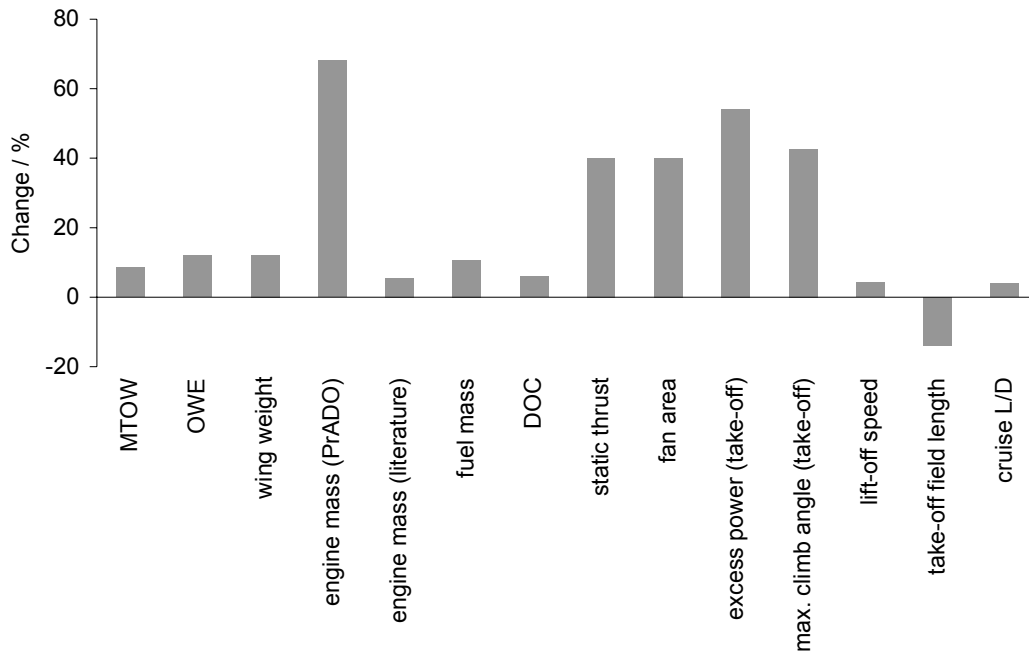
Figure 6.1 Results of PrADO design analysis, high-powered A/C compared to reference A/C (baseline)

6.1.2   Results and Verification of Engine Map Calculations

The engines used have been compared with engines currently available in today's aircraft industry (table 6.1). This analysis showed that PrADO scales the engine mass by almost 70 % that is an absolute increase of 1.1 tons whereas engines in literature differ in their masses only by 6 %. Thus, this deviation of estimated engine weights (1.1 tons) in PrADO is most likely to be responsible for such a significant impact on structural weights as presented in figure 6.1. However, PrADO scales the engine according to engine cycle parameters. As a logical consequence, the estimated engine weight is in PrADO significantly higher. Additionally, it can be seen, due to a higher MTOW more fuel is required to accomplish the required design mission. Direct Operating Costs (DOC) per flight hour are fractionally influenced. PrADO scales the new fan diameter identical to the increase in static thrust of 40 %. Excess power increases that in turn enhances climb performance. Maximum climb angle is shifted to a higher margin. The high-powered aircraft additionally accelerates faster that decreases take-off field length although lift-off speed slightly increases due to a higher structural mass.

Engines designed in PrADO are primarily dependent on turbine exhaust temperature margins as presented in figure E.3. Both engines feature identical maximum permissible temperatures that are crucial for determining engine operating conditions at a given altitude and Mach number. Fan mass flow rate out of PrADO responds to an engine thrust change accordingly and increases with higher Mach numbers (figure E.4). Core mass flow rate is correspondingly lower but also influenced by the Mach number. Computed fan rotational speed as derived in this thesis responds to an engine thrust increase almost identical in slope to fan mass flow rate (figure E.5). Considering the engine with increased static thrust the gradient of fan rotational speed decreases and the maximum fan rotational speed out of the whole engine map results to N1 = 80 % at maximum thrust setting, which is far from a satisfying result. Thus, fan blade exit flow angle ζ (or fan blade trailing edge angle as in figure E.5) has been adjusted to 26° to obtain a better agreement. Results show that the new derived fan rotational speed at a maximum thrust setting ranges between N1 = 80 % and N1 = 100 %. This would mean, that at take-off, maximum engine thrust i.e. static thrust is achieved at N1 = 80 %. This value is slightly too low and also not satisfying since fan rotational tip speed is crucial for fan noise prediction especially during take-off. The last adjustment has been made by further increasing the fan blade exit flow angle ζ to shift all curves to higher values. With $\zeta = 35°$ for the more powerful engine maximum fan rotational speed ranges now from N1 = 90 % and N1 = 110 % (figure E.9). For the reference engine fan blade the exit flow angle has been adjusted to $\zeta = 12°$ respectively (equation 4.15).

Table 6.1   Engine models used

Engine type	Parameter					
	Static thrust [kN]	Fan diameter [m]	Bypass ratio [-]	100% N1 [rpm]	TET [K]	comparable to[c]:
Reference engine	98	1.46	6.2	5000[a]	1533.15	CFM56-5A4
Ref. engine with incr. static thrust	137	1.72	5.5	5000[b]	1533.15	CFM56-5B2

Notes:

[a]   as stated in **FAA E37NE 1996**

[b]   as stated in **FAA E28NE 1998**

[c]   compared with data as in **Roux 2007**

Propulsive efficiency η_P, calculated out of PrADOs primary and secondary jet velocity results, is somehow stretched over the new range of engine thrust to meet approximately the same values at maximum thrust of each engine (figure E.6). Fan nozzle exhaust temperatures are decreasing with an increasing altitude as expected (figure E.7). The slope as well as absolute

values of fan pressure ratios increase with higher altitudes as expected since less thrust can be produced and ambient air pressure decreases (figure E.8). Application of corrected quantities has an insignificant influence on fan rotational speed results (figure E.9). However, the range of obtained maximum fan rotational speeds is slightly stretched which is actually not desirable. The influence of corrected quantities upon fan total temperature rise is more significant. The range of obtained results is enlarged as well (figure E.10).

A further adjustment of derived engine parameters has been made. It seemed to be necessary to adapt primary jet velocity v_9 to values of the DLR engine map. The DLR engine map was the only available source of information covering relevant engine parameters and has therefore been used as a baseline to compare obtained engine map results out of PrADO. The DLR engine map suggests a primary jet velocity range of $v_9 = 340 – 402$ m/s at relevant Mach numbers and flight altitudes, whereas PrADOs primary jet velocity ranges from $v_9 = 530$ m/s to $v_9 = 543$ m/s (table 6.2). In contrast, primary and secondary cross-sectional areas A_9 and A_{19} out of PrADOs engine cycle analysis are smaller compared with those of the DLR engine map. The area ratio A_{19}/A_9 is less effected than the stated absolute values. Jet velocities and cross-sectional areas are decisive for jet noise prediction. Hence, both cross-sectional areas as well as primary jet velocities have been adapted to meet approximately those values of the DLR engine map. But still, all calculations are made with the derived engine map out of PrADO. On a later basis it has been seen that differences in those parameters in <u>overall</u> noise impact on ground are of negligible amplitude (figure E.26)

Table 6.2   Variations in relevant parameters for jet noise prediction

Engine type	parameters relevant for jet noise prediction				
	A_{fan} m²	A_{19} m²	A_9 m²	A_{19}/A_9 -	v_9 (range) m/s
DLR CFM56-5A5	2.364	1.044	0.315	3.314	340 - 402
PrADO CFM56	1.667	0.871	0.175	4.977	530 - 543
PrADO GE90	9.749	4.726	0.602	7.850	520 - 530

Thrust available decreases with increasing airspeed. Thrust required shows a minimum at low airspeeds, preferably at initial climb airspeeds. Both have been plotted against each other with a dependency on the engine throttle setting τ at standard sea level conditions (figures E.11and E.12). For the considered aircraft with increased static thrust, thrust available lines are moved to higher levels as expected. A minor change in the characteristic of thrust required curves of the high-powered aircraft (figure E.12) is a consequence of increased overall aircraft weights

and a change in aircraft performance (lift-to-drag ratio L/D changes as shown in figure 6.1). At an airspeed of approximately $v = 135$ m/s a slight buckling of all thrust available lines can be noticed. This decrease in slope of all curves is due to turbine exhaust temperature (TET) margins as in figure E.3. At standard sea level the above mentioned airspeed equals a Mach number of 0.4 at which TET margins become predominantly effective by derating the engine. As a consequence, engine output is limited and decreases more rapidly after passing the Mach number threshold of 0.4. The maximum difference in thrust available (e.g. with $\tau = 1$) and thrust required can be found by moving a vertical line between those curves until the length has reached a maximum. In our case the airspeed v_{H35} at which the aircraft reaches the obstacle height of about 35 ft has been found to be close enough to the maximum excess thrust for each aircraft configuration. Therefore, with this in mind, each aircraft uses along its first climb segment maximum available excess power. This is not equivalent with the maximum rate of climb as can be seen in figures E.13 and E.14.

6.1.3   Segmented Flight Trajectories

The climb trajectory is in accordance with a modified ATA-procedure (chapter 4.3). The landing gear is retracted when the aircraft passes the obstacle height of 35 ft. The aircraft climbs with maximum climb angle and climb configuration (flaps extended 10°, slats extended 18°) to 1500 ft where a cutback is performed. High lift devices are retracted and the aircraft is in a clean configuration to perform an accelerating climb until reaching the x-coordinate threshold of $x = 25$ km. To maintain comparability between both aircraft true air speeds should be at least comparable at the end of the trajectory. The high-powered aircraft, however, features already a raised true air speed at the cut-back altitude compared to the reference aircraft. A compromise has been found by selecting an approximate identical true air speed growth (trajectory in figure E.16) throughout both second climb segments that are flown with identical climb angles. As a result, the high-powered aircraft does not need so much engine thrust for the required acceleration along the flight path. As can be seen in figure E.15 the high-powered aircraft performs its second climb segment with 60 % thrust whereas the reference aircraft needs 80 % of available engine thrust and both feature the same growth in true air speed along the flight path. The influence of increased structural masses upon the

high-powered aircraft can be seen when comparing both thrust required lines in figure 6.2. The high-powered aircraft needs more engine thrust to maintain the climb with constant climb angle. This might not be solely due to an increased maximum take off mass. The high-powered aircraft is also flying at a higher airspeed that increases aerodynamic drag.

Finally, noise analysis results depicted in figures E.16 through E.25 indicate that the high-powered aircraft has a significant lower noise impact on ground with respect to the reference aircraft. Noise contour plots have been cut along the x-axis and obtained SPL(A) (figure E.16) or EPNL (figure 6.2) split into major noise contributors: fan, airframe and jet noise. This allows for a thorough analysis and has been derived for the flyover reference with $y = 0$ and for the sideline with $y = 450$ m for both, SPL(A) and EPNL. Results of examined noise contours of constant EPNL as depicted in figure 6.2 are summarized in table 6.3.

Table 6.3   Evaluation of noise contours of constant EPNL

Aircraft type	Noise contour area of constant EPNL					
	Total area [km²]	65 EPNdB [km²]	70 EPNdB [km²]	75 EPNdB [km²]	80 EPNdB [km²]	85 EPNdB [km²]
Reference A/C	1800.00	289.58	199.61	112.15	62.88	17.80
High-powered A/C	1800.00	252.03	172.13	97.77	47.76	8.87
Green Freighter	1800.00	284.61	187.44	109.10	49.59	12.17

As shown in figure 6.2 all noise contours of constant EPNL below 85 EPNdB extend to the limits of the observer array. Furthermore, it is clearly visible that the noise contour area of 85 EPNdB is less in the noise plot for the high-powered aircraft (middle illustration) than in the plot for the reference A/C (top illustration). This supplementary is reflected by table 6.3, which contains computed areas of constant EPNLs out of the noise plots in figure 6.2. The 85 EPNdB noise contour area is decreased by 50 % (figure 6.3). Recognizable is also a somewhat smaller 73 EPNdB "belt" along the x-axis in figure 6.2 of the high-powered aircraft. Again, this is also reflected by table 6.3 although contours are examined for 75 EPNdB and 80 EPNdB. However, by evaluating contours of lower constant EPNLs the difference in compared areas diminishes. Possibly, this is because those noise contour areas are cut at the edge of the observer array. Another reason might be that effective perceived noisiness weighting smoothes discrete levels in the noise plot especially far from the source that are primarily influenced by atmospheric damping and the decreasing radial distance R. As can be seen in equations 3.20, 3.21 and 3.23 mean square sound pressures are inversely
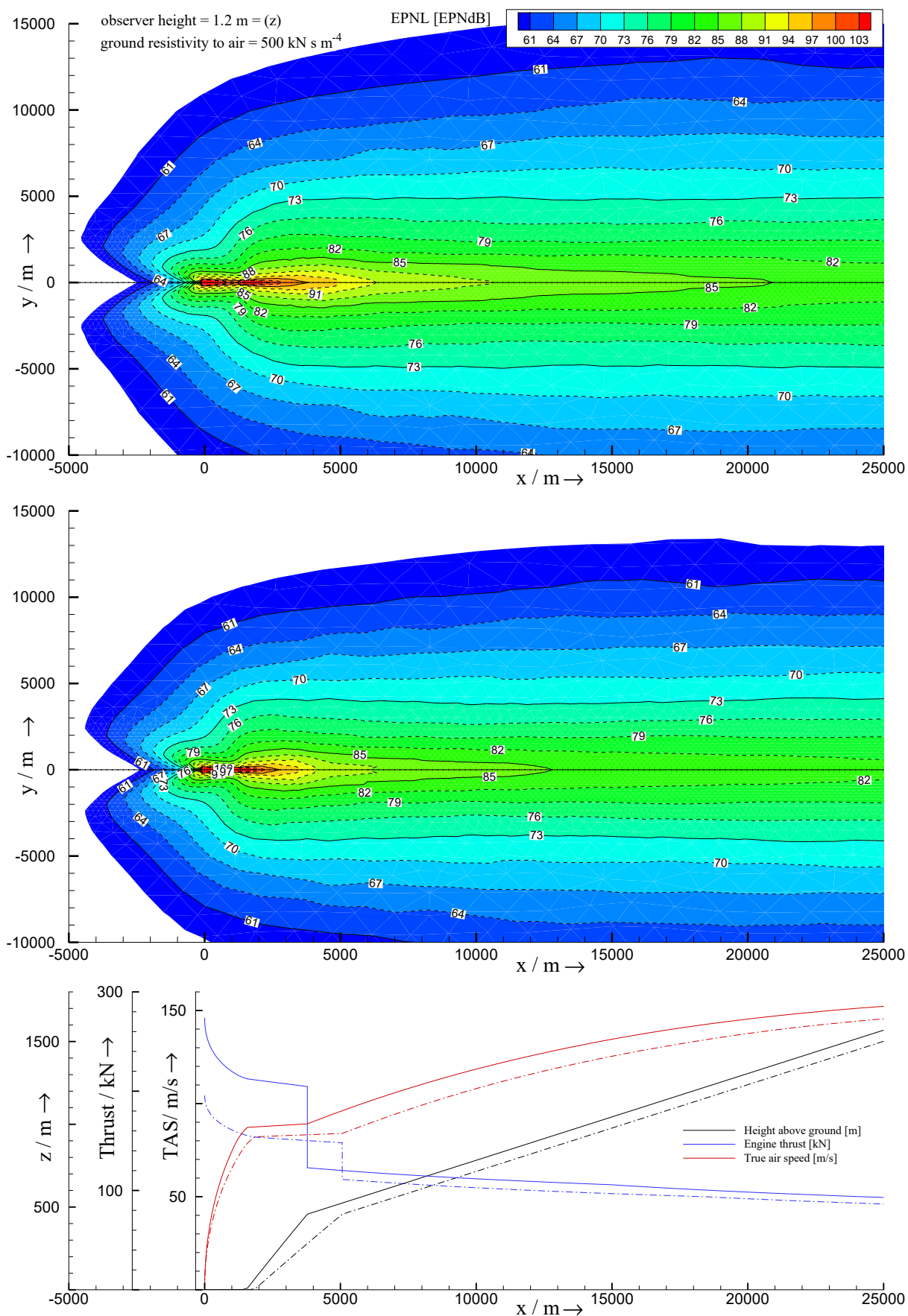
Figure 6.2   Noise contour plot in EPNL of the reference aircraft (top) v. the high-powered aircraft (middle) during take-off.

proportional to the squared radial distance R^2. This exponential characteristic is also clearly reflected in figure 6.3.

noise contour of constant EPNL / EPNdB $\longrightarrow$
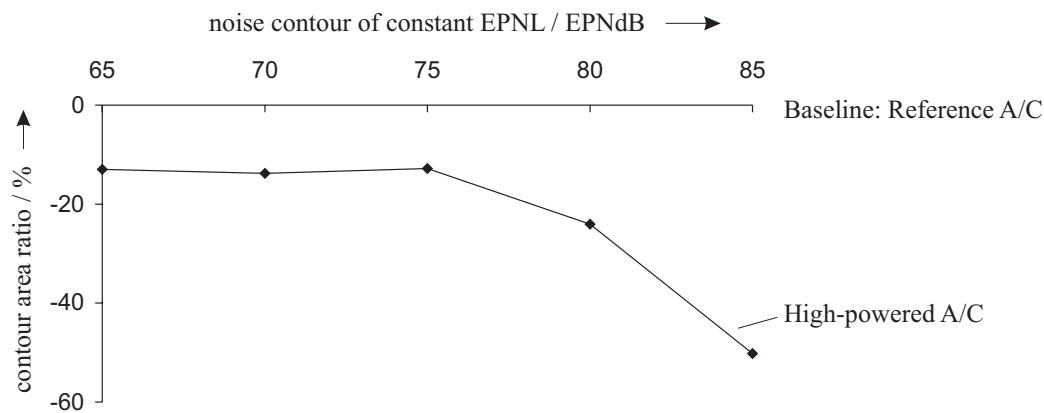
Figure 6.3   Change in noise contours of high-powered A/C with respect to reference A/C

6.2   Green Freighter Aircraft Noise Analysis

To show a further application of a noise analysis conducted by PANAM with data derived out of PrADO a conventional aircraft as used and investigated in the Green Freighter project has been chosen. The Green Freighter is a joint research project of Hamburg University of Applied Sciences, IFL, Airbus Deutschland GmbH and Bishop GmbH. Conventional as well as unconventional aircraft configurations are taken into consideration with the main focus on environmentally friendly and economic aircraft operation. One of the challenges to be met is low noise impact on ground during night operations that becomes especially important for aircraft freighters (**Scholz 2008**). The Green-Freighter is a twin engine, subsonic cargo aircraft with 330 tons maximum take-off weight, 110 tons maximum payload and a design range of about 8850 km. Maximum cruise speed is Mach 0.84 and the aircraft is powered by two turbofan engines with a static thrust of about 489 kN comparable to a GE90 engine (depicted in figure E.29). By considering such a big aircraft, semi-empirical noise source models in PANAM that are based on an aircraft, comparable in size and thrust to the reference aircraft as used in this thesis, may not be able to deliver accurate sound levels. This is the first time that sound source models are tested beyond their range of applicability.

For the GE90 engine rotor stator spacing and hub-to-tip ratio have been derived out of a cross-sectional drawing from **Stanford 2008**. The fan blade exit flow angle has been slightly adjusted to $\zeta = 37°$ resulting in the same maximum fan rotational speed range ± 10 % N1 as above. Primary jet velocity v_9 as well as primary- and secondary nozzle areas A_{19} and A_9 have been accepted as derived out of PrADOs engine cycle analysis although the discrepancy in the calculated fan area A_{fan} and the primary nozzle area A_{19} seems to be too high. However, a fully expanded jet comprises a somewhat smaller cross sectional area and secondary nozzle area A_{19} does not include primary nozzle area A_9.
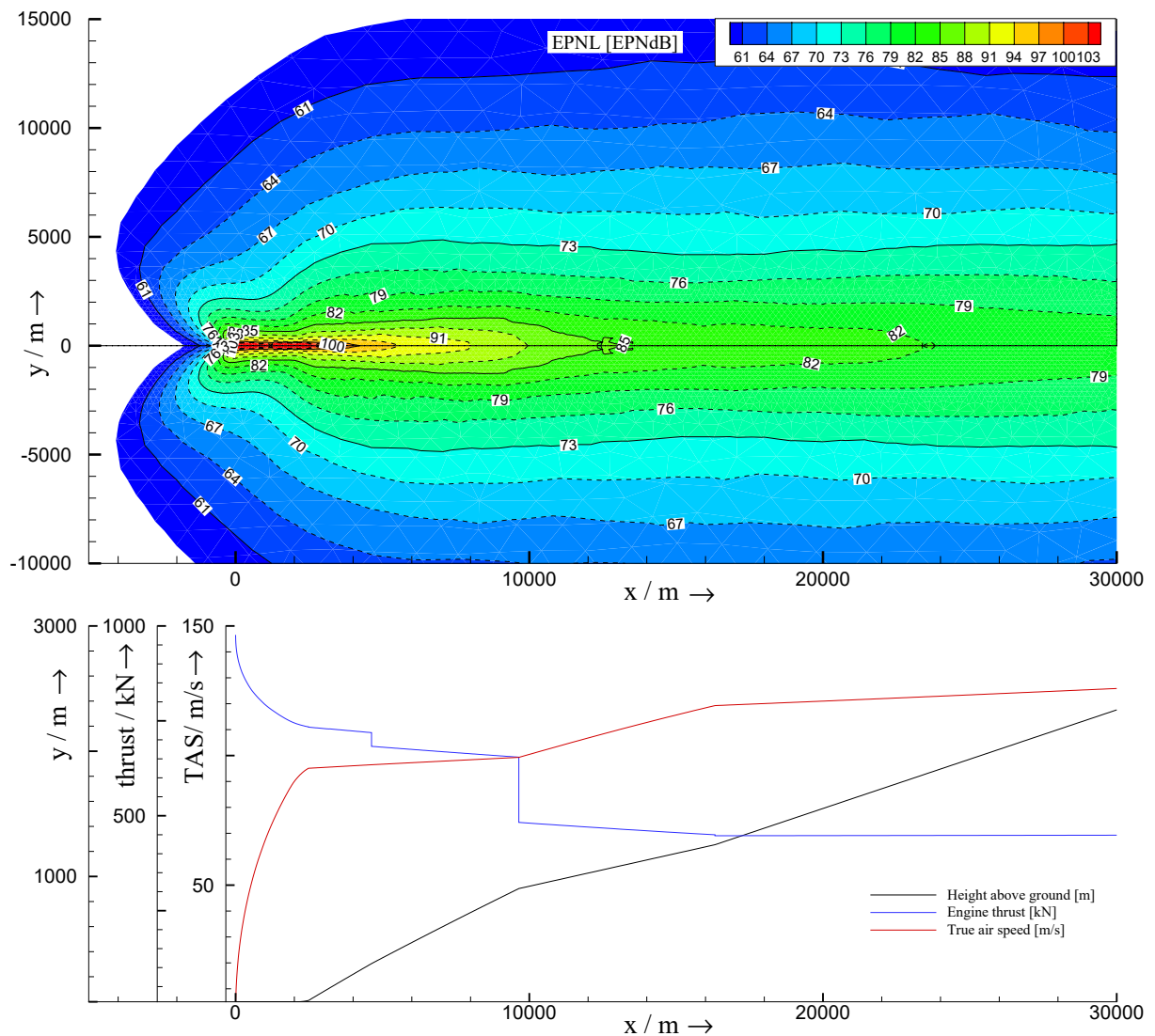
Figure 6.4   Noise contour plot in EPNL; departure of Green Freighter

The flight trajectory for the green freighter has been chosen according to a suggested noise abatement departure procedure as in **ICAO 2007** (page 13, profile 13). The aircraft takes-off with take-off power in take-off configuration (flaps deployed 10° and slats 18°) and climbs

with maximum climb angle to 3000 ft where a cutback is performed. In contrast to the afore prescribed modified ATA-procedure for short- to medium range aircraft the aircraft here changes from take-off power to climb power (approximated by $\tau = 0.95$) at 1000 ft. After cutback the aircraft accelerates in a clean configuration to 250 kts with a reduced climb angle before it then goes into the constant speed climb as depicted in figure E.30.

Noise analysis results are depicted in figures 6.4 and E.31. Again, contour plots have been cut along the *x*-axis and obtained SPL(A) or EPNL split into major noise contributors. SPL(A) are to be found in figure E.32 and EPNL in figure E.33. Noise contour areas of the green freighter during departure are summarized in table 6.3.

6.3   Verifications with ICAOs Noise Data Base

Noise analysis of the Green Freighter for a departure indicates valuable results especially when comparing calculated EPNLs at the aircraft noise certification flyover point with ICAO aircraft noise certification measurement results (**ICAO 2008a**) of an aircraft similar in weight and engine thrust (table 6.4). Flyover EPNL is almost identical whereas the calculated sideline EPNL is below the reference value. Sideline reference is the greatest noise level along the displaced runway centre line during departure (**FAR Part 36**, A36.9.2.1(b)).

Table 6.4   Comparison of calculated EPNL with ICAO reference levels

Aircraft type	EPNL at noise certification reference positions					
	Flyover calculated EPNdB	Flyover ICAO EPNdB	Sideline calculated EPNdB	Sideline ICAO EPNdB	Approach ICAO EPNdB	ICAO ID[b] -
Reference A/C	90.8	85.5[a]	93.8	94.9	96.1	AIRBUS_10519
High-powered A/C	86.8	x	92.0	x	x	no A/C found
Green Freighter	92.6	91.5	92.0	99.3	99.7	BOEING_13746

Notes:

[a]   aircraft with 118 kN engine thrust and 70 tons MTOW

[b]   Identification number for document used (**ICAO 2008a**)

Although the trajectory for flyover measurements, as stated in relevant wordings of law (figure D.14), seems to be identical at least in the procedure, no information can be extracted out of **ICAO 2008a** during which departure noise measurements have been conducted. As a

matter of fact, ICAOs certification reference values should be used solely as approximate levels of reference. EPNL values during approach as mentioned in table 6.4 are for information only since no comparison should be made with flyover- and sideline reference values that are a result of a departure.

Verification of noise analysis results of the short- to medium range aircraft with ICAOs noise data base is virtually not possible since no reference aircraft has been found in the database similar in aircraft mass and engine thrust. Nevertheless, the difference in 5 EPNdB (table 6.4) at flyover is significant when comparing flyover levels with an aircraft of at least similar aircraft mass. On the other hand, the ICAO trajectory used for noise measurements is in this case also unknown. No related aircraft configuration has been found for the high-powered aircraft as investigated in this thesis.

6.4   Directivity Plots

Directivity characteristics of fan, jet and airframe source models are dissociated from the overall resulting directivity (figures E.35 through E.48). Fan noise radiates in all directions and remains significant either with the engine at full thrust or at idle. Comparison of the derived directivity is possible with the directivity correction for fan noise according to **Heidmann 1979** as depicted in figure D.12. Jet noise, on the contrary, radiates largely backwards, gets heavily influenced by thrust setting and almost diminishes with the engine at idle. Comparisons of obtained directivities are possible with directivities after **Stone 1983** as depicted in figure D.13. In depicted figures, the strong influence of the airspeed upon airframe noise becomes clearly visible and indicates how important airframe noise can become at high airspeeds especially during idle descent. A shape of a dipole is recognizable that is probably due to slat noise modelling. Consequences of convective amplification upon directivities can be identified. A further discussion is provided below the figures in appendix E.1.

7   Discussion

Short- to medium range aircraft configurations

Engine thrust has been altered in order to evaluate the influence of an increased maximum climb-angle on noise impact on ground during take off. The modified ATA-procedure can be flown with reduced thrust that reduces noise radiating from the engines. Thus, take-off distance increases and the aircraft fly-over altitude decreases due to a reduced climb angle and a longer take-off run. Less thrust at lower altitudes is opposed to noise impact on the ground. To overlook the influence of the maximum climb-angle on noise impact on the ground, both aircraft have been considered to operate at maximum continuous thrust during their initial climb segment. As discussed in the preceding chapter, the first climb segment is performed with maximum available excess power and not with the maximum rate of climb (figures E.11 through E. 14). Equation 4.23 shows that the rate of climb is linear dependent on the airspeed. Increasing the airspeed above v_{H35} reduces excess power and thus maximum climb angle. The rate of climb, though, is still increasing until reaching a higher airspeed than v_{H35}. This is because airspeed exerts a strong influence upon the rate of climb. For our case, however, a greater rate of climb is not desirable (on a first proposal) since a downsized maximum climb angle decreases the distance between aircraft and observer. As a result, the first climb segment is conducted with maximum available excess power and not at maximum rate of climb because it is expected to influence the noise impact on ground in a positive way by bringing the aircraft far from the ground as quickly as possible. In contrast, an acceleration of the aircraft up to the airspeed for maximum rate of climb would take place above the runway where noise is not so keenly punished. So acceleration close to the ground with a following steep climb segment with maximum rate of climb could also show noise reduction capabilities.

The high-powered aircraft produces smaller EPNL noise contour areas on the ground compared with the reference aircraft especially for high EPNLs. Noise contours during the first climb-segment are more compact in the area of x = ±5 km. This is because the high-powered aircraft reaches cutback altitude at a lesser flyover distance on ground. The reference aircraft performs its cutback in a 20 % decrease in engine thrust. In contrast, the high-powered aircraft decreases thrust by 40 %. Here, it has to be mentioned that both engines feature identical maximum rotor-tip Mach numbers at fan design point M_{TRD}, primary- to secondary

jet area ratios A_{19}/A_9 (absolute values scaled by 40 % according to the suggested fan diameter increase) and the same margin for primary jet velocities v_9 (both engines have been adapted to values of the DLR engine map). Decreasing engine thrust by 40 % and fan rotational speed by, say, 40 % reduces the rotor-tip relative Mach number and therefore the discrete tone noise radiating from the fan. A cutback of about 20 % as performed for the reference aircraft also reduces the fan noise but compared to the cutback of 40 % the fan noise is significantly higher. This effect is additionally provoked by a lower altitude of the reference aircraft (figures E.17 through E.20 for SPL(A) and figures E.22 through E.25 for EPNL). Jet noise for the high-powered aircraft is lower, which is in accordance with fan noise results. The difference in jet noise between both aircraft seems to be higher although absolute jet areas are greater compared to those of the reference engine. Therefore, the influence must originate from a reduced jet velocity. Again, jet velocities are lower for the high-powered aircraft because of the cutback of 40 % in engine thrust. Therefore, jet noise is significantly lower. In contrast, the airframe noise of the high-powered aircraft is higher although the distance to the observer is greater compared with the reference aircraft. Geometrical dimensions are the same for both aircraft. Wing loading (that is also an input parameter for airframe noise prediction) is however slightly increased for the high-powered aircraft. Thus, those parameters cannot be responsible for the depicted difference in airframe noise. As a matter of fact, the airspeed is the driving parameter, which is scaled to at least to the power of five for calculating SPLs, and higher after the cutback for the high-powered aircraft.

Above mentioned results are reflected in calculated SPL(A) as well as EPNL at flyover as well as along sideline reference. Very high discrepancies (figure E.17) during the take-off roll ($x = 0$ to $x = 2$ km) are a result of inaccuracies in calculated engine parameters and source modelling. Source models in PANAM are designed for the acoustic far field only, which is not the case with the aircraft close i.e. the source close to the observer or microphone. However, discrepancies emerging from predicted fan rotational speed could have a greater influence upon this characteristic. Other minor discontinuities in two-dimensional SPL(A) noise plots along the x-axis are possibly due to the Doppler effect and resulting one-third octave band frequency jumps. Those discontinuities are smoothed in EPNL plots.

A later investigation of the reference aircraft with engine map results out of PrADO showed that the influences on discrepancies on jet noise are in this case of negligible amplitude for aircraft preliminary design. In figure E.26 it can be seen that in the vicinity of break release

SPLs(A) radiating from the reference aircraft with no changes in the engine map are approximately 2 dBA higher compared to SPLs(A) of the reference aircraft with the PrADO engine map adapted to the DLR engine map. This discrepancy diminishes with an increasing x-coordinate. Overall sound levels (SPL(A) or EPNL) are almost not affected by this over prediction of jet noise (figures E.26 through E. 28).

Absolute predicted EPNL at flyover are too high for the reference aircraft. Here, it has to be mentioned that the trajectory used for flyover measurements is unknown. However, computed contour areas are comparable to those of the Green Freighter. Therefore, computed noise levels are actually too high for this aircraft. This might be due to an over prediction of engine noise out of implemented source models in PANAM (see chapter 3.2.1, validation of PANAM) and also due to the fact that the reference aircraft could not have been found in the ICAO database with its overall mass and engine thrust. Thus, the reference aircraft might be equipped with too small engines. EPNLs for the high-powered aircraft would better agree with ICAOs reference levels.

Green Freighter aircraft

Calculated EPNL at flyover for the Green Freighter is very close to the ICAO value in contrast to the calculated EPNL at sideline. Responses of altered thrust, height and airspeed are clearly visible in the SPL(A) plot in figure E.31. Obtained results of jet noise seem to be too low. Out of figures E.32 and E.33 it can be seen that the jet noise is approximately 15 EPNdB under fan and airframe noise. Thus, having sound pressure summation on an energy basis in mind, jet noise could actually in this case be energetically neglected. Overall sound pressure levels might not change after such an action. This under prediction of jet noise (figure E.33) might be the reason for a calculated sideline EPNL being 7 EPNdB lower than the ICAO level (table 6.4). In contrast, with a higher jet noise EPNL at flyover also raises. Again, the trajectory used for flyover measurements is unknown which has to be kept in mind when comparing those sound levels. As a conclusion, on the one hand jet noise is seen as one of the major contributors to aircraft noise and is therefore in our case under predicted. On the other hand no information has been found in literature that clearly indicates that jet noise must be of at least the same amplitude as fan noise especially for a modern turbofan engine with a high bypass ratio like the GE90.

When comparing figure E.32 with E.17 it is identifiable that more discrepancies can be found in sound pressure levels of the Green Freighter. Slight peaks in the curve (especially for airframe noise levels at $x = 16$ km) are a result of sharp changes in the trajectory. This effect could not be explained at first view and requires further discussion and investigation. Those very little in amplitude but frequent discrepancies between $x = 10$ km and $x = 16$ km are because of the accelerating climb. Due to a constant increase in aircraft speed the program might switch from a given line in the engine map to a following line reserved for a higher Mach number. Therefore, discrepancies in the engine map, especially, in fan rotational speed become here in this case clearly visible. The slope of the three (fan, jet and airframe) curves in SPL(A) exhibit an identical slope between $x = 2$ km and $x = 10$ km along $y = 0$. At sideline the curves are disordered and exhibit an uncorrelated behaviour. This might be due to changed lateral directivities that are influenced e.g. by the dipoles of airframe noise source models.

General

It is interesting to see that noise radiating from the fan is in all cases determining (figures E.17 and E.32) and is additionally almost not affected by the cut-back. Primary and secondary jet velocities have been calculated with PrADO. In the case of the two short- to medium range aircraft jet velocities seemed to be too high and have been adapted to lower values (similar to those of the DLR engine map). For the Green Freighter, however, computed jet velocities out of PrADO appeared to be useful and have therefore been accepted and used for noise analyses. In the first case jet noise levels are predicted comparable to fan noise levels during the first climb segment. In the second case, jet noise sound levels seem to be too low during the initial climb segment. Here, airframe noise is more dominant and almost at the same level of fan noise that could also be a reason of an inaccuracy of predicted airframe noise with semi-empiric noise source models that are based on noise measurements of an Airbus A319. On the other hand the Green Freighter features greater high-lift devices, wings, landing gear lengths, etc. which would actually be in accordance with a significant higher predicted airframe noise. Positive to see is that airframe noise levels are in both cases decreasing at the cut-back because at this point the aircraft is in a clean configuration with no slats or flaps deployed. With an increasing airspeed the airframe noise levels are however increasing again and become decisive with the aircraft far from the runway. In conclusion, as long as no direct relations between fan-, jet- and airframe noise levels are known (at least not found in available literature), it cannot be said which levels are predicted more or less accurate. In first instance, relevant output parameters of PrADO (primary- and secondary jet velocities and

nozzle areas, fan rotational speed, etc) must be scrutinised for each individual type of engine. Secondly, the prediction capability of larger aircraft with the help of noise source models in PANAM that are based on Airbus A319 noise measurement results must be further investigated.

8 Summary and Concluding Remarks

The built interface necessary for the interconnection of PrADO and PANAM was derived by applying the generally accepted formulas that have been adapted to meet specified requirements. A thorough explanation of necessary assumptions and their associated effects upon predicted noise levels is the result of that adaptation. The derived interface is usable and offers a possibility for further investigations in the related topic of aircraft noise reduction on a generic level.

The effective perceived noise level is a result of the former D-weighting and judges aircraft noise in terms of annoyance where perceived loudness is used as a basis. OASPLs(A) are approximately 10 dB higher than calculated EPNLs. Noise source models as used in PANAM are described either as acoustic monopoles or dipoles or use predefined parametric characteristic directivities. Out of considered sound propagation effects, the response of convective amplification is directly reflected in two-dimensional noise contour plots.

PANAM in the current version is able to evaluate aircraft noise of conventional aircraft configurations with one horizontal tailplane. Implemented source models provide at first appearance valuable results in noise impact on ground regardless of aircraft size.

Inaccuracies in computed fan rotational speed are the result of treating the fan flow isobar and isentropic and a further assumption of a constant exit flow angle at the fan blade trailing edge. Repercussions of that are kept within limits for the prediction of overall sound pressure levels. Maximum climb angle is observed throughout climb trajectory calculations and exhibits no direct influence upon predicted sound impact on ground whereas discontinuities in the trajectory are reflected in relevant noise contours.

Fan blade tip speed, primary- and secondary jet velocities as well as cross sectional areas are decisive for engine noise prediction. The former can be adapted to meet approximate maximum levels by accommodating the exit flow angle. For the latter, results out of PrADO are to be surveyed before conducting a noise analysis.

Due to the definition of segmented departure trajectories various noise abatement procedures can be designed and evaluated. Prerequisites to adapt for approach trajectories have been created.

A drastic reduction in noise impact on ground can be achieved by keeping the propulsion system at a lower level. Jet noise gets positively, heavily influenced with the engine running at lower thrust settings whereas fan noise remains dominant. A positive influence on airframe noise can be exerted by lowering the airspeed.

Changes in aircraft configuration, condition and performance are reflected in noise contour areas. By using the scale of effective perceived noisiness, changes in noise contours are diminished but still enough in magnitude to be directed as an objective function into multidisciplinary optimization.

Bearing all aspects and limitations in mind, with the help of the derived interface it is now possible to investigate interactions of noise reduction at source, modification of aircraft design parameters and aircraft performance at the same time. For the conceptual status of aircraft preliminary design, the evaluation of differences in noise contour areas is satisfactory for an optimization process. Thus, tendencies can be demonstrated and influences of perceived noise exerted on the overall system aircraft evaluated. As a conclusion, a balanced approach towards aircraft noise reduction can now be implemented.

Acknowledgements

References

ACARE Report 2001 ADVISORY COUNCIL FOR AERONAUTICS RESEARCH IN EUROPE: The Challenge of the Environment. In: Strategic Research Agenda 1, Vol. 2 (ACARE Report). Brussels : ACARE, 2002 – URL: http://www.acare4europe.org (2008-07-23)

Airbus 2007 AIRBUS. Working Towards Greener Skies : The Airbus Family. Blagnac Cedex : Airbus S.A.S., 2007 (information brochure)

ANSI 1995 Standard ANSI S1.26-1995 (R2004). *Method for Calculation of the Absorption of Sound by the Atmosphere*. Abstract available under URL: http://webstore.ansi.org/ (2008-06-25)

Bertsch 2007 BERTSCH, Lothar; DLR, Inst. of Aerodynamics and Flow Technology: Stand der Arbeiten zur akustischen Bewertung von Flugzeugkonfigurationen im Projekt QSTOL. Köln : DLR Braunschweig, 2007 (IB 124-2007/4). - Technical Report

Bertsch 2008 BERTSCH, Lothar; DOBRZYNSKI, Werner; GUÉRIN, Sebastian. In: 29TH AIAA AEROACOUSTICS CONFERENCE: Tool Development for Low-Noise Aircraft Design (Vancouver 2008). Vancouver : AIAA, 2008 (AIAA 2008-2995)

Bertsch 2008a BERTSCH, Lothar; KRAMMER, Philip; DLR, Inst. of Aerodynamics and Flow Technology: PANAM – a noise prediction tool for conceptual aircraft design. Köln : DLR Braunschweig, 2008 (IB 124-2008/902). Technical Report

Bies 2003 BIES, David A.; HANSEN, Colin H.: *Engineering Noise Control* : *Theroy* and *Practice*. London : Spon Press, 2003

Blauert BLAUERT, Jens; XIANG, Ning.: *Acoustics for Engineers*. Berlin : Springer, 2008

Bräunling 2001 BRÄUNLING, Willy J.G.: *Flugzeugtriebwerke*. Berlin : Springer, 2001

Clean Sky 2008 URL: http://www.cleansky.eu (2008-07-21)

CONCAWE 1981 Conservation of Clean Air and Water in Europe: *The Propagation of Noise from Petroleum and Petrochemical Complexes to Neighbouring Communities*. Report 4/81, 1981; URL: http://www.concawe.org (2008-06-25)

Crichton 2007 CRICHTON, Daniel: *Fan Design and Operation for Ultra Low Noise*. Cambridge, University of Cambridge, Dept. of Eng., Dissertation, 2007

DIN 45630 1971 Standard DIN 45630 December 1971. Grundlagen der Schallmessung : Physikalische und subjektive Größen von Schall

DIN 66261 1985 Standard DIN 66261 November 1985. Information Processing; Nassi-Shneidermann flowcharts symbols

DIN 9300 1990 Standard DIN 9300 October 1990. Aerospace; Concepts, quantities and symbols for flight dynamics; Aircraft motion relative to the air; ISO 1151-1 : 1988 modified

DLR Annual Report 2007 DEUTSCHES ZENTRUM FÜR LUFT UND RAUMFAHRT: Annual Analyses of the European Air Transport Market – Annual Report 2007. Köln : DLR, 2008

DLR News May 2008 DEUTSCHES ZENTRUM FÜR LUFT UND RAUMFAHRT: DLR Nachrichten – Das Magazin des Deutschen Zentrums für Luft- und Raumfahrt, May 2008. Köln : DLR e.V. in der Helmholtz-Gemeinschaft, 2008

DLR Report 2008   DEUTSCHES ZENTRUM FÜR LUFT UND RAUMFAHRT: Status report of the Institute of Aerodynamics and Flow Technology (AS). Braunschweig : DLR, 2008

Dowling 2006   DOWLING, Ann: Convective *Amplification of real simple sources*. In: JOURNAL OF FLUID MECHANICS DIGITAL ARCHIVE: Eng. Dept. Univ. of Cambridge : Camb. Univ. Press, 2006 – Abstract available under URL: http://www.journals.cambridge.org (2008-06-25)

Dunn 1973   DUNN D.G.; PEART N.A.: Boeing Commercial Airplane Company: Aircraft Noise Source and Contour Estimation. Seattle : Boeing Commercial Airplane Company, 1973 (Boeing D6-60233; NASA CR-114649). – Prepared for Ames Research Center, NASA. – referred to as "The Boeing Ames Method"

EN 61672-1 2003   Standard DIN EN 61672-1 October 2003. *Electroacoustics - Sound level meters - Part 1 : Specifications*

EN ISO 266 199   Standard EN ISO 266 May 1997. *Acoustics : Preferred frequencies*

FAA E28NE 1998   U.S. Dept. of Transportation, Federal Aviation Administration FAA: Type Certificate Data Sheet E28NE, 1998. – URL: http://www.content.airbusworld.com/SITES/Certification_Register/PDF-tcds/CFMI/CFM56-5-5A_US.pdf (2008-07-18)

FAA E37NE 1996   U.S. Dept. of Transportation, Federal Aviation Administration FAA: Type Certificate Data Sheet E37NE, 1996 – URL: http://www.airbusworld.com (2008-08-01)

FAR Part 36   FEDERAL AVIATION ADMINISTRATION: *Noise Standards : A/C Type and Airworthiness Certification*. Dept. of Transportation, Subchapter C: Aircraft, Part 36; Washington D.C. – URL: http://www.faa.gov/ (2008-06-18)

Farokhi 2008   FAROKHI, Saeed: *Aircraft Propulsion*. Hoboken, NJ : Wiley, 2008

Fleming 2008   FLEMING, Gregg; MALWITZ, Andrew; BALASUBRAMANIAN, Sathya; et al.: Trends in Global Noise and Emissions from Commercial Aviation for 2000 through 2025. In: EUROCONTROL: *7th USA/Europe Air Traffic Management R&D Seminar* (*Barcelona 2007*). Brussels : EUROCONTROL, 2008 – URL: Spiegel Online 2008

Franosch 2003   FRANOSCH, Jan-Moritz P.; KEMPTER, Richard; FASTL, Hugo; et al.: Zwicker Tone Illusion and Noise Reduction in the Auditory System. In: The American Physical Socitey : *Physical Review Letters, Vol. 90, No. 17.* Baltimore : APS 2003 (DOI: 10.1103/PhysRevLett.90.178103)

Geoffrey 2004   GEOFFREY, A. Hill; OLSON, Erik D.: Applications of Response Surface-Based Methods to Noise Analysis in the Conceptual Design of Revolutionary Aircraft. In: AIAA: *10th AIAA/ISSMO Multidisciplinary Analysis and Optimization Conference* (*New York 2004*). Reston : AIAA, 200, pp. 1556-66

Heidmann 1979   HEIDMANN, Marcus F; NASA, Lewis Research Center: Interim Prediction Method for Fan and Compressor Source Noise. Washington, DC : NASA, 1979 (NASA TM X-71763). – Technical Memorandum

Heinze 1994   HEINZE, Wolfgang; Zentrum für Luft- und Raumfahrttechnik, Technische Universität Braunschweig: Ein Beitrag zur quantitativen Analyse der technischen und wirtschaftlichen Auslegungsgrenzen verschiedener Flugzeugkonzepte für den Transport großer Nutzlasten. Braunschweig : 1994 (94-01)

Heinze 2004   HEINZE, Wolfgang; ÖSTERHELD, C.M.; HORST, P.: *Multidisziplinäres Flugzeugentwurfsverfahren PrADO- Programmentwurf und Anwendung im Rahmen von Flugzeug-Konzeptstudien.* TU Braunschweig, Inst. of Aircraft Design and Lightweight Structures, Braunschweig : 2004 - PrADO software documentation.

Huff 2007   HUFF, Dennis L.; NASA, John H. Glenn Research Center: Noise Reduction Technologies for Turbofan Engines. Washington DC : NASA, 2007 (NASA/TM-2007-214495) – http://gltrs.grc.nasa.gov/

ICAO 2007   INTERNATIONAL CIVIL AVIATION ORGANIZATION: Review of Noise Abatement Procedure Research & Development and Implementation Results : Discussion of Survey Results. Preliminary ed., Montréal : ICAO, 2007 – URL: http://www.icao.int/env/ReviewNADRD.pdf

ICAO 2008   INTERNATIONAL CIVIL AVIATION ORGANIZATION: Balanced Approach to Aircraft Noise Management. Montréal : ICAO, Air Transport Bureau, Environmental Unit, Aircraft Noise – URL: http://www.icao.int/icao/en/env/noise.htm (2008-07-23)

ICAO Annex 16 1989 INTERNATIONAL CIVIL AVIATION ORGANIZATION: Excerpts of ICAO Annex 16. In: SMITH, Michael J.T.: *Aircraft Noise*. Cambridge : Cambridge Univ. Press, 1989, pp. 301-18

ICAO 2008a   INTERNATIONAL CIVIL AVIATION ORGANIZATION: ICAO Noise Data Base. Montréal : ICAO – URL: http://noisedb.stac.aviation-civile.gouv.fr/find.php (2008-08-18)

Ishii 2005   ISHII, Hirokazu; GOMI, Hiromi; OKUNO, Yoshinori: Flight Tests of Helicopter Noise Abatement Operations. In*: 31st European Rotorcraft Forum* : 2005

ISO 9613-1 1993   Standard DIN ISO 9613-1 June 1993. Acoustics - Attenuation of sound during propagating outdoors. Part 1: Calculation of the absorption of sound by the atmosphere

ISO 9613-2 1999   Standard DIN ISO 9613-2 October 1999. Acoustics – Attenuation of sound during propagation outdoors. Part 2: General method of calculation

Kollmeier ca. 2006   KOLLMEIER, Birger: *Erzeugung, Ausbreitung, Messung und Bewertung von Schall.* Oldenburg, University Oldenberg, Institut of Physics, Lecture Notes, ca. 2006 – URL: http://medi.uni-oldenburg.de/download/docs/lehre/kollm_phystechmed_akustik/aku2.pdf (2008-06-20)

Lamancusa 2000   LAMANCUSA, J.S.: *Engineering Noise Control : Noise Metrics and Regulations.* Pennsylvania State University, lecture notes, 2000. – URL: http://www.mne.psu.edu/lamancusa/me458/ (2008-06-18)

LAnAb 2007   BUNDESMINISTERIUM FÜR WIRTSCHAFT UND TECHNOLOGIE: *Lärmoptimierte An- und Abflugverfahren (LAnAb) – Zusammenfassender Schlussbericht.* In: Forschungsverbund Leiser Verkehr, Projekt 1600 Lärmoptimierte An- und Abflugverfahren. Berlin : 2007

Le Duc 2008   LE DUC, A.; SPIEGEL, P.; GUNTZER, F.; et al.: Simulation of complete helicopter noise in maneuver flight using aeroacoustic flight test database. In: American Helicopter Socitey: 64th Annual Forum and Technological Display. Montréal : 2008

Leifsson 2005   LEIFSSON, Leifur T.: *Multidisciplinary Design Optimization of Low-Noise Transport Aircraft.* Blacksburg, Virginia Polytechnic Institute and State University, Aerospace Engineering, Dissertation, 2005

Leifsson 2006   LEIFSSON, Leifur T.; MASON, William H.; SCHETZ, Joseph A.; et al.: Multidisciplinary Design Optimization of Low-Airframe-Noise Transport Aircraft. In: AIAA: *44th AIAA-Aerospace Sciences Meeting and Exhibit* (*Reno Nevada 2006*). Reston : AIAA, 2006

Lockard 2004   LOCKARD, Daniel P.; LILLEY, Geoffrey M.: NASA Langley Research Center : The Airframe Noise Reduction Challenge. Washington DC : NASA, 2004 (NASA/TM-2004-213013) – http://naca.larc.nasa.gov/

Mattingly 1996   MATTINGLY, Jack D.: *Elements of Gas Turbine Propulsion*. New York : McGraw-Hill, Inc., 1996

Maughan 1987   MAUGHAN, C.; CHADHA, G.: *The Acoustic Doppler Effect*. In: INSTITUTE OF PHYSICS ELECTRONIC JOURNALS: Physics Education 22, No. 4, July 1987, pp. 256-258. URL: http://www.iop.org/EJ (2008-06-25)

Merziger 1999   MERZIGER, Gerhard; WIRTH, Thomas: *Repetitorium der Höheren Mathematik*. Hannover : Binomi, 1999

Mistry 2007   MISTRY, S.; SMITH, H.; FIELDING, J.P.: Development of Novel Aircraft Concepts to Reduce Noise and Global Warming Effects. In: AIAA: *7th AIAA Aviation Technology, Integration and Operations Conference* (*Belfast 2007*). Reston : AIAA, 2007, pp. 593-601 (Report No. AIAA 2007-7753)

Norton 1989   NORTON, Michael P.: *Fundamentals of noise and vibration analysis for engineers*. Cambridge : Cambridge Univ. Press, 1989

Olson 2006   OLSON, Erik D.; MAVRIS, Dimitri N.: Aircraft Conceptual Design and Risk Analysis Using Physics-Based Noise Prediction. In: AIAA: *12th AIAA/CEAS Aeroacoustics Conference* (*Cambridge Massachusetts 2006*). Reston : AIAA, 2006

Phillips 2004   PHILLIPS, Warren F.: *Mechanics of Flight*. New Jersey : Wiley, 2004

Pott-Pollenske 2006   POTT-POLLENSKE, Michael; DOBRZYNSKI, Werner; BUCHHOLZ, Werner; et al.: Airframe Noise Characteristics from Flyover Measurements and Predictions. In: AIAA/CEAS: *Aeroacoustics Conference 2006*. Reston : AIAA, 2006, Paper 2006-2567

Raymer 1999   RAYMER, Daniel P.: *Aircraft Design : a conceptual approach*. 3rd ed. Reston : AIAA Education Series, 1999

Roux 2007   ROUX Élodie: *Turbofan and Turbojet Engines : Database Handbook*. Blagnac: Éditions Élodie Roux, 2007

Scholz 1999   SCHOLZ, Dieter: *Lecture Notes in Aircraft Design*. Hamburg, Hamburg University of Applied Sciences, Dept. of Automotive and Aeronautical Engineering, lecture notes, 1999

Scholz 2008   AERO – AIRCRAFT DESIGN AND SYSTEMS GROUP: *The Green Freighter Project*. Hamburg University of Applied Sciences, Faculty of Eng. and Computer Science, Dept. of Automotive and Aeronautical Eng. Research Focal Point Aeronautical Eng. – URL: http://gf.profscholz.de/ (2008-08-17)

Silent Aircraft Initiative 2008 URL: http://silentaircraft.org/ (2008-07-21)

Smith 1989   SMITH, Michael J.T.: *Aircraft Noise*. Cambridge : Cambridge Univ. Press, 1989

Snecma 2007   SNECMA – SAFRAN GROUP: About SILENCE(R). Courcouronnes, France : Snecma – SAFRAN Group, 2007, URL: http://www.snecma.com//IMG/pdf/Fact_sheet_Silencer_programme_ OK.pdf (2008-07-21)

SOURDINE 2008   SOURDINE (Study of Optimisation procedURes for Decreasing the Impact of NoisE. URL: www.sourdine.org (2008-07-21)

Spiegel Online 2008   SPIEGEL ONLINE: CO2-Ausstoß der Luftfahrt könnte dramatisch ansteigen. Hamburg : Spiegel Verlag, May 2008 – URL: http://www.spiegel.de/wissenschaft/mensch/0,1518,552002,00.html (2008-07-23)

Stanford 2008   STANFORD UNIVERSITY: GE90 cross-sectional drawing. Center for Integrated Turbulence Simulations. – URL: http://ctr-sgi1.stanford.edu/CITS/ge90r.jpeg (2008-08-16)

Stone 1982   STONE, James R.; GROESBECK, Donald E.; ZOLA, Charles L.: Conventional Profile Coaxial Jet Noise Prediction. In: AIAA: *7th Aeroacoustics Conference* (Palo Alto 1981). Reston : AIAA, 1982, Paper 81-1991

TecPlot 2006   Software Package. Used version: BURSTEIN, Jenya; FOWLER, Scott; HUNTER, Karen; et al.: *Tecplot 360*. Bellevue, WA : Tecplot, Inc., 2006

Truax 1999   TRUAX, Barry: *Handbook for Acoustic Ecology*. 2nd edition. Simon Fraser University, Sonic Research Studio School of Communication. Cambridge : Cambridge Street Publishing, 1999. URL: http://www.sfu.ca/sonic-studio/handbook/ (2008-06-25)

Werner-Westphal 2008 WERNER-WESTPHAL, Christian; HEINZE, Wolfgang; HORST, Peter: Multidisciplinary Integrated Preliminary Design Applied to Unconventional Aircraft Configurations. In: AIAA: *Journal of Aircraft* (*AIAA Aerospace Sciences Meeting & Exhibit Reno 2007*). Reston : AIAA, 2008, pp. 581-90 (DOI: 10.2514/1.32138)

Wilson 1989   WILSON, Charles E.: Noise Control : Measurement, Analysis, and Control of Sound and Vibration. New York : Harper & Row, 1989

Wolfe 2006   WOLFE, Joe: *Music Acoustics*. The University of New South Wales; School of Physics : 2006 - URL: http://www.phys.unsw.edu.au/ /jw/dB.html (2008-06-26)

Woodward 2004   WOODWARD, Richard P.; HUGHES, Christopher E.: NASA, John H. Glenn Research Center : Noise Benefits of Increased Fan Bypass Nozzle Area. Washington DC : NASA, 2004 (NASA TM-2004-213396) – http://gltrs.grc.nasa.gov/

X-Noise 2008   URL: http://www.xnoise.eu (2008-07-21)

Xue 2006   XUE, Min; ATKINS, Ella M.: Noise-Minimum Runway-Independent Aircraft Approach Design for Baltimore-Washington International Airport. In: AIAA: *Journal of Aircraft, Vol. 43, No. 1, January-February 2006*. Reston : AIAA, 2006

Appendices

Appendix A: Figures for Chapter 1 and Chapter 2

AIRFRAME NOISE

Main Wings

Fuselage

Spoiler

Trailing edge devices

Engine nacelle spillage at low speeds

Leading edge devices

Tailplane

Landing gear and wheelbays

Jet

Fan Inlet

Fan Exhaust

ENGINE NOISE

Trubine and Core
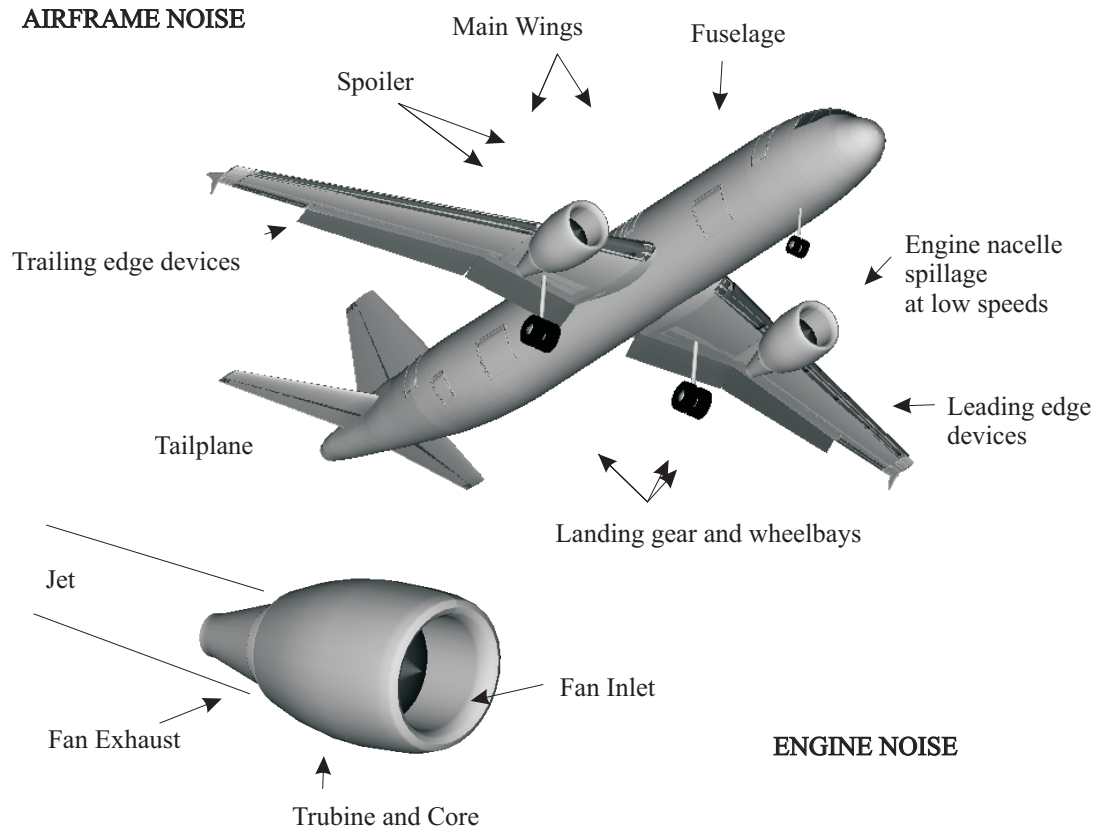
Figure A.1 Airframe and engine noise sources, adapted from **Smith 1989** (p. 42) and **Bertsch 2008** (p.14)

Figure A.2 The SAX-40 of the Silent Aircraft Initiative (from **Silent Aircraft Initiative 2008)**

Figure A.3   Model of the LNA configuration in the acoustic wind tunnel Braunschweig (from **DLR Report 2008)**
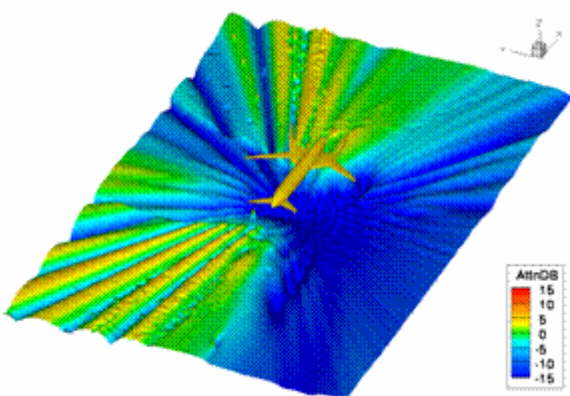
Figure A.4   Attenuation footprint (from **DLR Report 2008)**

"Attenuation footprint of source above starboard wing of full scale LNA for 314 Hz. Aircraft height 120 m, footprint size in x-y: 2 km x 1.4 km" **(DLR Report 2008)**

Appendix B: Figures and Tables for Chapter 3
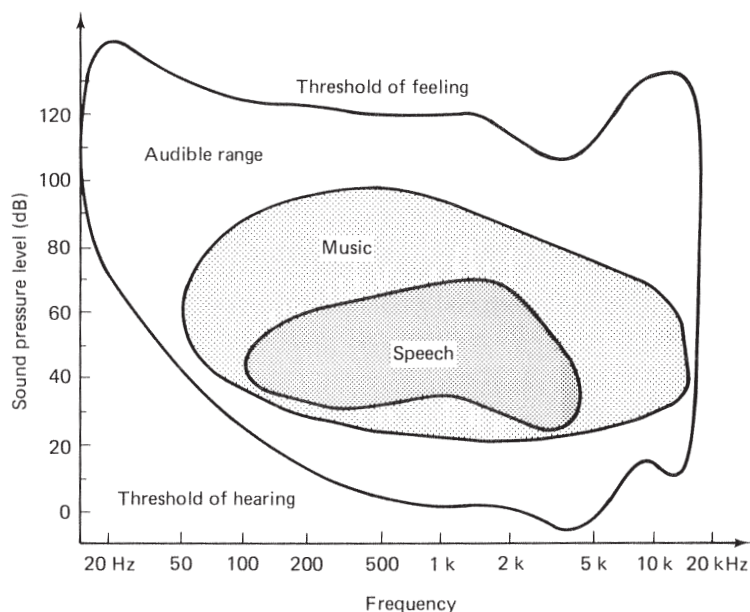
Figure B.1 "SPL v. frequency for the audible range, typical musical range, and range of speech." (from **Wilson 1989**, p. 14)

Table B.2 Perceived noisiness $n(i,k)$ as function of frequency of constant SPL's (60 dB and 90 dB). Bold values designate the maximum i.e. $n(k)$.

1/3 octave centre frequency (Hz)	$n(i,k)$ Noy at SPL: 90dB const.	$n(i,k)$ Noy at SPL: 60dB const.	multiplier m (-)	$n(i,k)*m$ (90dB)	$n(i,k)*m$ (60dB)
50	13.50	0.59	0.15	2.025	0.089
63	14.90	1.00	0.15	2.235	0.150
80	17.10	1.40	0.15	2.565	0.210
100	19.70	1.81	0.15	2.955	0.272
125	21.10	2.08	0.15	3.165	0.312
160	22.00	2.51	0.15	3.300	0.377
200	26.00	2.93	0.15	3.900	0.440
250	27.90	3.26	0.15	4.185	0.489
315	29.70	3.57	0.15	4.455	0.536
400	32.00	4.00	0.15	4.800	0.600
500	32.00	4.00	0.15	4.800	0.600
630	32.00	4.00	0.15	4.800	0.600
800	32.00	4.00	0.15	4.800	0.600
1000	32.00	4.00	0.15	4.800	0.600
1250	36.80	4.59	0.15	5.520	0.689
1600	47.60	6.01	0.15	7.140	0.902
2000	54.70	6.90	0.15	8.205	1.035
2500	62.70	7.92	0.15	9.405	1.188
3150	**67.20**	**8.49**	**1.00**	**67.200**	**8.490**
4000	67.20	8.49	0.15	10.080	1.274
5000	62.70	7.92	0.15	9.405	1.188
6300	58.60	7.39	0.15	8.790	1.109
8000	47.60	6.01	0.15	7.140	0.902
10000	38.70	4.89	0.15	5.805	0.734
x	x	x	$N(k)$:	191.475	23.3805

Table B.1   Data of A-, C-, D-weighting for the 1/3 octave band centre frequencies within the audible range and SPL data of constant perceived noisiness 0.1

One-third octave centre frequency (Hz)	A-network[a] (dB)	C-network[a] (dB)	D-network[b] (dB)	SPL (n = 0.1 Noy)[c] (dB)
10.0	-70.4	-14.3	.	-
12.5	-63.4	-11.2	.	-
16.0	-56.7	-8.5	.	-
20.0	-50.5	-6.2	.	-
25.0	-44.7	-4.4	.	-
31.5	-39.4	-3.0	-16.0	-
40.0	-34.6	-2.0	-14.0	-
50.0	-30.2	-1.3	-12.8	-49.0
63.0	-26.2	-0.8	-10.9	-44.0
80.0	-22.5	-0.5	-9.0	-39.0
100.0	-19.1	-0.3	-7.2	-34.0
125.0	-16.1	-0.2	-5.5	-30.0
160.0	-13.4	-0.1	-4.0	-27.0
200.0	-10.9	0.0	-2.6	-24.0
250.0	-8.5	0.0	-1.6	-21.0
315.0	-6.5	0.0	-0.8	-18.0
400.0	-4.8	0.0	-0.4	-16.0
500.0	-3.2	0.0	-0.3	-16.0
630.0	-1.9	0.0	-0.5	-16.0
800.0	-0.8	0.0	-0.6	-16.0
1000.0	0.0	0.0	0.0	-16.0
1250.0	0.6	0.0	2.0	-15.0
1600.0	1.0	-0.1	4.9	-12.0
2000.0	1.2	-0.2	7.9	-9.0
2500.0	1.3	-0.3	10.6	-5.0
3150.0	1.2	-0.5	11.5	-4.0
4000.0	1.0	-0.8	11.1	-5.0
5000.0	0.5	-1.3	9.6	-6.0
6300.0	-0.1	-2.0	7.6	-10.0
8000.0	-1.1	-3.0	5.5	-17.0
10000.0	-2.5	-4.4	3.4	-21.0
12500.0	-4.3	-6.2	1.4	-
16000.0	-6.6	-8.5	-0.5	-
20000.0	-9.3	-11.2	-2.5	-

Notes:

[a]   data as in **EN 61672-1 2003**

[b]   data from **Norton 1989** (p. 247)

[c]   derived out of table noys as a function of SPL in **ICAO Annex 16 1989** (Table 2-1.)
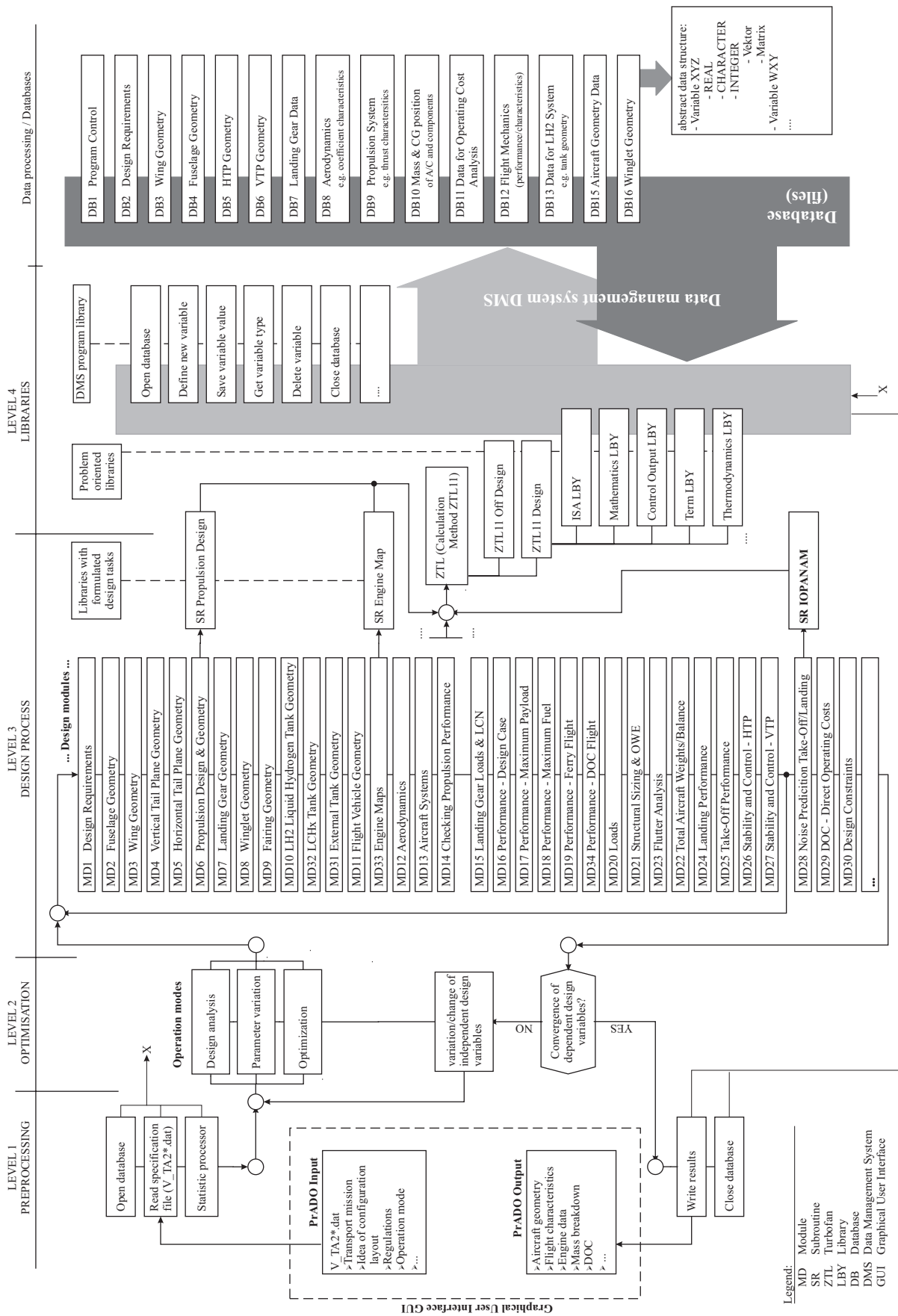
Figure B.2 PrADO process overview with an example of a possible library structure for an engine design. Figure adapted from **Heinze 1994** (pp. 191-2) and **Werner-Westphal 2008** (p. 582)

Appendix C: Figures and Tables for Chapter 4

C.1 PANAM Input Parameters

Table C.1   Requested geometrical parameters out of PrADO for A/C noise analysis with PANAM

Description	Variable name	Data of Ref. A/C	Unit	Data-base[a]	Out-put[b]
Airfoil wing					
max. wing loading/take-off	FBELS	600.0	kg/m²	15	1
max. wing loading/landing	FBELL	527.0	kg/m²	15	1
wing span	BF	33.9	m	3	1
mean aerodynamic chord/wing	TMUEF	4.2	m	3	1
medial wing sweep/leading edge LE	PHIVKF	27.5	deg	3	1
degree of occupation of wing span with LE flap	~~FNKBESF~~	0.8	-	3	0
medial dihedral angle/quarter chord line/wing	ZHI25F	4.3	deg	3	1
medial wing sweep/trailing edge TE	PHIHKF	12.3	deg	3	1
spoiler length (BF)/averaged/η-coordinate	BL_SPOI	16.6	m	calc	1
slat check/existing of slats	~~SLAT~~	1.0	-	calc	0
slat chord/averaged	SLAT_T	0.5	m	calc	1
slat length (BF)/averaged/η-coordinate	SLAT_L	26.2	m	calc	1
flap check/existing of flaps	~~FLAP~~	1.0	-	calc	0
flap chord/averaged	FLAP_T	0.9	m	calc	1
flap length (BF)/averaged/η-coordinate	FLAP_L	23.2	m	calc	1
Horizontal tailplane HTP					
span of HTP	BH	12.4	m	5	1
mean aerodynamic chord HTP	TMUEH	2.7	m	5	1
medial sweep/trailing edge/HTP	PHIHKH	12.9	deg	5	1
medial dihedral angle/quarter chord line/HTP	ZHI25H	6.077	deg	5	1
Vertical tailplane VTP					
No. of vertical tail planes VTP	~~NS~~	1.0	-	6	0
span of VTP	BS	5.9	m	6	1
mean aerodynamic chord, VTP	TMUES	4.0	m	6	1
medial sweep/trailing edge/VTP	PHIHKS	16.1	deg	6	1
medial dihedral angle/quarter chord line/VTP	ZHI25S	90.0	deg	6	1
Landing gear					
No. of nose gears	NBUG	1.0	-	7	1
No. of main gears	NHAUPT	2.0	-	7	1
length of nose gear leg/unloaded spring	BFW_L	2.3	m	calc	1
No. of axles/nose gear	BFW_NA	1.0	-	calc	1
tire diameter/nose gear	BFW_RD	0.8	m	calc	1
length of main gear leg/unloaded spring	HFW1_L	3.0	m	calc	1
No. of axles/main gear (left and right identical)	HFW1_NA	1.0	-	calc	1
tire diameter/main gear	HFW1_RD	1.2	m	calc	1
length of main gear leg/unloaded spring	~~HFW2_L~~	3.0	m	calc	0
No. of axles/main gear	~~HFW2_NA~~	1.0	-	calc	0
tire diameter/main gear	~~HFW2_RD~~	1.2	m	calc	0
chord length/wing-fusealge connection	TRF	6.1	m	3	1
Fuselage					
max. fuselage width/outer cross section	DARY	4.0	m	4	1
Engines					

Description	variable name				
No. of engines	NTW	2.0	-	8	1
Additionally needed for calculation					
Airfoil wing					
geometric vector/plan view/wing 1	R1GEOF1	vector	x	3	0
geometric data/wing 1/spar 1	SPHOF1H1	vector	x	3	0
geometric vector/front wing box/wing 1	R1GEONKF1	vector	x	3	0
geometric vector/aft wing box/wing 1	R1GEOHKF1	vector	x	3	0
rear wing box/wing 1	SPHKF1	vector	x	3	0
Landing gear					
data of i-th nose gear leg	R1BEINi	vector	x	7	0
data of i-th wheel	R1RADi	vector	x	7	0

Notes:

[a]   number of database as in figure A.2

[b]   1 indicates that the value is written into the geometric file as an output

0 indicates that output is not passed

Table C.2   Input Parameters for calculating engine noise

Description	Data CFM56-5A4	Unit	variable name		program version[a]	
			PANAM[b]	PrADO[b]	former	present
Fan and Jet Noise						
radiation angle[c]	variable	°	ang	N/A	c by PN	c by PN
no. of frequency bands[d]	27	-	TOB	N/A	s by PN	s by PN
Fan Noise						
rotor-stator spacing	2	-	RSS	N/A	s by PN	i by Pr-DB
no. of rotor blades	36 (38)		NOBLA	NFANROT	s by PN	i by Pr-DB
no. of outlet guide vanes	70		OGV	NFANSTA	s by PN	i by Pr-DB
max. fan rotor speed	78	cycles/s	n1_max	(UNDWMAXB)	s by PN	i by Pr-DB
ground effect[e]	boolean	true/false	inlet_*	N/A	c by PN	c by PN
fan total temp. rise[f]	variable	K	DTt	FanTTR	s by PN	c by Pr
design tip rel. Mach no.[g]	1.35		MTrd	-	s by PN	i by Pr-DB
tangential tip Mach no.	variable	-	Mt	(VCFAN)	c by PN	c by PN
tip relative Mach no.[h]	variable	-	MTr	(Mt,MTr)	c by PN	c by PN
total mass flow	variable	kg/s	Qm	MPKT	i fr. Map	c by Pr
rotor speed[i]	variable	cycles/s	fb (drehz1)	(XN1)	i fr. Map	c by Pr
Jet Noise						
flight velocity	variable	m/s	FlightSp*	N/A	c by PN	c by PN
temperature T18	variable	K	Tts	T9II	i fr. Map	c by Pr
temperature T8	variable	K	Ttp	T9I	i fr. Map	c by Pr
velocity v18	variable	m/s	Us	V9II	i fr. Map	c by Pr
velocity v8	variable	m/s	Up	V9I	i fr. Map	c by Pr
area A18	variable	m²	As	Q9S	i fr. Map	c by Pr
area A8	variable	m²	Ap	Q9	i fr. Map	c by Pr
additionally needed						
Hub-to-Tip Ratio	0.389	-	H2TR	HUBTOTIP	s by PN	i by Pr-DB
fan-radius of angle	0.72	m	N/A	SECTFANR	N/A	i by Pr-DB
fan blade angle	57	°	N/A	SECTFANA	N/A	i by Pr-DB

Notes:

[a]   data set(s), calculated(c) or imported(i) by PANAM (PN) or PrADO (Pr) via database (DB)

[b]   var. names in brackets not directly related – data correlation possible through simple conversion

c angle between engine centreline and vector to the observer on the ground - depending on observer array and flight position

d fixed by engine noise modules: **Heidmann 1979**, **Stone 1983**

e set; depending on present flight altitude; character name: "inlet_distortion"

f in former version set at constant 40.01K

g is not calculated and used for all frequency bands

h resulting of tangential and incident Mach number

i also referred to as blade passing frequency

Table C.3   Trajectory parameters for PANAM

Description	Unit	Variable name PANAM	Variable Name PrADO / or parameter value
Calculated:			
consecutive number	-	KPOINT	J1
Time coordinate	s	T	FLUGP(1,J1)*60
X-coordinate	m	X0ANN	FLUGP(2,J1)*1000
Z-coordinate[a]	m	Z0ANN	(FLUGP(3,J1)-HFLS)*1000
Flight-path climb angle	°	GAMANN	FLUGP(17,J1)
Inclination angle[b] (Euler)	°	ATTANN	FLUGP(21,J1)+FLUGP(17,J1)
True Air Speed TAS	m/s	CV0ANN	FLUGP(5,J1)/3.6
Engine thrust	N	SCHUB	FLUGP(12,J1)*1000
Gear position	-	IDGEAR	IDGEAR(J1)
Flaps	°	FLAP	XFLAP(J1)
Slats	°	SLAT	XSLAT(J1)
Set at constant value:			
Y-coordinate	m	Y0ANN	0
Air-path bank angle	°	BANANN	0
Azimuth angle (Euler)	°	DIRANN	90
Flight-path azimuth	°	CRSANN	90
Wind angle	°	WINANN	0
Wind velocity	m/s	VW	0
Acceleration	m/s²	AGC	0
Arc length (projected)	m	SIGMA	0
Rotor speed N1	%	RSPEED	0
Spoiler position	-	IDSPOI	0

Notes:

a HFLS = aerodrome elevation

b FLUGP(21,J1) = angle of attack: Inclination angle = Flight-path climb angle + angle of attack with all other Euler angles at zero and no wind influence: flight-path- equals air-path axis system

C.2 Complementary to Chapter 4

atmosphere

long nacelle

secondary/ambient shear layer

primary/secondary shear layer

nozzle

short nacelle

initial region   interaction region   mixed flow region
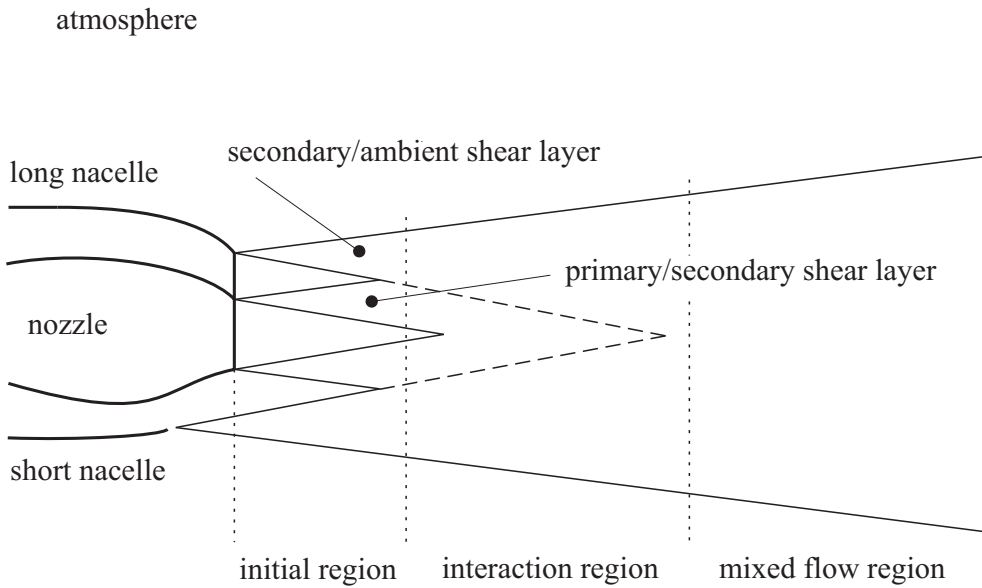
Figure C.1   Schematic of a coaxial jet for a turbofan engine with separate exhaust nozzles.

*Upper half engine equipped with long nacelle (adapted from **Crichton 2007**, p. 175). Lower half engine equipped with short nacelle. Both designs are treated the same way for jet noise prediction.*

TURBOFANS WITH INLET GUIDE VANES (IGV)

FIRST STAGE OF TURBOFANS WITHOUT IGV'S

IGV STATOR   ROTOR   STATOR

AIRFLOW

ROTOR

STATOR

AIR FLOW

C_1 C_2 C_3 C_4

$S_1 = C_2/C_1$, $S_2 = C_4/C_3$

RSS = MINIMUM OF (S_1, S_2) $\approx$ 100

WHERE RSS IS THE MINIMUM ROTOR

SPACING IN PERCENT

C_1 C_2

RSS = C_2/C_1 $\times$ 100

WHERE RSS IS THE ROTOR/ STATOR SPACING

IN PERCENT
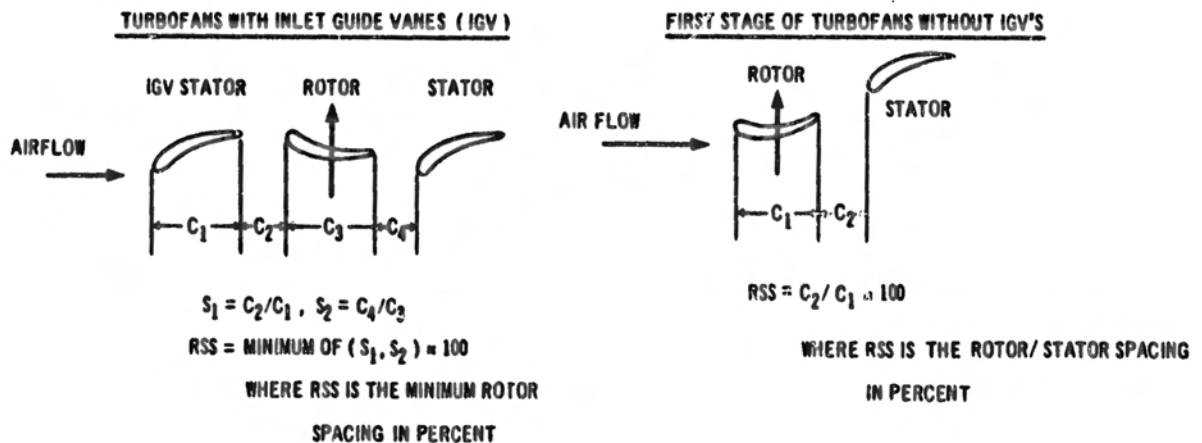
Figure C.2   Rotor-stator spacing for a fan (from **Dunn 1973**, p. 132)
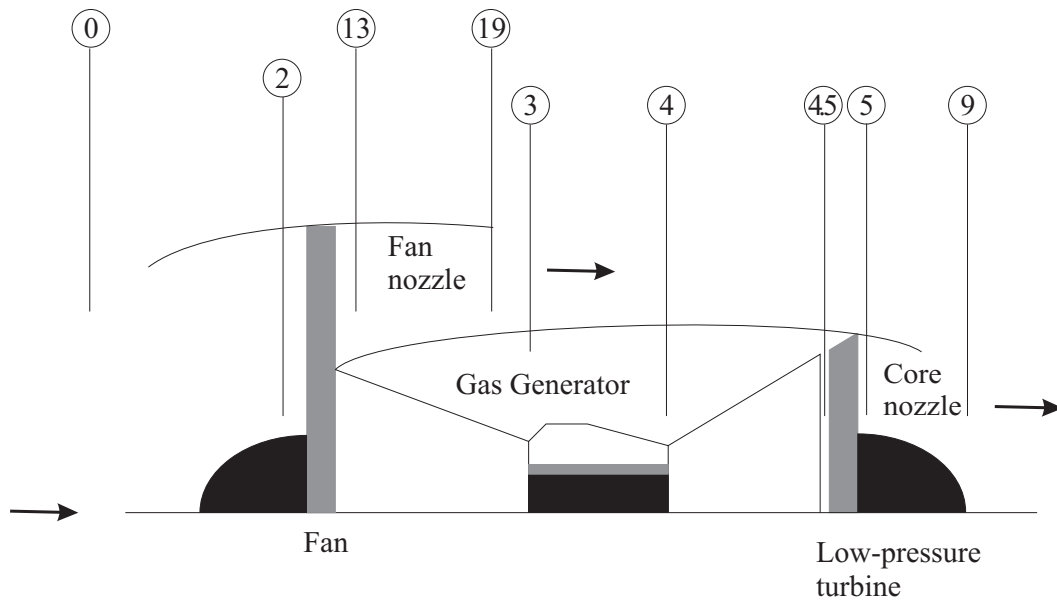
Figure C.3   Engine station numbering of a separate-exhaust turbofan engine with two spools (adapted from **Farokhi 2008**, p. 180)
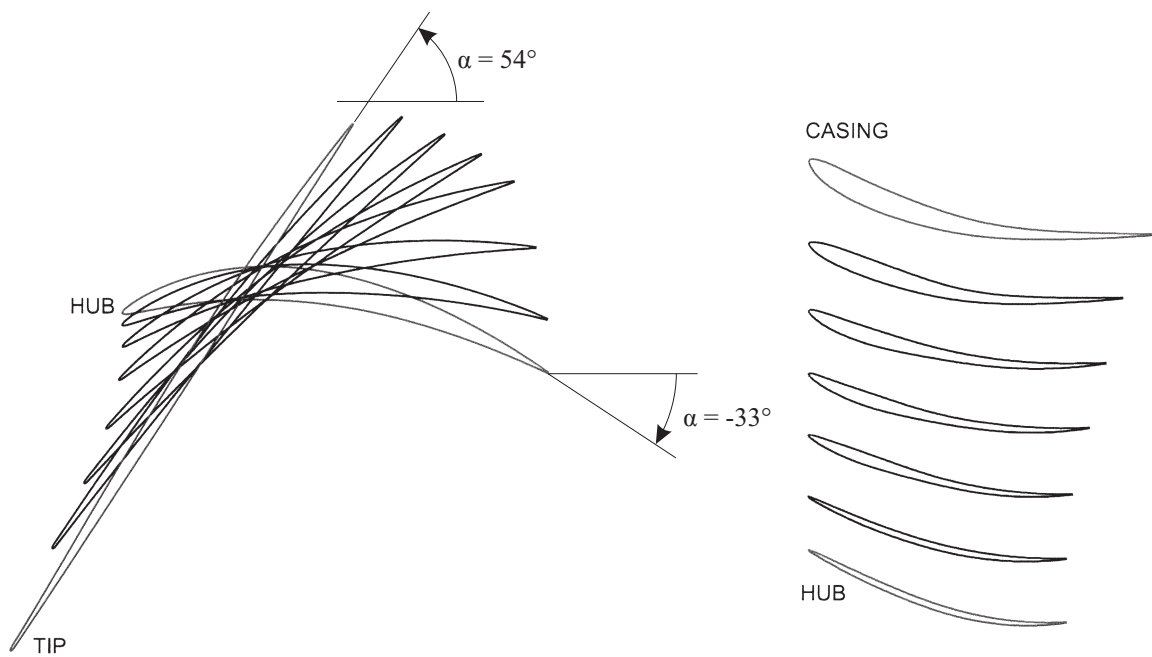
Figure C.4   Rotor and outlet guide vanes blade sections (from **Crichton 2007**, p. 210), α according to the definition used

Figure C.5   Typical fan stage maps (from **Mattingly 1996**, p. 674)

The left graph in figure C.5 represents the characteristics of a low noise fan with a reduced tangential Mach number. The right map shows a fan stage with a considerably higher pressure ratio with supersonic fan blade tip speeds. Data is presented in terms of corrected quantities.

Figure C.6   Euler angles in an isometric view (from **Phillips 2004**, p. 621) – notation changed to LN 3900 standards

The airplane is originally pointing to the north. The earth-fixed axis system (x_0, y_0, z_0) is first rotated about the z_0-axis through an angle Ψ, followed by a rotation about the y-axis by an angle Θ, and finally rotated about the x-axis by an angle Φ that yields into the body-axis system (x_f, y_f, z_f). A different order of the rotations results in another orientation. Roll, pitch and yaw can be related to but are not identical to the Euler angles e.g. the bank angle β is derived out of rotation about the x_0-axis whereas in difference the roll movement is derived out of a rotation about the x_f-axis. The axes of the aircraft movements of roll, pitch and yaw are always perpendicular to each other whereas those of the Euler angles are not (Phillips 2004, p. 620).

Appendix D: Figures and Tables for Chapter 5
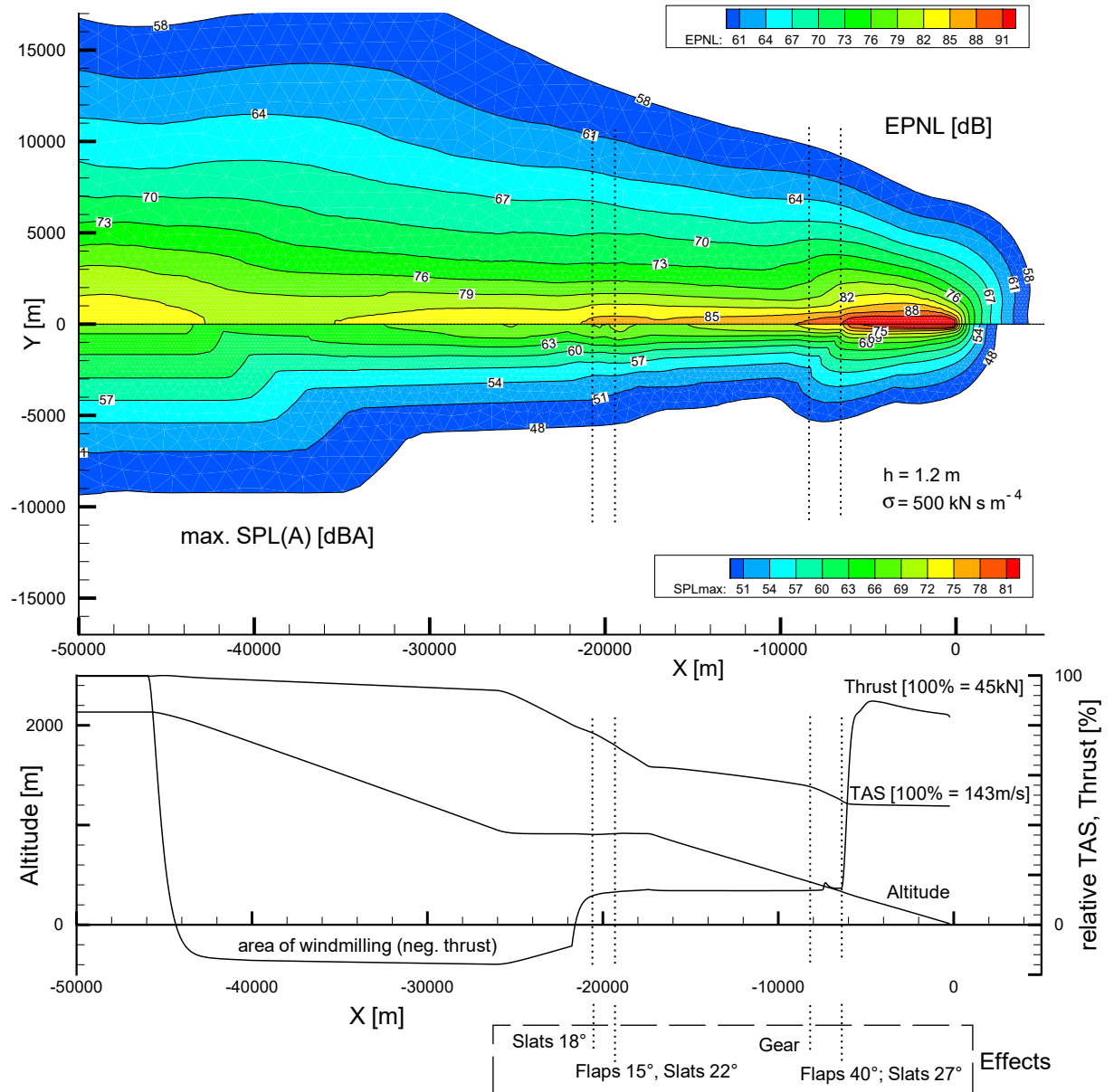
Figure D.1   Low Drag-Low Power approach noise contour plot of the reference aircraft (from **Bertsch 2008**, p. 16) with an optimized trajectory from the DLR Inst. of Flight Systems and engine map data from the DLR Inst. of Propulsion Technology.
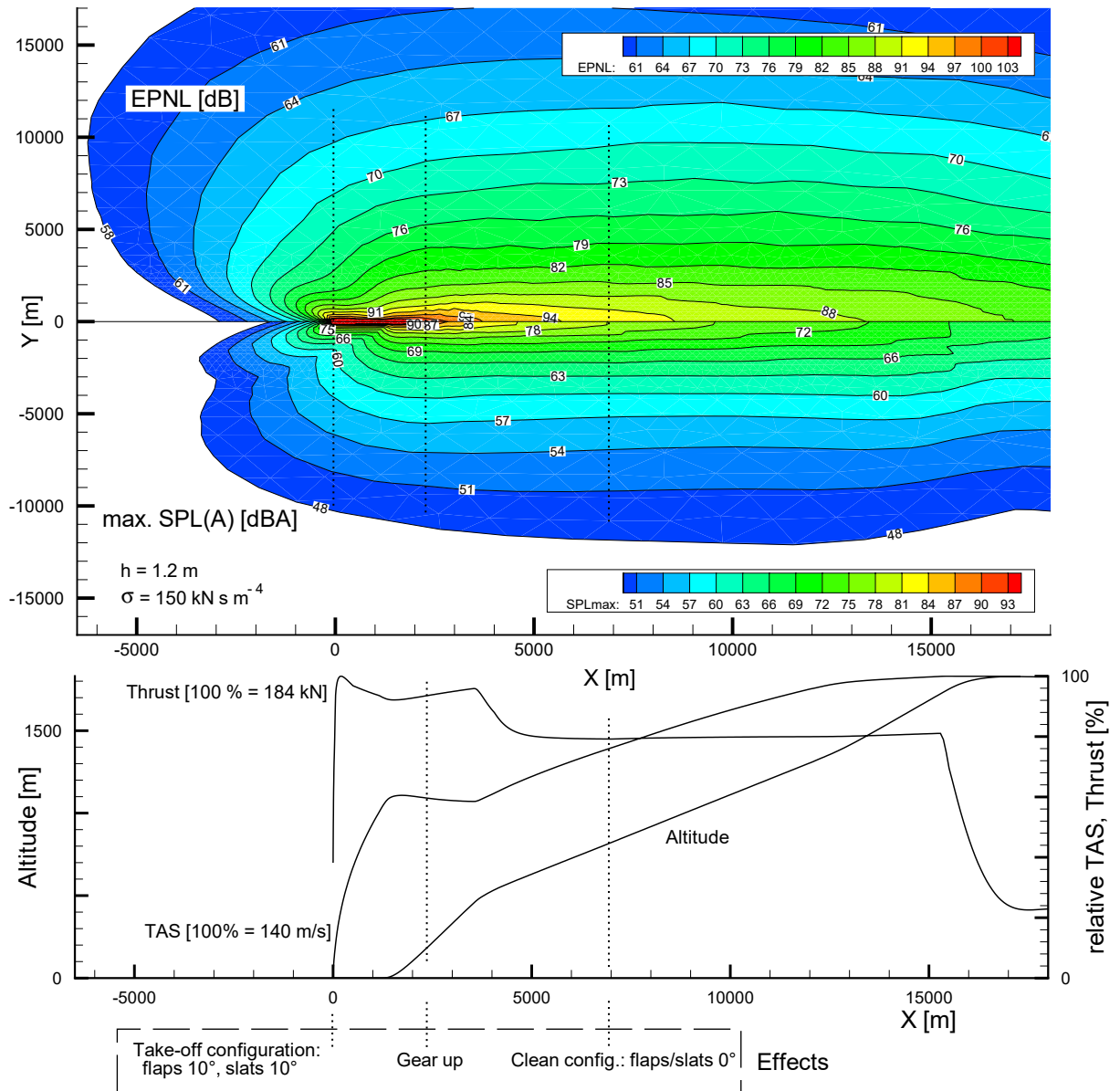
Figure D.2   Modified ATA-departure noise contour plot of the reference aircraft (from **Bertsch 2008**, p. 17) with an optimized trajectory from the DLR Inst. of Flight Systems and engine map data from the DLR Inst. of Propulsion Technology.
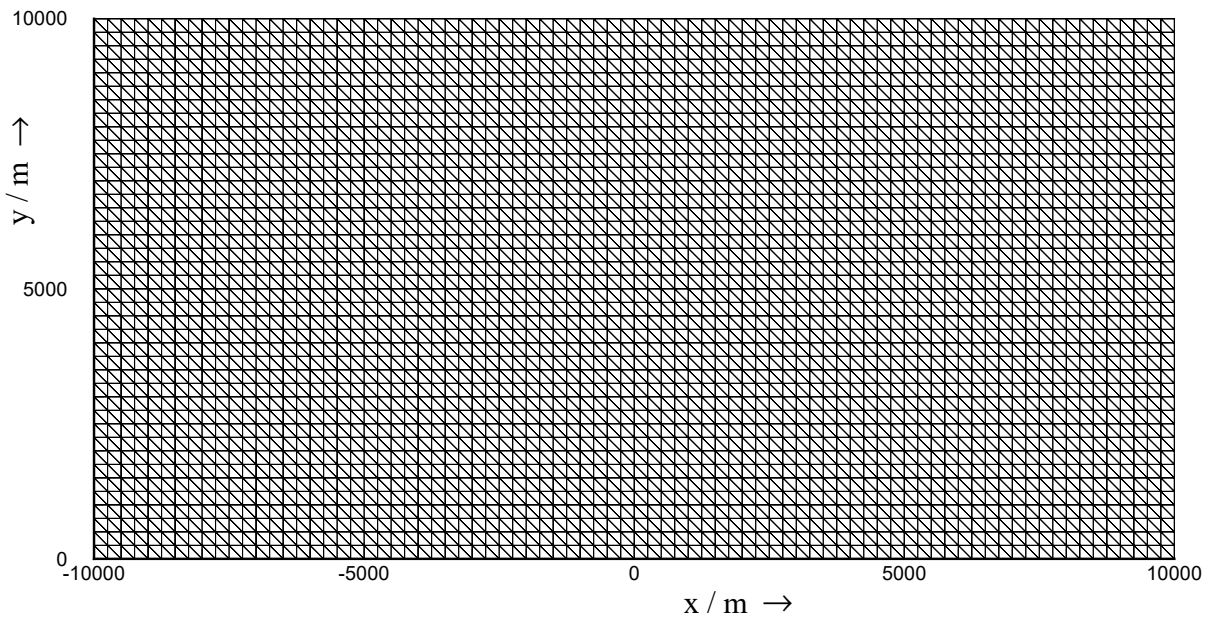
Figure D.3   Observer array on ground (structured mesh; 10 km x 20 km)
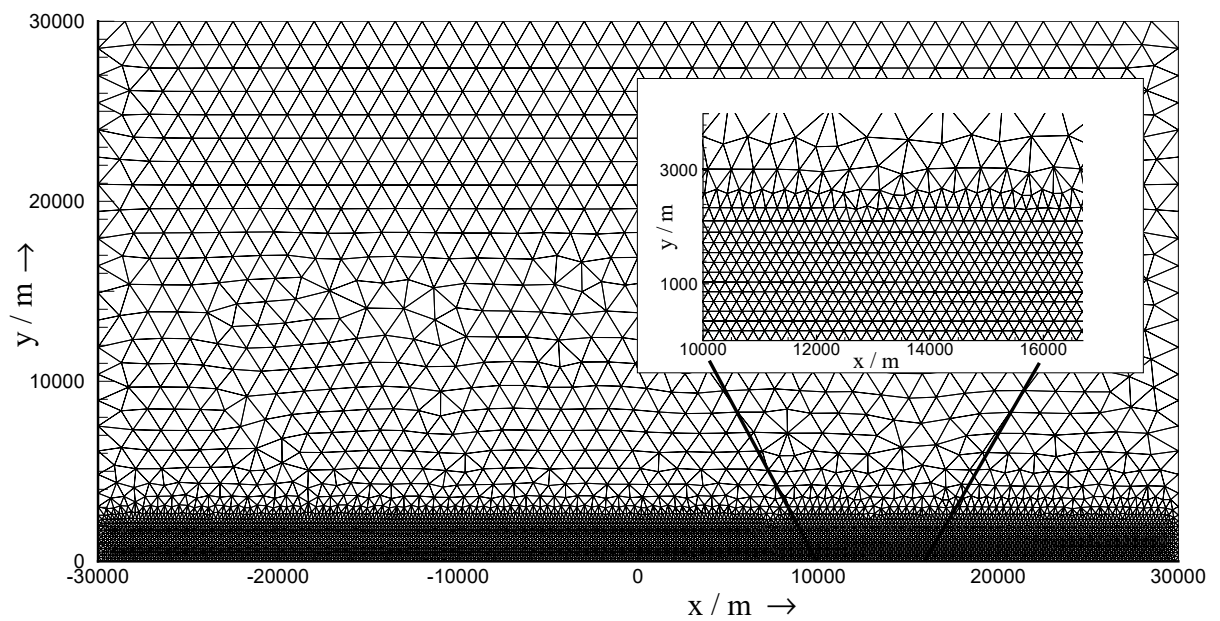
Figure D.4   Unstructured observer mesh (30 km x 60 km)
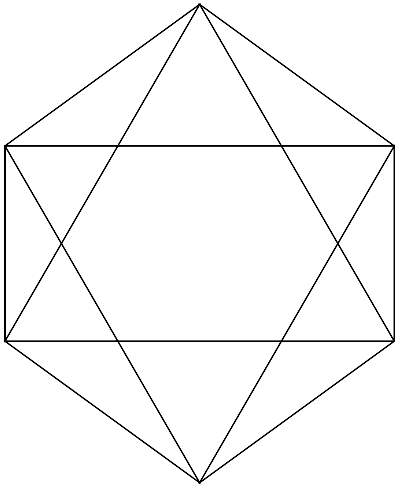
Figure D.5   Starting grid: Octahedron n = 0
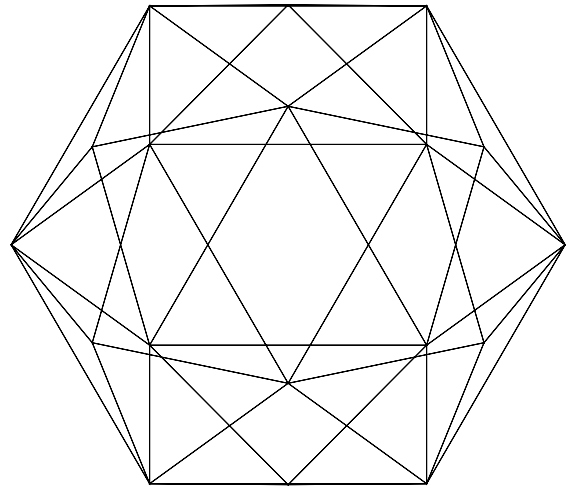
Figure D.6   Spherical grid refining n = 1
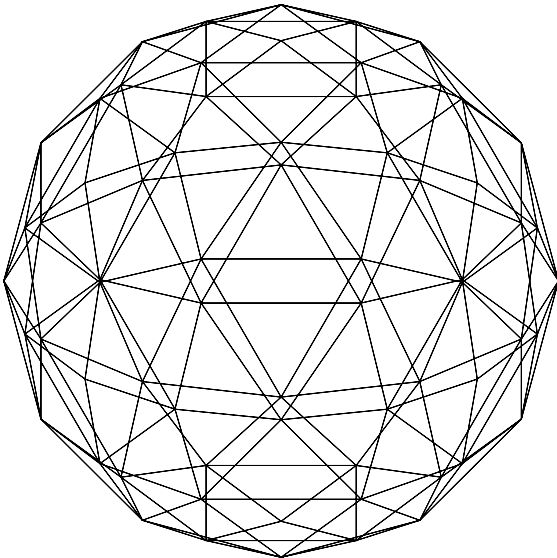
Figure D.7   Spherical grid refining n = 2
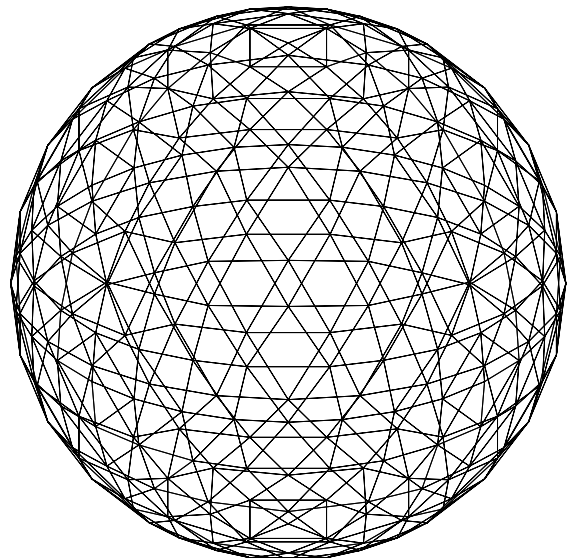
Figure D.8   Spherical grid refining n = 3
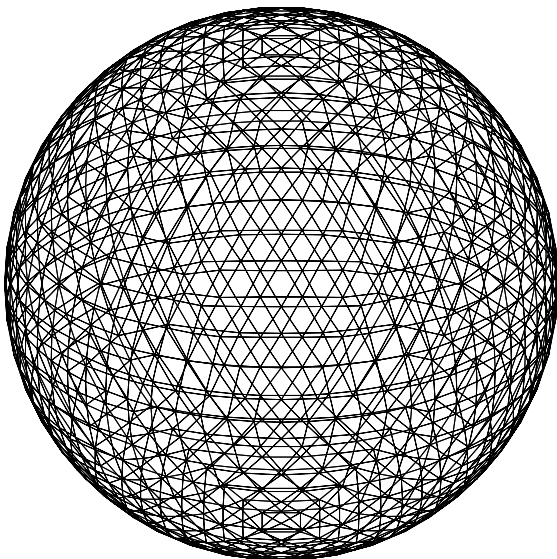
Figure D.9   Spherical grid refining n = 4
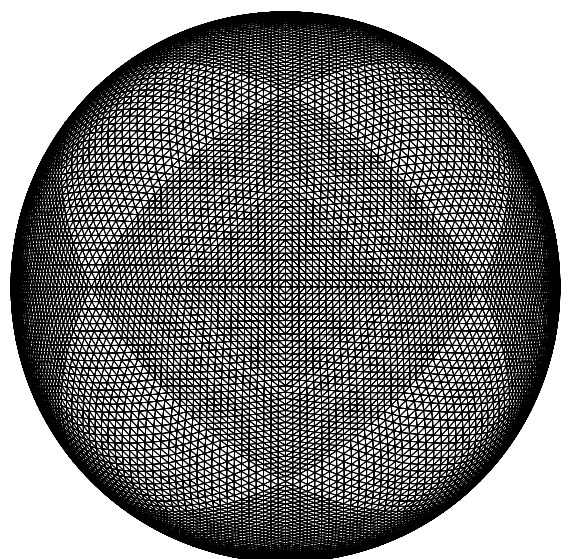
Figure D.10   Spherical grid refining n = 6
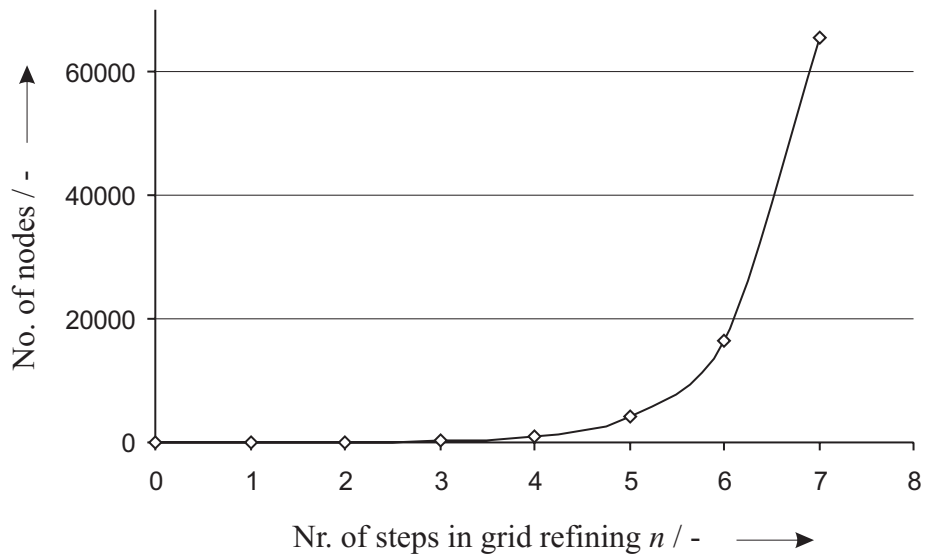
Figure D.11   Exponential increase in number of nodes for spherical grid refining
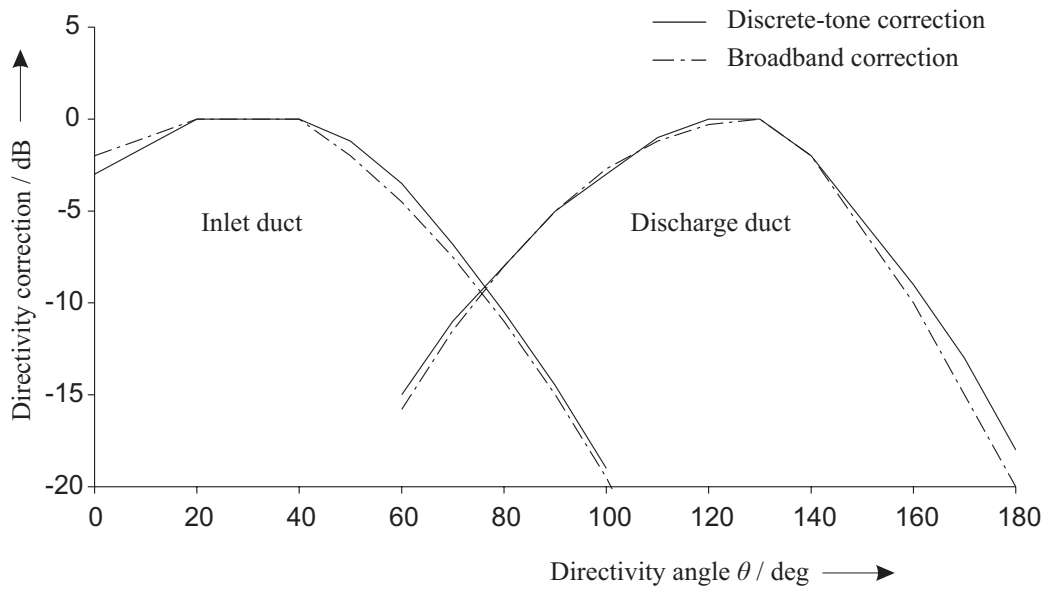
Figure D.12   Directivity correction for fan noise (data from **Heidmann 1979**), (definition of θ in figure D.11)
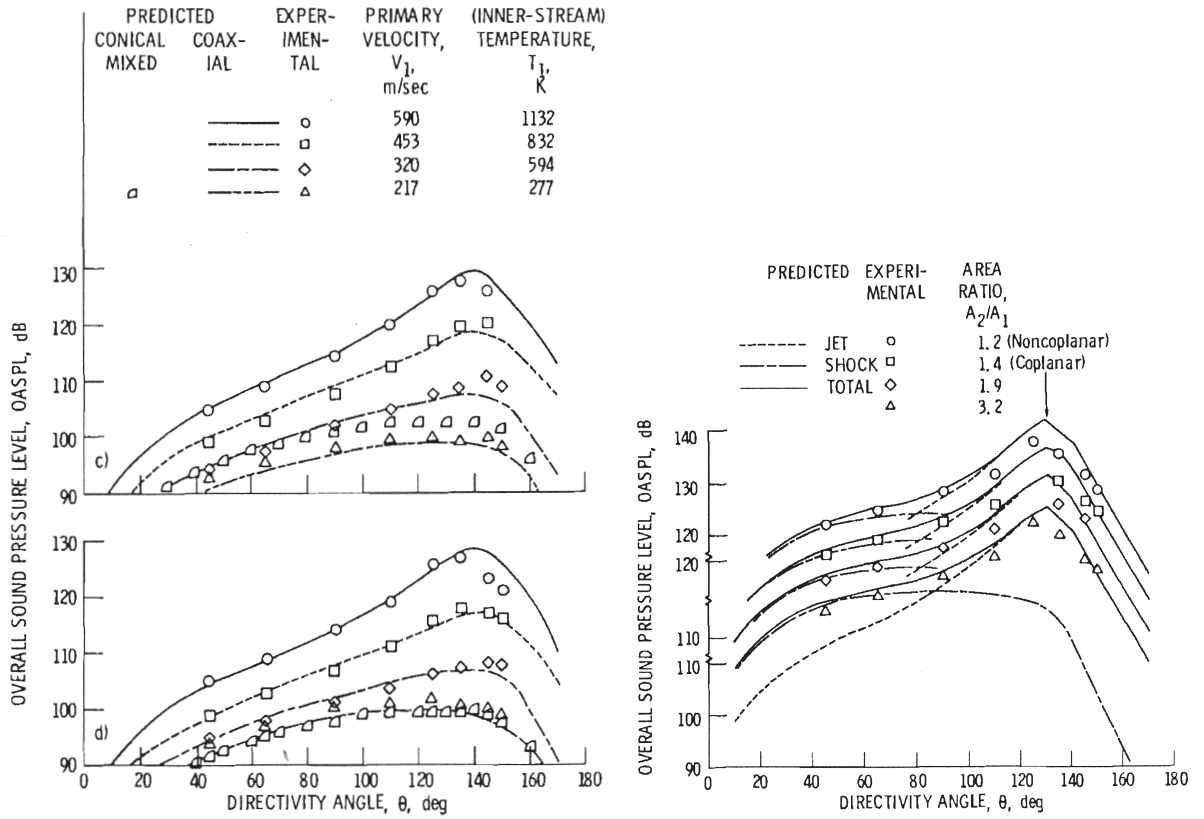
Figure D.13 Influence of primary velocity v_9 and area ratio A_{19}/A_9 on jet noise (from **Stone 1983**).

Left illustration: *lossless free-field OSAPL directivity on 5.0 m sideline (v19 = 215 m/s, T19 = 279 K) for coplanar jets. Top: A19/A9 = 1.9, bottom: A19/A9 = 3.2*

Right Illustration: *Supersonic jet mixing and shock noise, lossless free-field OASPL directivity on 5.0 m sideline (high primary Mach number M_9 = 1.38, high primary velocity v_9 = 790 m/s, v_{19} = 216 m/s, T_9 = 1130 K. T_{19} = 278 K, A_9 = 10 cm,*

Here, directivity angle θ is defined as the angle between the positive x_f-axis, as defined in this thesis, and the radiation towards the observer within the x_f-z_f-plane.

120 M (394 FT)
ALTITUDE

3 DEGREE
GLIDE SLOPE

TAKEOFF
REFERENCE

6500 M
(3.5 N. MI.)

SIDELINE
REFERENCE
450 M
(0.25 N.MI.)

2000 M
(1.08 N. MI.)

APPROACH
REFERENCE
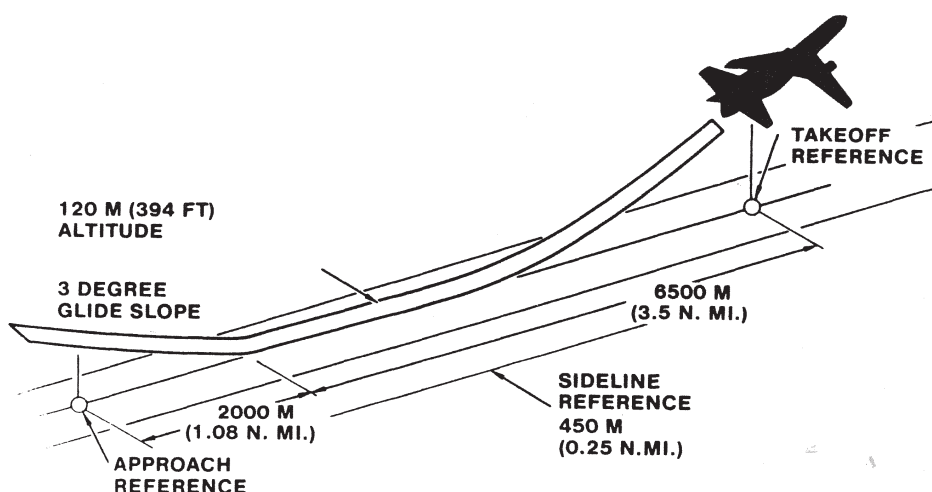
Figure D.14   The three noise certification reference positions (from **Smith 1989**, p. 25)

The approach reference is defined as the point 2000 m before touch down, take-off reference is defined as the point 6500 m after break release and both are on the (extended) runway centre line. Sideline reference is obtained from a 450 m lateral displaced runway centre line.

*As specified in **FAR Part 36** (A36.9.2.1 (a) and (b), Takeoff Profile):*

"The airplane begins the takeoff roll ... lifts off ... and begins its first climb at a constant angle .... Where thrust or power (as appropriate) cut-back is used, it is started ... and completed at a̲ [authors note] point .... From here, the airplane begins a second climb at a constant angle...."

"... lateral noise measuring station, which is located on a line parallel to, and the specified distance from, the runway center line where the noise level during takeoff is greatest."

Appendix E: Figures and Tables for Chapter 6
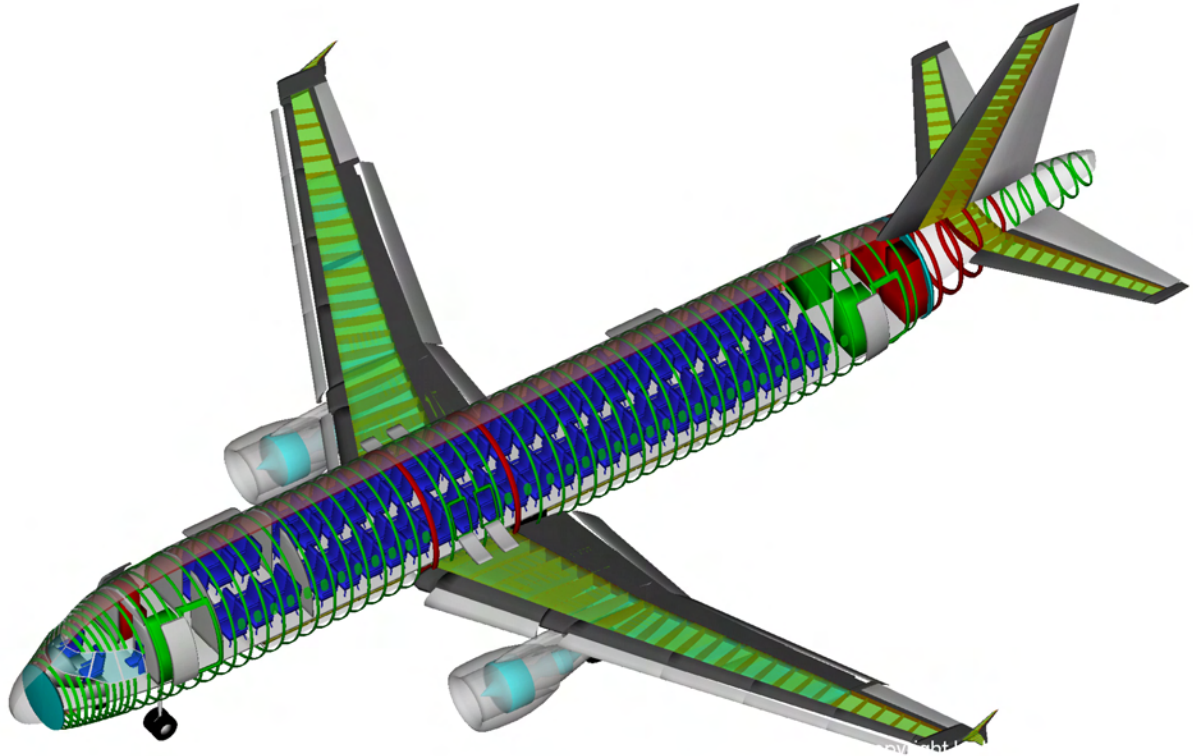
Figure E.1   PrADO 3D-drawing of the reference aircraft
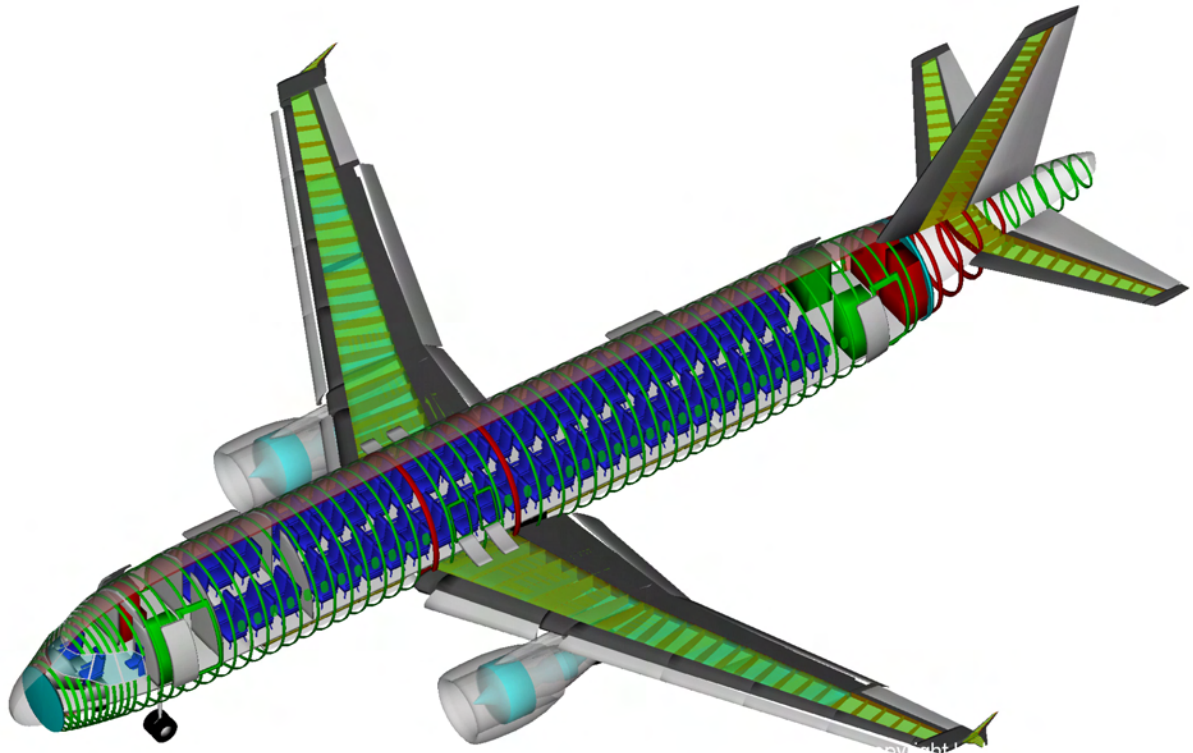
Figure E.2   PrADO 3D-drawing of the high-powered A/C (slight increase in engine diameter noticeable)
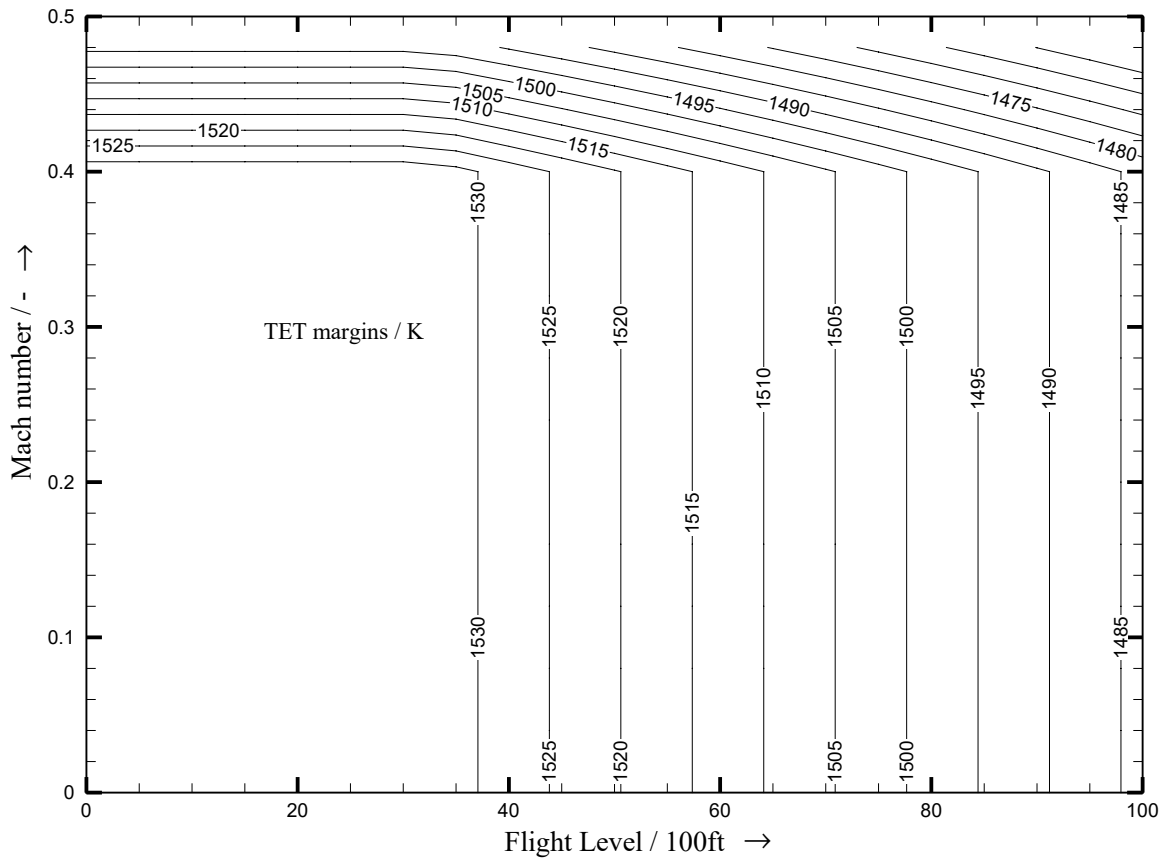
Figure E.3   Turbine exhaust temperature limits v. Mach number and flight level (both engines)
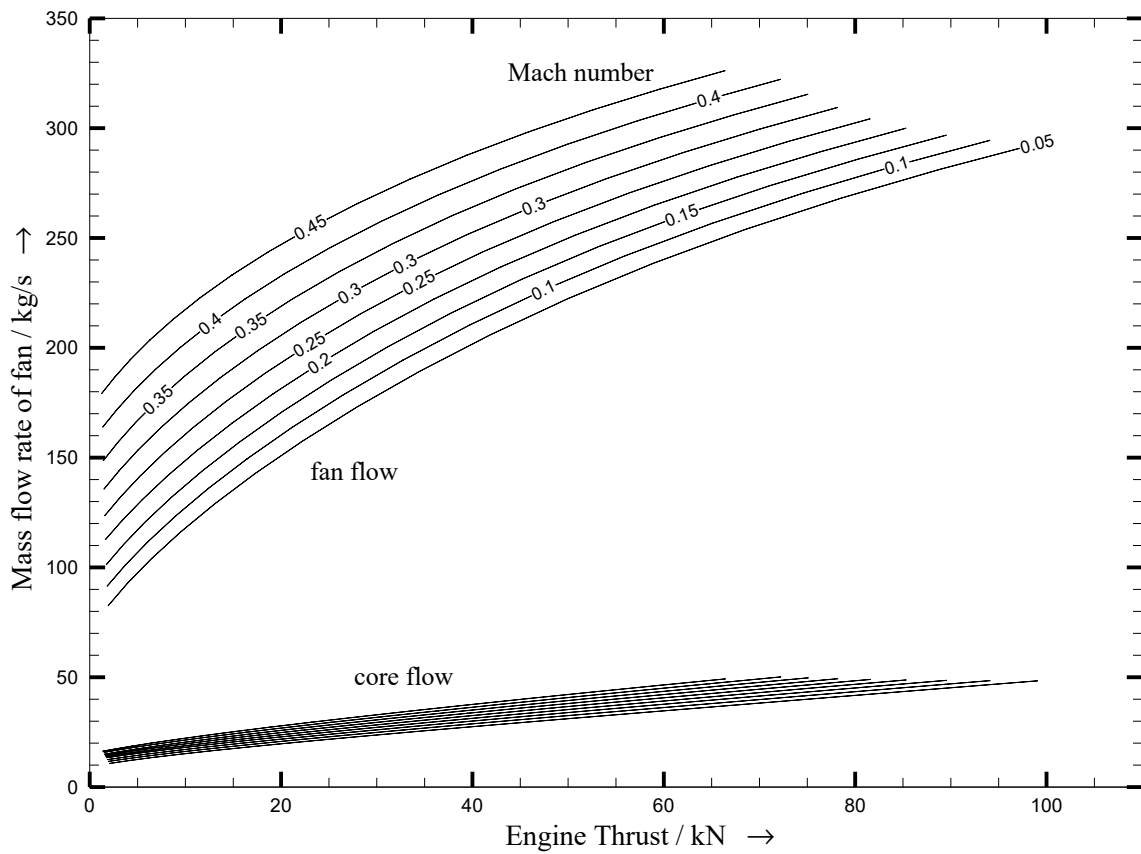
Figure E.4   Fan (and core) flow v. thrust and Mach number (FL = 0; reference engine)
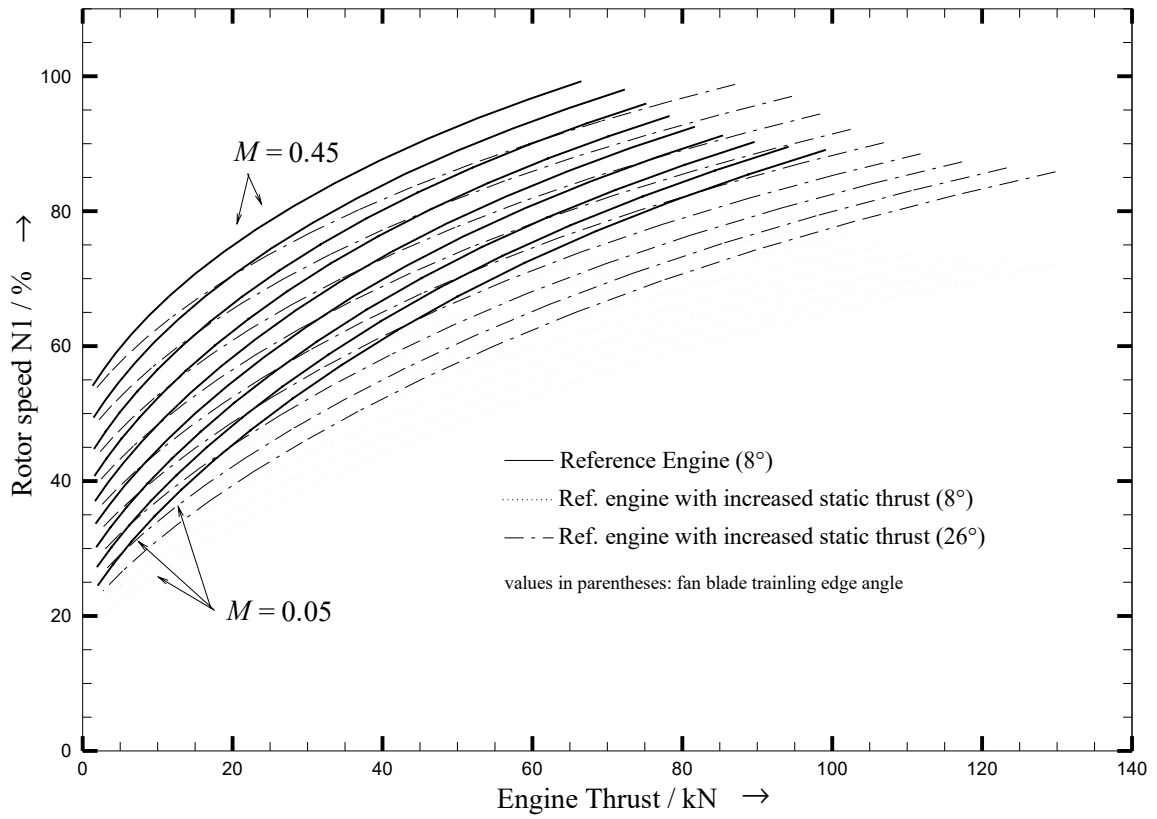
Figure E.5   Rotor speed N1 v. thrust and Mach number for both engines at FL = 0
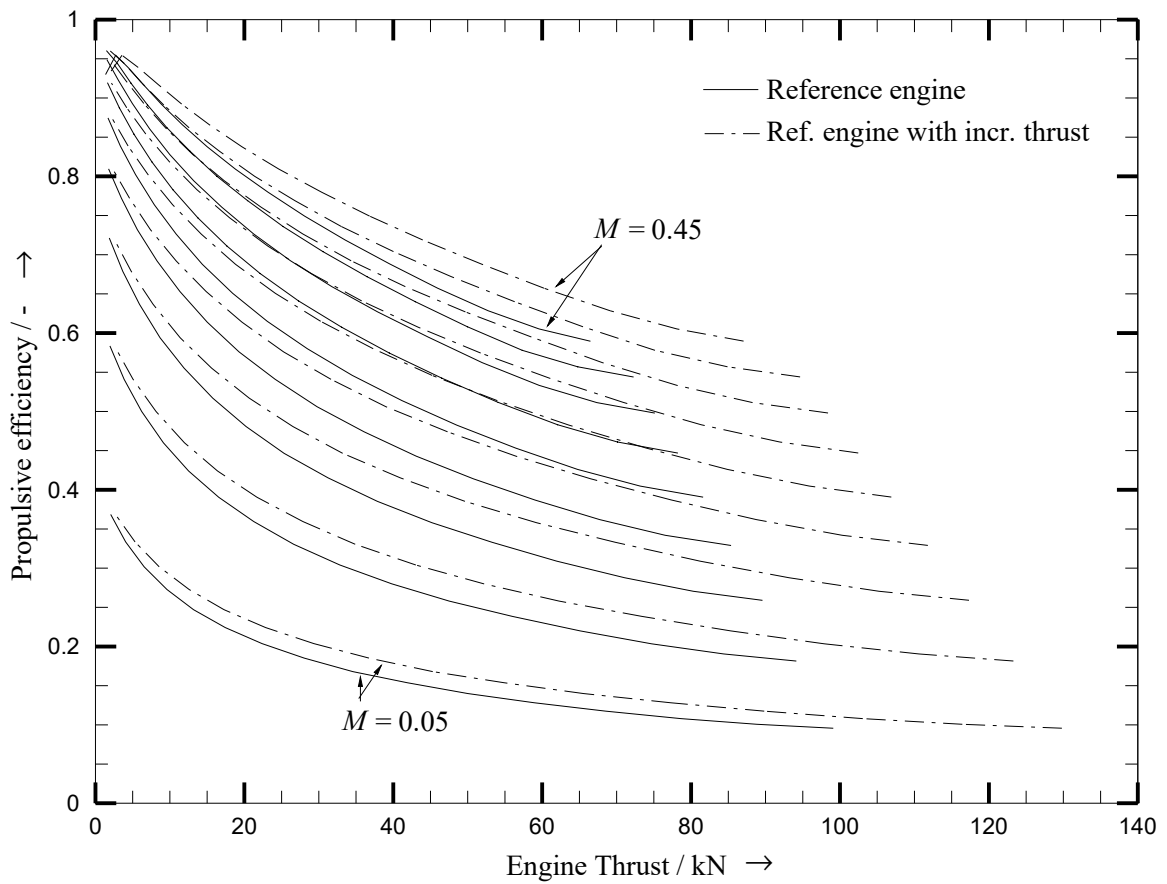
Figure E.6   Propulsive efficiency v. thrust and Mach number for both engines at FL = 0
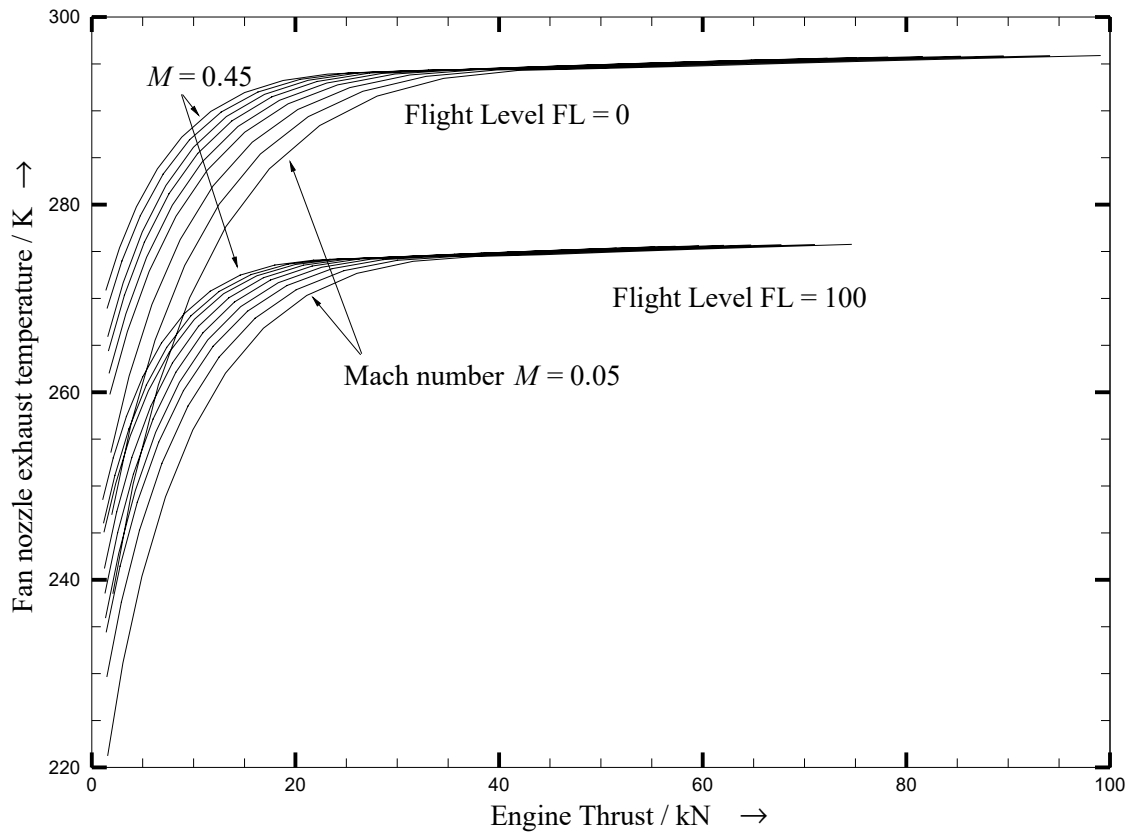
Figure E.7   Fan nozzle exhaust temperature v. thrust and Mach number (reference engine)
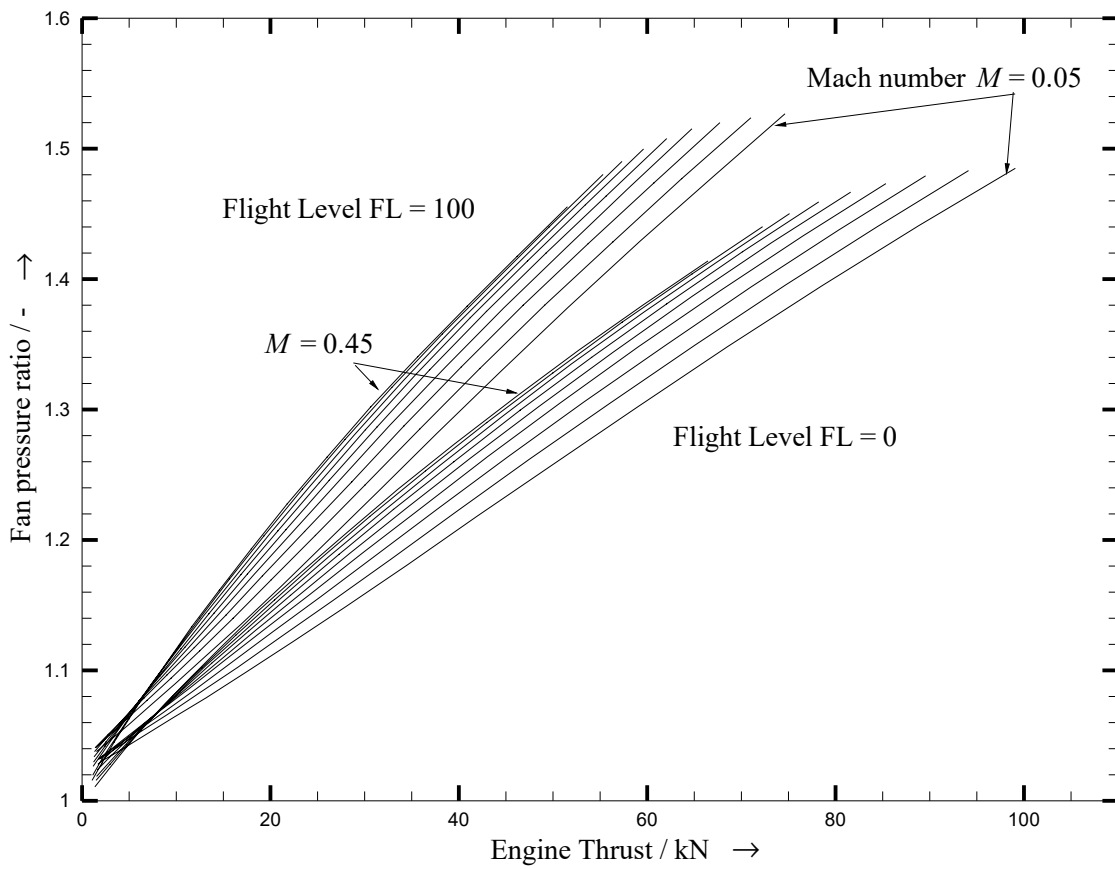
Figure E.8   Fan pressure ratio v. thrust and Mach number (reference engine)
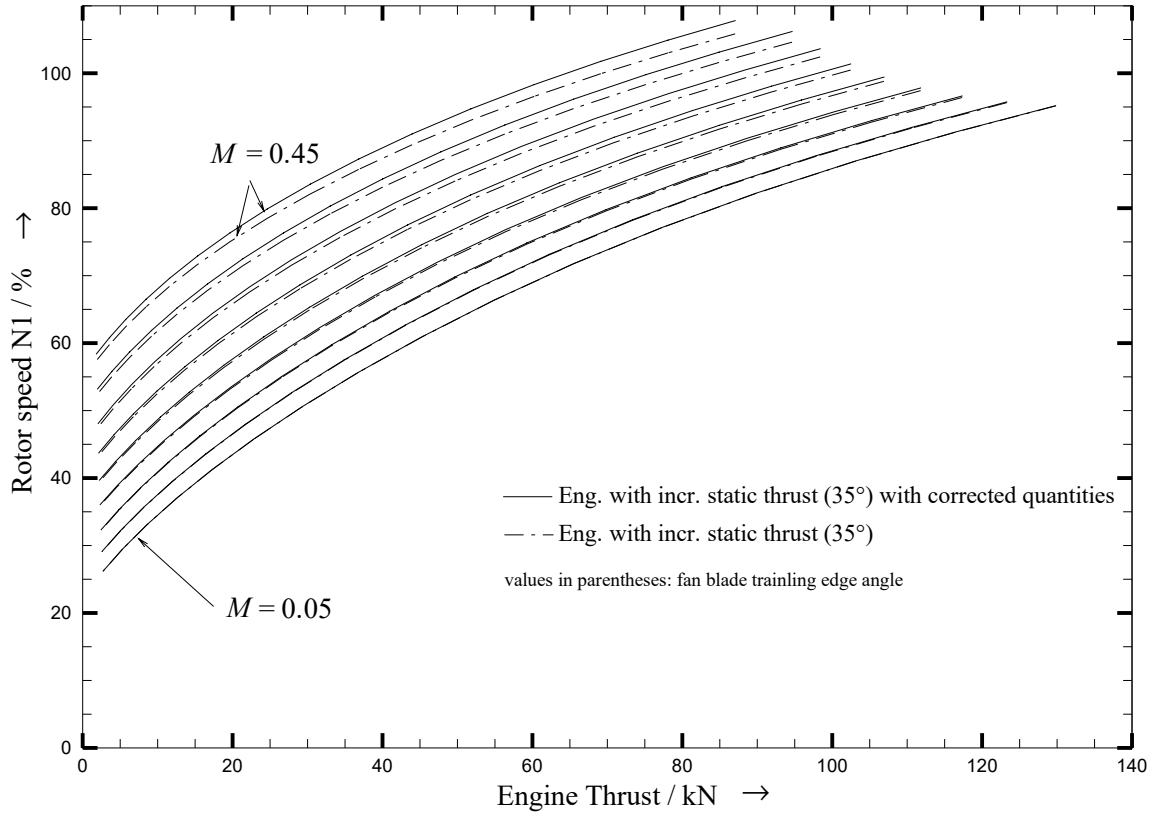
Figure E.9   N1 v. thrust, engine with increased static thrust (overpowered), corrected v. uncorrected quantities at FL = 0
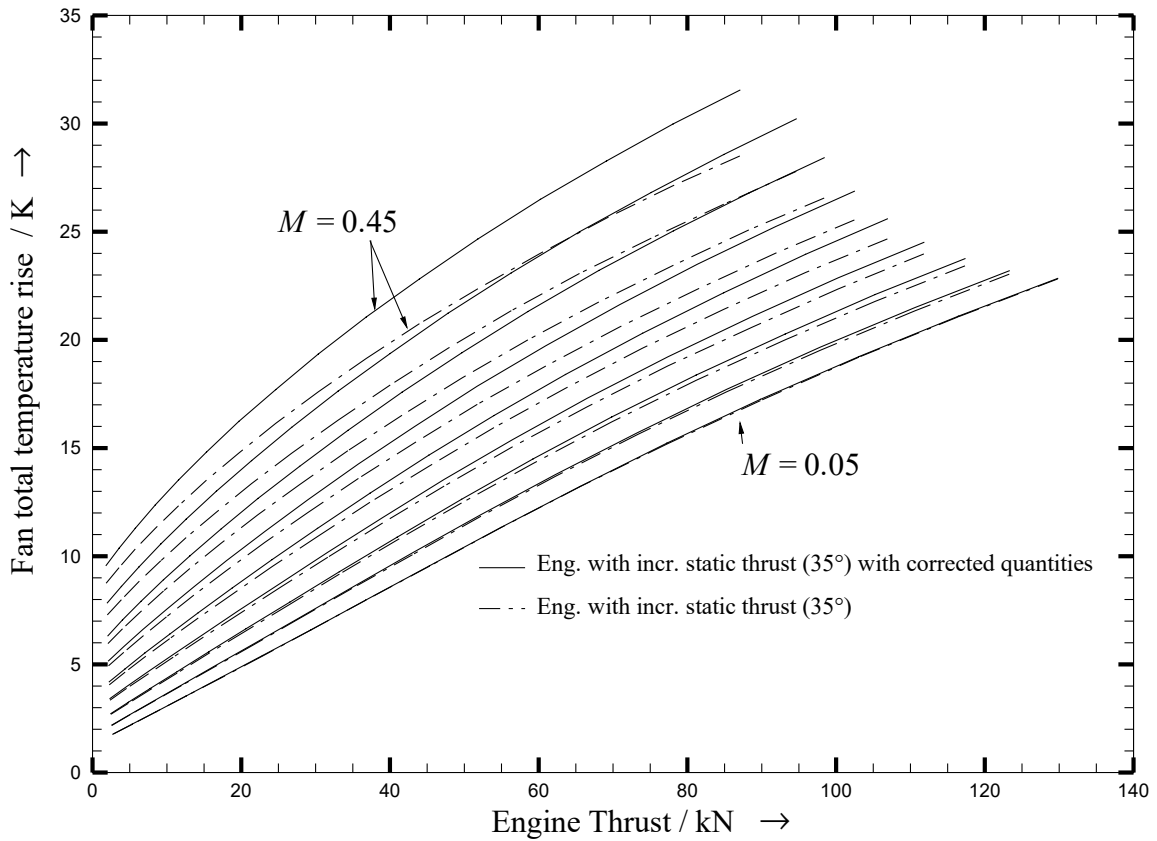
Figure E.10   Fan total temperature rise v. thrust and Mach number, engine with increased static thrust (overpowered), corrected v. uncorrected quantities at FL = 0
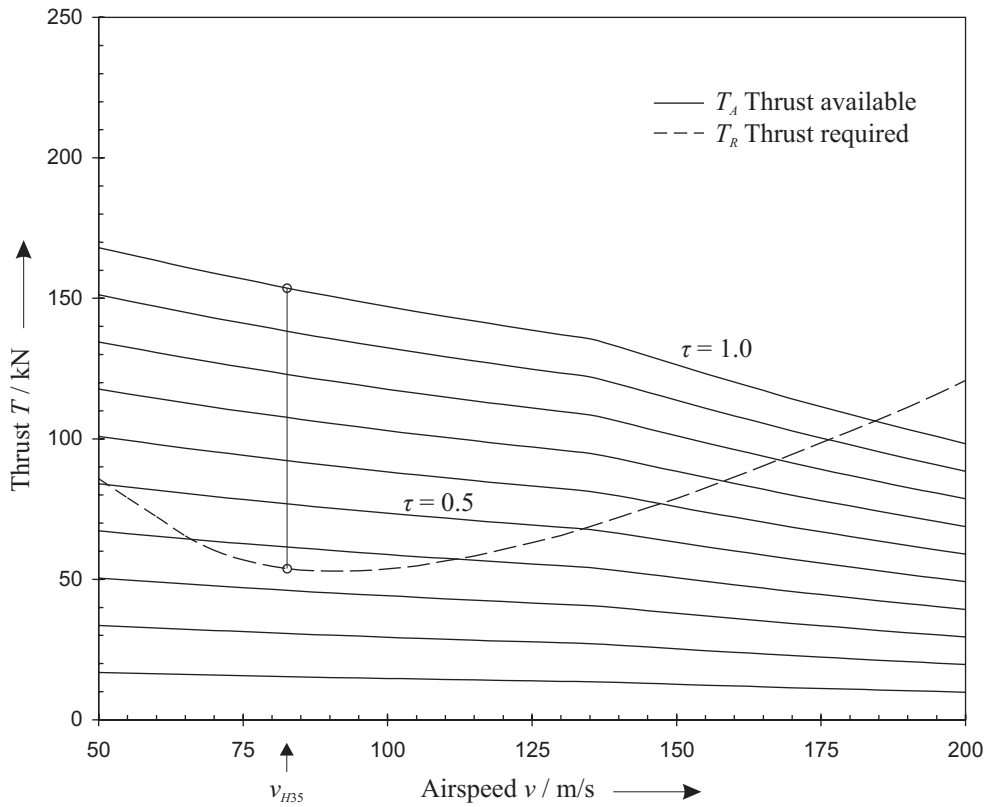
Figure E.11   Thrust available and thrust required at standard sea level – reference A/C with parameter τ as engine throttle setting (0 – 100 %)
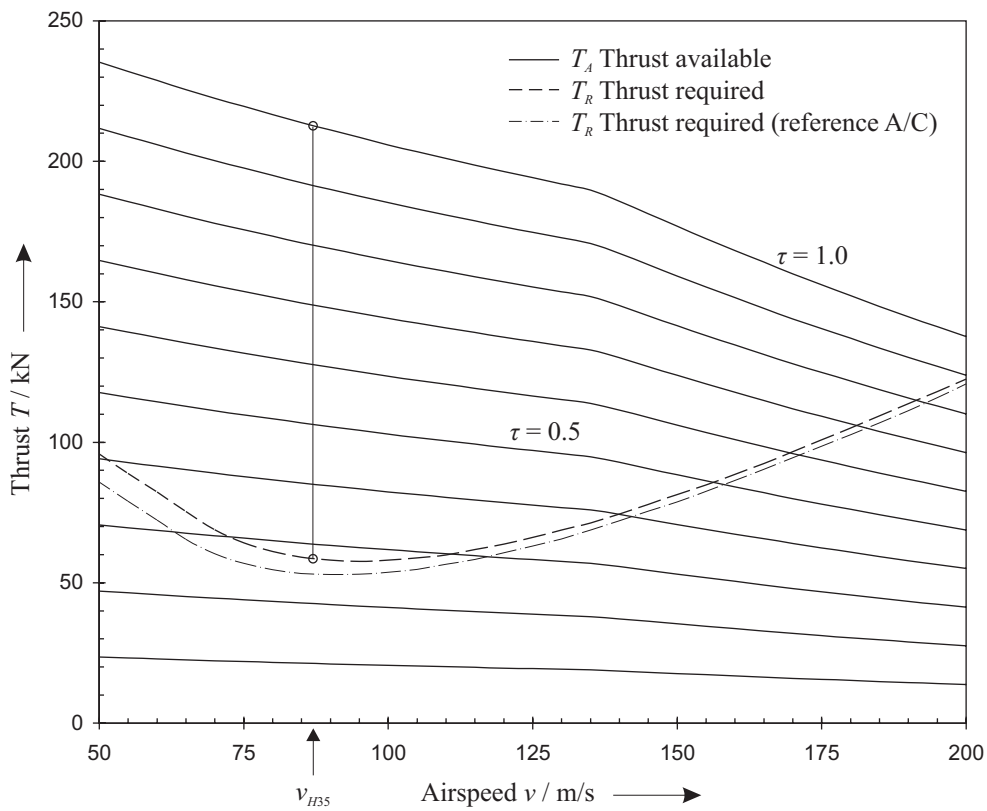
Figure E.12   Thrust available and thrust required at standard sea level – high-powered A/C
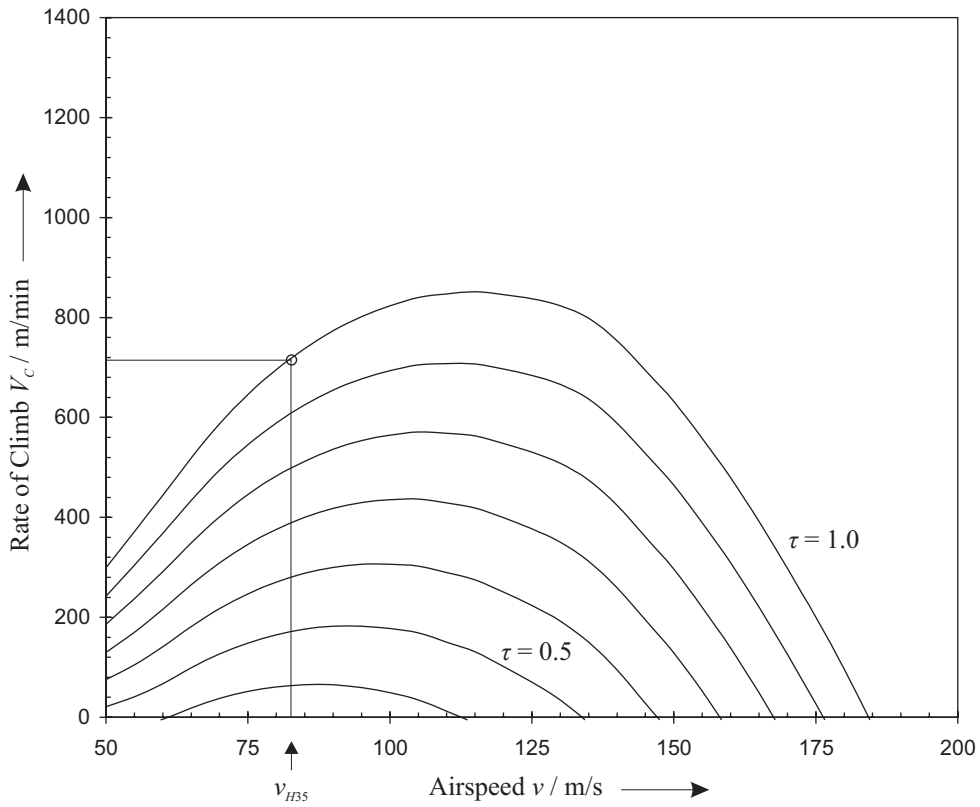
Figure E.13   Rate of climb level at standard sea level – reference A/C
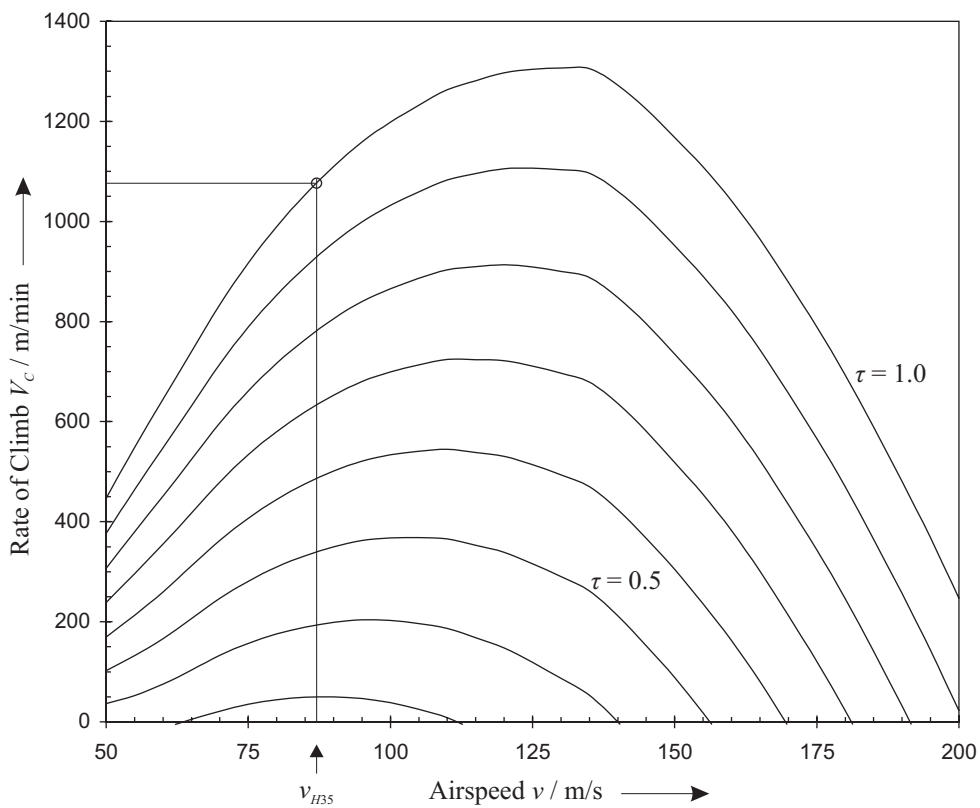
Figure E.14   Rate of climb level at standard sea level – high-powered A/C
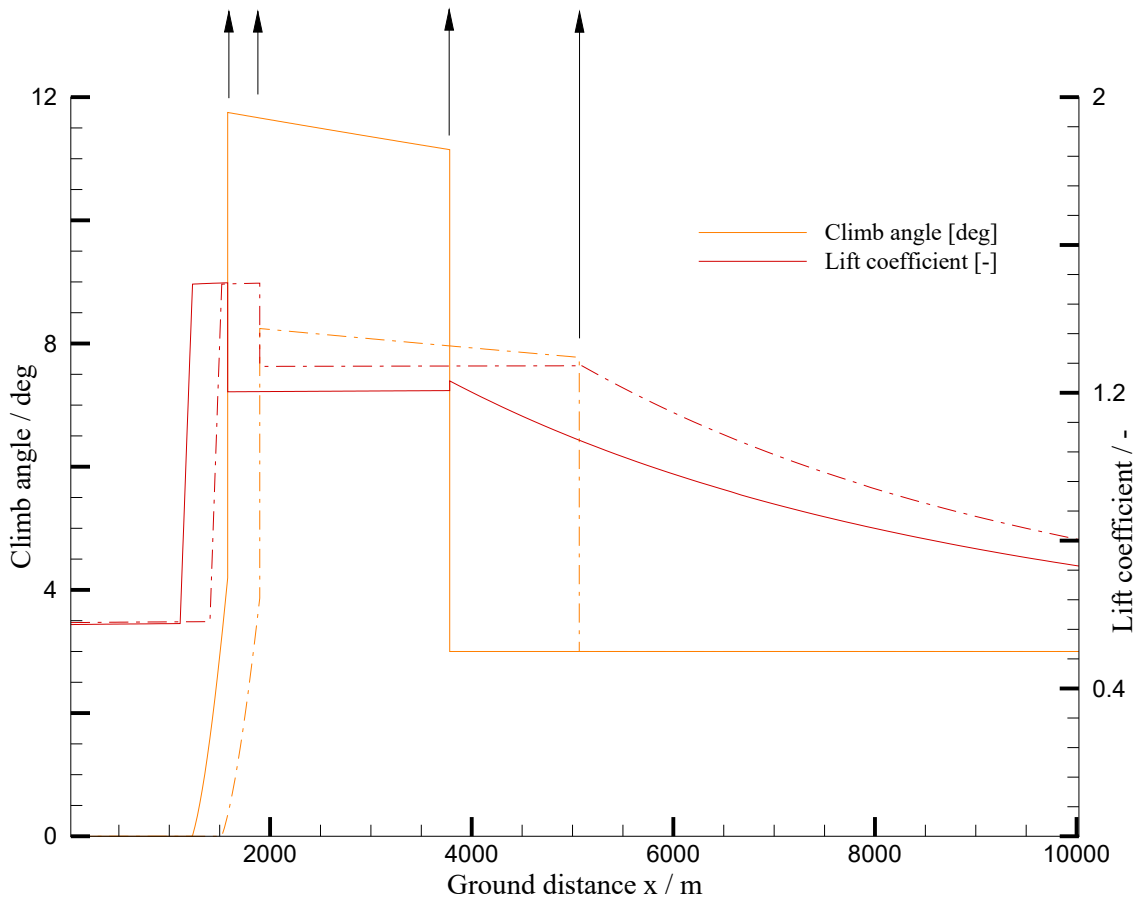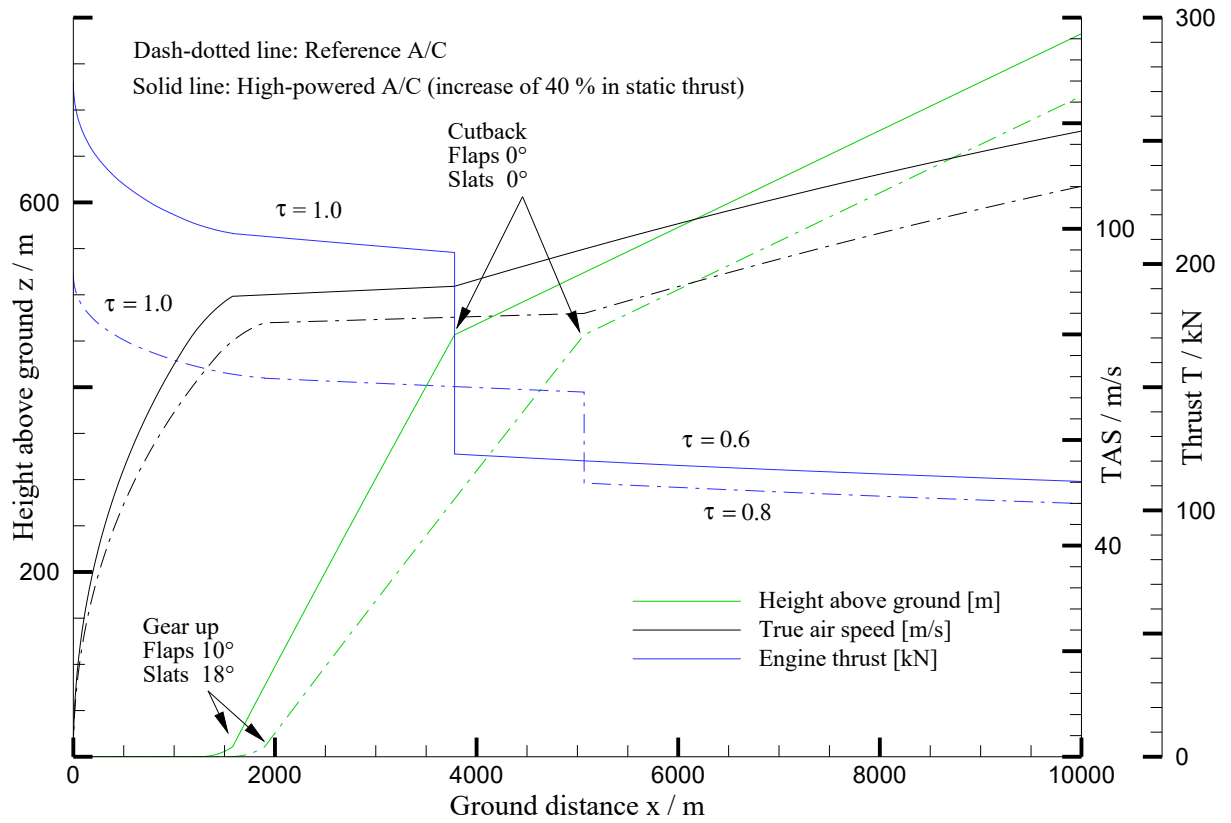
Figure E.15 Climb trajectory; reference A/C (dash-dotted) v. high-powered A/C, flight mission: flight with maximum payload. Engine throttle setting τ (0 – 100 %)
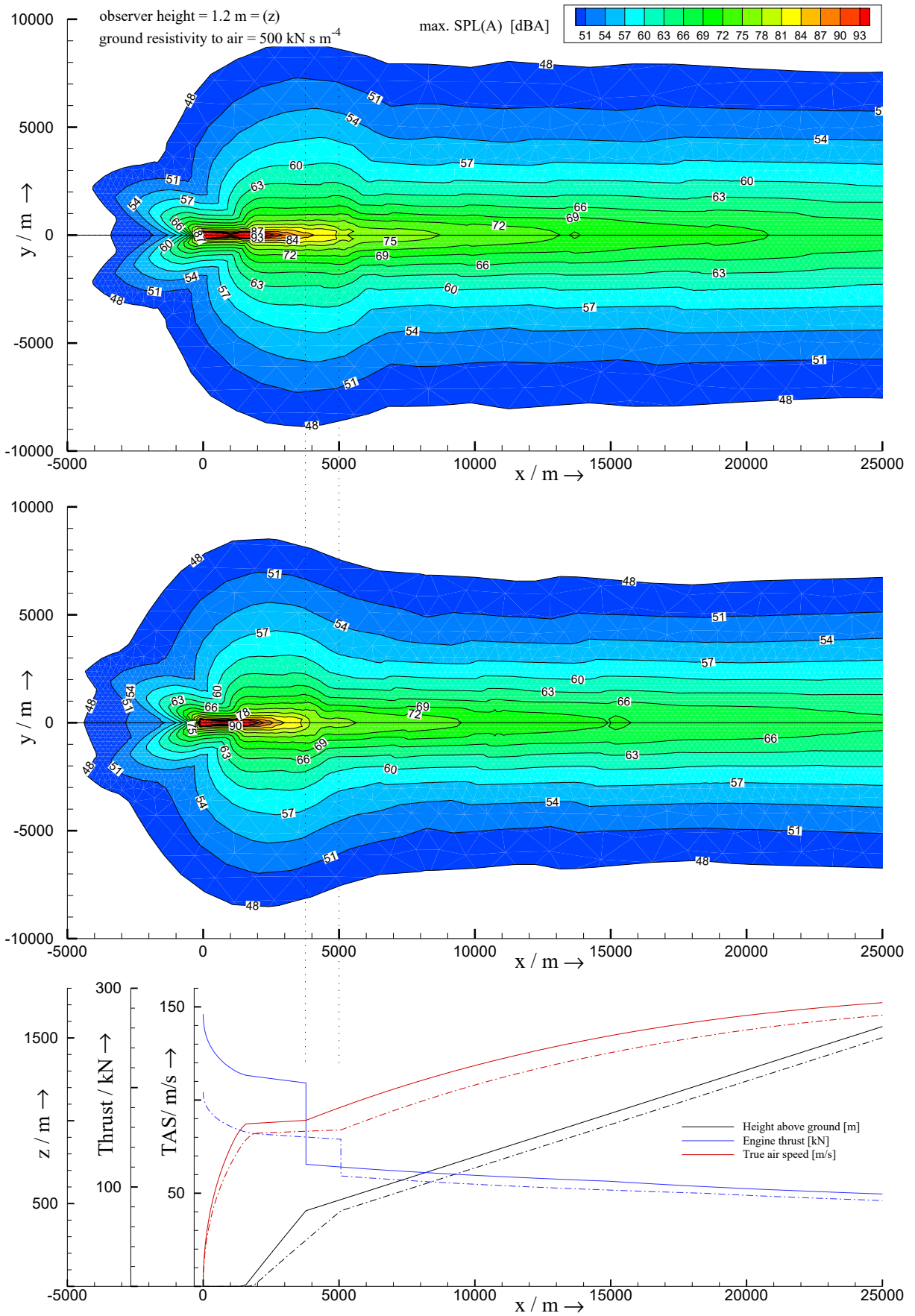
Figure E.16 Noise contour plot in max. SPL(A); departure; reference A/C (top illustration; dash-dotted line) v. high-powered A/C (middle illustration; solid line)
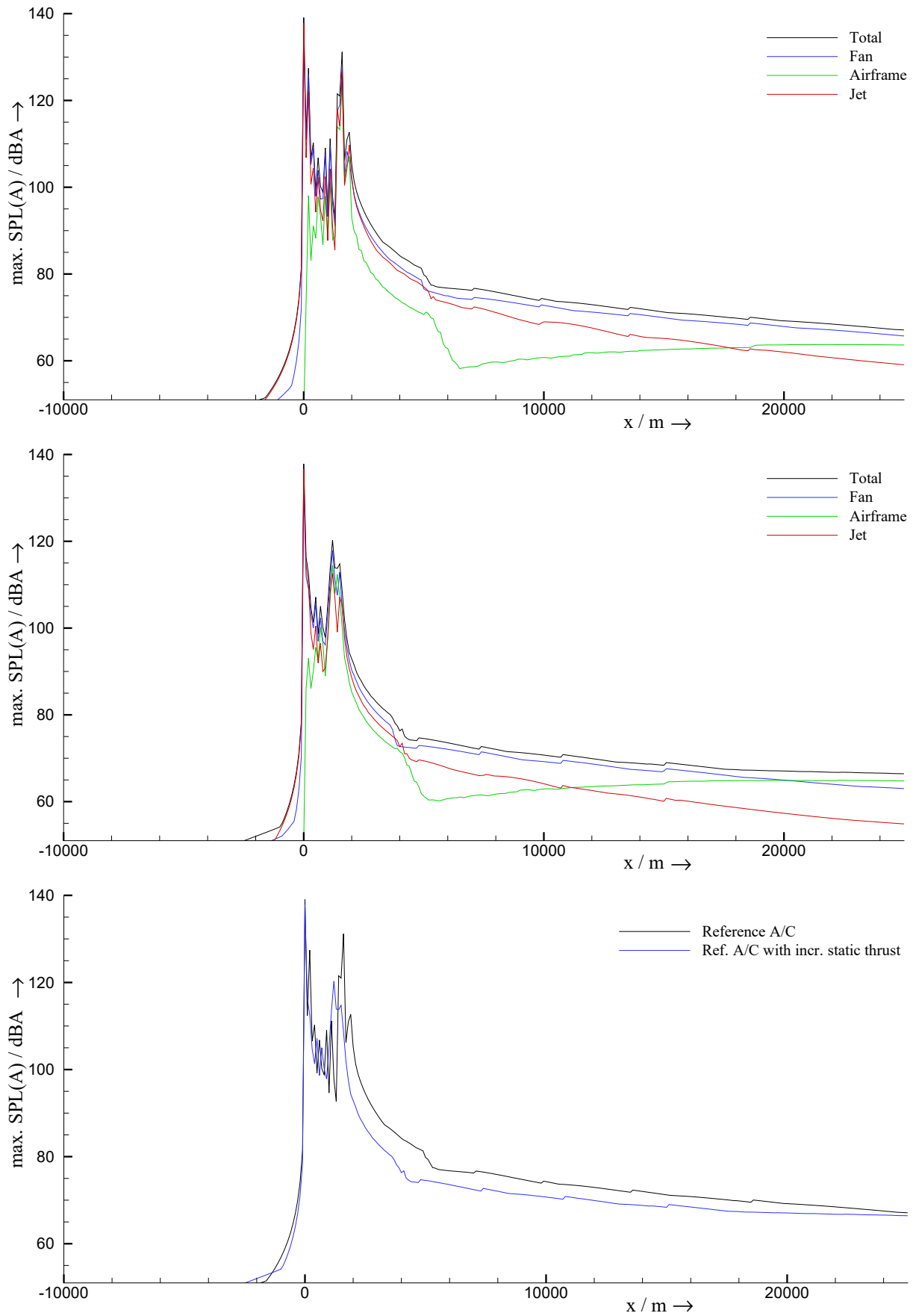
Figure E.17   Max. SPL(A) along *x*-axis, *y* = 0; departure; reference A/C (top) v. high-powered A/C (middle)
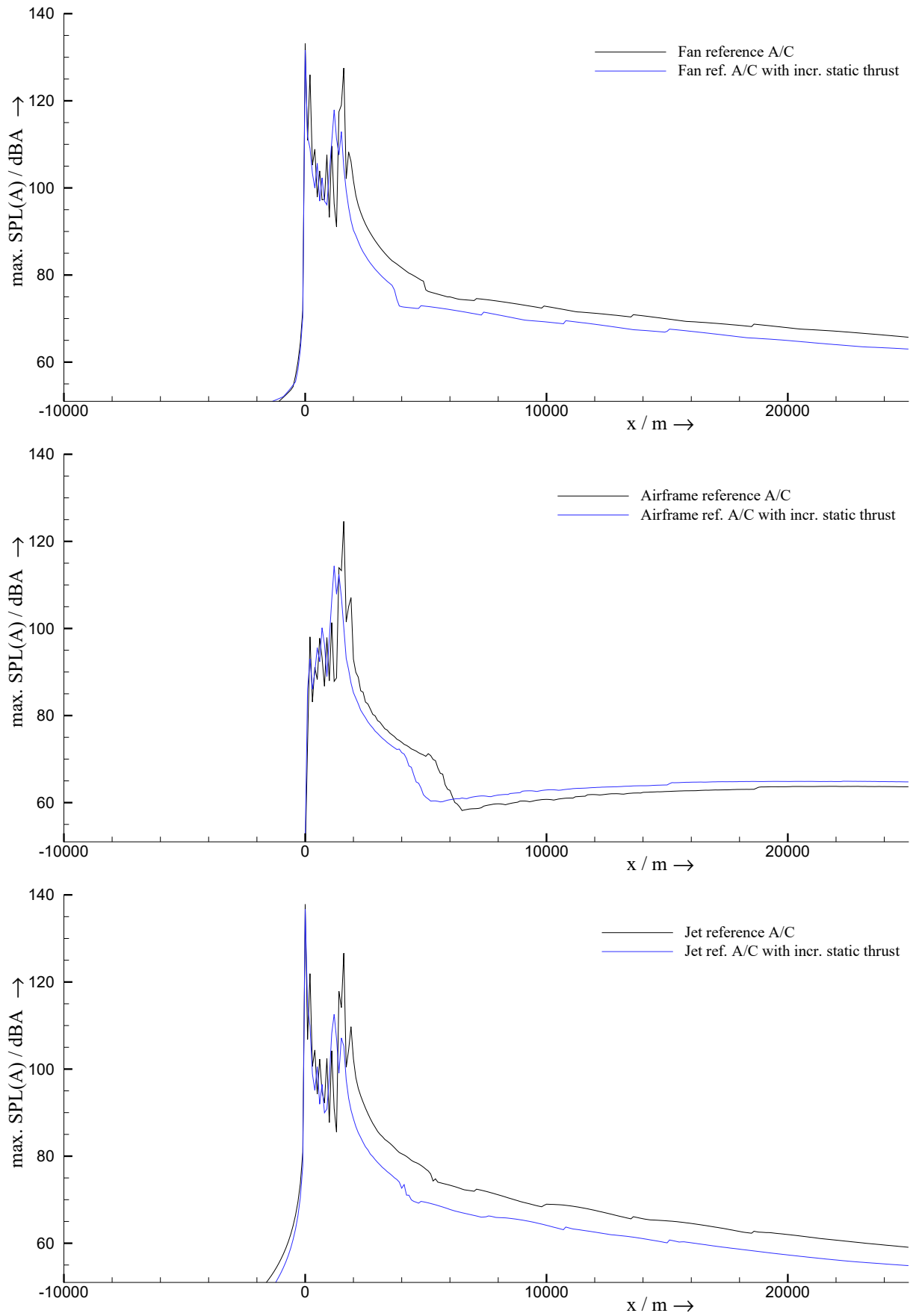
Figure E.18   Max. SPL(A) along *x*-axis, *y* = 0; departure; fan-, airframe-, and jet noise components of reference A/C v. noise components of high-powered A/C
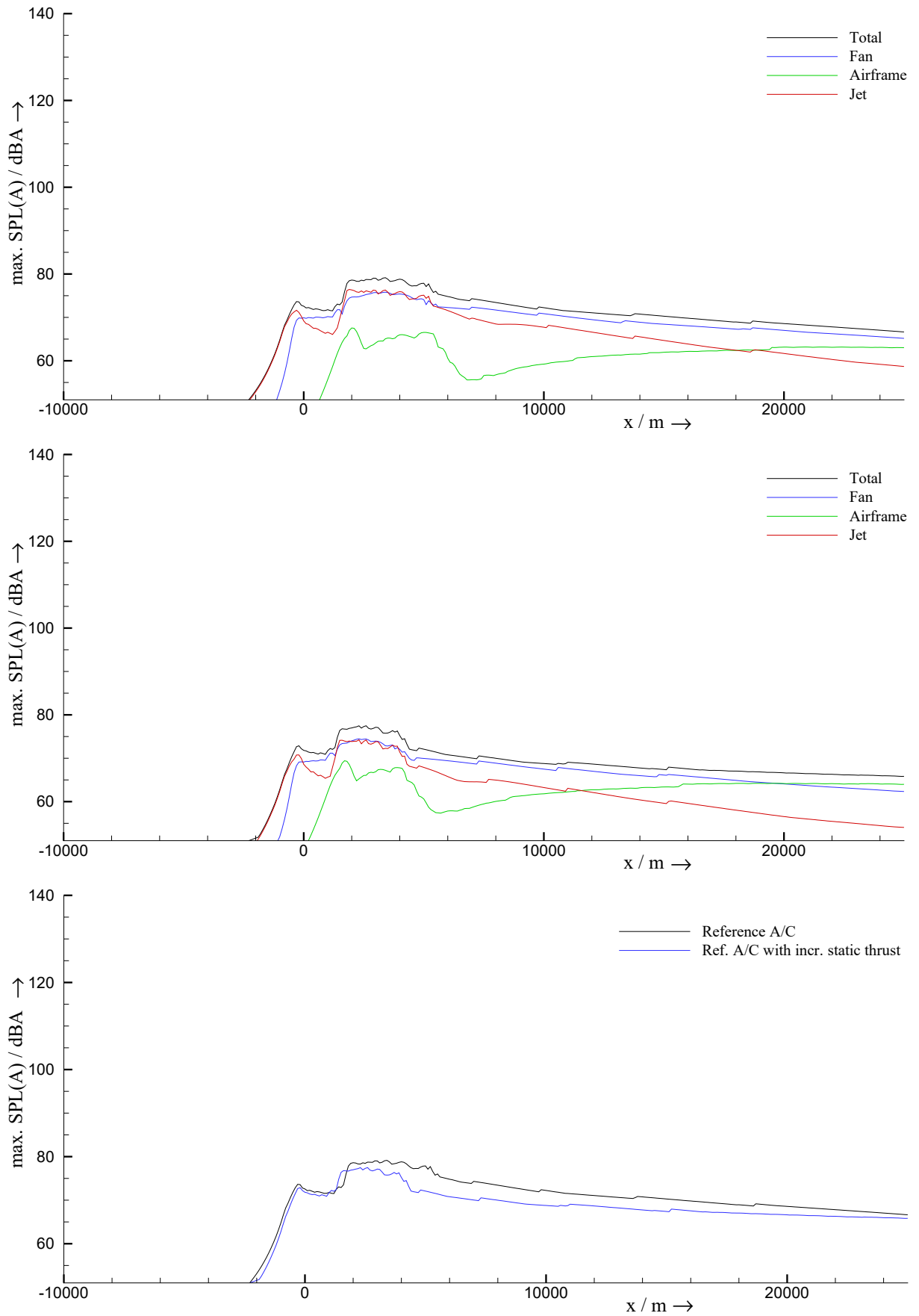
Figure E.19 Max. SPL(A) along *x*-axis, sideline *y* = 450 m; departure; reference A/C (top) v. high-powered A/C (middle)
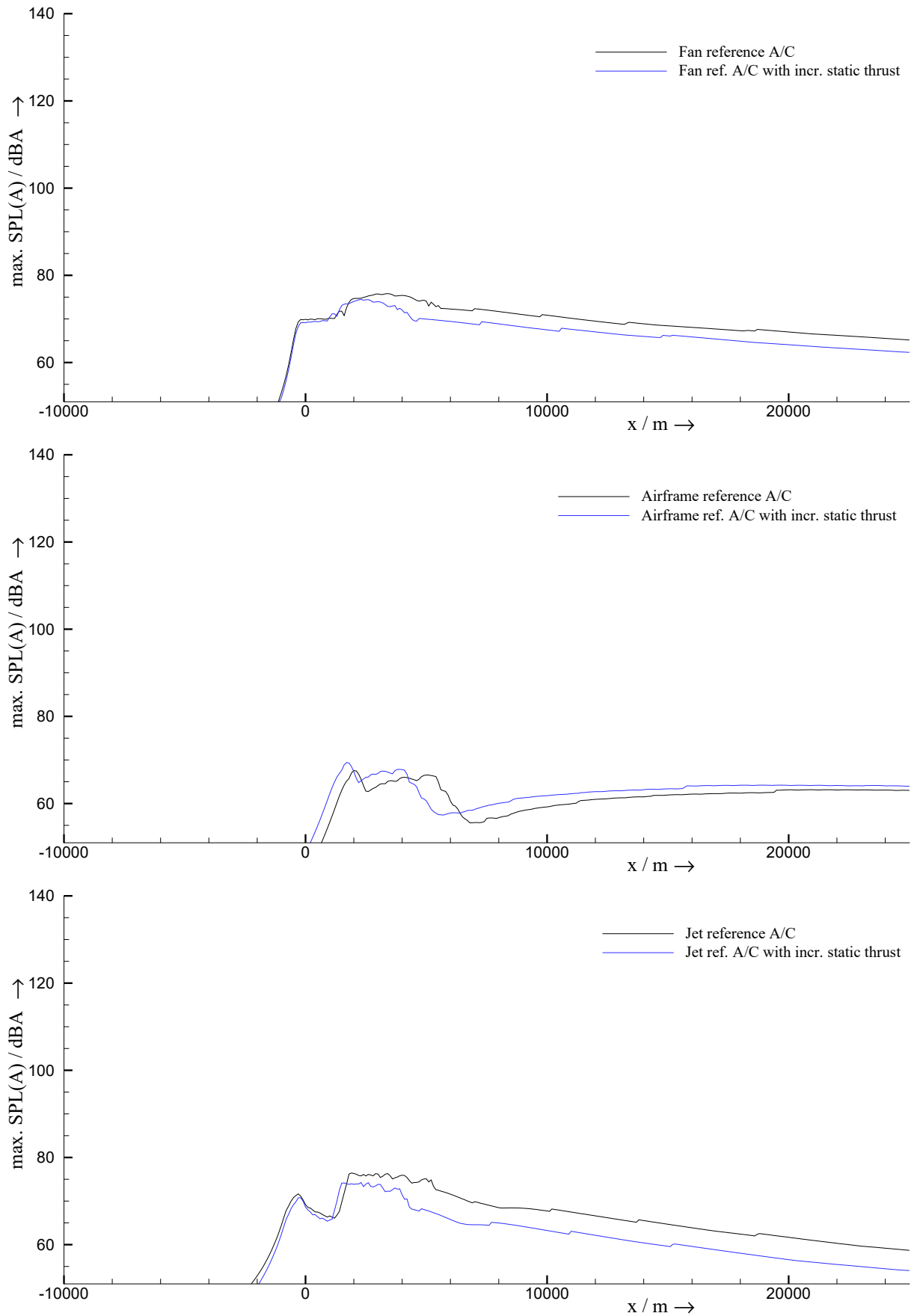
Figure E.20   Max. SPL(A) along *x*-axis, sideline *y* = 450; departure; fan-, airframe-, and jet noise components of reference A/C v. noise components of high-powered A/C
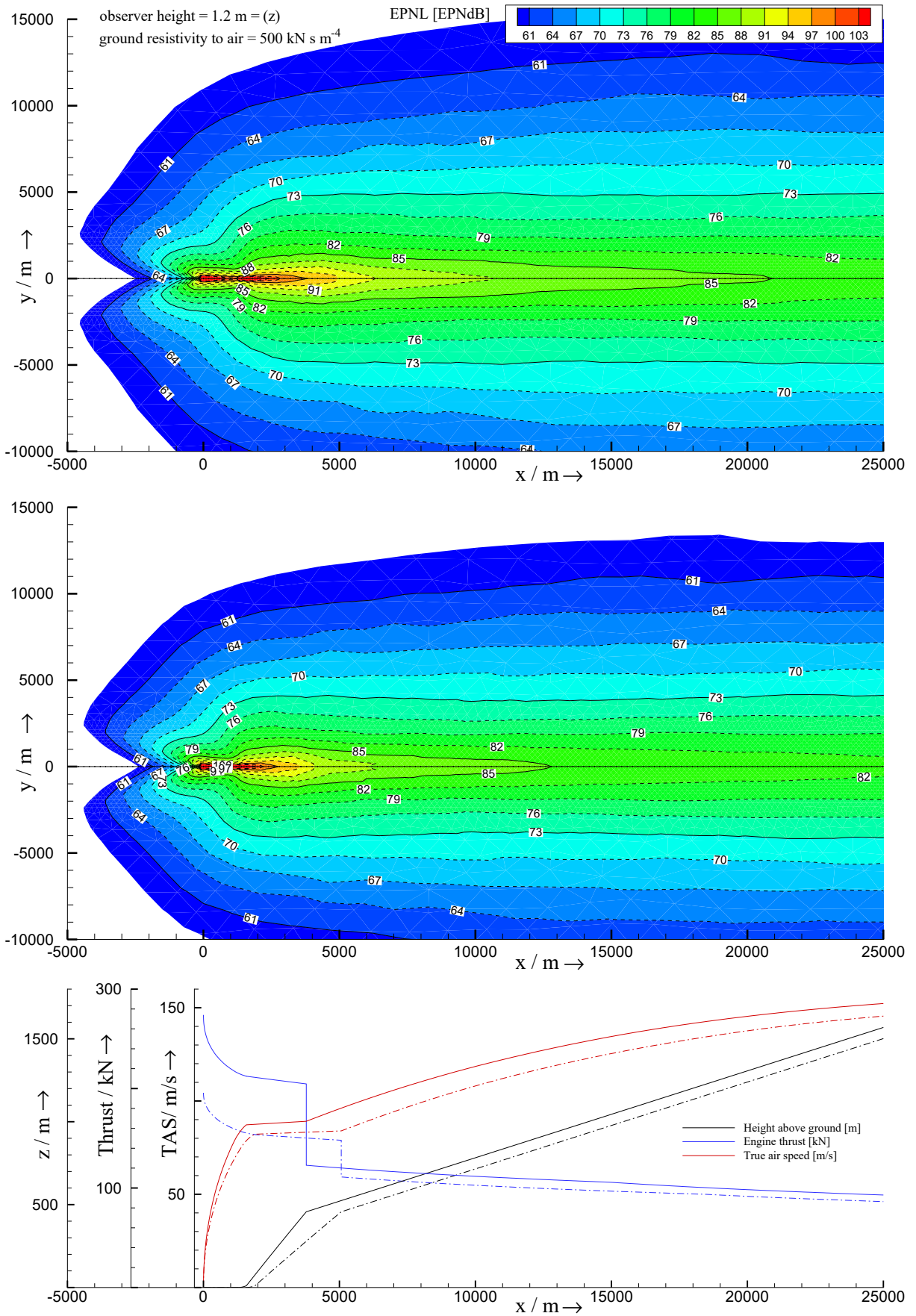
Figure E.21   Noise contour plot in EPNL; departure; reference A/C (top illustration; dash-dotted line) v. high-powered A/C (middle illustration; solid line) (identical to figure 6.2).
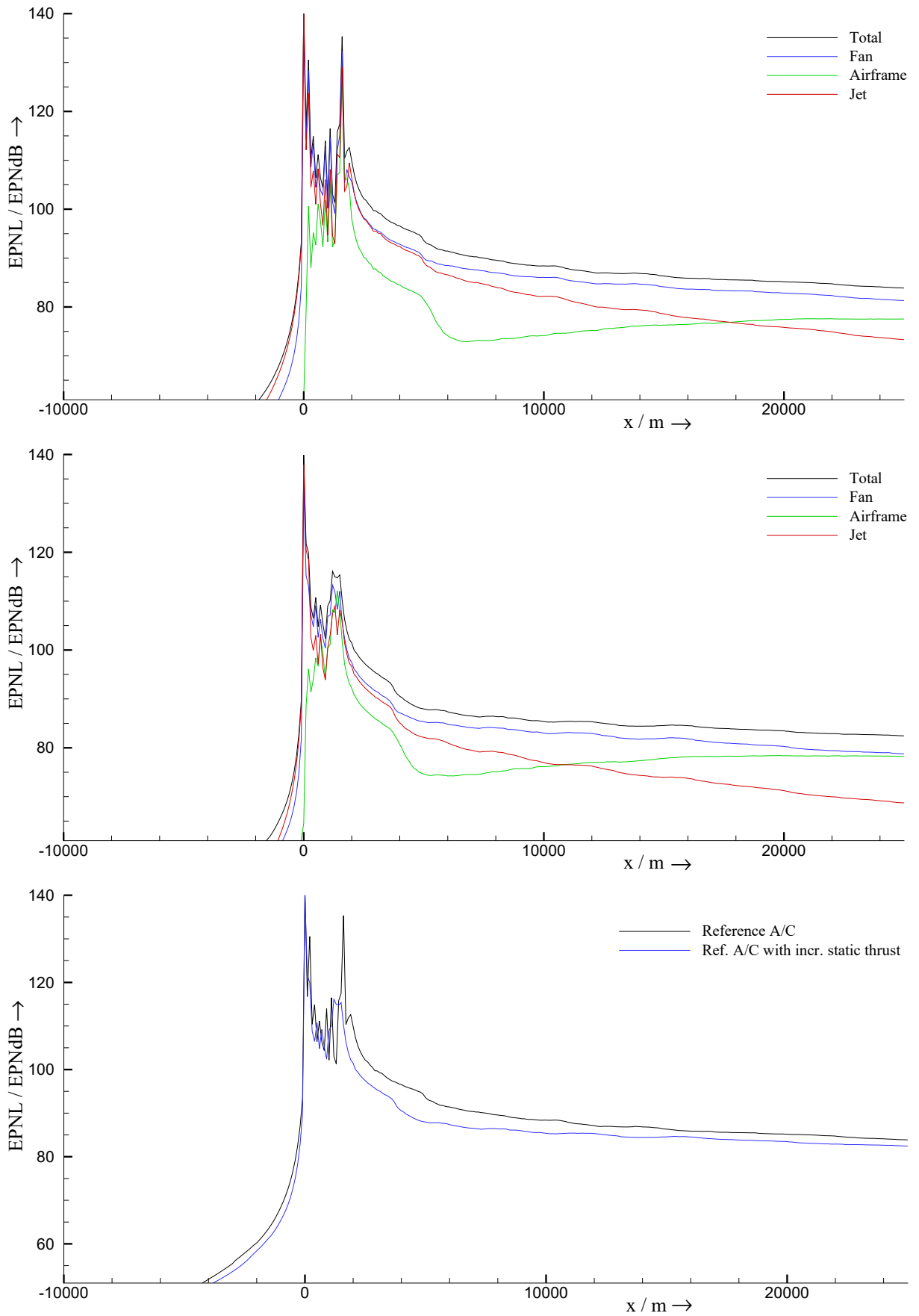
Figure E.22   EPNL along *x*-axis, *y* = 0; departure; reference A/C (top) v. high-powered A/C (middle)
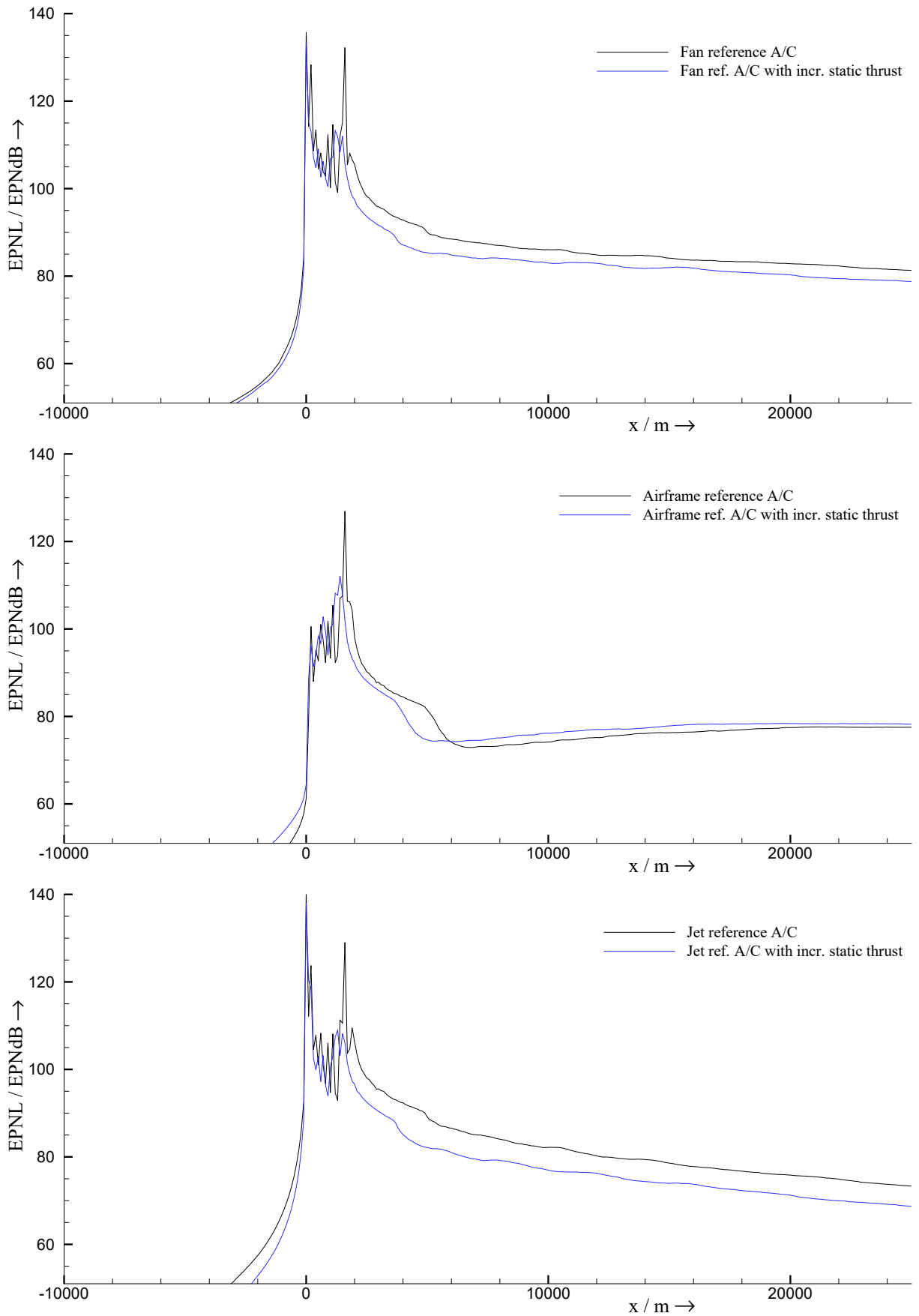
Figure E.23   EPNL along *x*-axis, *y* = 0; departure; fan-, airframe-, and jet noise components of reference A/C v. noise components of high-powered A/C
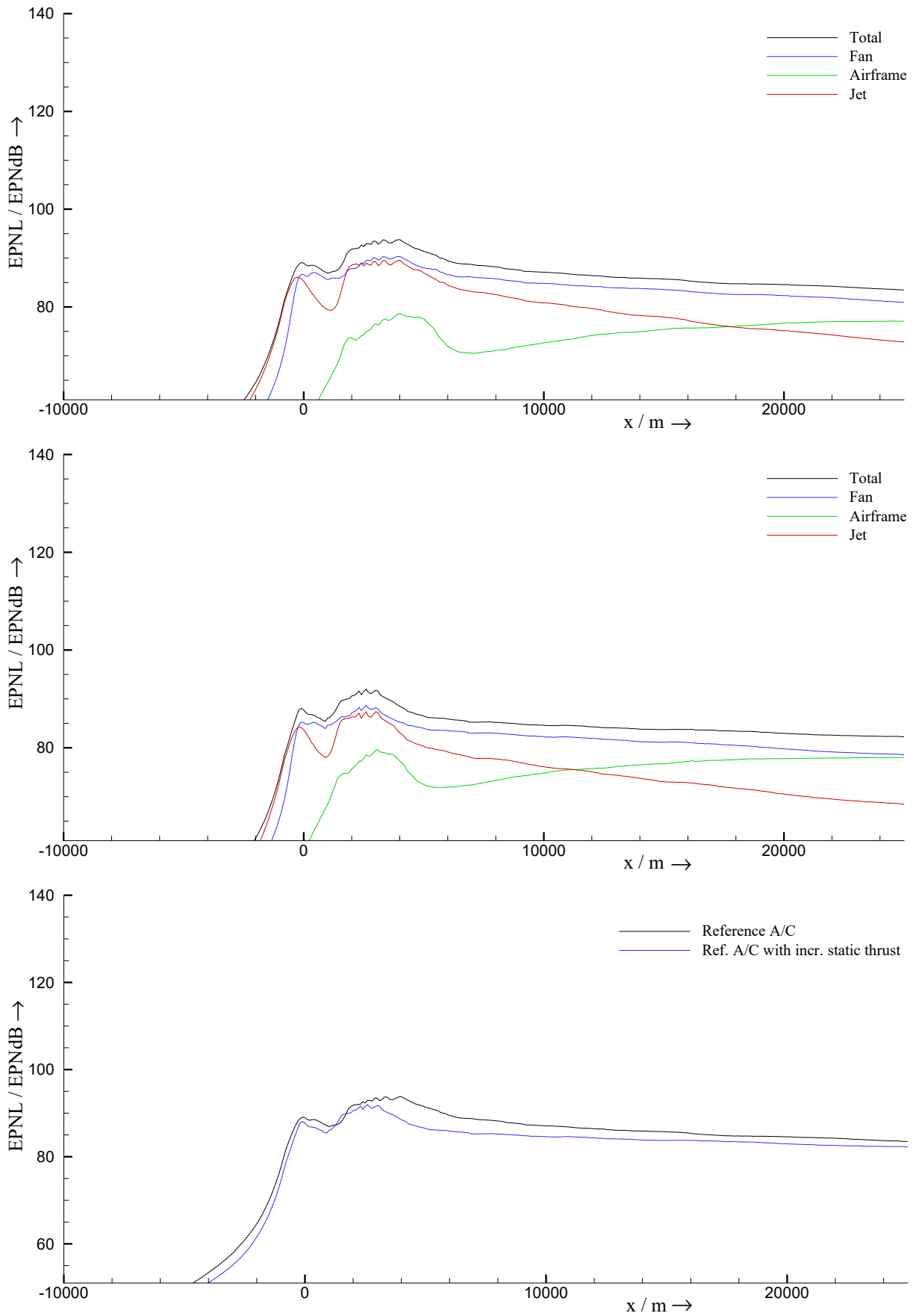
Figure E.24 EPNL along *x*-axis, sideline *y* = 450 m; departure; reference A/C (top) v. high-powered A/C (middle)
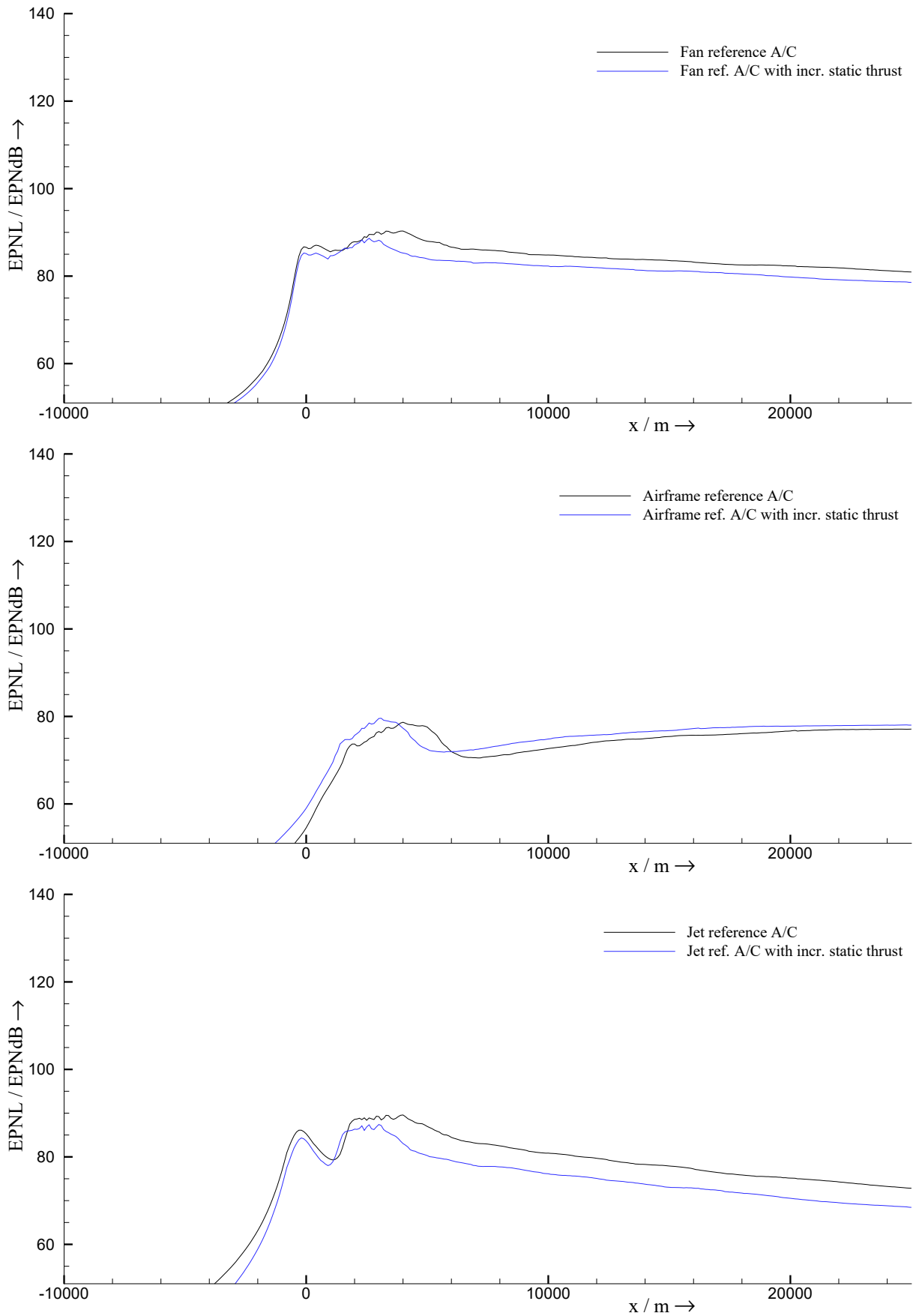
Figure E.25   EPNL along *x*-axis, sideline *y* = 450; departure; fan-, airframe-, and jet noise components of reference A/C v. noise components of high-powered A/C
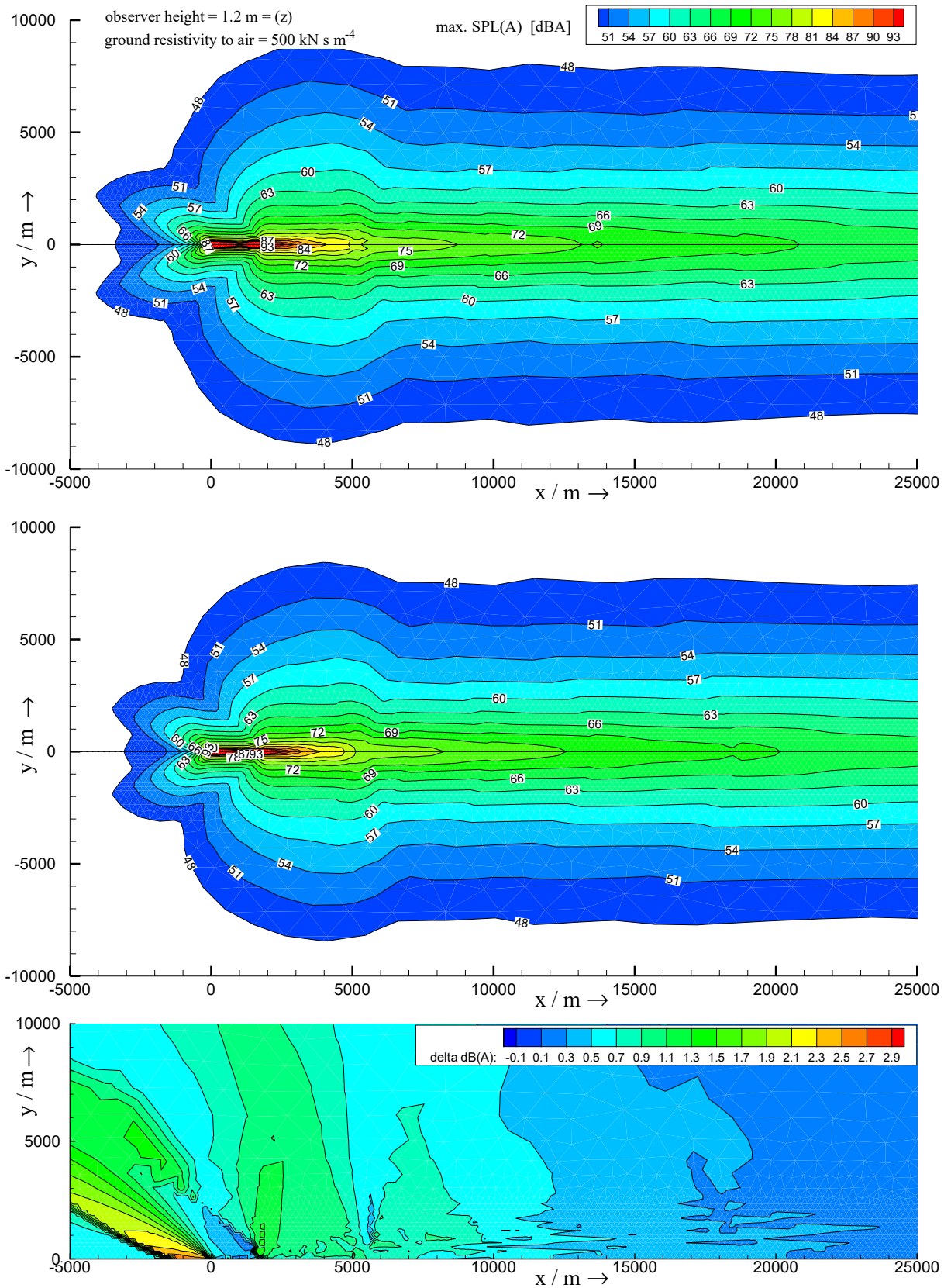
Figure E.26   Max. SPL(A) of reference A/C with the engine map adapted to DLR engine map (top) v. max. SPL(A) of reference A/C out of PrADO with no changes in the engine map (middle); bottom: top minus middle
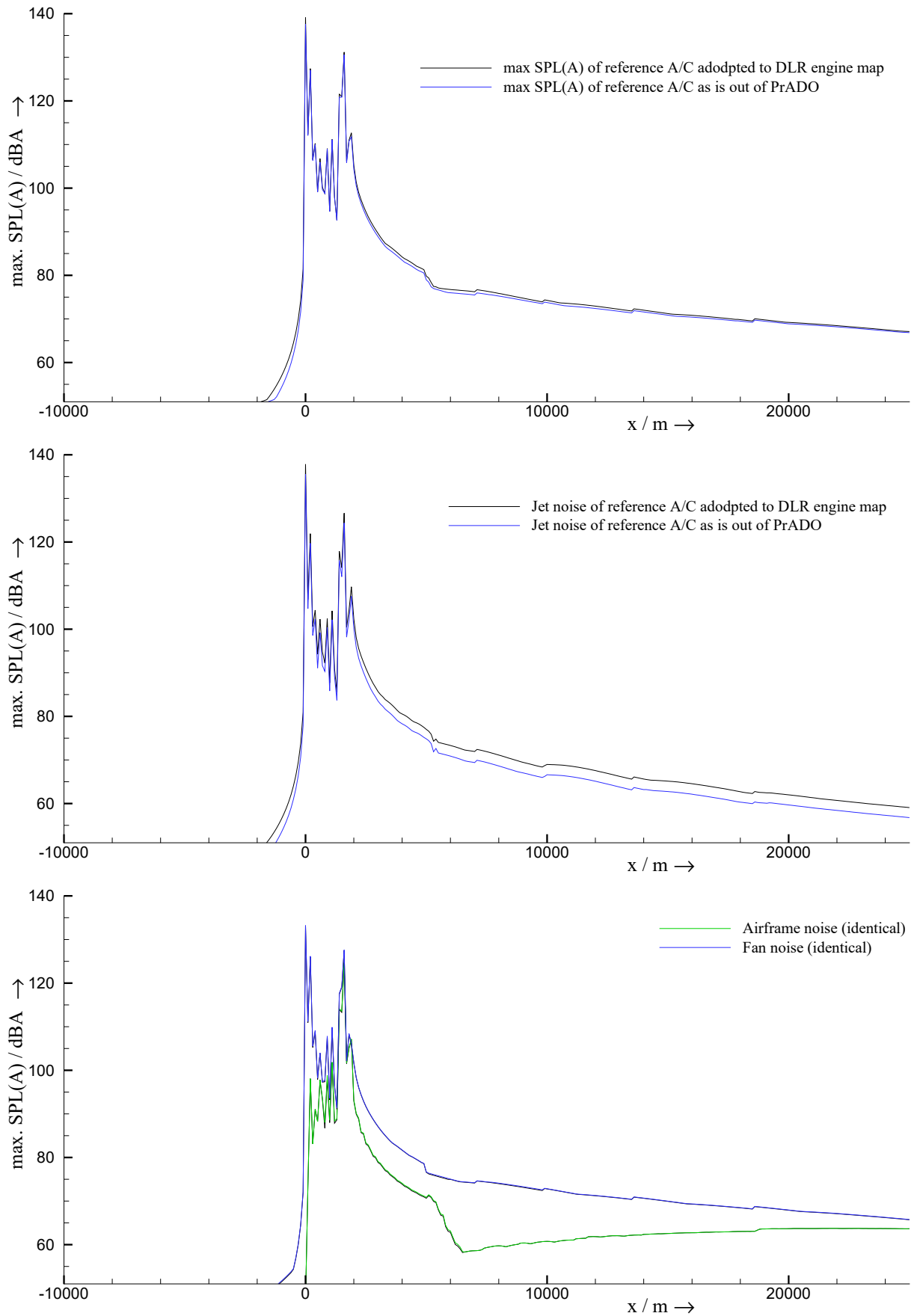
Figure E.27 Max. SPL(A) along *x*-axis, *y* = 0; departure; reference A/C adapted to DLR engine map v. reference A/C out of PrADO
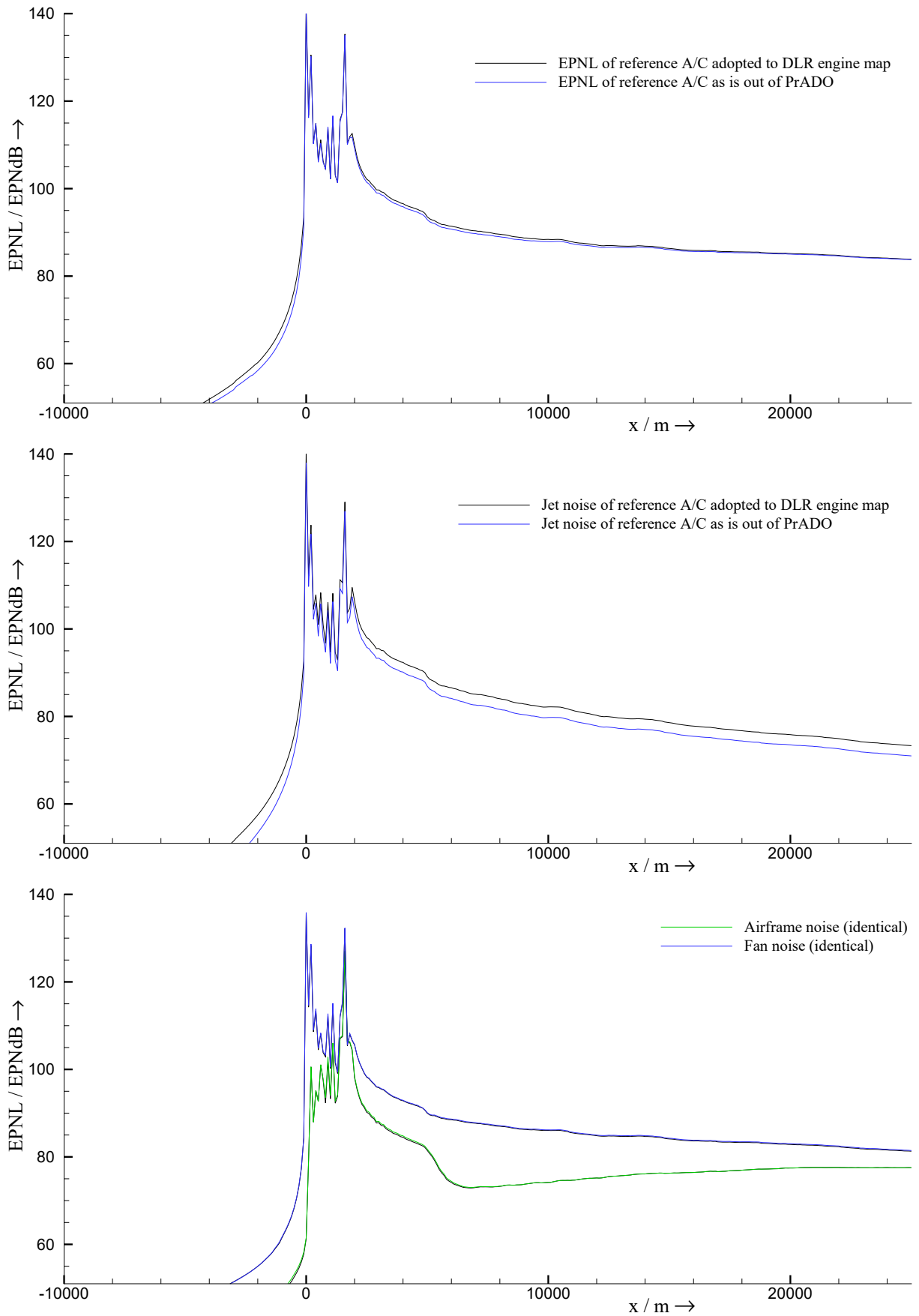
Figure E.28   EPNL along *x*-axis, *y* = 0; departure; reference A/C adapted to DLR engine map v. reference A/C out of PrADO
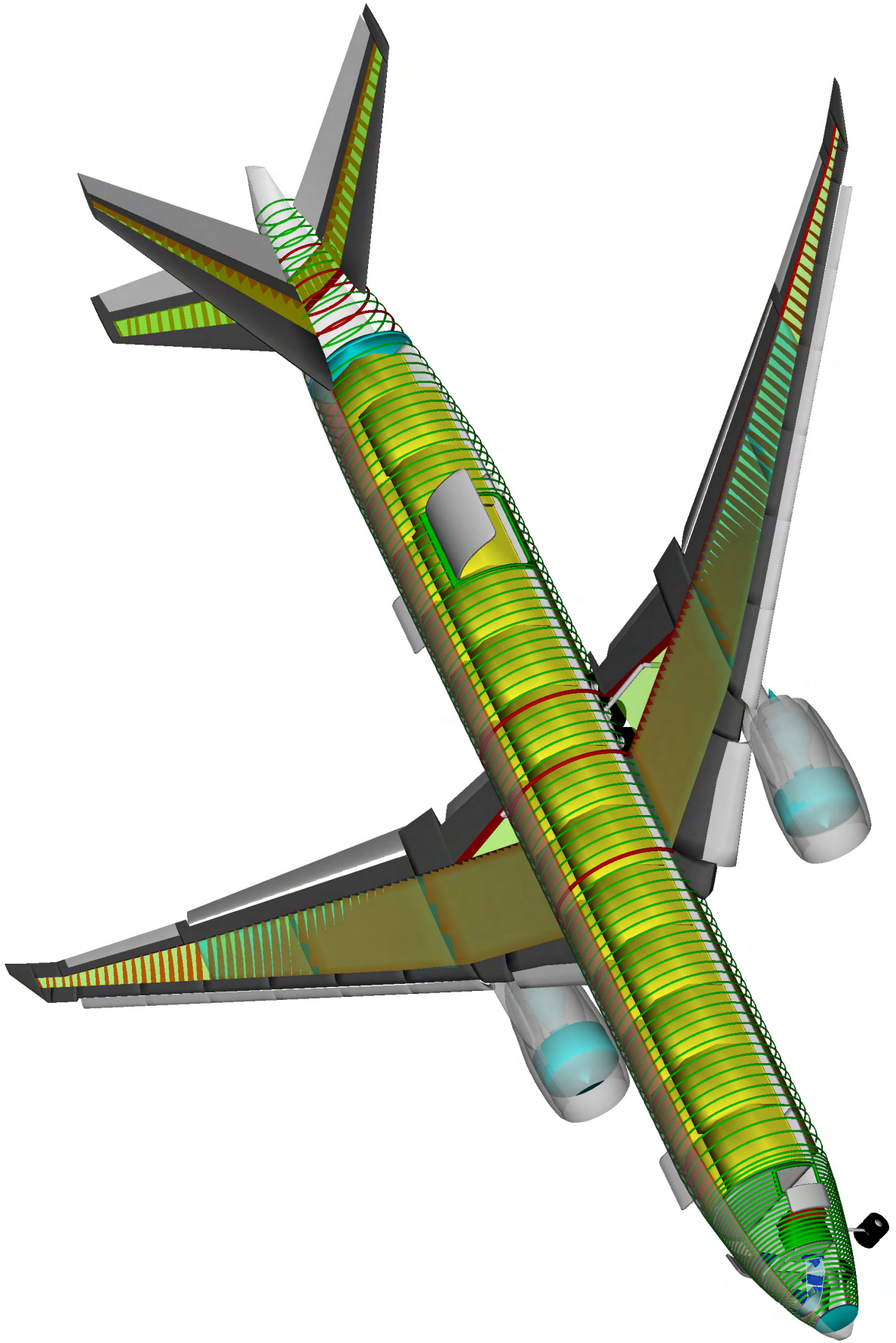
Figure E.29   PrADO 3D-drawing of Green-Freighter A/C
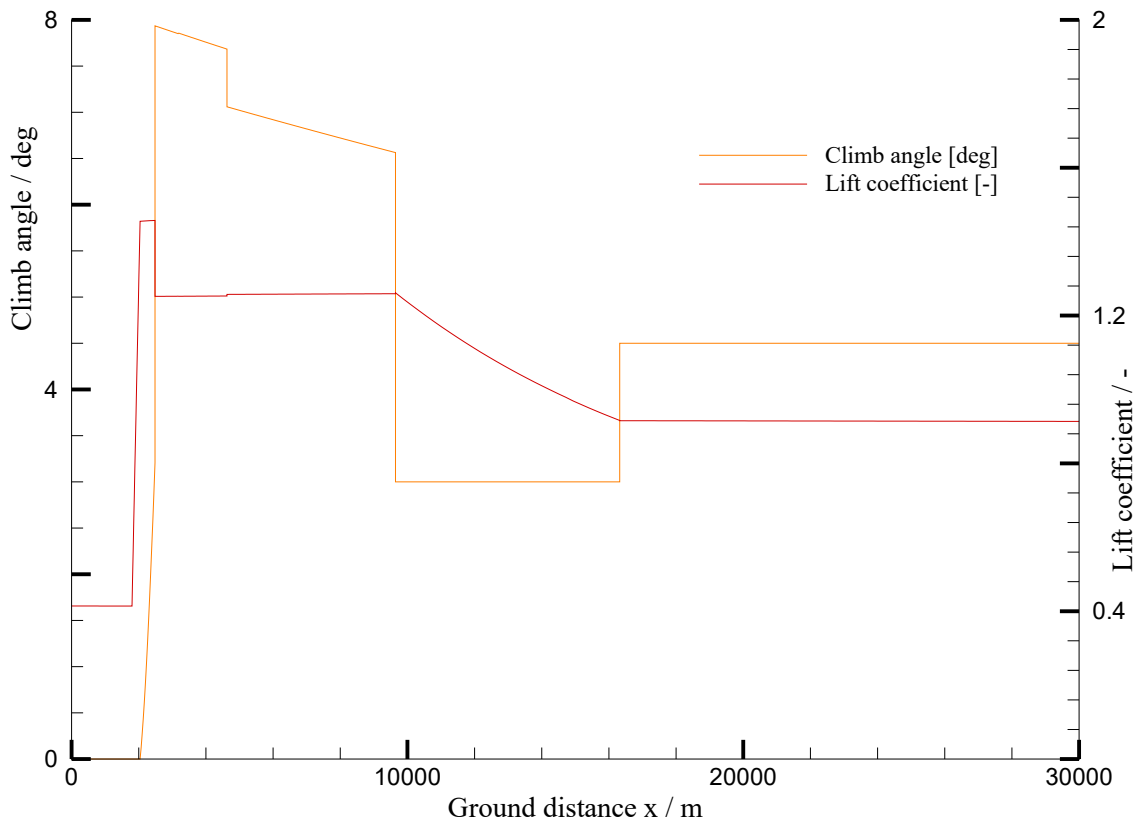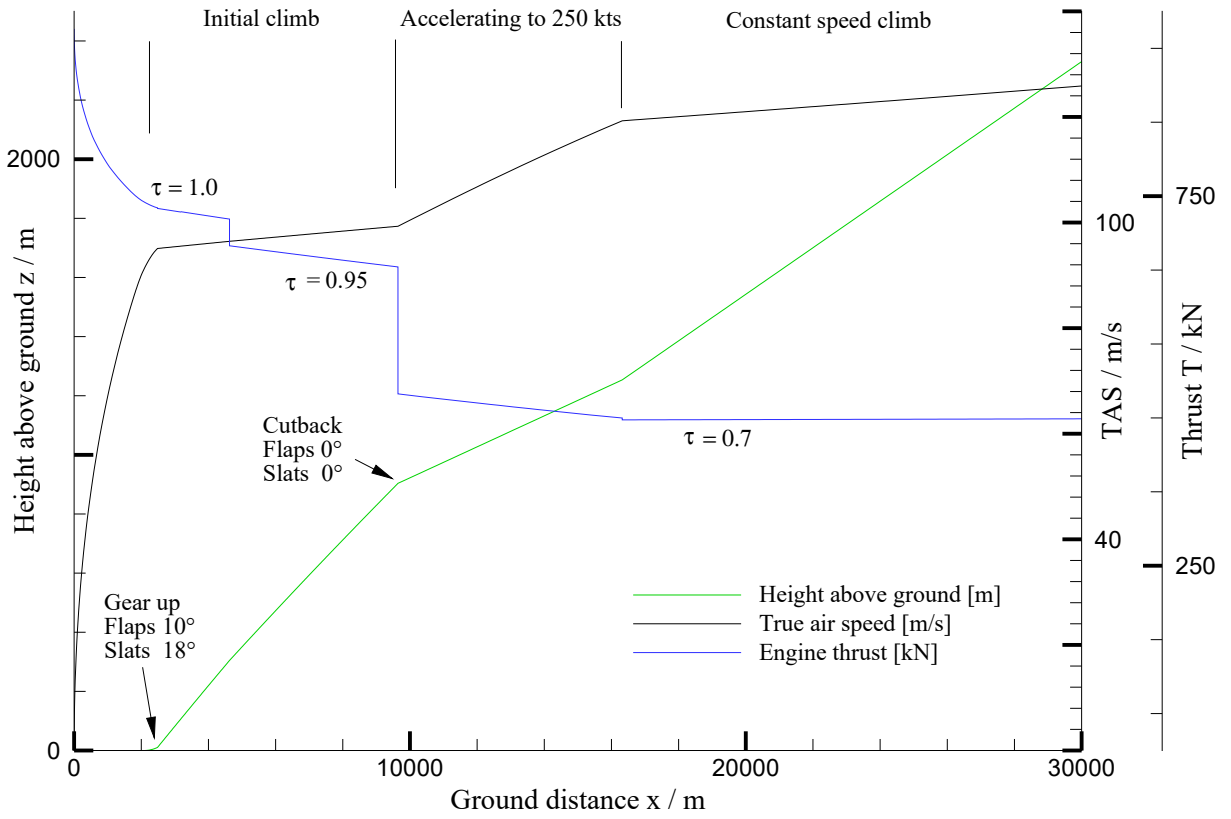
Figure E.30 Climb trajectory (ICAO NADP departure) of Green Freighter A/C, flight mission: flight with maximum payload. Engine throttle setting τ (0 – 100 %)
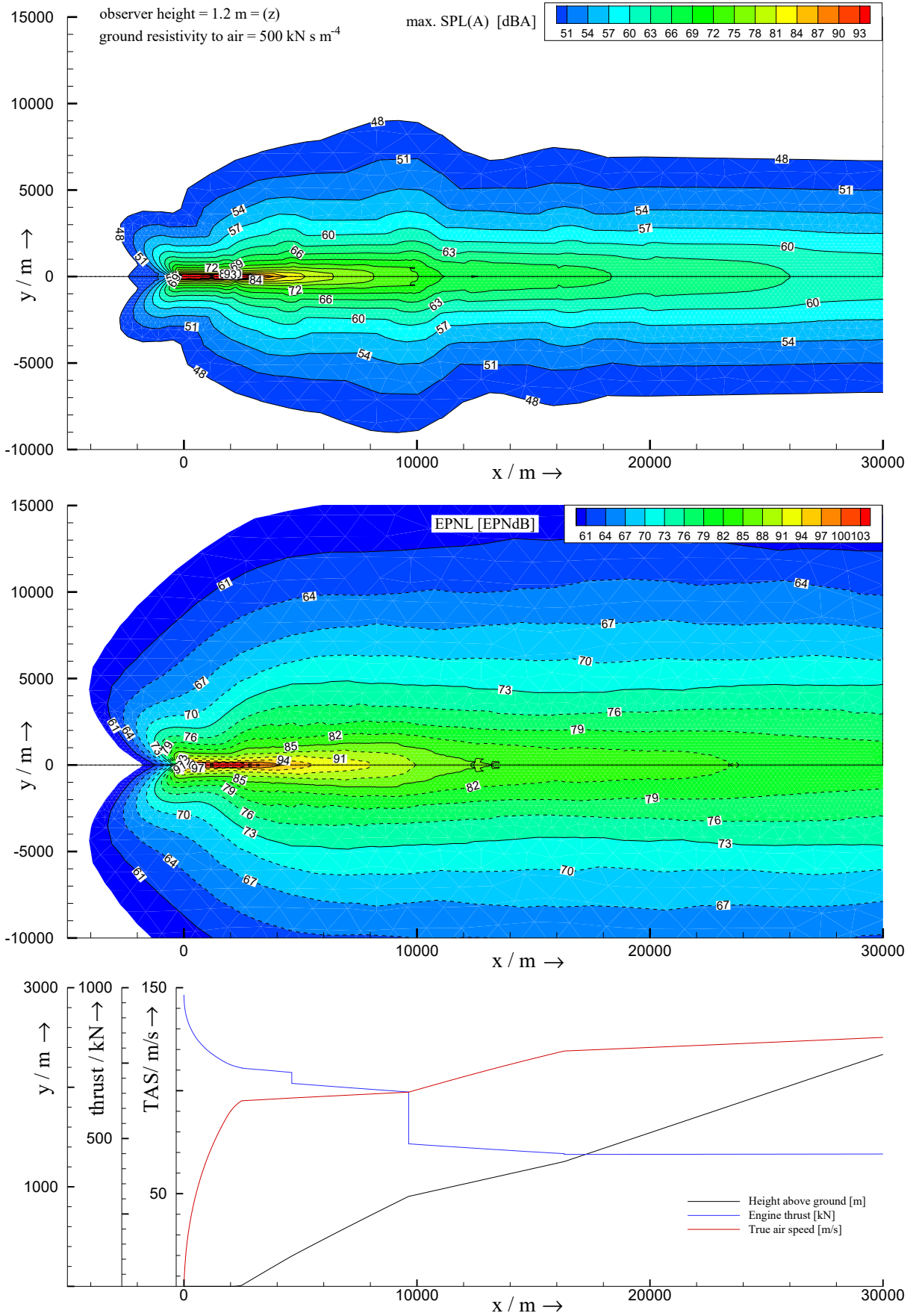
Figure E.31 Noise contour plot in max. SPL(A) vs. EPNL; ICAO departure of Green Freighter A/C (middle plot identical to figure 6.4)
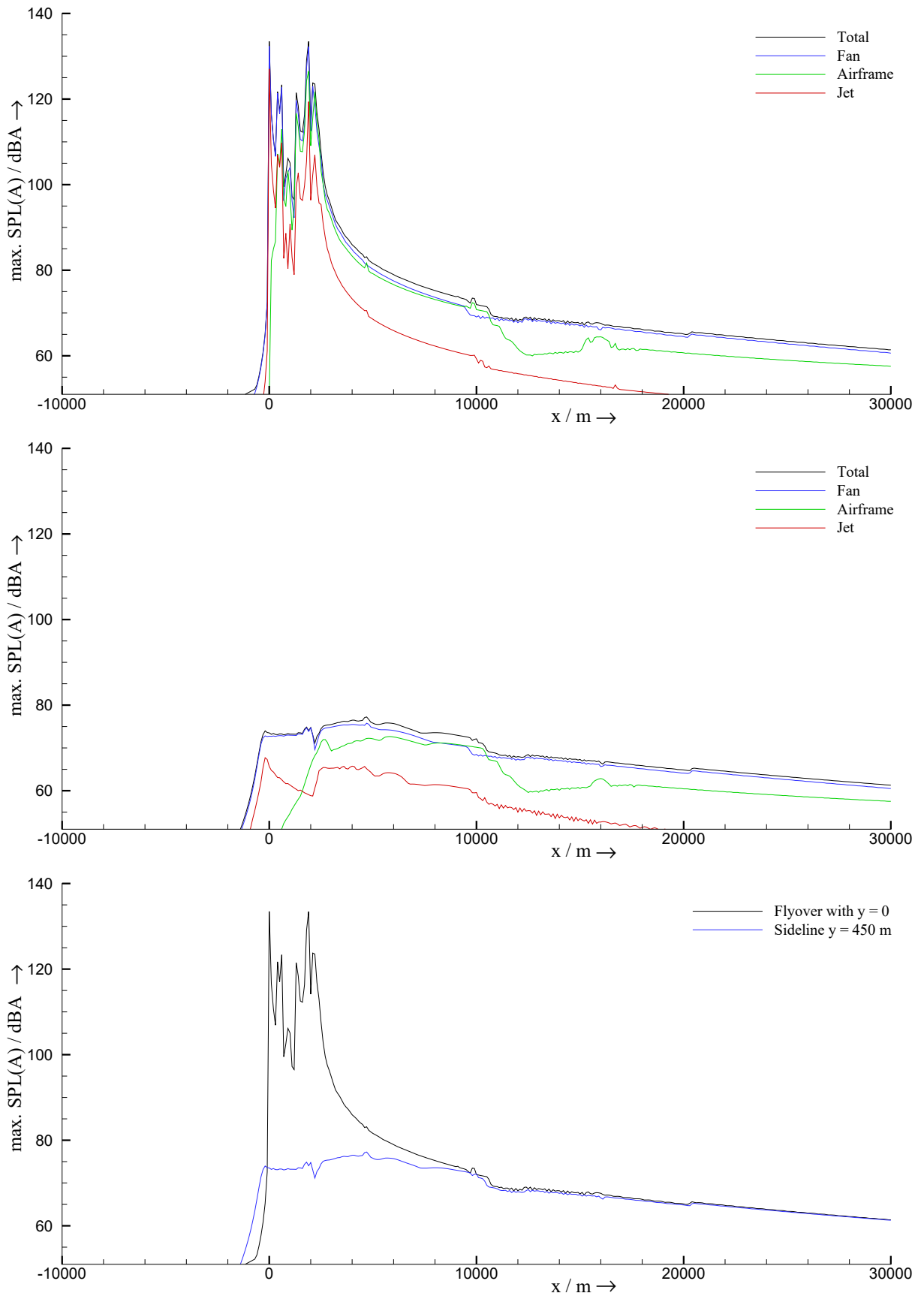
Figure E.32 Max. SPL(A) along *x*-axis, flyover (top) and sideline (middle); ICAO NADP departure of Green Freighter A/C
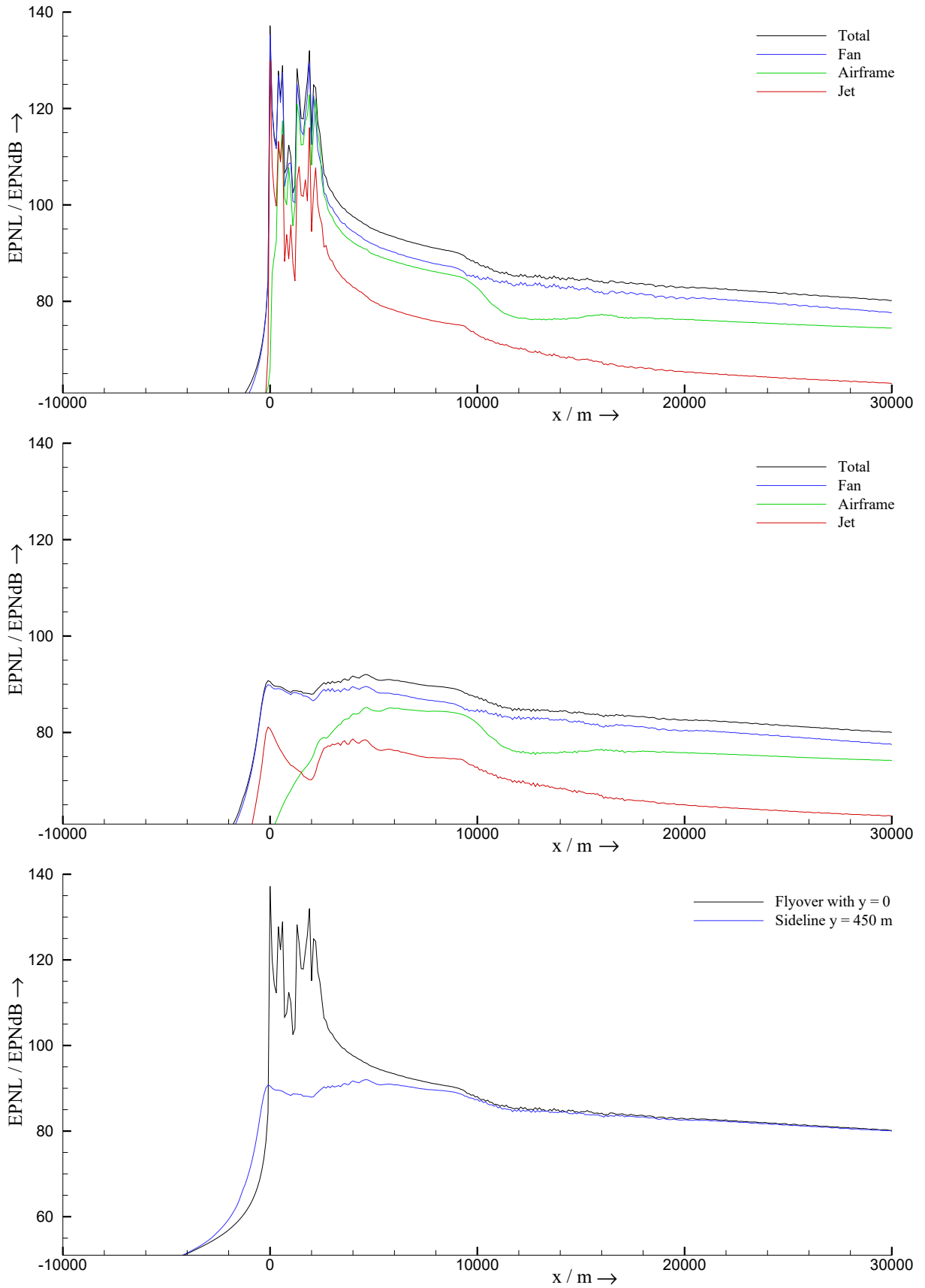
Figure E.33   EPNL along *x*-axis, flyover (top) and sideline (middle); ICAO NADP departure of Green Freighter A/C

E.1 Directivity Plots

Table E.1 Overview of varied parameters and A/C configurations for directivity plots

Fig. #	Description	N1 %	Thrust kN	TAS m/s	γ °	Θ °	α °	Gear -	Flap °	Slat °
	Engine									
E.35	Engine at max thrust	100	160	85	x	x	x	x	x	x
E.36	Engine at idle	70	64	85	x	x	x	x	x	x
E.37	Jet at max thrust	100	160	85	x	x	x	x	x	x
E.38	Jet at idle	70	64	85	x	x	x	x	x	x
E.39	Fan at max thrust	100	160	85	x	x	x	x	x	x
E.40	Fan at idle	70	64	85	x	x	x	x	x	x
	Airframe									
E.41	High lift at high speed	x	x	105	-3	2.5	5.5	ext.	15	22
E.42	High lift at low speed	x	x	75	-3	2.5	5.5	ext.	15	22
E.43	Clean at high speed	x	x	105	-3.6	-1	2.6	retr.	0	0
E.44	Clean at low speed	x	x	75	-3.6	-1	2.6	retr.	0	0
	Total climb									
E.45	Initial climb configuration	90	144	85	12	18	6	retr.	10	18
E.46	Climb configuration after cut back	80	106	130	5.5	9.5	4	retr.	0	0
	Total descent									
E.47	Idle descent configuration	0	-4	145	-3.6	-1	2.6	retr.	0	0
E.48	Glide slope configuration	85	140	68	-3	2.5	5.5	ext.	40	27
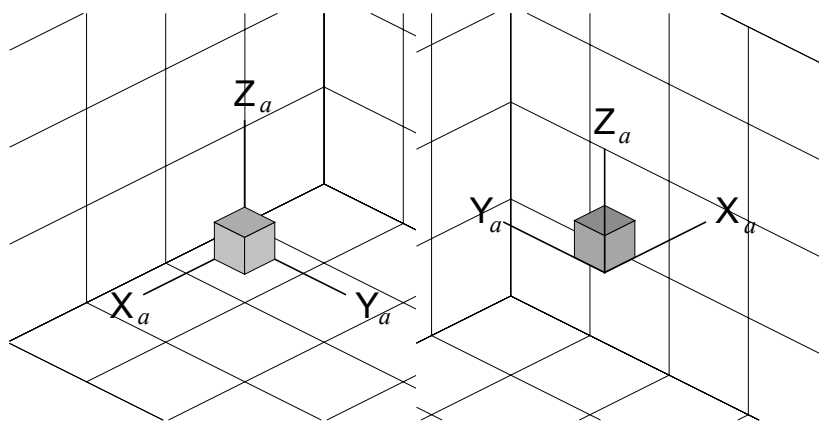
Figure E.34 Coordinate system definition for directivity plots.

a designates the air-path axis system. Therefore, the position of plots relative to the air-path axis system is defined through angle of attack α, and the position of the air-path axis system relative to the isometric coordinate view on the paper is defined through climb angle γ.

In left illustrations, the directivity plot is shown from the front side. In right illustrations the directivity plot is shown from the back side.
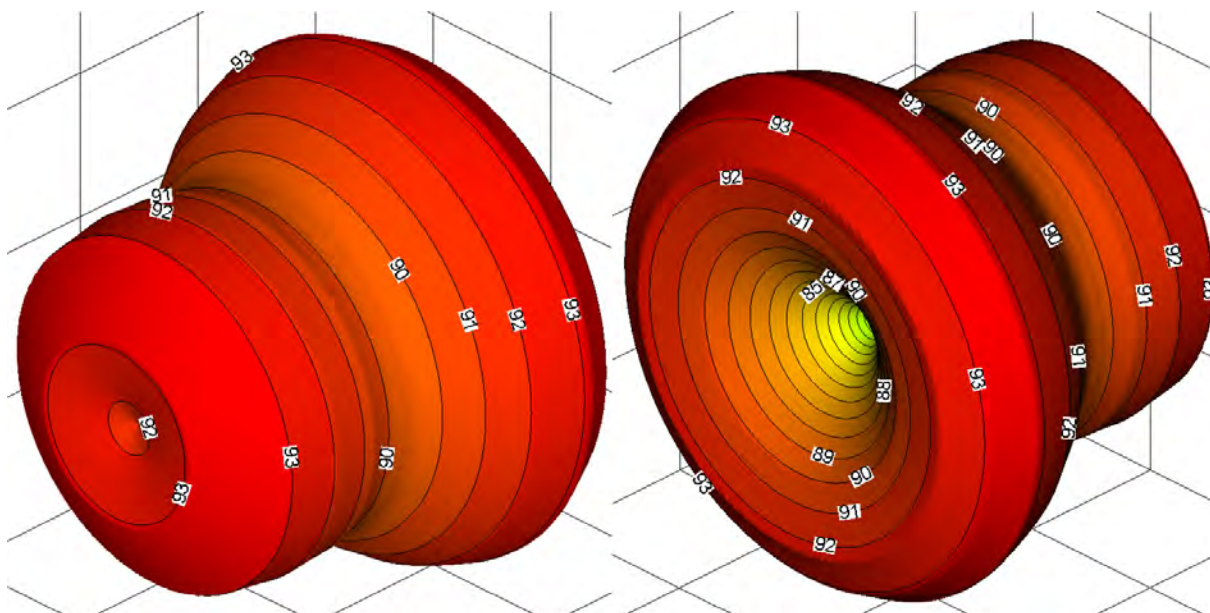
Figure E.35   Directivity plot: engine at maximum thrust
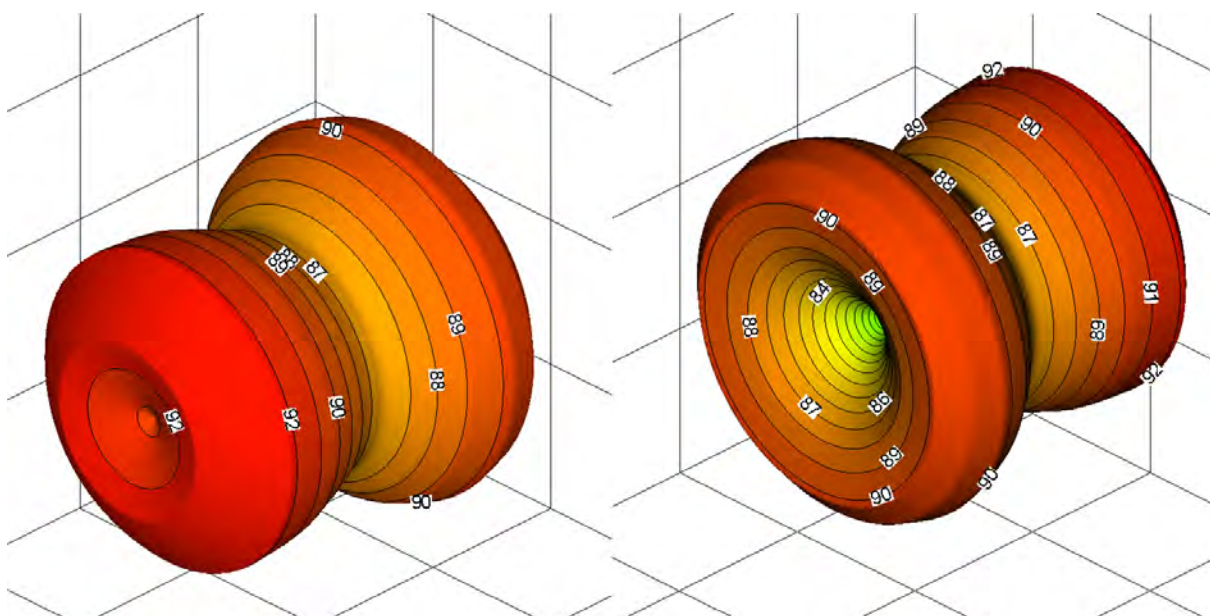
Figure E.36   Directivity plot: engine at idle

Sound pressure levels radiating forward are still comparable in form and in absolute levels in dBA although the condition of the engine changes from maximum thrust to idle. In contrast, SPL radiating backwards change remarkably that could be an answer of jet or fan source models. Noise radiating forward is (in our case with implemented source models) caused by the fan. Splitting the engine noise into its major contributors of fan- and jet noise will give more information (see directivity plots below)
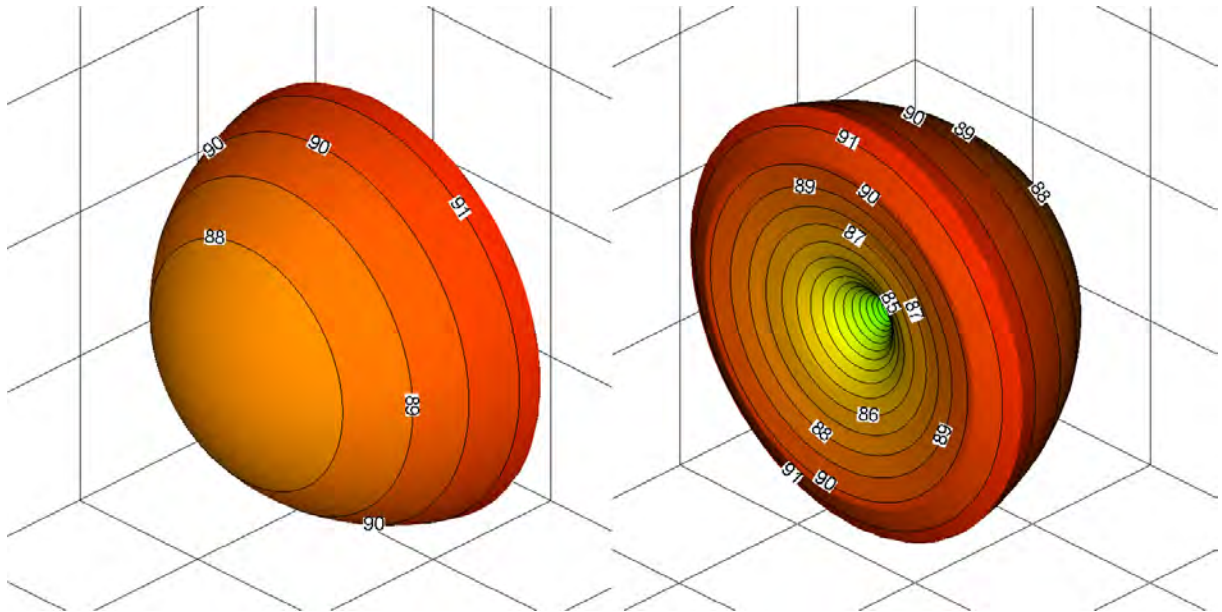
Figure E.37   Directivity plot: jet at maximum thrust
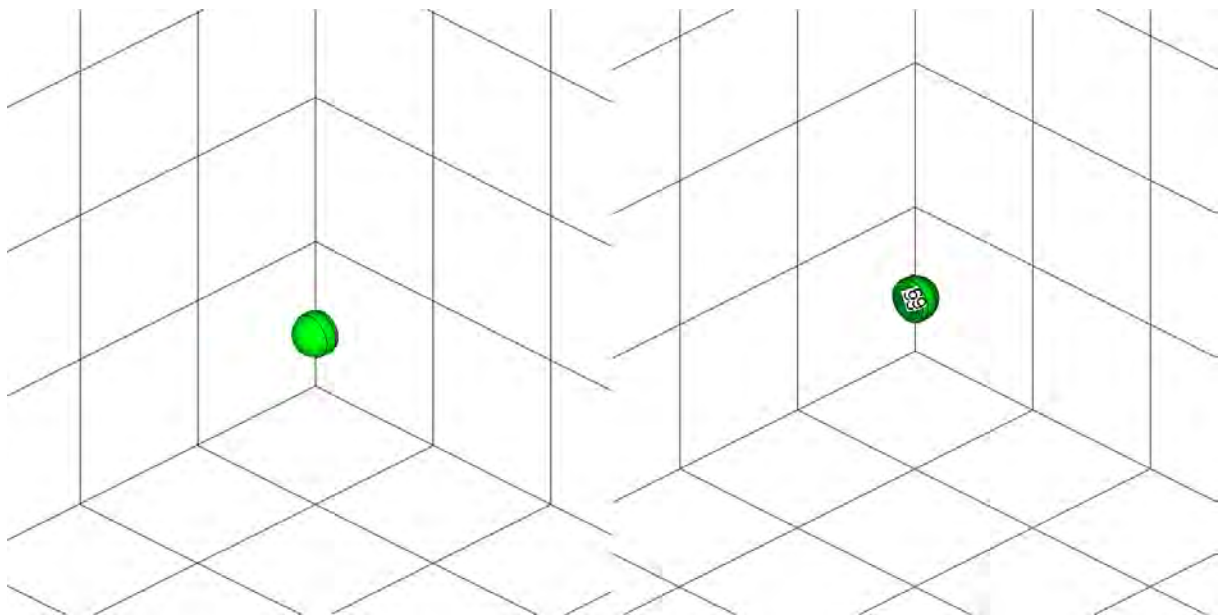
Figure E.38   Directivity plot: jet at idle

*Noise caused by the jet of an engine seems to be highly dependent on engine thrust setting and thus on primary-and secondary jet velocities. SPLs for the jet are identifiable 30 dBA lower compared to those with the engine at idle. The small size of the contour plot is a result of the logarithmic ratio of the decibel scale that is here, in the plot, reversed by scaling the distance (microphone – source) of relevant SPL(A) with the root-mean-square sound pressure that has been A-weighted before. As can be seen in the plot, jet noise does not radiate forwards. Comparisons of obtained directivities are possible with directivities after **Stone 1983** as depicted in figure D.13.*
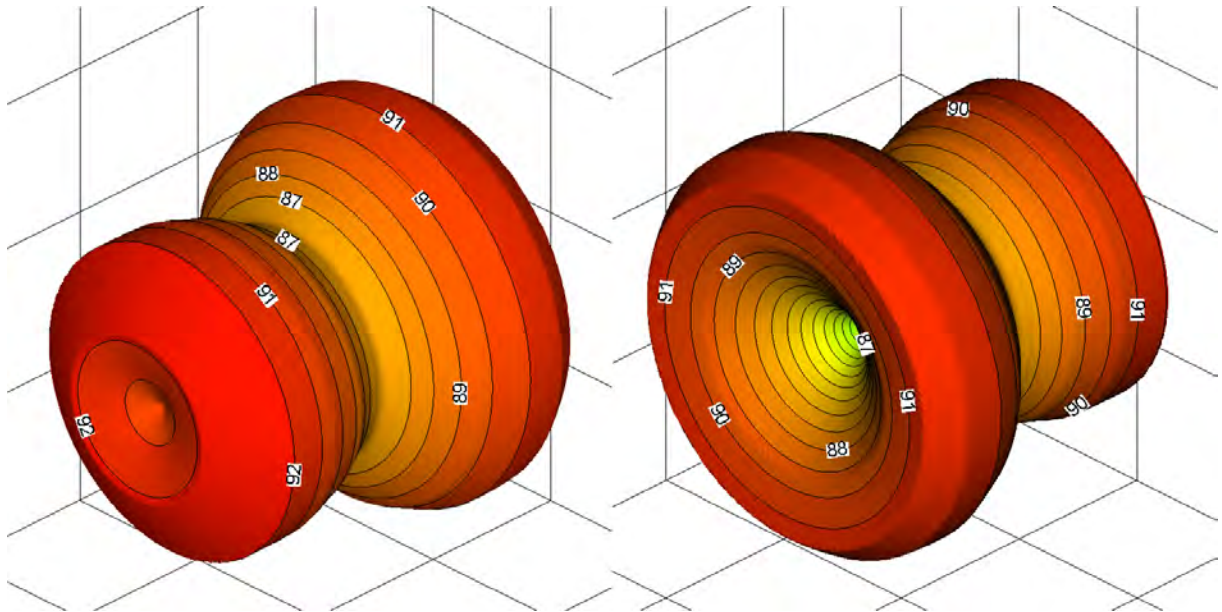
Figure E.39   Directivity plot: fan at max thrust
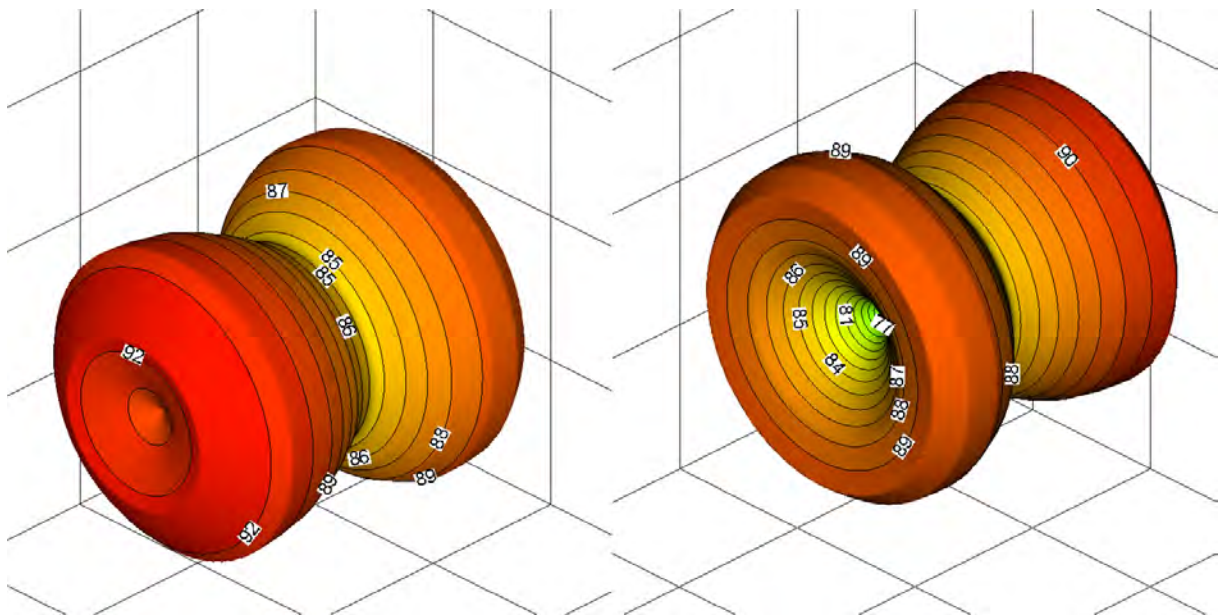
Figure E.40   Directivity plot: fan at idle

*Noise from the fan radiates forwards and backwards. Cutting these plots in half through the rotational x-axis would give the directivity correction for fan noise from **Heidmann 1979** as depicted in figure D.12. It can be seen that fan noise radiating forward does not change so much with a change in engine thrust setting. Fan noise radiating backwards shows at least a discrepancy in 2 dBA. However, as a result, fan noise is prevailing throughout all engine conditions. This result reflects the necessity of reducing fan noise to obtain lower noise impacts on ground.*
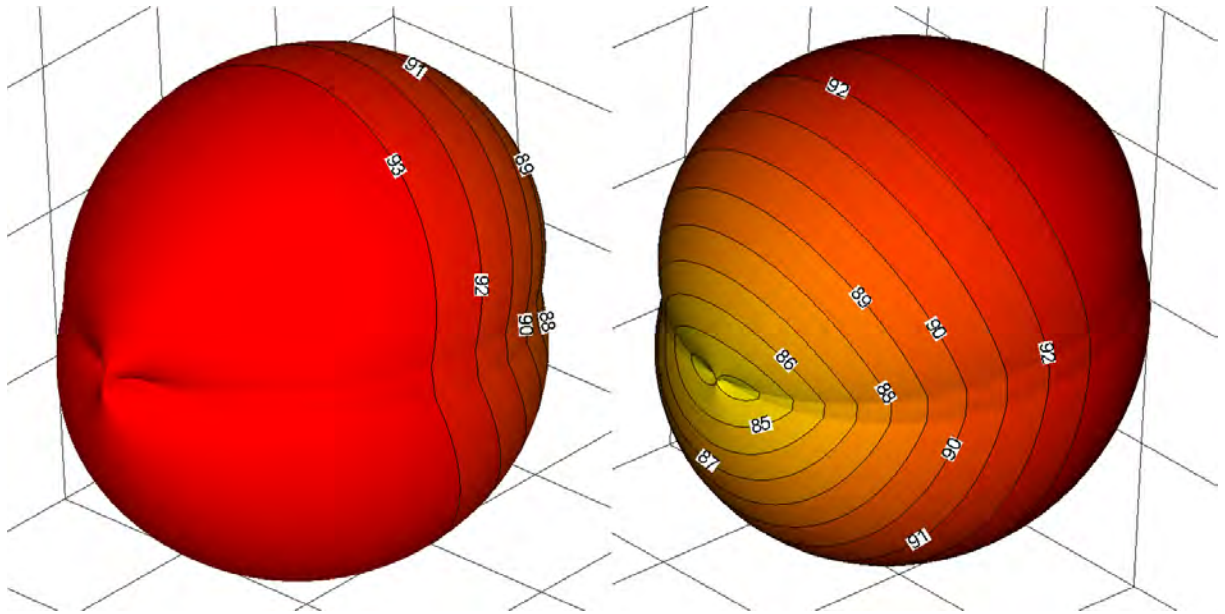
Figure E.41   Directivity plot: high lift at high airspeed
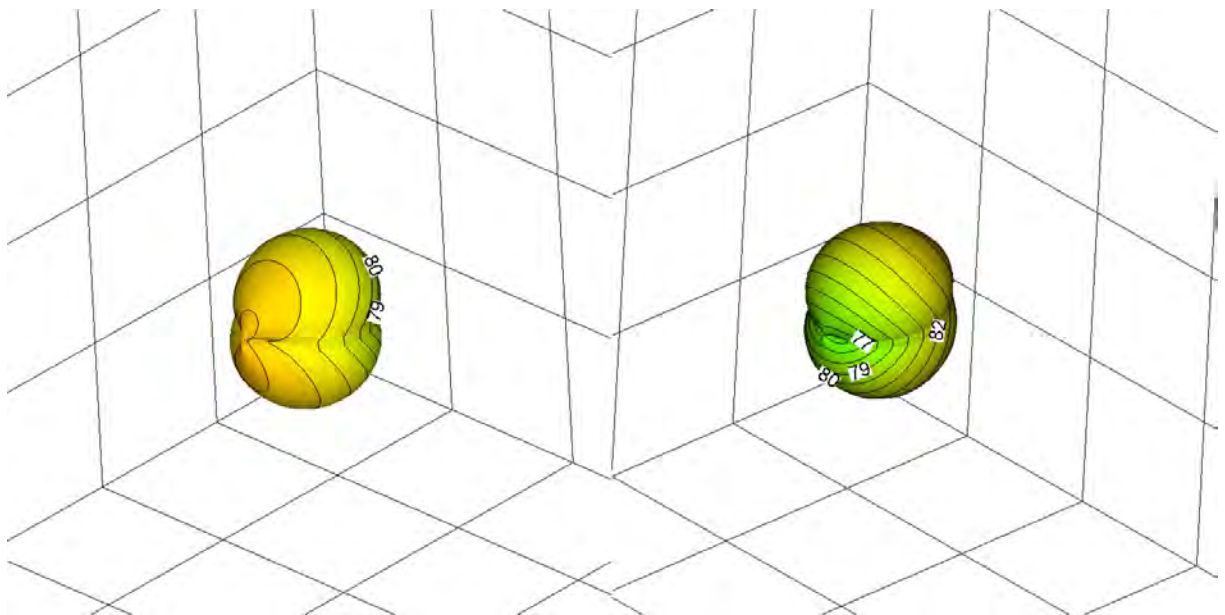
Figure E.42   Directivity plot: high lift at low airspeed

In above figures the strong influence of the airspeed upon airframe noise becomes clearly visible (airspeed scales SPLs at least to the power of five). The above figure exhibits higher SPL(A) compared to engine or jet SPL(A). This shows how important airframe noise can become at high airspeeds especially during idle descent. The form equals almost a pulsating sphere i.e. monopole. However, at low airspeeds (figure E.42) a dipole becomes visible.
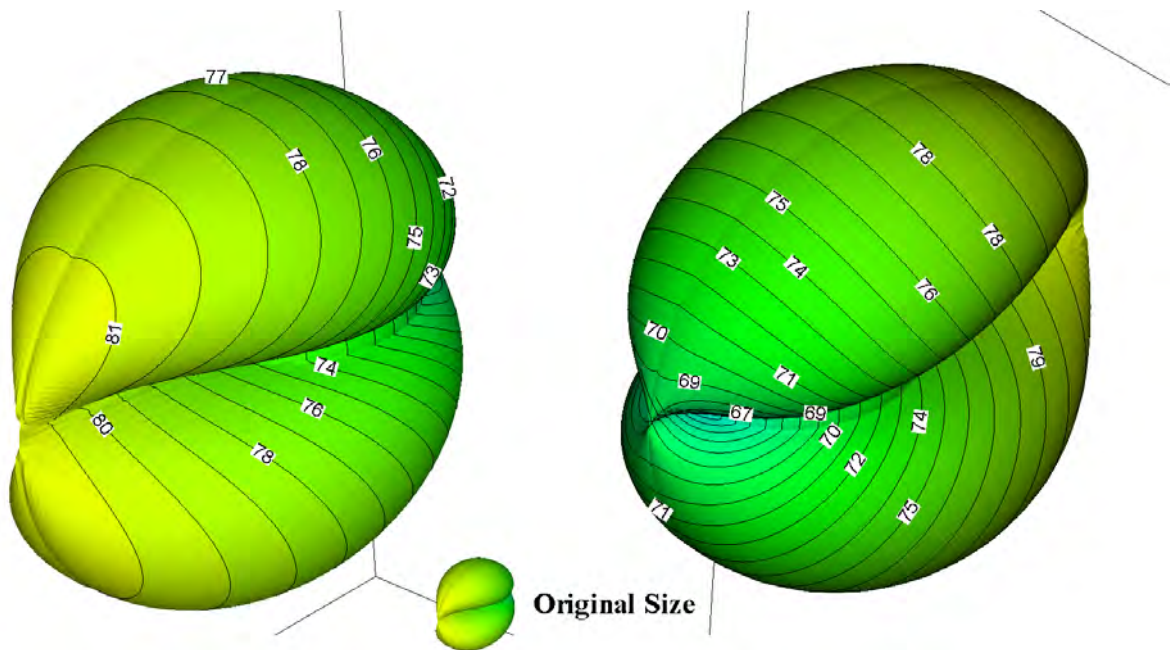
Figure E.43   Directivity plot: clean at high speed
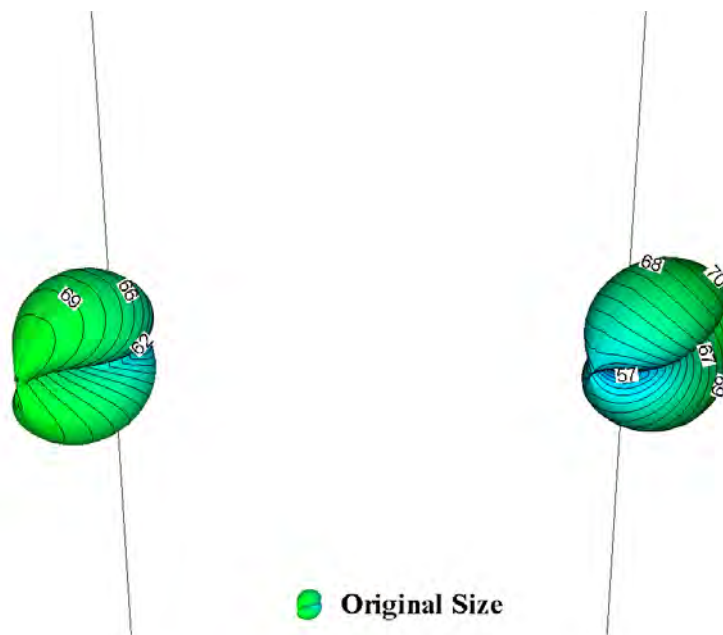
Figure E.44   Directivity plot: clean at low speed

With no slats and no flaps extended airframe noise that is in this case the noise of the clean aircraft becomes very small (compare original size in illustrations with E.41 and E.42) especially at low airspeeds. A shape of a dipole is recognizable although slats (modelled through dipoles) are retracted.
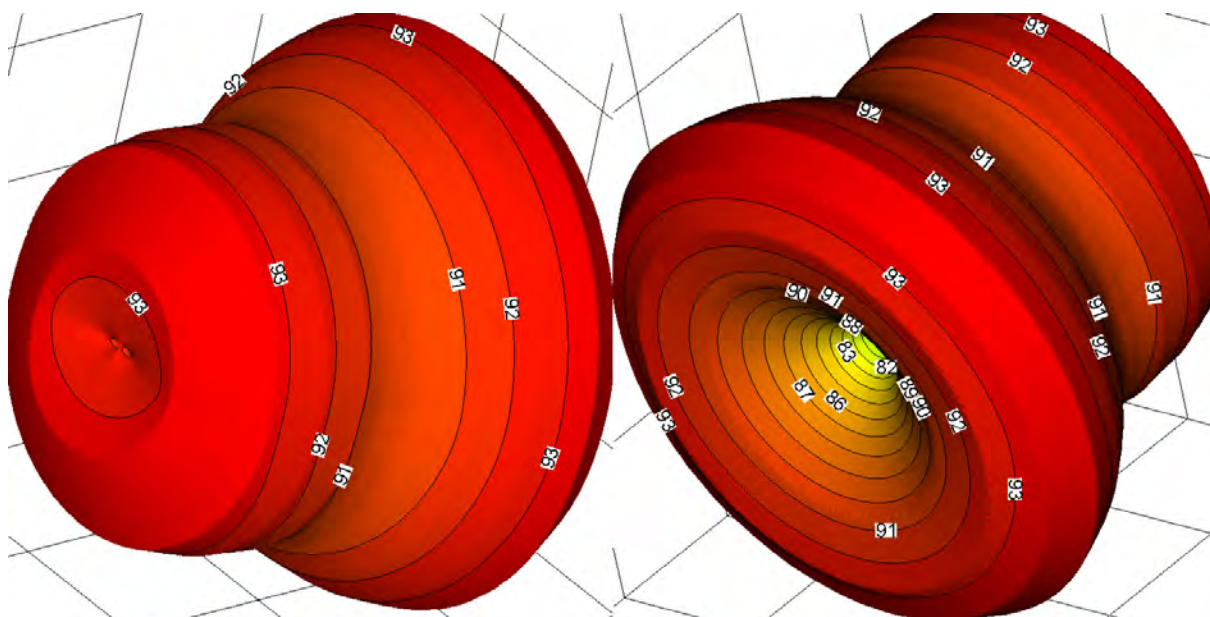
Figure E.45   Directivity plot: initial climb configuration
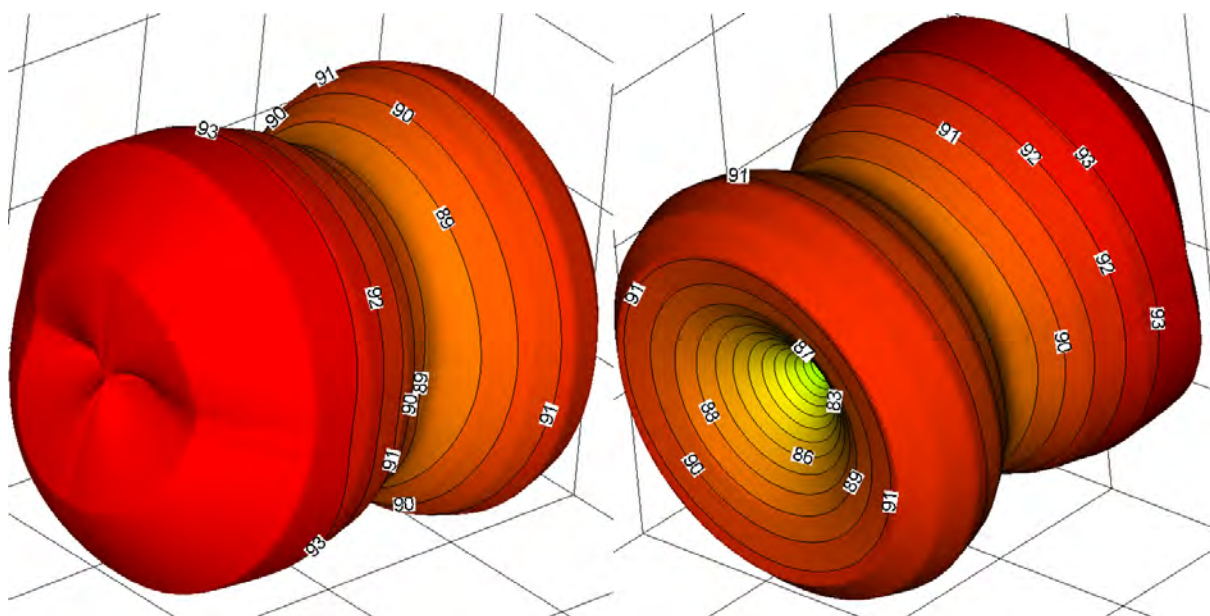
Figure E.46   Directivity plot: climb configuration after cut back

Due to the cutback fan noise radiating backwards and jet noise are lower (see above directivity plots), lowering the engine noise radiating backwards. This directivity plots are considering all noise sources (airframe and engine). It can be seen that the shape is equally to that of the engine directivities. However, the directivity in figure E.45 is of greater extend than that as in figure E.35. Airframe directivities can only be assumed to be responsible for a slight oval shape. In figure E.46 convective amplification becomes visible on fan noise.
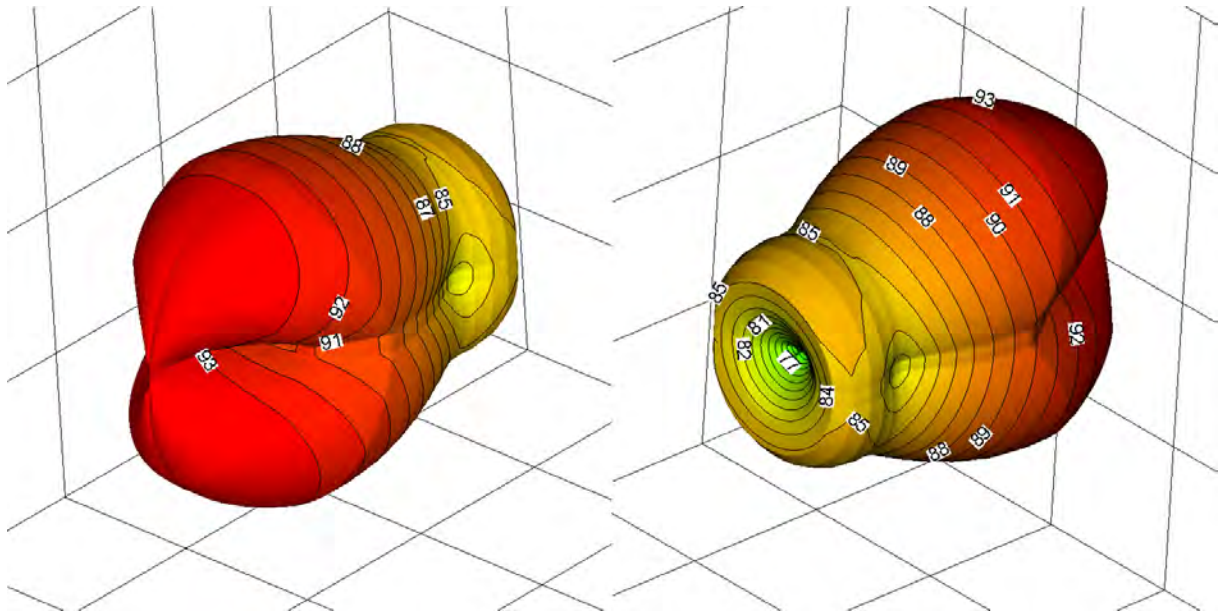
Figure E.47   Directivity plot: idle descent configuration
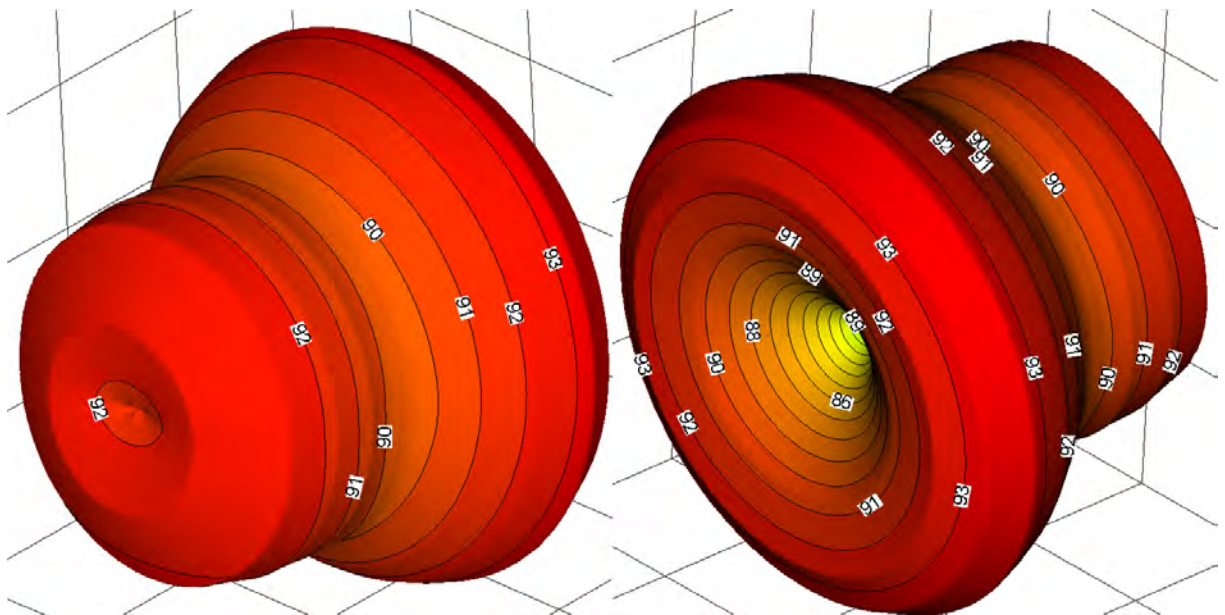
Figure E.48   Directivity plot: glide slope configuration

In figure E.47 the engine is at idle but additionally in a windmilling condition (compare figure D.1). Thus, engine noise is actually not accounted anymore within PANAM although e.g. the fan blades are still turning. Here again, a dipole becomes visible that is heavily influence by convective amplification. Noise that radiates backwards is close to be of neglecting amplitude. In figure E.48 the engine is now running at 85 % N1. Thus, engine characteristics are dominant.

Appendix F: Specification File for IOPANAM

```
C !!!!!!!!!!!!!!!!!!!!!!!!!!!!!!!!!!!!!!!!!!!!!!!!!!!!!!!!!!!!!!!!!!!!!!!
C !!                                                                 !!
C !! File:          V_IOPANAM                                        !!
C !! Originator:    Philip Krammer                                   !!
C !! Date:          17/08/2008                                       !!
C !! Description:   - Definitions for module IOPANAM                 !!
C !!                - Definition of (approach) and departure         !!
C !!                  procedure segments for calculating             !!
C !!                  trajectories as an input for PANAM             !!
C !!                - supplementary to DB8 (engine map calculation)  !!
C !!                                                                 !!
C !!!!!!!!!!!!!!!!!!!!!!!!!!!!!!!!!!!!!!!!!!!!!!!!!!!!!!!!!!!!!!!!!!!!!!!
C
C --------------------------------------------------------------------
C ---                                                              ---
C ---      ADD of Database DB12                                    ---
C ---                                                              ---
C ---      P A N A M   D E F I N I T I O N                         ---
C ---                                                              ---
C --------------------------------------------------------------------
C
C
C -------------
C EXPLANATIONS
C -------------
C
C IMD28P0      : control parameter/noise analysis execution with
C                =0   noise propagation model - IFL 2004
C                =1   PANAM (Parametric Aircraft Noise Analysis Module)
C                     - DLR 2007
C
C IOPNDEF      : This matrix holds the definition elements for noise
C                calculation with PANAM
C                PANAM can be started in 2(k) different modes.
C
C                The vector elements have the following meaning:
C
C                k              -   Row Index
C                                   =1 Departure
C                                   =2 Approach
C
C                IOPNDEF(1,k)   - control parameter
C                                   =0 no calculation
C                                   =1 calculation
C                IOPNDEF(2,k)   - type of noise sources to be calculated
C                                   = 0    airframe noise only
C                                   = 1    engine noise only
C                                   = 2    engine and airframe noise
C                                   = 3    landing gear noise only
C                                   = 4    flaps only
C                                   = 5    slats only
C                                   = 6    spoiler only (source model to be
C                                          implemented in PANAM)
C                IOPNDEF(3,k)   - control parameter / noise animation
C                                   =0 no calculation
C                                   =1 calculation
C                IOPNDEF(4,k)   - control parameter / isometric surfaces
```

```
C                                                =0 no calculation
C                                                =1 calculation
C                IOPNDEF(5,k)    -  control parameter / ground influence
C                                                =0 free field
C                                                =1 ground reflection
C                IOPNDEF(6,k)    -  control parameter / array height
C                                                   (observer height)
C                                                =0 0m
C                                                =1 1.2m
C ----------
C DATA SETS
C ----------
<-IMD28P0       -   control parameter/noise analysis module
  0  2  1  1
  1
<-IOPNDEF       -   configuration definition for PANAM
  0  2  1  18
  1  2  0  1  1  1
  1  2  0  1  1  1
  1  2  0  1  1  1
C
C
C -----------------------------------------------------------------------
C ---                                                                 ---
C ---      ADD of Database DB12                                       ---
C ---                                                                 ---
C ---      P A N A M   F L I G H T   T R A J E C T O R I E S          ---
C ---                                                                 ---
C -----------------------------------------------------------------------
C
C CONTENTS:
C         -  Definition and explanation of departure segments
C         -  Information specifying departure segments
C         -  Definition and explanation of approach segments
C         -  Information specifying approach segments
C
C -----------------------------------------------------------------------
C
C PRINCIPAL SET-UP
C
C    '          '      '          '        '         '             '          '
C    '          '      '      _ -'         '     _ -'              '      _ _ -'
C    '          '      '_ _ ¯  '           '_ _ ¯  '              '_ _ ¯  '
C    '          '      '- ¯     '   +  '- ¯     '   +  ... +  '- ¯     '
C    '     /'   '      '        '        '        '             '        '
C    '-----´ '         '---------'        '---------'            '---------'
C    '          '      '          '        '         '             '          '
C    take-off        segment i        segment i+1              segment n
C
C TAKE OFF SEGMENT:
C
C No inputs are needed for this segment. The airplane accelerates with 100%
C of available thrust, rotates at V2 and climbs up to the obstacle height
C (FAR). Flaps are in start configuration, the gear is fully extended.
C
C
C CLIMB SEGMENT A: climb with constant speed up to a desired altitude. With
C                 a constant flight speed the rate of climb will be
C                 adjusted, engine thrust not. Flight speed is set to the
C                 flight speed from the segment before (end speed). If the
```

```
C                        speed is to be changed an acceleration segment F1206 has
C                        to be calculated (flown) in advance
C
C       '          '  H(END)      PARAMETERS OF SEGMENT A:
C       ' v=const-'                V(IAS) = Indicated Air Speed     [m/s]
C       '  _  -   '                H(END) = Altitude end of segment  [m]
C       '-        '                TS     = thrust setting           [%]
C i ' "F1201" '  (i+1)            MAL    = Mach number limitation   [ ]
C ' '---------'    '               FLAPS(i)= flap setting            [°]
C       '          '               GEAR(i) = landing gear position   [ ]
C
C
C CLIMB SEGMENT B: climb with constant climb angle until reaching the
C                  desired true air speed V_TAS(END) or the final alt.
C                  H(END), which ever is first reached along the flight
C                  path. Climb angle will be adjusted if exceeding maximum
C                  climb angle.
C
C       '          '  V(END)      PARAMETERS OF SEGMENT B:
C       '     _  -'  H(END)        GAMMA   = climb angle             [°]
C       '  _  -   '                V(END)  = TAS end of segment     [m/s]
C       '-        '                TS      = thrust setting          [%]
C i ' "F1206" '  (i+1)            MAL     = Mach number limitation  [ ]
C ' '---------'    '               FLAPS(i) = flap setting           [°]
C       '          '               GEAR(i)  = landing gear position   [ ]
C                                  H(END)  = Altitude end of segment [km ]
C
C
C -------------
C EXPLANATIONS
C -------------
C
C IOPNDED : This vector describes the climb trajectory in terms of putting
C           the segments mentioned above into a sequence. Each segment has
C           its own input parameters
C
C           The vector elements have the following meaning:
C
C           IOPNDEP(1)       -   No. of segments
C
C           IOPNDEP(1+1)     -   No. of vector/segments elements (total row)
C           IOPNDEP(1+2)     -   Type of climb segment
C                            = 1    climb segment A
C                            = 2    climb segment B
C
C           i-th climb segment TYPE A
C           IOPNDEP(3+1)     -   number of sampling points
C           IOPNDEP(3+2)   km    requested height margin (beginning up to
C                                the end of segment)
C           IOPNDEP(3+3)   %     thrust setting
C           IOPNDEP(3+4)   -     Mach number limitation
C           IOPNDEP(3+5)   -     control parameter of flaps and landing gear
C                                condition
C                                =1 Slats/Flaps retracted/LDG retracted'
C                                =2 Slats/Flaps retracted/LDG extended'
C                                =3 Slats/Flaps in Take-Off Configuration/
C                                   LDG retracted'
C                                =4 Slats/Flaps in Take-Off Configuration/
C                                   LDG extended'
C                                =5 Slats/Flaps in Approach Configuration
C                                   during Landing/LDG retracted'
```

```
C                                      =6 Slats/Flaps in Approach Configuration
C                                         during Landing/LDG extended´
C                                      =7 Slats/Flaps in Landing Configuration/LDG
C                                         retracted'
C                                      =8 Slats/Flaps in Landing Configuration/LDG
C                                         extended'
C           IOPNDEP(3+6)    -    control parameter - reserved
C           IOPNDEP(3+7)    -    control parameter
C                                =1 temporary max. thrust
C                                =2 maximum continuous thrust
C           IOPNDEP(3+8)   deg   minimum allowed climb angle
C           IOPNDEP(3+9)   deg   maximum allowed climb angle
C           IOPNDEP(3+10)   -    control parameter
C                                =0 no tecplot output of trajectory
C                                =1 output
C
C           i-th climb segment TYPE B
C           IOPNDEP(3+1)    -    number of sampling points
C           IOPNDEP(3+2)   km    requested height margin (beginning up to
C                                the end of segment)
C           IOPNDEP(3+3)    %    thrust setting
C           IOPNDEP(3+4)    -    Mach number limitation
C           IOPNDEP(3+5)    -    control parameter of flaps and landing gear
C                                condition
C                                =1 Slats/Flaps retracted/LDG retracted'
C                                =2 Slats/Flaps retracted/LDG extended'
C                                =3 Slats/Flaps in Take-Off Configuration/
C                                   LDG retracted'
C                                =4 Slats/Flaps in Take-Off Configuration/
C                                   LDG extended'
C                                =5 Slats/Flaps in Approach Configuration
C                                   during Landing/LDG retracted'
C                                =6 Slats/Flaps in Approach Configuration
C                                   during Landing/LDG extended´
C                                =7 Slats/Flaps in Landing Configuration/LDG
C                                   retracted'
C                                =8 Slats/Flaps in Landing Configuration/LDG
C                                   extended'
C           IOPNDEP(3+6)    -    control parameter - reserved
C           IOPNDEP(3+7)    -    control parameter
C                                =1 temporary max. thrust
C                                =2 maximum continuous thrust
C           IOPNDEP(3+8)   deg   climb angle (will be adjusted if > than
C                                max. climb angle)
C           IOPNDEP(3+9)   m/s   N/A: requested TAS at the end of the
C                                segment
C           IOPNDEP(3+10)   -    control parameter
C                                =0 no tecplot output of trajectory
C                                =1 output
C
C
C ----------
C DATA SETS
C ----------
C
C short- to medium range A/C (150 PAX, 2 Eng., range: 4800 km, M = 0.78)
C -------------------------------------------------------------------
C *** IOPANAM departure trajectory (modified ATA (DLR)) ***
C
C Reference A/C
C
```

```
<-IOPNDEP
  0  3  1  37
  3.
  12. 1.  120. 0.446  100.  0.8  3. 1. 2. 0.  45.   1.
  12. 2.  250. 1.348   80.  0.8  1. 1. 2. 3. 128.6 1.
  12. 1.   30. .100    55.  0.8  1. 1. 2. 0.  1.    1.
C
C High-powered A/C
C
C <-IOPNDEP
C  0  3  1  37
C  3.
C  12. 1.  120. 0.446  100.  0.8  3. 1. 2. 0.  45.   1.
C  12. 2.  250. 1.348   60.  0.8  1. 1. 2. 3. 128.6 1.
C  12. 1.   30. .100    50.  0.8  1. 1. 2. 0.  1.    1.
C
C *** IOPANAM departure trajectory (climb with cut back) ***
C
C  <-IOPNDEP
C   0  3  1  25
C   1.
C   12. 1.  200. 0.446  100.  0.8  3. 1. 2. 0.  45.   1.
C   12. 2.  200. 0.262   80.  0.8  1. 1. 2. 3. 128.6 1.
C
C
C
C green freighter A/C
C ------------------
C
C  (initial climb to 1000ft
C   climb with climb power up to 3000ft
C   retracting flaps and accelerating to 250kts
C   climb with 250kts up to 10000ft
C
C  <-IOPNDEP       -   IOPANAM departure trajectory
C  0  3  1  49
C  4.
C  12. 1.  100. 0.294  100.  0.8  3. 1. 2. 0.   45.   1.
C  12. 1.  200. 0.599   95.  0.8  3. 1. 2. 0.   45.   1.
C  12. 2.   30. 0.350   70.  0.8  1. 1. 2. 3.  128.6 1.
C  12. 1.  150. 1.500   70.  0.8  1. 1. 2. 4.5   4.5 1.
C
C
C
<-IOPNAPP        -    IOPANAM approach trajectory
C                     SOURCE CODE TO BE IMPLEMENTED


C
C
C ----------------------------------------------------------------------------
C ---                                                                      ---
C ---      ADD of Database DB8                                             ---
C ---                                                                      ---
C ---      A D D I T I O N A L   E N G I N E   P A R A M E T E R S  ---
C ---      under point 3.4 in DB8 - Data of Fan                           ---
C ----------------------------------------------------------------------------
C
C ------------
C EXPLANATIONS
C ------------
C UNDWMAXBN          : planned maximum low pressure spool speed N1 in %
```

```
C                               associated with parameter UNDWMAXB
C
C                               for CFM56: 102% (http://www.airbusworld.com - FAA
C                                          Type Certificate Data Sheet)
C                               for GE90:  100% (no reference found)
C
C RSS                 : Rotor Stator Spacing (data exclusively for PANAM)
C
C                               CFM56-5B  : 2.0
C                               GE90      : 2.0
C
C SECTFANA            : fan blade trailing edge angle relative to rotational
C                       axis at 0.5 * fan radius
C
C                               CFM56-5A4 : 12°
C                               CFM56-5B2 : 35°
C                               GE90      : 37°
C
C HUBTOTIP            : Hub to Tip Ratio (data exclusively for PANAM)
C
C                               CFM56-5B  : 0.389
C                               GE90      : 0.347
C                                    (http://ctrsgi1.stanford.edu/CITS/ge90r.jpeg
C
C ----------
C DATA SETS
C ----------
<-UNDWMAXBN %        planned maximum low pressure spool speed N1
  0  3  1  1
  102.
<-RSS        -       Rotor Stator Spacing
  0  3  1  1
  2.0
<-SECTFANA   °       fan blade trailing edge angle at 50% fan radius
  0  3  1  1
  8.
<-HUBTOTIP   -       Hub to tip ratio
  0  3  1  1
  0.389
```

F.1   Changes in the PrADO Environment

Within subroutine "get_PrADO_Projectpath(npd,projectdir)" subfolder "panam" added to the project tree.

New project, "PANAM", added in workspace "PrADO_TA2". Files created in the directory "PrADO_MAIN". FORTRAN fixed format source files added to the new project:

- iopanam.for – control routine. Calls all other subroutines and programs, executes PANAM, reads results and writes them back into PrADO database
- f1206.for – slightly modified PrADO climb segment (f1206.for)
- iopn_ClimPerf.for – determines the max. climb angle, for one flight condition or for a straight climb to reach a desired altitude
- iopn_EngMap.for – output of an engine map in the format for PANAM; calculation of fan rotational speed
- iopn_geometry.for – writes necessary geometric parameter out of PrADOs databases; checks the A/C configuration. calculates flap- and spoiler length\width averaged over the wing
- iopn_trajectory.for – simulates a departure, checks the empennage, writes data in the format for PANAM and provides a Tecplot file (**TecPlot 2006)** for visualization.

Within \LBY\TAS_LBY\md28.for new control parameter added which allows for selection between conventional noise prediction and PANAM.

New environmental variable needed: PANAM_HOME with :\PrADOSYSTEM\PANAM
PANAM   is   started   with   a   system   call.   Executable   is   in   the   folder:
PrADOSYSTEM\PANAM\BIN\main.exe

Results of IOPANAM are written into D:\PrADOSYSTEM\PrADO\PROJEKTE\PrADO-TA2*ProjectName*\panam

Results of PANAM are written into: …\PrADOSYSTEM\PANAM\Ausgabedateien

Glossary

Absorption

Absorption is a reduction of reflected sound energy and depends on material properties. Thus, the sound energy striking the material surface will not be totally reflected. This must not be mistaken with the transmission loss through a material (**Wilson 1989**, p. 539)

Acoustics

"(1) The science of sound, including the generation, transmission, and effects of sound waves, both audible and inaudible. (2) The physical qualities of a room or other enclosure (…) that determine the audibility and perception of speech" (**Wilson 1989**, p. 540)

Air-path axis system

has an air-path axis (x-axis), pointing in the direction of the flight velocity vector, a lateral air-path axis (y-axis) and a normal air-path axis (z-axis) (**DIN 9300 1990**)

Aural

"Of or pertaining to the ear or hearing" (**Wilson 1989**, p. 540)

A-weighted sound level

The human ear is more sensitive at speech range frequencies. The A-weighted sound level in dBA, reduces the effects of the low and high frequencies with respect to the behaviour of the ear in the medium frequency range (**Wilson 1989**, p. 539)

Background noise

"The total of all noise in a system or situation, independent of the presence of the desired signal. In acoustical measurements, the term "background noise" is also used with the same meaning as "residual noise."" (**Wilson 1989**, p. 540)

Band

"A segment of the frequency spectrum" (**Wilson 1989**, p. 540)

Band centre frequency

"The designated (geometric) mean frequency of a band of noise or other signal …" (**Wilson 1989**, p. 540)

Body axis system

has the longitudinal axis pointing forward (defined by the reference plane) and the transverse axis perpendicular to the reference sphere, positive to starboard (**DIN 9300 1990**). It is a Cartesian system. Positive angle of attack occurs with a positive z-axis component of the airplane's velocity vector (**Phillips 2004**, p. 602).

Broadband noise

"Noise components over a wide range of frequencies." (**Wilson 1989**, p. 540)

Conventional aircraft configuration or tail aft aircraft. Characterized by a fuselage and a wing as well as a horizontal tailplane and vertical tailplanes on the tail of the aircraft (**Scholz 1999**, p. 4.7)

deciBel (decibel)

"dB – The decibel is a measure, on a logarithmic scale, of the magnitude of a particular sound intensity by reference to a standard quantity that represents the threshold of hearing." (**Smith 1989**, p. 285)

Displacement, elongation

"… displacement of an oscillating particle from its resting position." (**Blauert 2008**, p. 5)

Earth-fixed axis system

Has an x-y plane normal to the local gravitational vector. X-axis is pointing north and the y-axis is pointing east. It is a Cartesian system with the simplification that the Earth radius is large compared to the distance travelled by an airplane (**Phillips 2004**, pp. 601-2).

Exit flow angle

is the angle between the direction of fluid flow at blade exit relative to machine rotational axis

Far field

"… at a sufficient distance from the source, the sound pressure … decreases 6 dB with each doubling distance from the source … Also, the sound particle velocity is in phase with the sound pressure … Regions closer to the source, where these two conditions do not hold, constitute the near field …" (**Wilson 1989**, p. 542) "The acoustic far-field is defined as those distances greater than or equal to ten times the acoustic wavelength of interest, or ten times the characteristic source dimension." (**Dunn 1973**, p. 13)

Footprint (Noise)

"The shape and size of the geographical pattern of noise impact …" (**Wilson 1989**, p. 543)

Free field

"A sound field in which the effects of obstacles or boundaries (or reflecting ground plane, author's note) on sound propagated in that field are negligible." (**Wilson 1989**, p. 543)

Frequency analysis

"… is a process by which a time-varying signal is transformed into its frequency components" (**Bies 2003**, p. 41)

Hub-to-tip ratio

Hub radius divided by tip radius

Loudness

"The judgement of intensity of a sound by a human being. Loudness depends primarily upon the sound pressure of the stimulus." (**Wilson 1989**, p. 544)

Noise

"Any sound that is undesirable because it interferes with speech and hearing, or is intense enough to damage hearing, or is otherwise annoying." (**Wilson 1989**, p. 544)

Noise level [Sound level, author's note]

"This is an A-weighted sound pressure level as measured directly using a sound-level meter on "slow" response, … specified by the California Department of Transport for monitoring airport noise." (**Smith 1989**, p. 287)

Octave

"An octave is the interval between two sounds having a basic frequency ratio of two …" (**Wilson 1989**, p. 545)

Particle velocity

"… alternating velocity of an oscillating particle." [must not be mistaken with the speed of sound, authors note] (**Blauert 2008**, p. 5)

Pure tone

"A sound wave whose waveform is that of a sine wave." (**Wilson 1989**, p. 545)

Random noise

"An oscillation (sound pressure or vibration) whose instantaneous magnitude and frequency are not specified for any given instant of time … "(**Wilson 1989**, p. 546)

Reference plane

The reference plane is the plane of symmetry if one exits. Within this plane the longitudinal and normal axis have to be found (**DIN 9300 1990**). In most cases, aircraft have one plane of symmetry, the x-z plane.

Root mean square (rms)

"The root-mean-square value of a quantity that is varying as a function of time is obtained by squaring the function at each instant, obtaining the average of the squared values over the interval of interest, and taking the square root of this average …" (**Wilson 1989**, p. 546)

Sound

"Sound is the sensation produced at the ear by very small pressure fluctuations in the air." (**Bies 2003**, p. 12)

Sound intensity

"… sound power per effective area, … that is the area component perpendicular to the direction of energy propagation." (**Blauert 2008**, p. 5)

Sound power

"The total amount of energy radiated into the atmospheric air per unit time by a source of sound" (**Wilson 1989**, p. 547)

Sound pressure

"… alternating pressure as caused by particle oscillation" (**Blauert 2008**, p. 5)

Sound pressure level

"The root-mean-square value of the pressure fluctuations above and below atmospheric pressure due to a sound wave …" (**Wilson 1989**, p. 547)

Spectrum

"The description a sound resolved into components, each of different frequency." (**Wilson 1989**, p. 548)

Spherical wave

"A sound wave in which the surfaces of constant phase are concentric spheres. A small (point) source radiating into an open space produces a free sound field so spherical waves. " (**Wilson 1989**, p. 548)

Third-octave band

"A frequency band whose cutoff frequencies have a ratio of 2 to the one-third power, which is approximately 1.26 …" (**Wilson 1989**, p. 587)

Tone

"A sound of given pitch. A pure tone has a sinusoidal waveform." (**Wilson 1989**, p. 549)

Unconventional aircraft

configurations differ at least in one basic feature out of the design features of a conventional aircraft configuration (characterized by a fuselage and a wing as well as a horizontal tailplane and vertical tailplanes located at the tail of the aircraft (**Scholz 1999**, p. 4.7)